UNIVERSITÀ DEGLI STUDI DI NAPOLI "FEDERICO II"

SCUOLA DI DOTTORATO "SCIENZE DELLA TERRA"
"Giuseppe De Lorenzo"

Dottorato in Scienze ed Ingegneria del Mare

in consorzio con
SECONDA UNIVERSITÀ DI NAPOLI
UNIVERSITÀ "PARTHENOPE" NAPOLI
in convenzione con
ISTITUTO PER L'AMBIENTE MARINO COSTIERO – C.N.R.
STAZIONE ZOOLOGICA "ANTON DOHRN"

XXI ciclo

Tesi di Dottorato

Mediterranean tephrochronology: new insights from high-resolution analyses of a 200.000 years long composite sedimentary record

Candidato: Dott.ssa Stella Tamburrino

Tutor: Dott. Ennio Marsella

Co-Tutors: Prof. Lucia Civetta
Dott. Mario Sprovieri

Il Coordinatore del Dottorato: Prof. Bruno D'Argenio

ANNO 2008

Contents

Abstract

Marine sediments represent excellent archives for reliable recording of tephra layers produced by explosive volcanic eruptions due to their about continuous accumulation. Investigation on tephra layers in Mediterranean sediments contributes to better understanding of the dispersion patterns of erupted volcanic material and of the magmatic evolution of the Mediterranean volcanic provinces over large time scales. Due to the proximity of a number of volcanic sources, the Mediterranean sea represents an ideal location for tephrostratigraphic and tephrochronological studies. Several papers have already provided a solid and reliable tephrostratigraphic scheme data for this area (e.g. Keller et al. 1978; Paterne et al. 1986, 1988, 1990; Calanchi et al. 1994) useful for large scale correlations.

This work presents an integrated tephrostratigraphic and tephrochronologic study, carried out on three sedimentary cores collected in the central Mediterranean area. The KC01B (Ionian basin, 36°15.25′N, 17°44.34′E), MD01_2474G (N-Stromboli canyon, 39°10.44', 15°2.72') and ODP Leg 160 Site 963A (Sicily strait, 37°01.938', 13°10.896') were studied in details and used to continuously cover the stratigraphic interval of the last 200 ky. Generation of high-resolution age models based on astronomical tuning of the records, isotope stratigraphy, AMS ^{14}C dating and quantitative eco-biostratigraphy represented a unprecedented frame for accurate and reliable definition of ages for the detected tephra layers. The presented results take into account nineteen crypto-tephra and tephra layers singled out throughout the three sedimentary records. These tephras are distributed in a time span ranging from ca 7 kyr to 200 kyr B.P. (zone Y, X, V according to the tephrostratigraphic framework of Keller et al., 1978). Some tephra layers are here described for the fist time, while other volcanic deposits, well-known in the literature, were reconsidered in order to better constrain dating and volcanic sources. Major and trace elements analysis carried out by WDS and LA_ICP-MS techniques on well preserved pumice, scoria and glass shards, allowed to definitively characterise the different tephras and to correlate them to the activity of major volcanic sources located in the central Mediterranean area (Aeolian arc, Etna volcano, Campania Plain and Pantelleria island). In particular, for the first time, this research work accurately reconstructed the recurrent volcanic activity of the Aeolian arc and Pantelleria island and identified one younger Ischia explosive eruption, earlier poorly known. Despite further investigations are needed to provide definitive insights on these more complex tephrostratigraphic events, this work represents a considerable advancement in Mediterranean tephrostratigraphy allowing confirmation of eruptive events already known and the detection of the new ones.

Riassunto

I sedimenti marini rappresentano un archivio naturale in grado di preservare grazie al loro quasi continuo tasso di sedimentazione, i livelli di tefra prodotti dalle eruzioni vulcaniche. La caratterizzazione geochimica dei tefra nei sedimenti marini contribuisce al miglioramento delle conoscenze circa l'evoluzione magmatica delle province vulcaniche che insistono nell'area mediterranea in un ampio range temporale. Grazie alla presenza di numerosi vulcani attivi, il mare Mediterraneo rappresenta un sito ideale per interpretazioni di carattere tefrostratigrafico e tefrocronologico. Attualmente esistono in letteratura numerosi lavori che forniscono per questa area, consistenti ed affidabili schemi tefrostratigrafici utili per correlazioni a grande scala (Keller et al., 1978; Paterne et al., 1986, 1988, 1990; Calanchi et al., 1994).

Questo lavoro di ricerca presenta uno studio integrato di tefrostratigrafia e tefrocronologia, effettuato su tre carote marine prelevate nel Mediterraneo centrale. Sono state studiate in dettaglio le carote KC01B (bacino Ionico, 36°15.25'N, 17°44.34'E), MD01_2474G (N-Stromboli canyon, 39°10.44', 15°2.72') e ODP Leg 160 Site 963A (stretto di Sicilia, 37°01.938', 13°10.896') che ricoprono l'intervallo stratigrafico degli ultimi 200 ka. Per la definizione della cronologia di tutti i tefra studiati sono stati realizzati ed adottati "age-models" ad alta risoluzione basati su calibrazione astronomica, stratigrafia isotopica, datazioni radiometriche ed eco-biostratigrafia quantitativa. I tefra identificati nei tre records (19 crypto-tefra e tefra) ricadono in un intervallo temporale tra ~ 7 ka e ~ 200 ka B.P. (zone X, Y, V proposte da Keller et al., 1978). Le analisi effettuate per la caratterizzazione geochimica dei tefra studiati (in termini di elementi maggiori, minori e REE) sono state eseguite con l'utilizzo di WDS e LA-ICP-MS su campioni di pomici, scorie e vetri vulcanici, al fine di poter individuare una correlazione con le principali sorgenti vulcaniche del Mediterraneo (arco vulcanico delle Eolie, Etna, piana Campana e Pantelleria). In particolare, in questo lavoro di ricerca sono stati individuati livelli di tefra ascrivibili alla attività vulcanica delle isole Eolie, di Pantelleria e dell'isola di Ischia, poco noti in letteratura. Sebbene ulteriori approfondimenti siano necessari per meglio definire dal punto di vista tefrostratigrafico i tefra su detti, questa tesi rappresenta un ampliamento considerevole delle conoscenze sulla attività vulcanica esplosiva italiana.

1 Introduction

During the Quaternary, including prehistoric and historical period, several volcanoes have been active in the Mediterranean area. In particular, two major source regions of activity were represented by the Italian (Tuscan, Roman, Campanian, Aeolian, Sicilian), and the Aegean volcanic provinces including the Central Turkey. The explosive character of those activities, the eastward prevalent dispersion of plumes related to the prevalent NW wind pattern in the Mediterranean region and the highly variable and distinctive chemical composition of magmas and volcanic deposits make the Mediterranean an *ideal* area for application of tephrostratigraphy and tephrochronology.

The record of volcanic eruptions substantially demonstrates that their occurrence is a random episode. Actually, the explosive events are related to a number of interdependent factors: degree of gas saturation of the magma, tectonic movements around and within the magma chamber, rates of recharge of the magma reservoirs, ect.

From a geological point of view, the volcanic eruptions can be considered as instantaneous geologic events and, therefore, the associated deposits (named *tephra,* a Greek word originally used by Aristotele to describe volcanic eruptions in the Aeolian Islands and meaning all volcanic deposits e.g. fall, fallout ect, and/or *cryptotephra* when the layers are represented by material not visible to naked eye), are potentially synchronous time horizons intercalated in the sedimentary sequences at regional scale. They offer a sound opportunity to date volcanic eruptions and appropriately define sources and geological dispersion patterns of different explosive events. A number of recent papers (e.g. Calanchi et al., 1988; Narcisi 1996; Narcisi and Vezzoli 1999; Keller et al., 1978; Paterne et al., 1985, 1986, 1988) demonstrates that the tephrostratigraphy represents an appropriate tool for stratigraphic high-resolution correlations of marine sedimentary sequences in a number of geological settings (e.g., marine platforms, deep seas, lakes, ect.). Noticeably, the higher sedimentary continuity of the marine record ensures a better preservation of the tephrostratigraphic events.

In the last years, chemical characterization of tephra layers was carried out by more and more sophisticated analytical techniques capable to provide appropriate precision and accuracy of the measurements. In particular, EDS/WDS and Laser Ablation ICP-MS (LA-ICP-MS) techniques currently allow to detect concentrations of elements present at very low levels in single glass shards thus extending the tephrostratigraphic approach to very thin volcanic deposits in the sedimentary record.

Accurate and detailed investigations of tephras in the marine records, is currently considered a priority to improve our knowledge of the volcanic activity in different geographical areas and therefore to better assess potential volcanic hazard. Actually apart from a number of examples related to the destrutive effects of plinian eruptions that form high and great volcanic clouds with consequent wide geographical dispersion of ashes, generally proximal deposits are mostly used to define eruptive styles and dynamics of related source-events. Moreover, each single volcano produces deposits with variable major-elements chemistry, although it is not generally evident a systematic behaviour according to an ensemble of processes related to the evolution of the magma chamber prior to eruption. Besides, while on land the proximal pyroclastic deposits can be characterised by distinctive geochemical trends related to the magma evolution, in the coeval marine record it is not ever the case. Actually, dispersion of volcanic ash under effect of "filtering" of the dispersion patterns of transported matter produces an effect of not-systematic change in relative proportions and composition of minerals with distance from the eruptive area. This effect reflects in significant changes in bulk chemical composition of tephras.

Apart from such a number of methodological and conceptual problems, detailed analysis of tephra in the sedimentary archives is currently considered a sound method for appropriate stratigraphic reconstruction and correlation of regionally distributed sedimentary records and, once combined to radiometric methods and/or alternative dating approaches, a high-potential tool for reliable 0chronology of sedimentary archives (e.g., Keller et al., 1978; Paterne et al., 1986, 1988; Narcisi & Vezzoli, 1999, Wulf et al., 2004).

Three basic characteristics render tephra deposits suitable for accurate stratigraphy and then geochronology:

- distinguishable chemical and petrographic features detected from fresh juvenile material;
- widespread dispersion, for potential regional and extra-regional correlations.

Accordingly, the "best tephra" is that is possible to clearly attribute to a well known volcanic event, in terms of chemical and petrographic features, identified and possibly dated on land. On the other hand, accurate integrated stratigraphic correlation and radiometric dating are essential to include the tephra in a precise geochronological framework useful for large-scale correlations. In recent years, adoption of new conceptual models combined to classic radiometric approaches, increased the accuracy and precision of sedimentary records dating. Nowadays, one of the more accurate chronological tools adopted for high resolution calibration of different kinds of geological archives (continental as well as marine sedimentary records) is related to the so-called astronomical time scale. The essential principle of this "absolute" time scale is the recognition of high resolution cycle patterns in the studied records. That cyclicity, potentially tied to changes in the orbital parameters and insolation values, represents a high-resolution "pace-maker" of the sedimentary record with an associated potential of age control determined by deterministic calculation of the main astronomical parameters. This approach allows one generation of age model with precision of about 10,000 years extended back in time to the last 50 My. Contemporary, recent analytical improvement extended the K-Ar and $^{40}Ar/^{39}Ar$ radiometric methods to dating late Neogene deposits with high precision and accuracy making this radiometric technique an excellent tool for appropriate construction of sedimentary age models. The ^{14}C radiometric dating (at least for the last 24 kyr), represents a suitable technique for generation of accurate age models in the sedimentary records. Last but not least, an innovative high-resolution chronological tool for generation of age models for the last 70 ky is related to the recognition of abrupt climate changes in climate-sensitive proxy sedimentary records correlated to the same events recognised in ice core archives where high-resolution counting of yearly-layering provides unprecedented accurate dating.

This research work aims at reconstructing a new and detailed geochemical dataset of distal tephra recorded from a composite record of three sedimentary cores for which a highly precise age model is available and/or is here defined (in particular for MD01_2474G core). The three cores made part of a number of researches that rendered them key records for defining reliable chronological framework and paleoceanographic evolution of the Mediterranean basin for the last 1 Myr.

The main objectives of the thesis can be synthesised in the following points:

- to improve the tephrostratigraphy of the last 200 ky and define a high-resolution tephrochronology for the same interval in the Mediterranean area;
- to identify poorly known volcanic events mainly related to the Pantelleria and Aeolian volcanic activity;
- to check the real potential of tephrochronology as reliable tool for generation of high-resolution age models for Quaternary Mediterranean sedimentary records.

Hereafter a synthetic description of the main chapters of this thesis.

Chapter 1	**Introduction** – The first Chapter includes a synthetic overview of the main high-resolution chronology tools for marine sedimentary records along with a systematic reconstruction of the literature information available for tephrostratigraphy and tephrochronology of the last 200 kyr in the Mediterranean basin. Limits of the tephrostratigraphic methods are discussed in detail.
Chapter 2	**Material: the studied sedimentary records** – The studied sedimentary records along with the analised tephra layers, are presented and described in detail.
Chapter 3	**Analytical methods** – All the analytical techniques adopted for generation of the different age models and to characterise the geochemistry of the different studied tephra layers are described.
Chapter 4	**Results** – The results of the chemical analyses of the tephra layers are reported and commented in relation to potential volcanic sources.
Chapter 5	**The age models** – The Chapter refers to the generation of high-resolution age models, achieved in this study and/or available in the literature, for precise and reliable dating of the studied marine sedimentary records.
Chapter 6	**Discussion** – This Chapter takes into account potential attribution of the tephra layers to single volcanic activities and dating of them with particular consideration to those poorly known. At the end of the chapter a synthetic scheme displays a comparison between ages reported in this study for the recognised tephra layers and those reported for the same events by Keller et al. (1978).
Chapter 7	**Conclusions**
Appendix A:	**ARM profile of the MD01_2474G core and correlation result tephra layers**
Appendix B:	**Oxygen isotopes from the MD01_2474G core**
Appendix C:	**Chemical analysis of tephras from: KC01B core, MD01_2474G core and ODP Leg 160 Site 963A**
Appendix D:	**Primitive mantle and chondrite values used for normalization trace elements**
Appendix E:	**Whole-cores photos of KC01B, MD01_2474G and OPD Leg 160 Site 963A**

1.1 Methods for high-resolution chronology of marine sedimentary records

1.1.1 The astronomically tuned time scale

The climate of the Earth varies over a broad range of time-scales, from a few seconds, in association of atmospheric turbulence, to some billions of years in relation to tectonic changes. Apart from this irregular variability, a restricted group of (quasi)periodic signals seem to systematically pacemake the Earth’s climate system.These Periodic astronomically variations of the insolation value are substantially related to some orbital parameters: precession, obliquity and eccentricity of the Earth's orbit. These orbital parameters describe the shape of the orbit of the Earth around the Sun and the orientation of the rotation axis of the planet with respect to its orbital plane. Due to gravitational forces between the Earth and the Moon and between the Earth and the other planets those orbital parameters are not constant but oscillate very slowly. A short description of those three main orbital parameters that influence the climate system of the Earth (Fig. 1.1) are hereafter described.

Obliquity

The tilt or obliquity (ε) of the Earth is defined as the angle between the Earth's rotational axis and the normal of the orbital plane. Because the Earth is not exactly a sphere, the Sun and the Moon exert a torque on its equatorial bulge which results in a change of the obliquity. The component with by far the largest amplitude has a period of 41 ka. This period appears stable for at least the last 1.5 Ma. Over long time-scales it shortens going back in time due to the shortening of the Earth-Moon distance, i.e. from 41 ka (present day) to 29 ka at 500 Ma BP.

Eccentricity

The Earth's orbit around the Sun is an ellipse. The Sun is roughly located in one of its two foci. The eccentricity (e) of the Earth's orbit is defined as $e = c/a$ where a is the ellipse semi-major axis which measures the size of the ellipse and c is the distance from focus to centre. The most important period in the series expansion for eccentricity is 413 ka while the next four periods range from 95 to 131 ka which contribute to a peak which is often referred to as the 100 ka eccentricity cycle. The sixth period is 2.3 Ma which has been observed in very long geological records.

Precession

The locations along the Earth's orbit where the Sun is perpendicular to the equator at noon are called equinoxes. The Earth's rotational axis rotates (or *precesses*) around the normal to the orbital plane like a spinning top. This rotation causes a clockwise movement of the equinoxes (as well as the *solstices*) along the Earth's orbit and this is called *precession of the equinoxes*. The quasi period of this precession of the equinoxes is 25.7 ka relative to the stars. However, for the climate, only the movement of relative to perihelion (the location of the Earth's orbit closest to the Sun) is important. This relative movement is called climatic precession and is measured by $\tilde{\omega}$ ($\tilde{\omega}=\Omega+\omega$) which is the angle between vernal equinox and perihelion, measured counter clockwise. The combination of the perihelion movement and of the precession of the equinoxes results in a period of the climatic precession of about 20 ka.

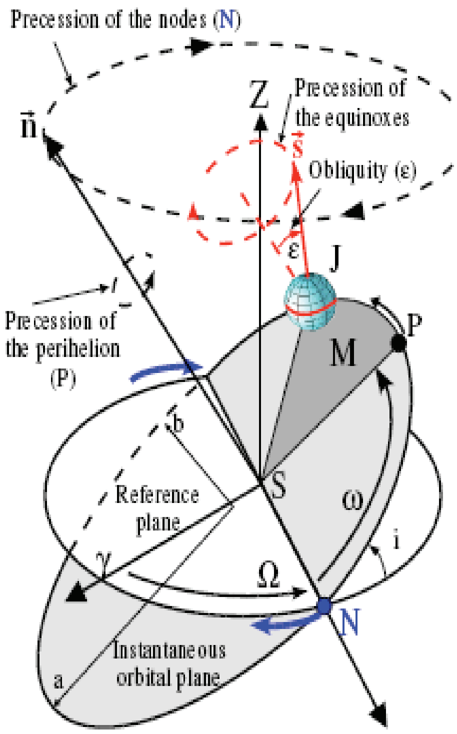

Fig. 1.1 Main orbital elements of the Earth's movement around the sun.

When an accurate calculation of the orbital parameters is confirmed, the insolation for any latitude and at any time of the year can be computed. Changes in the orbital parameters strongly affect the strength and the spatial and seasonal pattern of the insolation received by the Earth eventually resulting in climatic oscillations. The expression of these orbital induced climate oscillations seems faithfully recorded in sedimentary archives of widely different age and environment.

Lithologic alternation in sedimentary sequences attributed to orbital perturbations of the insolation curve and this to climate-ocean dynamics can be used like instrument to construct high resolution and accurate geochronological scales. A precise astronomical time scale based on a number of high resolution sedimentary records extends to the base of the Serravallian ~ 14 million of years (Shackleton et al., 1995; Hilgen et al., 1995; Lourens et al., 1996, Hilgen et al. 2003). A key effort to construct the Astronomical Time Scale of the Neogene was come out on sedimentary sequences of the Mediterranean basin where a highly rhythmic alternation of homogenous marls and organic rich strata (named *sapropels*), astronomically driven, represented a suitable clock for dating the sedimentary record. Actually, sapropels formation appears directly controlled by discharge of the river Nile influenced by the strength of the African monsoon. When the fresh water discharge increases, the salinity of the surface water decreases with a resulting weakens of the thermohaline circulation and consequent oxygen depletion at the bottom. Regarding the Pleistocene, it is characterised by rhythmic changes of climatic conditions from cool to warm, with different climatic effects in different parts of the world. However, what is distinctive about the Quaternary is not only the occurrence of repeated warm or cold episodes but the combination of both the high amplitude and the frequency of such variations. The repeated correspondence between the rhythm of environmental changes preserved in Quaternary fossil records and Earth's orbital ones has given origin to the theory of astronomical forcing on climatic changes. If external (astronomical) variables are the slow-varying forcing factors of Quaternary climate, the variations produced are the resultant of complex positive and negative *feedback* mechanisms internal to the climate system. Such feedbacks are necessary to translate the slight changes of solar heating into climatic variations, and probably contribute to limit the magnitude of such oscillations within a limited interval, and to modulate the rapidity of the changes. The response of the climate system to any (internal or external) forcing factor is nonlinear, and the physical mechanisms by which they are translated in global climate variations are still not completely understood. Appropriate tuning of sedimentary records with astronomical from calls for a number of assumptions: the sequences of interest should be continuous in time, unaltered, and the "real" climatic signal should have to be separable from non-climatic "noises". Moreover, the climatic dependence of each proxy has to be *calibrated* in order to estimate as precisely as possible the magnitude of climatic variations associated to each response. The technique of astronomical tuning of sedimentary records is at the present the most appropriate dating method for time calibration of Neogene sediment records. The ATS provides an age control every 10.000/20.000 years, corresponding to the precession frequency. Therefore the orbital tuning method is far more precise than that achievable by radiometric dating alone (Hilgen et al., 1999). The error of an astronomically tuned timescale is systematic and includes a few thousand years, based on the assumption of a constant (mostly unknown) time lag between a change in orbital insolation and the following climate response. Within this inaccuracy, the tuning approach provides a reliable and absolute timescale for magnetic reversal stratigraphy, biostratigraphy, oxygen isotope stratigraphy, and, of course, records of climate and oceanographic variability that transfer the astronomical record of varying insolation into quasi-cyclic sedimentological variability.

1.1.2 Radiometric ^{14}C and $^{40}Ar/^{39}Ar$ dating methods: limits, accuracy and precision

^{14}C dating method

The method most routinely employed to date marine fossils and sediments spanning the last ca. 25,000 years is the radiocarbon dating. ^{14}C method has been precisely calibrated by dendrochronology back to the beginning of the Holocene (Stuiver et al., 1998) and may be considered as the most accurate dating tool for the last 12 Kyr. The general sources of uncertainty that constrain the precision and accuracy of radiocarbon dates obtained from marine samples, are:

- ✓ analytical precision (laboratory),
- ✓ factor affecting the geological integrity of dated materials (stratigraphical),
- ✓ *"marine reservoir errors"*,
- ✓ and calibration procedures.

Analytical precision

The 1σ analytical error range for most conventional radiocarbon measurements are commonly of the order of 80–150 radiocarbon years, which limit the potential to date events at a higher temporal resolution.

Apparent age

The problem of "apparent age" is prevalent in the marine realm, but the main causes in this context are ocean circulation processes and variations in the rate of carbon exchange between the oceans and the atmosphere. The resulting "*marine reservoir error*" is probably the most serious and widespread source of error affecting radiocarbon dates obtained from marine samples. Other factors that may complicate the interpretation of radiocarbon age models are fossil recycling (reworking), contamination during coring or other sampling procedures, and isotopic fractionation. Furthermore, small fossils may be mobile in the sediment column and hence radiocarbon data-sets based on selected macrofossil samples are not necessarily superior to those based on bulk sediments. Therefore the integrity of the results generated through both methods needs to be tested of time in time for every investigated site.

"Marine reservoir effect"

The *marine reservoir effect* is an off-set in ^{14}C age between organisms that derive their carbon from the marine environment and contemporaneous terrestrial organisms (Ascough et al., 2005). The modern reservoir effect in near-surface ocean waters generally varies between about 200 and more than 750 ^{14}C years and averages around 400 ^{14}C years. Recent evidence has shown, however, that modern ocean surface reservoir ages vary with latitude and circulation effects. Evidence of marked regional departures from R_t (standard correction) has led to efforts to define local correction factors, which are expressed as deviations from R_t, termed ΔR (Reimer and Reimer, 2001). In particular samples from deep water basins tend to have large reservoir errors, while the gradient in radiocarbon age between surface and deep waters may also have varied over time.

Radiocarbon calibration

The internationally accepted standard model for radiocarbon calibration, INTCAL04 (Reimer et al., 2004), is based upon radiocarbon-dated tree-ring samples for the sector that extends from the present back to ca. 11.9 kyr BP (tree-ring yr). Although the use of tree-ring samples provides the most rigorous calibration data available, calibration of Holocene radiocarbon dates is not without problems, due principally to short-term oscillations in atmospheric radiocarbon content. In fact, remains that calibration frequently introduces an additional error term, over and above those associated with laboratory precision and uncertain geological context and the uncertainties introduced by calibration increase dramatically in the case of radiocarbon age estimates older than Holocene. The part of the INTCAL04 calibration data-set which dates between approximately 15,585 and 11,500 years BP (the 'Lateglacial' period) is primarily based on radiocarbon-dated *laminated sediments* from the Cariaco Basin (tropical Atlantic). Beyond 15,585 cal BP, and extending back to ~ 24,000 year BP, INTCAL04 is based on paired *^{14}C/U-series* dates obtained from corals. The radiocarbon dating of this part of the INTCAL04 data-set is thus based predominantly on marine samples which may be affected by a marine reservoir error. Although there is some reason for believing that this error may not have varied significantly during the last 25,000 years or so (Hughen et al., 2004), this is by no means certain. Problems of calibration are even more acute for radiocarbon ages greater than ca. 25 kyr BP.

Currently two techniques are possible in order to determine the relationship between ^{14}C of a sample:

- ✓ Method of Libby, that it is the dating with a conventional method for the measure of the radioactive activity β of the champion,
- ✓ Method AMS, based on the Atomic Mass Spectroscopy (AMS) with particle accelerators of type Tandem, that it allows the direct measurement of the relationship between Carbon atoms and of its radioisotope.

$^{40}Ar/^{39}Ar$ dating method

Recent analytical development expended the K-Ar and $^{40}Ar/^{39}Ar$ methods to date very young rocks (Late Pleistocene-Holocene) with high precision makes his techniques an important tool of geochronology.

K/Ar method

^{40}K isotope is radioactive and decays to ^{40}Ca and ^{40}Ar. Hence the error in the age calculation for K-Ar clock is solely dependent on precision and accuracy of the $^{40}Ar_{rad}/^{40}K$ measurements. Determination of $^{40}Ar_{rad}$ in young volcanic rocks (and minerals) is complicated due to low quantities of radiogenic argon in comparison to overwhelming amount of the atmospheric argon. To overcome the problem special analytical procedures such as unspiked K-Ar technique (Cassignol et al., 1978; Gillot and Cornette, 1986) and isotope dilution technique by the atmospheric argon have been developed.

Measured amount of ^{40}Ar in a dated sample consists of radiogenic argon ($^{40}Ar_{rad}$), which was accumulated from ^{40}K since mineral crystallisation, and non-radiogenic argon ($^{40}Ar_{n-rad}$), which was initially trapped by the mineral during its crystallisation ($^{40}Ar_{ini}$) and impregnated after by the atmospheric pressure into intercrystalline defects ($^{40}Ar_{atm}$).

$^{40}Ar/^{39}Ar$ method

The $^{40}Ar/^{39}Ar$ method differs from the conventional K-Ar method in that the determination of potassium is replaced by determinations of artificially created ^{39}Ar due to $^{39}K_{(n,p)}{}^{39}Ar$ reaction with fast neutrons. For this purpose sample is irradiated in a nuclear reactor. $^{40}Ar/^{39}Ar$ age calculation includes two major sources of errors: 1) instrumental errors on peak measurements and blank corrections, and 2) errors on J-factor and Ca, K, Cl correction factors. Errors, which results from K-Ar calibration of the age monitors, Ca and K correction factors, are systematic and often are not considered for the final error propagation in the $^{40}Ar/^{39}Ar$ age. However, for calibration of other methods these errors have to be accounted for but special studies on inter-calibration of the age monitors were performed to reduce that source of systematic errors in $^{40}Ar/^{39}Ar$

dating (e.g. Baksi et al., 1996; Renne et al., 1998). $^{40}Ar/^{39}Ar$ method is advantageous in comparison to K-Ar method despite the more complex procedure. First of all, a $^{40}Ar/^{39}Ar$ ratio is measured from the same aliquot of a sample. It reduces problem of inhomogeneous distribution of potassium, which is one of the sources of uncertainty in K-Ar method. Secondly, there is no need for absolute concentrations of argon isotopes to be determined. It increases precision of the method and allows samples with small amount of argon be analysed. Third, as only isotopic ratios have to be known, it can be measured in fractions of gas released from a sample at different temperatures. These advantages have lead to development of stepwise-heating and laser fusion techniques.

Stepwise-heating technique

In the *stepwise-heating* technique a sample is incrementally heated from a low temperature until its final melting. Each portion of gas released at several temperature steps is analysed separately. Measured $^{36}Ar/^{40}Ar$ and $^{39}Ar/^{40}Ar$ ratios are also analysed in the inverse isochron coordinates. In a case of good linear relation between measured values for different temperature steps the x-intercept yields $^{39}Ar/^{40}Arrad$ ratio, while the y-intercept provides information on the $^{40}Ar/^{36}Ar$ ratio of initially trapped argon. If the requirements of closed isotopic system are fulfilled total fusion and isochron $^{40}Ar/^{39}Ar$ ages must be equal within analytical precision, and the $^{40}Ar/^{36}Ar_{ini}$ ratio, estimated from the inverse isochron diagram, must be 295.5. Hence, the inverse isochron approach gives additional control on both the analytical conditions and natural isotopic disturbances.

Laser fusion technique

In the $^{40}Ar/^{39}Ar$ *laser fusion* technique gas is released by melting of the sample with a continuous wave laser. The advantage of the $^{40}Ar/^{39}Ar$ total fusion technique is in that the very small samples, such as single crystals or individual grains of ultimately fresh rock matrixes, can be analysed and in that K and Ar will be determined in the same sample. $^{40}Ar/^{39}Ar$ stepwise-heating by the laser system is also possible. At last the $^{40}Ar/^{39}Ar$ dating method is, at present, the most precise and accurate geochronological tool for a range from 10 ka up to several Ma. Hence, the $^{40}Ar/^{39}Ar$ method may provide a reference time-scale for calibration of other methods such as $^{230}Th/^{234}U$, ^{10}Be etc., commonly used for dating of the Quaternary sediments.

1.1.3 A climatic driven (millennial to century scale) late Pleistocene chronology: the D/O and Heinrich events

Paleoclimate studies have revealed the general high-frequency instability of Late Pleistocene climate on timescales of a few millennia, centuries or even decades (e.g., Broecker et al., 1992; Johnsen et al., 1992; Dansgaard et al., 1993; Grousset et al., 1993; Bender et al., 1994; Kotilainen et al., 1995; Porter and An, 1995; Behl et al., 1996; Mayewski et al., 1996; Schulz et al., 1998; Cacho et al., 1999; Cacho et al., 2000; Martrat et al., 2004; Sierro et al., 2005; Sprovieri et al., 2006; Frigola et al., 2007), with rapid coolings (stadials) and warmings (interstadials) periods generally referred to as Dansgaard/Oeschger (DO) millennial oscillations (Dansgaard et al., 1993; Bond and Lotti, 1995). Moreover, a number of massive ice rafted detritus episodes, called Heinrich events (HE) occurred in the North Atlantic during some of the coldest stadials at the end of long-term cooling trends that include several DO oscillations (Heinrich, 1988; Bond et al., 1992, 1993).

One of the most valuable archive that records abrupt climate changes is represented by the polar ice-cores (e.g., ice core project GISP-2, GRIP; Johnsen et al., 1992; Dansgaard et al., 1993; Bender et al., 1994; Mayewski et al., 1996; N-GRIP members, 2004; EPICA Community Members, 2006) reaching several hundred thousand years back in time. In particular, the Northern ice cores (NGRIP, GRIP, GISP and many others) have been accurately dated by annual layer counting, flow models, wiggle matching to existing time scales or a combination hereof. Supported by annual layer counting, the collected stable isotope profiles, in particular those of oxygen, provided invaluable information about sudden climate changes in the recent past unlocking the state of the ocean-climate system during the last 70-100 ky.

A total of 25 abrupt Dansgaard/Oeschger events spanning the 125-11 ky time interval can be recognised in the ice core records, the last corresponding to the abrupt warming of the Younger Dryas termination at approximately 11,550 years BP. On the other hand, it has been postulated that the deposition of these major IRD layers resulted from catastrophic iceberg calving along the ice sheet margins of the North Atlantic (Bond et al., 1992; Broecker et al., 1992) (Fig. 1.2).

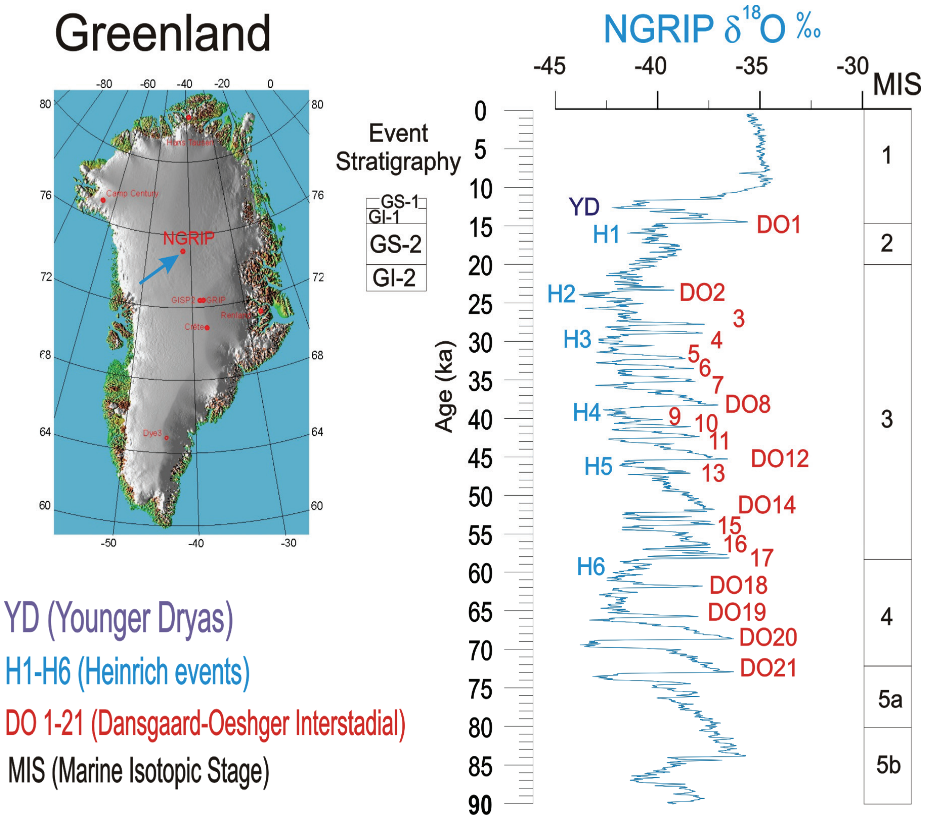

Fig. 1.2 Timing of Heinrich events an Dansgars-Oeschger events (Bond, 1992, 1993; NGRIP members, 2004; Hemming, 2004) inferred from geochemical records ($\delta^{18}O$ signal) of ice core NGRIP.

Moreover, minor IRD events were (Bond and Lotti, 1995) associated with all DO climatic oscillations, demonstrating that IRD events occurred much more frequently than previously thought, although they were recorded only in cores taken in the vicinity of the ice sheet margins. Iceberg melting during HE affected the hydrology of the North Atlantic Ocean, particularly the latitudes between 40°N and 55°N (Ruddiman, 1977) where the major IRD layers were deposited and planktonic foraminifera show pronounced decreases in $\delta^{18}O$ values, indicating the presence of meltwater (Heinrich, 1988; Grousset et al., 1993; Cortijo et al., 1997; Elliot et al., 1998, 2001).

A number of recent papers offer evidence of reliable recording of abrupt climate changes associated to the D/O and HE events in the sedimentary records of the Mediterranean basin (Cacho et la., 1999; Sierro et al., 2005). The high sensibility of the Mediterranean sea to record near instantaneous climate changes is related to the reduced volume of the basin, its restricted communication with the open ocean, the geographical position at the boundary between the subtropical/monsoon regime and the temperate westerlies, and renders this area extremely attractive to reliably document, in an amplified way, the major climate changes influencing the intermediate northern latitudes.

Thus, direct correlation of climate-sensitive proxy signals recorded in super-expanded sedimentary records of the Mediterranean basin to high-resolution time calibrated ice-core records, represents an excellent tool for dating, at century scale, sedimentary sequences spanning the last ~100 ky.

Summarising, precision of the Ar/Ar dating method can be assessed around a ~1.5% while that of the ^{14}C method range in the order of magnitude of 50-200 years at least for the 0-24ky interval. Astronomically tuned age model conceptually constrains dating in an interval related to the precessional cycle (±10 ky) although accurate and high-resolution investigation of sedimentary records could further improve the precession of the ages associated to such a kind of approach. Finally, dating of sedimentary succession based on a so-called climate-based chronology of the late Pleistocene (down to ~100 ky) can be considered precise at the same order of magnitude of the age model generated for the ice-core records and generally assumed ranging in a 0-600 years material from the younger to the oldest part of the record where counting of ice layers results unreliable and is substituted by less accurate models of ice-flow. Particularly, in the time interval related to the Marine Isotope Stage 4 where some of the tephras studied in this research occur, precision (2σ) associated to the calculated ages is about ±200 years.

1.2 Active volcanism in the Mediterranean region during the last 200 kyr

The explosive nature of the volcanic activity in the Mediterranean region over the last 200 kyr was intensively explored during the last decades (e.g., Keller et al., 1978; Thunell et al., 1979; McCoy 1981; Paterne et al., 1986, 1988, 1990; Vezzoli, 1991; Narcisi & Vezzoli, 1999; Calanchi et al., 1998; Siani et al., 2004).

The origin of the ash layers in this region is related to two main sources: the Italian and Aegean volcanic provinces. The products of the volcanic activity related to the two areas can be clearly identified in central-eastern Mediterranean sediments dominated by the north-westerly wind patterns and close to the volcanic sources (Keller et al., 1978). Actually, volcanism in the Aegean volcanic province is thought not to provide distal tephra to the western-central Mediterranean due to unfavourable prevailing wind pattern that distributes ashes towards the east. On the other hand, significant in differences major and trace-element concentrations of tephras allow our to clearly distinguish products from the Aeolian Arc, the Campanian volcanic provinces, and the Aegean Arc.

Hereafter synthetic view of the main source areas characterised, during the past 200 kyr, by eruptive activities and potentially recorded in sedimentary archives of the Mediterranean basin is presented.

Italian volcanic provinces

Campanian volcanoes

The Campania Province (Fig. 1.3) represents the southernmost sector of the Plio-Quaternary volcanic belt along the Italian peninsula.

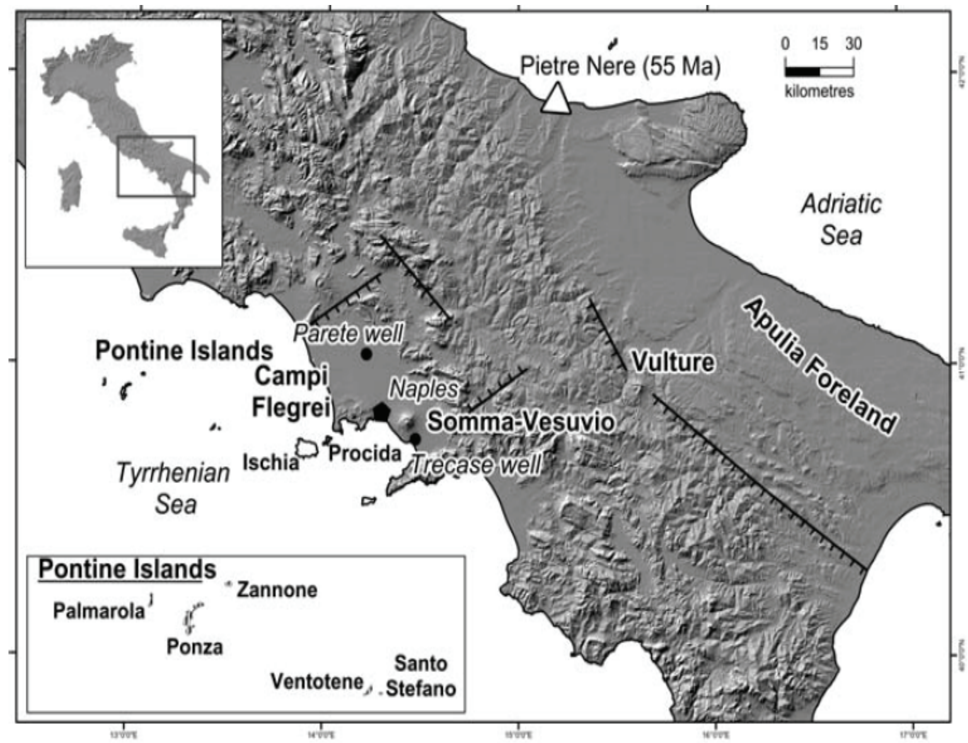

Fig. 1.3 Location map of the Campanian volcanoes, Pontine Islands and Mount Vulture (from Peccerillo 2005).

It is formed by the active volcanoes of Somma-Vesuvio, Ischia and Campi Flegrei (Phlegraean Fields), and by the islands of Procida and Vivara. The Pontine Islands (Ponza, Palmarola, Zannone, Ventotene and Santo Stefano) are also sometimes included in the Campania Province, although petrological data suggest that only the eastern islands (Ventotene and Santo Stefano) and the younger rocks from Ponza (about 1 Ma) have chemical compositions comparable to those of some Campanian volcanoes. Volcanic rocks in Campania and Pontine Islands range from mafic to felsic and mostly a silica undersaturated potassic to ultrapotassic behaviour. Mafic rocks with K_2O contents close to calc-alkaline basalts have been found both as lavas and as lithic ejecta at Ventotene and Procida-Vivara (D'Antonio and Di Girolamo, 1994; De Astis et al., 2004). Pliocene (about 4.5 Ma old) calc-alkaline rhyolites occur at Ponza, and 2 Ma old calc-alkaline basalts to andesites have been found by borehole drilling beneath the Campanian Plain north of Campi Flegrei (Pappalardo et al., 1999; Civetta et al., 1997; D'Antonio et al., 1999; Orsi et al. 1995). Mount Vulture is a 0.8 to 0.1 Ma old stratovolcano rising as an isolated cone about 100 km east of Vesuvio. Although the Vulture rocks are alkaline and undersaturated in silica, they are enriched in both sodium and potassium, and show a distinct composition with respect to other alkaline volcanoes in central-southern Italy.

A summary of ages and compositional chemistry of volcanism in Campania, the Pontine Island and Vulture is given in Table 1.1.

Vulacano		Age	Volcanology and Petrolgy
Somma-Vesuvio		30 kyr to 1944 AD	Stratovolcano (Mount Somma) with multiple caldera and an intracaldera cone (Vesuvio) formed of slightly to strongly silica undersaturated trachybasalt and leucite-tephrite to trachyte and phonolite.
Campi Flegrei		About 0,2 Ma to 1538 AD	Multicentre volcanic complex with two nested calderas and several monogenetic cones and maars, formed of prevailingly pyroclastic rocks with trachybasalt to trachyte-phonolite composition.
	Ischsia Island	150 kyr to 1302 AD	Volcano-tectonic horst formed of prevaling pyroclastic rocks with trachybasaltic to dominant trachytic composition.
	Procida Island	55 kyr to 17 kyr	Coalescing explosive centres formed of basalt, K-trachybasalt to trachyte pyroclastics.
Ventotene Island		0,8 Ma to <130 kyr	Stratovolcano with a caldera formed of basalt, K-trachybasalt to trachyte lava flows, domes (Santo Stefano) and pyroclastics.

Tab. 1.1 Schematic sketch of ages and chemical composition of Campania volcanoes.

The *Somma-Vesuvio* is a high volcanic complex in which an older stratovolcano truncated by a summit caldera (Somma) hosts a younger cone (Vesuvius). The ages of both the beginning and the end of explosive activity at Somma and Vesuvius, as well as the number and size of explosive eruptions, which characterized the eruptive history of the volcanic complex, are controversial. According to Santacroce et al. (2003), explosive activity at Somma begun 18 kyr ago and four Plinian episodes and eight-ten minor explosive eruptions occurred, sub- Plinian to Vulcanian in style, up to the 79 A.D. eruption. In the post 79 A.D.–1944 time span, the recent Vesuvius cone was formed by effusive and Strombolian activity. The largest eruptions of this period of activity occurred in 472 A.D. and 1631 A.D. and were sub-Plinian in size. The products of the most ancient activity are slightly silica saturated (K-trachytes to K-latites), whereas they evolved through time to undersaturated K-rich products (phonolites–phonotephrites–tephrites) (Santacroce et al., 1987).

The *Campi Flegrei* is a volcanic field characterized by several monogenic centres and two nested calderas. Activity is older at least than 60 ka (Orsi et al., 1996; Pappalardo et al., 1999, 2002). Two prominent eruptions characterize the Campi Flegrei volcanic activity from 60 kyr ago to the present time: the Campanian Ignimbrite (**CI**) and the Neapolitan Yellow Tuff (**NYT**) eruptions. The *CI* eruption occurred ~ 39 kyr (De Vivo et al., 2001) as a large-volume pyroclastic flow associated to a phreatoplinian event of phonolitic-trachytic pyroclastics. The *NYT* eruption is an important phreatomagmatic episode linked to the origin of the present Campi Flegrei caldera (Orsi et al., 1996). Recently a ^{14}C age of 12.1±0.17 kyr (range of calibrated ages 13.8–14.3 ka) on NYT was obtained by Siani et al. (2001, 2004). While $^{40}Ar/^{39}Ar$ dating method give an age of 14.9 kyr (Deino et al., 2004). The post NYT Campi Flegrei activity is represented by phreatomagmatic episodes and minor magmatic events with vents located inside the caldera. The chemical compositions of the products vary in the range trachybasalt–alkali trachyte and, on the whole, are K enriched with respect to Na (Rosi & Sbrana, 1987). The latest eruption dates back to 1538 AD when the Monte Nuovo phonolitic cone was formed. After this eruption, Campi Flegrei has been subjected to a number of volcanic crises characterised by strong soil uplift and intense shallow seismicity, but no eruptions have occurred. The main unrest events in the past 40 years, took place in 1969-72 and 1982-84, and generated uplifts of 170 and 180 cm, respectively (e.g. Orsi et al., 1996).

Volcanic activity at Procida Island is mainly represented by hydromagmatic eruptions from small monogenic centres, spanning the age range 55-17 kyr (D'Antonio & Di Girolamo, 1994; D'Antonio et al., 1999; De Astis et al., 2004). The erupted material consists of scoriae, hyaloclastites, accessory lithics and pumices, which are interfingered with and sometimes hardly distinguishable from pyroclastic deposits from Ischia and Campi Flegrei. Compositions range from basalt to trachyte. Overall, the rocks at Procida and Vivara closely resemble the potassic series from Ischia, although mafic compositions are much better represented at Procida.

The volcanic activity at Ischia Island spans along the late Pleistocene-Holocene period. Stratigraphic studies and radiometric dating indicate several phases of activity (e.g. Gillot et al., 1982; Poli et al., 1987; Civetta et al., 1991). The lowest exposed rocks are older than 150 ka, and consist of pyroclastic products with intercalated lava flows and paleosols. A second phase of activity (150 ka to 75 ka) is represented by several lava domes emplaced along a semicircular structure, probably a caldera rim. A third phase (55-20 ka) was opened by a caldera-forming ignimbritic eruption (Monte Epomeo Green Tuff) and was followed by explosive and effusive eruptions at different centres. The fourth phase (10 ka to 1302 AD) erupted lavas and some pyroclastics from monogenetic centres along extensional faults of the Ischia graben. The most important explosive events of the last 60 ka was the "*Monte Epomeo Green Tuff*" (MGT), a widespread ignimbritic deposit that covered the main part of the island (Brown et al., 2007), dated at ~ 55 ka. The last activity is the *Arso* lava flow erupted in 1302 A.D. The Ischia products are mainly alkali trachytic in composition and generally show Na/K≥1 (Vezzoli, 1988). The Ischia rocks are mildly undersaturated to oversaturated in silica and contain slightly lower alkalies and K_2O/Na_2O ratios than Campi Flegrei. The rocks of the first two stages are mainly trachytic lavas and pyroclastics. The Monte Epomeo Green Tuff and the following activity of the third phase are trachytic to phonolitic in composition with a few trachybasalts and shoshonites. During the last period of activity, latitic to trachytic lava and pyroclastics were erupted (Poli et al., 1987; Civetta et al., 1991).

The Island of Ventotene consists of a basal series of thin mafic lava flows cut by a caldera rim and covered by intermediate to felsic pyroclastic products. Santo Stefano is an eccentric lava dome covered by pyroclastic products. Pyroclastic rocks include fall, flow and surge magmatic and hydrovolcanic products, and contain lava lithics and cumulate xenoliths. Rock compositions range from basalt and trachybasalt to phonolite.

Sicilian volcanoes

The Sicily Province consists of several young to active volcanoes occurring in eastern Sicily, in the Sicily Channel and in the southern Tyrrhenian Sea. Etna is by far the best known among these volcanoes; other centres include Iblei, Pantelleria, Linosa, several seamounts in the Sicily Channel, the Island of Ustica and the Prometeo submarine lava field in the southern Tyrrhenian Sea (Fig. 1.4).

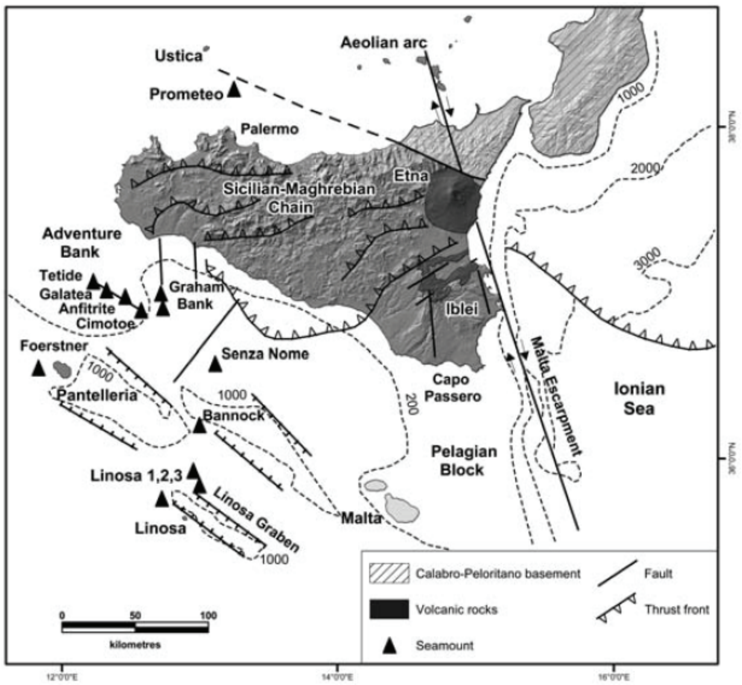

Fig. 1.4 Location map of Sicily volcanoes (from Peccerillo 2005).

The rocks have a variable petrochemical affinity, from tholeiitic to Na-alkaline, but all show typical intraplate trace element signatures (i.e. low LILE/HFSE ratios) and isotope compositions characterised by unradiogenic Sr, and radiogenic Nd. Ages range from about 7 Ma to present. A synthesis of ages, volcanological and petrological characteristics of Sicily volcanoes is given in Table 1.2.

Volcano	Age	Volcanology and Petrolgy
Etna	About 0,6 Ma to present	Several coalescing and superimposed stratovolcanoes mostly formed of lavas, spotted with hundreds of cinder cones, cut by three rift zones and by the Valle del Bove depression. Rocks include tholeiitic basalts followed by Na-alkaline rocks (trachybasalts, hawaiites and minor benmoreites and trachytes).
Pantelleria	320 to less than 10 kyr	Stratovolcano with central nested calderas formed of peralkaline rhyolitic (pantellerites) and trachytic ignimbrites and lava domes, with minor weakly Naalkaline basaltic lava flows and cinder cones.
Sicily Channel seamounts	Miocene to present	Several cones (Cimotoe, Tetide, Anfitrite, Graham, Senza Nome, Foestner, etc.) rising along NW-SE and N-S trending faults, formed of tholeiitic basalt, hawaiite and basanite.

Tab. 1.2 Schematic sketch of ages and composition in of sicilian volcano (from Peccerillo 2005).

Etna is an active stratovolcano. During the last 150 ka mainly lava flows were emplaced as a consequence of the formation of two stratovolcanoes: Trifoglietto (80–40 ka) and Mongibello (30 ka to Present). The most important of the five explosive phases which characterized the history of the volcano (Chester et al., 1987) occurred at the Ellittico eruptive centre (Coltelli et al., 2000), which 15 krs ago emplaced the *Biancavilla Formation*, benmoreitic in composition (De Rita et al., 1991).

Four main evolution stages have been distinguished for Mount Etna activity (Gillot et al., 1994; Branca et al., 2004). The first stage (580 to 225 ka) was characterised by emplacement of tholeiitic basalts, which were erupted over a wide area from the Iblean Plateau in the south to the Peloritani mountains in the north, and presently crop out as pillow-lavas, hyaloclastites and sills along the Ionian Sea coast north of Catania and along the south-western margin of the volcano (Corsaro & Cristofolini, 2000). Starting from about 220 ka, the volcanic activity concentrated in the Ionian coast and changed from tholeiitic to Na-alkaline (Branca et al., 2004). A number of central volcanoes (Ancient Alkaline Centres or Timpe Volcanoes) were constructed over a time span of about 100 ka (172 to 96 ka), and their remnants mainly crop out along the present-day margin of Etna. Successively, various cones (Tifoglietto, Cavigghiuni, Vavalaci etc.) making up the so-called Trifoglietto unit (Chester et al., 1985) were built up by effusive and explosive eruptions between about 80 to 60 ka (Gillot et al., 1994). Finally, the Mongibello stratovolcano was constructed between about 60 ka (80 ka according to Branca et al., 2004) to present. Older Mongibello activity built up the so-called Ellittico volcano, consisting of prevailing benmoreitic to trachytic lavas and pyroclastics, and was closed by a caldera collapse (at about 15 ka). Recent Mongibello activity (14 ka to present) has been characterised by dominant effusive eruptions and strombolian explosions, giving lava flows and scoria cones, which cover extensively the flanks of the Etna volcano. The Etna rocks have tholeiitic to Na-alkaline affinity, with a few products exhibiting a potassic alkaline tendency. Compositions range from basalt to hawaiite, mugearite, benmoreite and trachyte on the TAS diagram.

The Island of *Pantelleria* is a NW-SE elongated stratovolcano with two nested calderas (Fig. 1.5), built up by dominant peralkaline trachytes and rhyolites (pantellerites) and minor Na-transitional to mildly alkaline basalts.

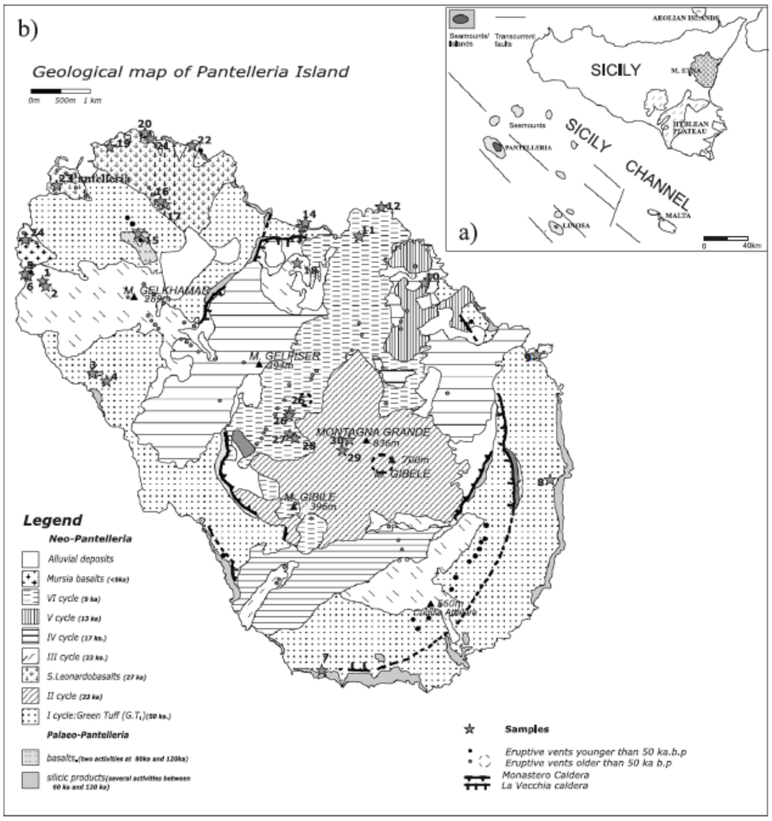

Fig 1.5 (a)Tectonic setting of the Sicily channel with location of volcanic occurrences.
(b) Pantelleria Volcano, geological and volcanological sketch map (from Avanzinelli et al., 2004).

The oldest dated rocks are 324 and 220 ka old, whereas the youngest dated activity on the island is about 4 ka-old (e.g. Civetta et al., 1984, 1988, 1998; Mahood & Hildreth,1986). Most of the volcanism at Pantelleria was explosive and emitted silicic peralkaline pyroclastic products and some lavas. Basaltic magmas have been erupted episodically (at 118, 83, 29 and less than 10 ka; Civetta et al., 1984, 1998; Mahood & Hildreth, 1986) by effusive and strombolian activity. Large explosive eruptions occurred at about 114 ka and 50 ka, and generated caldera collapses in the southeastern sector of the island (Orsi & Sheridan, 1984; Mahood & Hildreth, 1986). The younger collapse is associated with the deposition of the so-called Green Tuff, a complex pyroclastic trachytic to pantelleritic deposit, formed of ignimbrite, fall and surge beds (Orsi & Sheridan, 1984). Resurgence has taken place inside the younger caldera. Post-caldera silicic activity has occurred both inside and outside the caldera, whereas basaltic eruptions took place outside the calderas, in the north-western sector of the island. Based on the TAS diagram, the mafic volcanic rocks from Pantelleria are classified as basalt and hawaiite, whereas the silicic products fall in the trachyte and rhyolite fields. Mafic rocks show transitional to weakly alkaline petrochemical affinity (Civetta et al., 1984).

Aeolian arc

The Aeolian Islands archipelago is located offshore the eastern Sicily coastline. It consists of several stratovolcanoes forming seven main islands and several seamounts, which extend to the west and northeast of the emergent portion of the arc, around the Marsili basin (Fig. 1.6).

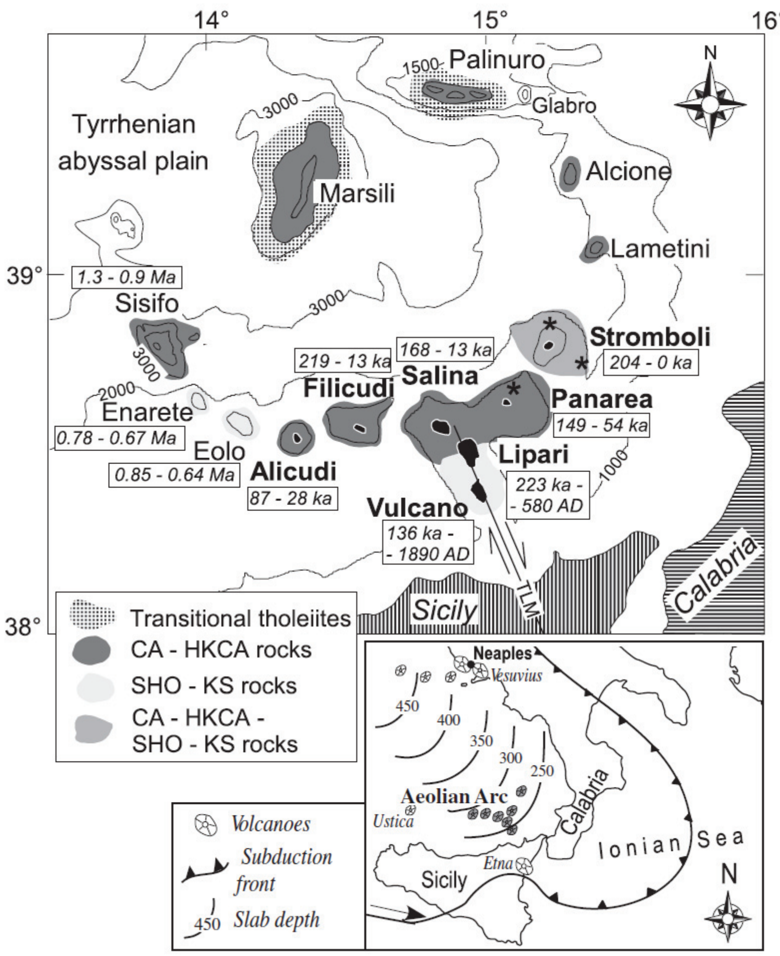

Fig. 1.6 Location of the Aeolian islands and seamounts with reported ranges of available radiometric ages and general composition of the rocks. TML: Tindari-Letojanni-Malta tectonic line. From Francalanci et al., 2007.

The volcanic activity exposed above the sea level took place entirely during the Quaternary, most probably from about 400 ka to the present. Rock compositions range from mafic to silicic, and show a calc-alkaline (CA), high-potassium calc-alkaline (HKCA) to shoshonitic (SHO) affinity (Fig. 1.7 Francalanci, 2007).

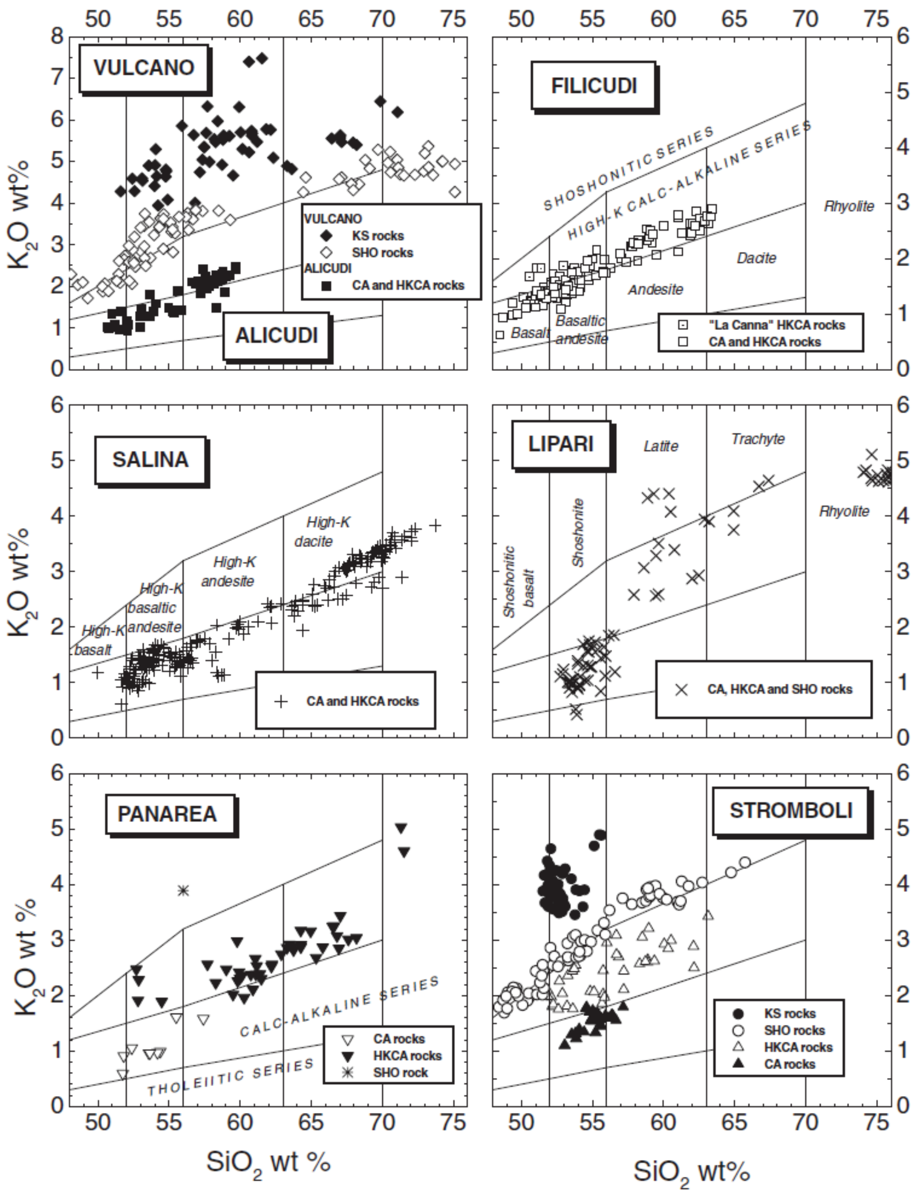

Fig. 1.7 K_2O versus SiO_2 classification diagram for the rocks of the Aeolian island arc (diagrams from Francalanci et al., 2007). CA—calc-alkaline series; HKCA—high-K alkaline series; SHO—shoshonitic series; KS—potassic series.

A few potassic alkaline rocks with a composition close to the Roman potassic series (KS) occur at Vulcano and Stromboli (e.g. Keller, 1982; Francalanci et al., 2004). Arc tholeiites have been dredged along some seamounts (Beccaluva et al., 1982). There are important variations of structural, volcanic and magmatic features along the arc. The Aeolian arc consists of three main sectors, each of which shows distinct magmatic, volcanic and structural features. The western sector includes the islands of Alicudi, Filicudi and

Salina, where the exposed volcanism developed along a W-E trending fault system, between approximately 0.4 Ma and 13 ka (Keller, 1980; Gillot, 1987). The volcanic islands active in the last 200 ka, located in the western part of the archipelago (De Rosa et al., 2003), are: Salina, Lipari and Vulcano. On the eastern section of the archipelago, volcanic activity occurred on the island of Panarea (submarine fumaroles and hot springs) and still persists on the island of Stromboli (mildly explosive strombolian volcanism). The activity, both effusive and explosive, mainly emplaced calcalkaline products with evolved compositions (from dacite to rhyolite), except for Stromboli volcano, where, at present, high-K to shoshonitic products are erupted both as lava flows and during the recurrent explosive phases (Armienti et al., 2007). Active volcanism is restricted to the central and eastern sectors. At Lipari, the last eruption occurred at about 580 AD, whereas at Vulcano it dates to 1888-1890 AD.

1.2.1 Tephrostratigraphy in the Mediterranean basin: a state of the art

A number of volcanoes in the Aegean and Italian volcanic provinces are known to have produced major eruptions which can be reliably recovered as discrete ash layers in deep-sea sediments of the central-eastern Mediterranean Sea, including the Aegean Sea and Marmara Sea (e.g., Pe-Piper & Piper, 2002, Margari et al., 2007). The Quaternary volcanic activity of the Italian Volcanic Provinces was concentrated west and northwest of the Calabrian Arc in the Tuscan, Roman, Campanian, Aeolian and Sicilian regions (e.g. Peccerillo, 2005). The Quaternary volcanic activity of the Aegean volcanic province was concentrated north of the Hellenic Arc on Methana and the islands of Milos, Santorini, Kos, Yali and Nisyros (e.g., Pe-Piper & Piper, 2002).

The first reliable medium-resolution marine tephrochronology was established by Keller et al. (1978) for the period beginning around 200 ky BP. Since then, systematic investigation of tephra distribution in the Mediterranean region (Keller et al., 1978; McCoy, 1981; Paterne et al., 1986, 1988), were extensively carried out either in lake deposits (e.g. Calanchi et al., 1998; Narcisi, 1996, Munno & Petrosino, 2004; Wülf et al., 2004), and in deep-sea sediments (e.g. Thunell et al. 1979, Vinci 1985, Vezzoli 1991, Calanchi et al. 1998, Narcisi and Vezzoli 1999, Siani et al. 2004). The nomenclature of "tephra zones", proposed by Keller et al. (1978) currently adopted by several researches, is made up with alpha-zone identifiers (V being the oldest, Z the youngest), and internal numerical tephra labels (W-1 being younger than W-3 etc.). For the Adriatic and Tyrrhenian records, the most significant popular works related to tephrostratigraphic reconstructions of the Pleistocene are those of Paterne et al. (1986, 1988). The authors labelled tephra layers with alphabetic letters for different potential volcanic sources (C for the Campanian volcanoes, E for the Aeolian volcanoes, Et for the Etna volcano, and V for the Somma–Vesuvius volcano) followed by progressive numbers pointing out the stratigraphic position of layers in time. Differently from the Keller's approach, those authors identified tephra not only by visual inspection but also by direct counting of volcanic glass abundance in sample collected from sedimentary records.

In Table 1.3 are listed the tephra layers with the potential volcanic sources and estimated ages, recognized in the last 200 kyr of central-eastern Mediterranean sediments (Keller et al. 1978 modified, Tab. 1.3).

Zone	Tephra layer code by Keller et al. 1978	Tephra layer code from papers published after Keller et al. (1978)	Tephra (marine and lacustrine archives)	Source area	Source	Estimated Age (ky)	References
Z (10 ky *Present*)			TM6	Somma-Vesuvius	Mercato	8,010±35 uncal. yr BP (^{14}C terr. Andronico et al. 1995); 8,154-9,691 (2σ) cal yr BP (Reimer et al. 2004); 9,620±480 varve cal. yr BP; 8,200 yr Oxygen-isotope stratigraphy (Paterne et al. 1988)	Wulf et al. 2007
			V1				Paterne et al. 1988
			TM5	Campi Flegrei	Agnano Monte Spina	4,100±400 yr BP ($^{40}Ar/^{39}Ar$ de Vita et al. 1999); 4,130±50 uncal. yr BP (Di Vito et al. 1999); 5390±270 varve yr (Wulf et al. 2007)	Wulf et al. 2007
	Z1		TM4	Somma-Vesuvius	Avellino	3,590±25 uncal. yr BP (^{14}C terr. Andronico et al. 1955); 3,551-4,158 (2σ) cal. yr BP (Reimer et al. 2004); 4,360 (^{14}C Santacroce et al. 2008); 4310±220 varve cal. Yr (Wulf et al. 2007)	Wulf et al. 2007
			TM3c		AP2	3,225±140 uncal. yr BP (^{14}C terr. Andronico et al. 1995); 3,136-3,735 (2σ) cal. yr BP (Reimer et al., 2004); 4150±210 varve yr (Wulf et al. 2007)	Wulf et al. 2007
			TM3b		AP3	2,710±60 uncal. yr BP (Andronico and Cioni 2002); 2,744-2,946 (2σ) cal. yr BP (Reimer et al., 2004); 4,020±200 varve yr (Wulf et al. 2007)	Wulf et al. 2007
	Z2			Santorini	Minoan	3370 yr (^{14}C Pichelr and Friederch 1976); 3565 cal yr (Hammer et al. 1987)	
			N3			2,9 - 3,5 cal. Yr (^{14}C with oxygen isotpe stratigraphy Asku et al. 2008)	Asku et al. 2008
		Z3		Turkey	Kolomvos	8-10	Mc Coy 1980,1981
		Z4				8-10	
		Z5				8-10	

Zone	Tephra layer code by Keller et al. 1978	Tephra layer code from papers published after Keller et al. (1978)	Tephra (marine and lacustrine archives)	Source area	Source	Estimated Age (ky)	References
Y (10-70 ky)			TM7a,b	Campi Flegrei	Agnano Pomici Principali	10,320±50 uncal. yr BP (^{14}C Di Vito et al. 1999), 11,972-12,385 (2σ) cal yr BP (Reimer et al. 2004); 9,200 yr Oxygen isotope stratigraphy (Paterne et al. 1986)	Wulf et al. 2007
			C1				Narcisi 1996
			L5				Paterne et al. 1986
	Y1		TM11	Etna	Biancavilla-Montalto ignimbrite	14,800 yr (^{14}C De Rita et al. 1991); 14,180±200 yr (^{14}C terr. Delibrias et al. 1986); 15,420±60, 15,050±70 yr (AMS ^{14}C Coltelli et al. 2000); 16,440±820 varve yr (Wulf et al. 2007)	Wulf et al. 2007; Siani et al. 2001; De rita et al. 1991; Vezzoli 1991; Calanchi et al. 1996
			Et1			14,18±0,2 kyr (^{14}C Delibrias et al. 1986)	Paterne et al. 1988
			490 cm			14,650 cal. yr (^{14}C Siani et al. 2004)	Siani et al. 2004
			TM8	Campi Flegrei	Neapolitan Yellow Tuff	14,900±400 yr BP ($^{40}Ar/^{39}Ar$ Deino et al. 2004); 12,100±170 uncal. yr BP (^{14}C Siani et al. 2001, 2004) after calibration at 2σ (13,582-14,669 cal yr BP (Reimer et al., 2004); 14,120±710 varve yr (Wulf et al. 2007); 12,300 yr Oxygen-isotope stratigraphy (Paterne et al. 1986)	Wulf et al. 2007
			L6				Narcisi 1996
			C2				Paterne et al.1986
			TM13	Somma-Vesuvius	Pomici di Base	18,300±150, 18,220±120 uncal yr BP (^{14}C Andronico et al. 1995 and Siani et al. 2004); 18,750±420-19,170±420 uncal. yr BP (^{14}C Bertagnini et al. 1998); 21,153-24,063 (2σ) cal yr BP (Reimer et al. 2004); 19,280±960 varve yr (Wulf et al. 2007)	Wulf et al. 2007
			L9			16250±130, 17050±40 (^{14}C Narcisi 1996)	Narcisi 1996
	Y2			Santorini	Cape Riva	18,050, 18,880 uncal. yr (^{14}C Picher and Friedrich 1976); 21,705±0.311 cal yr (Akrotiri, Eriksen et al. 1990); 22,300, 24,800 yr BP (after Lourens et al. 1996)	Wulf et al. 2002; Vinci 1985
			A1, A4, A9, G4				Asku et al. 2008
	Y3		TM15	Campanian province		26,9 kyr (Oxygen-isotope stratigraphy Paterne et al., 1988); 25,3±3 kyr (interpolation sapropel chronology Kraml, 1997); 30,67±0,23 (calibrate ^{14}C Di Vito et al. 2008); 23,93 varve yr (Wulf et al. 2004)	Wulf et al. 2007
			L10				Narcisi 1996
			SIMP1-e				Sulpizio et al. 2003
			C7				Paterne et al. 1988
			B2 (C45)/ A2 (C106) / S19				Munno & Petrosino 2004, 2007
	Y4			Santorini	Yali-C	30 kyr Oxygen-isotope stratigraphy (Federman and Carey 1980); 35 kyr ATS (Smith et al. 1996)	Vinci 1985
	Y5		TM18	Campi Flegrei	Campanian Ignimbrite	39,280±0,11 yr (K/Ar Cornette et al. 1983, $^{40}Ar/^{39}Ar$ De Vivo et al. 2001)	Wulf et al. 2004
			L12				Narcisi 1996
			B3 (C45)				Munno & Petrosino 2004
			1070-1075 cm				Wagner et al. 2007
			A2, A5, G1, G5			~ 35 kyr (oxygen isotope stratigraphy Asku et al., 2008)	Asku et al. 2008
			C-13		Citara Tuff (Ischia) or Campanin Ignimbrite	41,100±2,1 yr ($^{40}Ar/^{39}Ar$ Ton-That et al. 2001)	Ton-That et al. 2001; Paterne et al. 1986
			NIS	Aegean province	Nisyrios	29 cal. ky (Rehren 1988); 47,54 cal. ky (Limburg et Varekamp 1991); 46,8±5,69 cal. kyr (Margari et al. 2007)	Asku et al. 2008
	Y6			Pantelleria	Green Tuff	49,6 (Cornette et al. 1983); 45-50 (Mahood et Hildreth 1986)	Civetta et al. 1988, Cornette et al. 1983, Mahood & Hildreth 1986
	Y7		TM19	Campi Flegrei	M. Epomeo Green Tuff	55,4± 2,2 ky (K/Ar Gillot 1984); 50,1±1,3/55,8±1,8 kyr (K/Ar Vezzoli 1985); 55 ky (Poli et al. 1987); 55±3.5 kyr (K/Ar Vezzoli 1988); 55±2 kyr ($^{40}Ar/^{39}Ar$ Watts et al. 1996)	Wulf et al. 2004
			L14				Narcisi 1996
			C17				Paterne et al. 1988
			SAL 1,1				Lucchi et al. 2008
	Y8			Aeolian province		55 ky	

Zone	Tephra layer code by Keller et al. 1978	Tephra layer code from papers published after Keller et al. (1978)	Tephra (marine and lacustrine archives)	Source area	Source	Estimated Age (ky)	References
X (70-130 ky)	X1			Hellenic	Creta	70 ky (Keller et al. 1978); posterior to S3 (Vinci 1985); 71 ky Oxygen-isotope stratigraphy (Paterne et al. 1988)	Vinci 1985
			C (i) 8	Aeolina province			Paterne et al. 1988
		Y9	**TM21**		Petrazza Tuff (Str)	85,3±2/64,3±4,9 yr (Petrazza Hornig-Kjarsgaard et al. 1993; Gillot & Keller 1993); 73,5 yr (Astronomical age Kraml 1997); 74,54 varve yr (Wulf et al. 2004)	Wulf et al. 2004
			G 3				Asku et al. 2008
	X2			Campanian province	Ischia	70 ky	Vezzoli 1991
			C-22, cm 825			81 ky, 81,4 ky Oxygen-isotope stratigraphy (Paterne et al. 1985)	Paterne et al. 1985
			S13-14				Munno & Patrosino 2007
			TM22	Pantelleria	pre-GT	85,320 varve yr (Wulf et al. 2004); 77,10 ky Oxygen-isotope stratigraphy (Paterne et al. 1988); 79±4 kyr (Morche 1988)	Wulf et al. 2004
			P10				Paterne et al. 1988
			C-22	Roman province		89 ky; 87,000 (±7000) yr (Magri and Sadori 1999)	Paterne et al. 2008
			in **Magri and Sadori 1999**				Magri & Sadori 1999
	X3			Aeolina province	Salina	90 ky	
	X4			Etna		90 ky	
	X5		**TM24a,b**	Campanian province		97,770, 98,750 varve yr (Wulf et al. 2004)	Wulf et al. 2004
			SAL II				Lucchi et al. 2008
			C27	Roman province		103,500 yr prior to S4 (Paterne et al. 2008)	Paterne et al. 2008
			TAU1-b	Campanian province		105±2 kyr ($^{40}Ar/^{39}Ar$ Alllen et al. 1997)	Allen et al. 1997
	X6			Campanian province		107 ky	
			TN27(1)-(2)				Wulf et al. 2006
			S10, cm 975				Munno & Petrosino 2007
			SAL I				Lucchi et al. 2008
			SM1-2, SA			73±33 ky (uncorrected $^{40}Ar/^{39}Ar$ Marciano et al., 2008)	Marciano et al. 2008
			C-31/C-35	Roman province		107,6 ky, 121,500 yr (Paterne et al. 2008)	Paterne et al. 2008
W (130-165 ky)	W0		**P11**	Pantelleria		131 ky (Paterne et al. 08)	Paterne et al. 2008
	W1			Roman province	Vico	140 ky (Narcisi and Vezzoli 1999); 138±2 kyr/151±3 kyr (Carbognano and Sutri formation $^{40}Ar/^{39}Ar$, Perini et al. 2004)	Vezzoli 1991; Narcisi & Vezzoli 1999, Perini et al. 2004
			E-23	Aeolian province		143,400 yr (Paterne et al. 2008)	Paterne et al. 2008
			C-41	Roman comagmatic province	Somma-Vesuvio	145,100 yr (Paterne et al. 2008)	Paterne et al. 2008
			in **Vezzoli 1988**	Campi Flegrei	Monte Cotto/La Guardia - Castello di Ischia	147±3 and 140±3 kyr respectively (K/Ar Vezzoli 1988)	Vezzoli 1988
			C-42	Roman province	Vico-Vulsini	149 kyr (Paterne et al. 2008)	Paterne et al. 2008
			Et-3	Etna		149 kyr (Paterne et al. 2008)	Paterne et al. 2008
		W2		Santorini	Middle Pumice	<125 (prior to S5 Vinci 1985); 150 kyr (Keller et al. 1978)	Vinci 1985
		W3		Kos		161,3±1,1 kyr (Smith et al. 1996)	Vinci 1985
			P12	Pantellaria		164 kyr (Paterne et al. 2008)	Paterne et al. 2008
V (165-200 Ky)		**V0**		Pantellaria		170±21 kyr ($^{40}Ar/^{39}Ar$ Kraml 1997)	Scheld 1995
	V1			Santorini	Lower Pumice	170 kyr (Keller et al. 1978); within S6 (Vinci 1985)	Vinci 1985
	V2			Roman province		170 kyr (Keller et al. 1978)	
			E-25	Aeolian province		172 kyr (Paterne et al. 2008)	Paterne et al. 2008
			C-49	Roman/Campaian province		175,800 yr (Paterne et al. 2008)	Paterne et al. 2008
	V3			Kos		180 kyr (Keller et al. 1978)	
			C-50	Roman/Campaian province		182 kyr (Paterne et al. 2008)	Paterne et al. 2008
			C-51			183 kyr (Paterne et al. 2008)	Paterne et al. 2008
			P13	Pantelleria		192,500 yr (Paterne et al. 2008)	Paterne et al. 2008
			P14			193 kyr (Paterne et al. 2008)	Paterne et al. 2008
			C-55	Roman/Campaian province		193,400 yr (Paterne et al. 2008)	Paterne et al. 2008
			P-15	Pantelleria		197,400 yr (Paterne et al. 2008)	Paterne et al. 2008
			P-16			198 kyr (Paterne et al. 2008)	Paterne et al. 2008

Tab. 1.3 Tephrostratigraphy of the Central-Eastern Mediterranean deep-sea and lacustrine sediments <200 kyr; labels of tephra layers in the second column are from Keller et al., (1978); estimated ages of the tephras are based on their stratigraphic position in relation to sapropel layers, oxygen-isotope events, AMS ^{14}C and K/Ar-$^{40}Ar/^{39}Ar$ measurements.

1.3 Methodological approaches to tephrostratigraphy

Geochemical investigation of individual tephra layers relies on chemical analysis of juvenile components of deposits related to individual eruptional events such as the vitreous fraction glass shards, pumice fragments, scoria and or various pheno-crystal phases (e.g. feldspars, pyroxenes or oxides). These deposits frequently include reworked material such as older lithic fragments or material from previous eruptions and therefore, with increasing distance from the source, become more prone to contamination by other detritical material. Thus, a prerequisite for reliable correlations of tephra layers to land deposits clearly attributed to different volcanic eruptions, is that the geochemical composition of juvenile materials remain unaltered by diagenetic processes and/or laboratory analytical procedures (Pollard et al., 2003). Glasses, particularly when in form of small shards with a high surface to volume ratios, although prone to chemical alteration in both acidic and basic environments, are generally employed for tephrostratigraphy investigations of late Quaternary deposits.

Extraction of glass shards from sediments and cleaning procedures

Six main methods are generally applied for separation of tephra shards:

- grain-size separation;
- magnetic separation (using the *Franz* Isodynamic Magnetic Separator);
- separation with jolt table;
- gravimetric separation with heavy liquids;
- and the common separation *handpicking*;

with handpicking at binocular microscope considered the most efficient. Often, after any kind of separation, it is necessary a scrupulous washing of glasses minimizing breakage and improving separation of fine ash coatings. Washing is performed generally in distilled water and acetic acid to remove carbonate incrustations. However, a significant body of evidence suggests a high potential for glasses to be significantly affected by chemical alteration, depending upon the ratio between surface area and volume of the shards, molecular structure of glasses, solution pH, reaction kinetics, and temperature (Pollard et al., 2003).

Glasses are subjects to two main kinds of solution attack. In mildly basic to acidic environments (pH<9), the predominant mechanism is *ionic exchange* of cations from the 'terminal structure' of alkali ions (i.e. those associated with non-bridging oxygen sites) at the glass surface with hydronium ions (H_3O^+) from solution. Lost of cations results in the formation of a leached Si gel layer. In more basic media (pH>9), the predominant process appears related to *network dissolution*, in which the hydroxyl ions in solution disrupt the siloxane bonds in the glass surface, ultimately resulting in dissolution of glasses. The resulting non-bridging oxygen terminals are capable of dissociating other water molecules producing excess hydroxyls which, depending on the environment, may accumulate in the corrosion layer, increasing the pH and accelerating the dissolution of the network. This process also results in the stripping out of cations as the network degrades. Once the local pH has risen to greater than 9, the Si network begins to break up and silicon is removed into solution as $Si(OH)_4$, eventually resulting in complete dissolution of the glass Si network and, therefore, sample loss. The stability of vitreous material in any given environment appears to be primarily a function of chemical composition of the glass, with the proportions of Si and Al content determining molecular structure and, therefore, durability. A recent study (Pollard et al., 2003) suggests that while some tephras are relatively stable (although still potentially prone to chemical attack), many show a high potential for solubility. If the altered surface of shards is not removed by polishing the samples, then uncertainties will arise at the stage of geochemical correlation of the analysed tephras. The problem related to potential alteration of the chemical signature of the tephra layers after laboratory treatment is considered particularly significant for micro-tephras. It is vital therefore, that the less-corrosive procedures are employed during tephra extraction. An appropriate strategy to avoid alteration of the studied tephras was adopted in this research work.

Analytical procedures

Though adoption of appropriate protocols for glass shards cleaning represents a sensitive point for a correct interpretation of final chemical analyses, a suitable choice of the analytical methods for major and trace element measurements is crucial as well.

The main analytical techniques generally considered to measure concentrations of major and trace elements in glass shards are:

- **XRF** (**X**-**R**ay **F**luorescence),
- **INAA** (**I**nstrumental **N**eutron **A**ctivation **A**nalysis),
- **AAS** (**A**tomic **A**bsorption **S**pectrometry),

- **ICP-AES/ICP-MS** (**I**nductively **C**oupled **P**lasma-**A**tomic **E**mission **S**pectrometry and **M**ass **S**pectrometry respectively),
- **EPMA EDS/WDS** (**E**lectron **P**robe **M**icro **A**nalyse with **E**nergy **D**ispersion and with **W**avelength **D**ispersion respectively),
- **LA_ICP-MS (L**aser **A**blation_**I**nductively **C**oupled **P**lasma-**M**ass **S**pectrometry).

The choice of the most appropriate analytical method has to consider: i) the small dimensions of samples, ii) the irregular shapes of glass shards and iii) their potential inhomogeneity. In general methods for analysis of tephra deposits typically require the separation of relatively large volumes of material (generally between 0.5 and a few grams). In that case, analytical methods include "dry" X-ray analyses, or "wet" and "destructive" analyses by inductively coupled plasma spectrometry (ICP-AES/MS) following "acid digestion" of samples (by mixtures of HF, HNO_3 and/or HCl acids). For proximal tephra deposits, separation of the required amounts of juvenile glasses or mineral phases can be readily achieved using magnetic or density methods, followed by visual inspection. However, from fine-grained distal deposits or limited size samples such as deep-sea or ice cores for example, the separation of such relatively large volumes of material is difficult, if not impossible. Such a kind of bulk analysis related to measurements of solutions obtained by chemical attacks of a number of glass shards does not allow investigations on the potential tephrostratigraphy of single shards. This limitation is avoided by application of combined EPMA and LA-ICP-MS "micro-destructive" measurements. Both these techniques need of a small amount of material (few glass shards preventively cleaned) mounted on resin beads. Although EDS is commonly employed for X-ray microanalysis, there are undeniable benefits in using a wavelength dispersion spectrometer to provide increased sensitivity and resolution (in terms of peaks separation). Using EDS, all of the energies of the characteristic X-rays incident on the detector are measured simultaneously and data acquisition is therefore very rapid on the entire spectrum. However, the resolution of an EDS detector is considerably worse than that of a WDS spectrometer. The WDS spectrometer can acquire the high count rate of X-rays produced at high beam currents, because it measures a single wavelength at a time. Moreover the resolution of the EDS detector in a number of situations is limited by overlap of adjacent peaks. The increased resolution of WDS allows to easily identify peaks with absolute confidence. Last, but not least, WDS can deal with much higher X-ray intensities and therefore achieve detection limits significantly lower than EDS, and necessary for trace elements analysis. In practice, the techniques of EDS and WDS are complementary. The speed of EDS is used for the initial survey of a sample, and the resolution and dynamic range of WDS is used to check for overlaps and increase sensitivity. Combination of WD and ED spectra represents to date a routine and suitable approach.

While electron probe x-ray microanalyses techniques is especially used to collect major elements analyses, IC plasma-mass spectrometry generally represents the best techniques for analysis of trace elements glass shards. The ICP-MS has better sensitivity than ICP-AES, and 3/4 order of magnitude lower detection limits. If ICP-MS generally works with solutions introduced and nebulised in a spray chamber/torch area, vaporisation of solids by electro-thermal devices represents a suitable alternative for sample introduction in the detection area of the MS. The ability of high power lasers to produce ablation of micro-particulate material makes it an excellent choice for micro-sample analysis such as glass shards. Thus, the LA-ICP-MS analytical method combines micro-destructivity with the powerful capacity of analyzing a great number of trace and REE elements with high sensitivity in a very short time.

2 Material: the studied sedimentary records

2.1 Geographical distribution of the studied cores

This research is based on the study of three deep sea sedimentary cores (KC01B, MD01_2474G and ODP Leg 160 Site 963A) located in the central-eastern Mediterranean area (Fig.2.1).

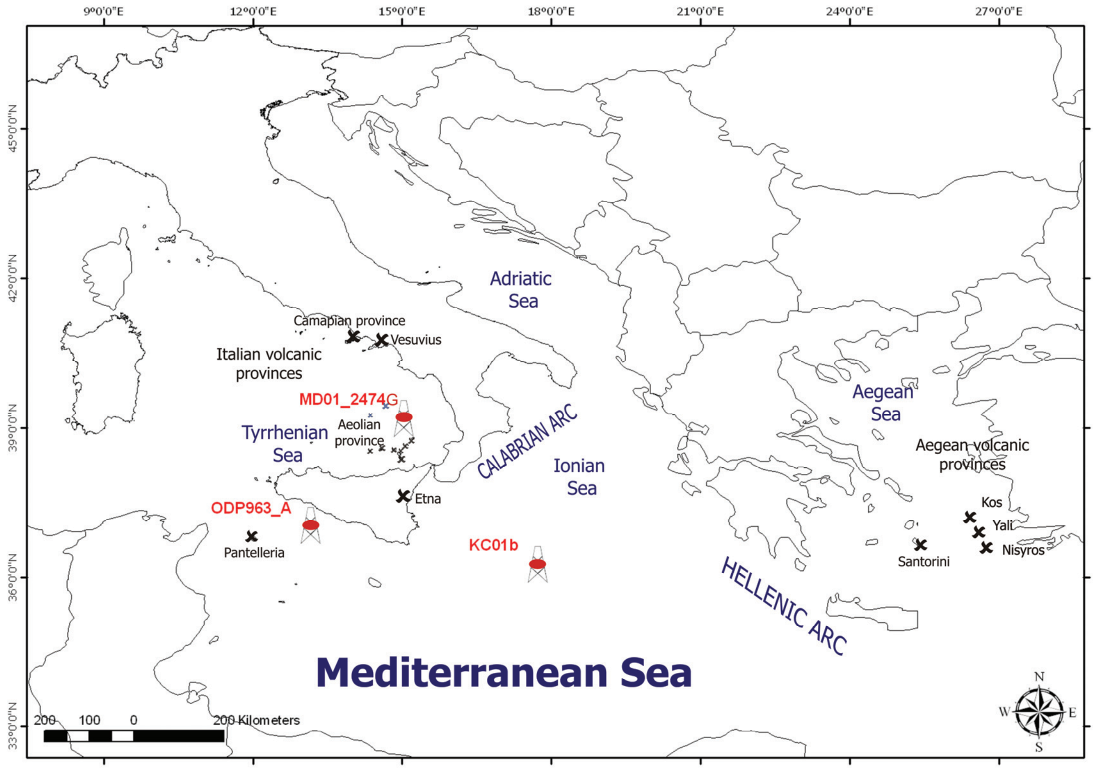

Fig. 2.1 Location map of the studied cores. The principal Quaternary volcanoes of the Italian and Aegean provinces are reported (dark crosses).

Geographical coordinates, depths and details of the collected cores are reported in Table 2.1.

Core	Latitude	Longitude	Depth b.s.l. (m)	Total core length (m)	Cruise	Area
KC01B	36°15.2'	17°44.3'	3.643	37	Mast-1, 1991	Pisano Plateau
MD01_2474G	39°10.44'	15°2.72'	2.131	15	Marion Dufresne, 2001	N-Stromboli Canyon
ODP Leg 160, Site 963A	37°01.938'	13°10.896'	481	199	ODP Leg 160, 1995	Sicily Channel

Tab. 2.1 Details of the studied cores in terms of geographical coordinates, depths, total core length, cruise.

The MD01_2474G and ODP Leg 160 Site 963A cores are located close to two main districts of Quaternary volcanic activity: the Aeolian arc and Pantelleria island, respectively.

The KC01B core is located in the central Mediterranean representing a key site to record the products of Italian volcanism during the past 200 kyr due to the prevalent NW direction of wind patterns of the basin.

For each core a high-resolution age model is available. The age model for the MD01_2474G is presented in this research work while for the other two records high-resolution dating is reported to previously published papers (e.g. Dekkers et al., 1994; Van Santvoort et al., 1997; Rossignol-Strick & Paterne, 1999; Lourens, 2004; Sprovieri et al., 2006; Incarbona et al., 2008). The three sedimentary cores overlap for a 20% of their time thus offering the opportunity to reliably construct a composite record for the last 200 kyr.

2.2 Nomenclature adopted for labelling tephra layers

The nomenclature adopted to label tephra layers collected from the core KC01B considers the nomenclature adopted by Lourens (2004), while for core MD01_2474G and ODP Leg 160 Site 963A labelling refers to the stratigraphic position of the layers in the succession starting from the youngest level and using consecutive alphanumeric codes. For the thickest tephra layers a number of samples from the stratigraphic intervals were collected and identified by consecutive letters. Greek letters were used to identify five tephra layers along core KC01B previously not recognised.

2.3 Description of the cores

2.3.1 The KC01B Core

The studied sediments are fine-grained, nannofossil-rich and contain sapropels, tephra layers, and silt layers. Color reflectance measurements of KC01B reported by Lourens (2004) are shown in Fig. 1a and 1b. Sapropels, tephra layers, and silt layers are all marked by low color reflectance. A total of 33 tephras were recognised and labelled by Lourens (2004) [I1–I33, (Tab. 2.2)]. Sampling of the core was carried out at the Department of Earth Sciences (Utrecht University) in march 2007.

Tephra layers of KC01B, KC01 and ODP Leg 160, Site 964			
	KC01B	KC01	ODP 964
Tephra	Level [a] m	Level [a] ccd	Level [a] ccd
I1	1.275	2.350	1.283
I2	3.370	4.505	2.465
I3	3.835	4.950	2.706
I4	4.930	6.245	3.972
I5	5.430	6.800	4.215
I6	6.240	7.910	4.965
I7	6.840	8.930	5.675
I8	7.490	9.710	6.324
I9	8.205	10.520	6.932
I10	10.160	12.410	8.592
I11	10.760		9.247
I12	11.010		9.439
I13	11.410	13.090	9.825
I14	11.690	13.420	10.210
I15	11.930	13.590	10.576
I16	12.720	14.335	11.385
I17	14.035	15.485	12.849
I18	14.255	15.685	13.099
I19	14.975	16.335	13.889
I20	16.540	17.845	15.449
I21	17.715	18.955	16.950
I22	18.125	19.360	17.443
I23	19.645	20.900	19.456
I24	20.285	21.510	20.014
I25	20.425	21.670	20.206
I26	20.675	21.840	20.36
I27	21.585	22.745	21.552
I28	23.285	24.175	23.514
I29	24.005	24.885	24.264
I30	24.505	25.500	24.822
I31	34.865		35.676
I32	35.240		36.080
I33	36.020		36.666

a) Levels in meters refer to the modified piston depths of KC01B and corrected composite depth of ODP Leg 160, Site 964 as used in Lourens 2004.

Tab. 2.2 Tephra layers and chronology of KC01B, KC01 and ODP Leg 160, Site 964 according to Lourens, (2004).

The previous reported tephra layers were re-sampled and five new ones (I1α, I1β, I10α, I10β and I32α) were identified and sampled by visual inspection of the core (Tab. 2.3 and 2.4).

KC01 B					
Level [a], m	Tephra [b]	Tephra nomenclature adopted in this study	Level [a], m	Tephra [b]	Tephra nomenclature adopted in this study
1,26	I1	I 1	14	I17	I 17
1,51	?	I 1 α	14	I18	I 18
1,57	?	I 1 β	15	I19	I 19
3,38	I2	I 2	17	I20	I 20
3,82	I3	I 3	18	I21	I 21
4,93	I4	I 4	18	I22	I 22
5,42	I5	I 5	20	I23	I 23
6,25	I6	I 6	20	I24	I 24
6,83	I7	I 7	20	I25	I 25
7,47 7,48 7,49	I8	I 8 a,b,c	21 21 21	I26	I 26 a,b,c
8,19 8,22 8,25	I9	I 9 a,b,c	22	I27	I 27
10,17	I10	I 10	23	I28	I 28
10,28	?	I 10 α	24	I29	I 29
10,72	?	I 10 β	25	I30	I 30
10,75	I11	I 11	35	I32	I 32
10,99	I12	I 12	35	?	I 32 α
11,43	I13	I 13	36	I33	I 33
11,70 11,72 11,73	I14	I 14 a,b,c			
11,93	I15	I 15			
12,72	I16	I 16			

[a] Levels in meters refer to the modified piston depths of KC01B (*Lourens, 2004*).

[b] Tephra label from *Lourens 2004*.

Tab. 2.3 Tephra layers recovered along the KC01B sedimentary core; in yellow the tephra layers studied in this PhD thesis.

Core	Tephra layer	Tickness (cm)	Sample	Volcanic constituents
KC01B	**I1**	<1		Black scoria, poorly vesiculated light grey micropumices with spherical vesicles, rare glass shards (Pl, cpx)
	I3	<1		Micropumices, spherical vesicles, tubular micropumice and glass shards (Pl, cpx and Bt)
	I9	6,5	I9a I9b I9c	Spherical vesicles, tubular micropumice and glass shards (Pl, Kf and Bt). Elongate and platy glass shards and blocky micropumices (Au, Pl, Kf and Bt)

Tab. 2.4 Lithological characteristics of tephras sampled in this study.

2.3.2 The MD01_2474G Core

Sedimentary core MD01_2474G (Lat. 39°10’44', Long. 15°02’72”, 2131 m water depth) was recovered in the southern Tyrrhenian sea during Marion Dufresne cruise 2001 (Fig. 2.2).

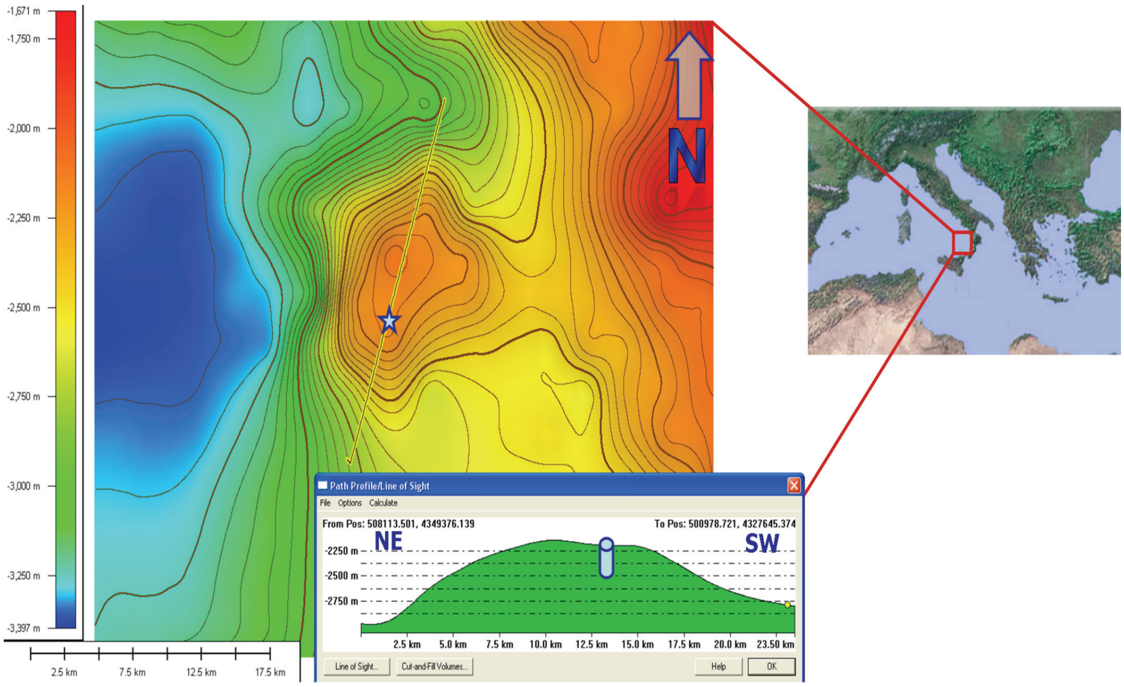

Fig. 2.2 Location map of core MD01_2474G. Bathymetric details with NE-SW path profile.

A detailed paleomagnetic and rock-magnetic study was carried out at the paleomagnetic laboratory of the LSCE at Gif sur Yivette (France) on U-channels collected from the 10 sections (total 14. meters) of the core. By using a cryogenic magnetometer natural remanent magnetization (NRM) as well as artificial magnetizations such as the isothermal (IRM) and the anhysteretic (ARM) remanence with a resolution of 1 cm (Appendix A). Were measured initially the choice of the tephra samples has been done on the basis of evident peaks of the ARM (from 400 to 1100 ARM, see Apppendix A), but then an accurate work to the binocular microscope allowed a definitive selection of the tephra layers. The paleomagnetic results indicate that the core was emplaced during the Brunhes Chron (last 780 kyr), but no geomagnetic excursion was identified throughout the core. By normalizing the NRM for concentration related parameters ARM and IRM, it is possible to reconstruct the relative paleointensity of the Earth magnetic field and the obtained results from the MD01_2474G core were compared with the reference curve for the last 70 kyr (NAPIS-75; Laj et al., 2000). On the base of these results we focused the investigations on the uppermost 6 sections (9 m) of the core and all the major peaks identified on the ARM profile were sampled from the U-channel as potential tephra layers (Tab. 2.5). A direct microscope analysis of the collected samples allowed a more appropriate confirmation of the presence of volcanic minerals/pumices/scoria. A total of 40 samples were collected from the core and picked in order to collect shards and/or pumices for geochemical analysis (Tab. 2.6).

MD01_2474G

Level [a], m	Tephra nomenclature adopted in this study	Level [a], m	Tephra nomenclature adopted in this study
0,08 0,09	MD1 a,b	3,56	MD16
0,19 0,20 0,21 0,22 0,23	MD2 a,b,c,d,e	3,61	MD17
0,51 0,53 0,54	MD3 a,b,c	4,0 4,1	MD18 a,b
0,61 0,62 0,63 0,64	MD4 a,b,c,d	4,1	MD19
0,66 0,67 0,68 0,69 0,70	MD5 a,b,c,d,e	4,3	MD20
1,1	MD6	4,4	MD21
1,2	MD7	4,50 4,52 4,54 4,57	MD22 a,b,c,d
1,18 1,19	MD8 a,b	4,6	MD23
1,30 1,31	MD9 a,b	4,96 4,97 4,98	MD24 a,b,c
1,74 1,75 1,76	MD10 a,b,c	5,1	MD25
1,86	MD11	5,3	MD26
2,06	MD12	5,58 5,59	MD27 a,b
2,30 2,31 2,33	MD13 a,b,c	7,01 7,06 7,11	MD28 a,b,c
2,60 2,61 2,62	MD14 a,b,c	7,2	MD29
3,42 3,47 3,52	MD15 a,b,c	7,3	MD30
		7,36	MD31
		7,41	MD32
		7,6	MD33
		7,8	MD34
		8,1	MD35
		8,11 8,12 8,13	MD36 a,b,c
		8,2	MD37
		8,3	MD38
		8,55 8,58	MD39 a,b
		8,8	MD40

[a] Levels in metres refer to the absolute piston depths of MD01_2474G.

Tab. 2.5 Tephra layers recovered along the MD01_2474G sedimentary core; in yellow tephra layers studied in this PhD thesis.

Core	Tephra layer	Tickness (cm)	Sample	Volcanic constituents
MD01_2474G	MD3	3	MD-3 a	Dark scoria, brown elongate glass shards (Kf and px)
			MD-3 b	Dark scoria, brown elongate and bubbly altered glass shards (Kf and px)
			MD-3 c	Dark vesicular scoria, brown curvy glass shards with tubular vesicles, rare light pumice
	MD10	3	MD-10 a	Rare dark scoria, rare light pumice, light vesicular glass shards (Kf)
			MD-10 b	Dark scoria, light yellow vesicular pumice, rare brown vesicular glass shards
			MD-10 c	Dark scoria, rare light pumice (Kf,px)
	MD11	1		Dark vesicular scoria, rare light pumice, brown elongate vesicular glass shards
	MD14	2	MD-14 a	Rare dark vesicular scoria, rare light pumice, rare light-beige vesicular glass shards (Kf)
			MD-14 b	Dark scoria, rare light pumice, rare brown glass shards
			MD-14 c	Rare dark scoria, rare light and brown vesicular glass shards
	MD15	10,8	MD-15 a	Dark scoria, rare light pumice, rare light-brown glass shards (Kf, px)
			MD-15 b	Dark scoria, beige vesicular pumice, rare light-brown glass shards
			MD-15 c	Dark scoria, rare light pumice, light-brown elongate and vesicular glass shards (Kf, px)
	MD18	5	MD-18 a	Dark scoria, rare light pumice, brown glass shards (Kf, px)
			MD-18 b	Dark vesicular scoria, light and bronw vesicular glass shards (Kf, px, bt)
	MD22	8,3	MD-22 a	Dark dense scoria, brown glass shards and light elongate pumiceous shards (Kf, px)
			MD-22 b	Dark dense scoria, brown vesicular glass shards and light elongate pumiceous shards (Kf, px)
			MD-22 c	Dark dense scoria, brown glass shards and light elongate pumiceous shards (Kf)
			MD-22 d	Dark dense scoria, brown glass shards and light elongate pumiceous shards (Kf, px)
	MD27	2	MD-27 a	Dense dark scoria, rare light and brown elongate glass shards (Kf, px)
			MD-27 b	Dense dark scoria, rare altered pumice, rare brown glass shards (Kf)
	MD28	11	MD-28 a	Light bubble-wall juction shards with strainght and linear ribs
			MD-28 b	Light bubble-wall juction shards with strainght and linear ribs
			MD-28 c	Light bubble-wall juction shards with strainght and linear ribs
	MD33	1		Dense scoria, light pumice, rare beige fragmented glass shards (Kf, px)
	MD35	1		Rare light pumice, light leongate and vesicular glass shards (Kf)

Tab. 2.6 Lithological characteristics of tephra sampled levels studied.

2.3.3 The ODP Leg 160, Site 963A Core

The ODP Site 963, Hole A, is located in the Sicily Channel (central Mediterranean), between the Adventure Bank to the northwest and the Gela basin to the southeast (Sicily Channel) (37°02.148′ N, 13°10.686′ E; 470.5 m below sea level and legth 199.4 m) (Fig.2.3).

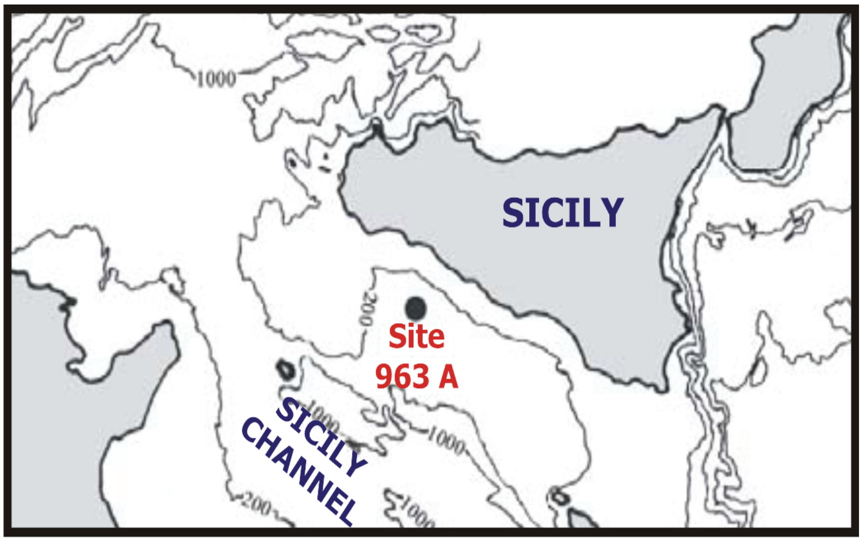

Fig. 2. 3 Bathymetric map of the Sicily Strait showing core location of ODP Leg 160, Site 963A.

Sediment of the ODP Leg 160 Site 963 A are generally olive to grey nannofossil rich clays, with disseminated pyrite and ash layers. No lithologic evidence of sapropels, turbidites or resedimented layers is present, even if a millimetric quartz sand horizon occurs in section 5 of core 3H (Emeis et al., 1996). A detailed description of the core is reported in Emeis et al. (1996).

The tephra layers interbedded within the hemipelagic deposits were identified by visual inspection (Appendix E) of the core. In this study a total of six tephra layers were analysed: ODP3/5-1, ODP6/3-2, ODP6/3-3, ODP6/3-4, ODP8/1-5 and ODP8/3-6 (Tab. 2.7 and 2.8).

ODP Leg 160, Site 963A		
Core	Level [a], mbsf	Tephra nomenclature adopted in this study
Site 963A 3H-5	20,8 20,9	ODP3/5-1 a,b
Site 963A 6H-3	47,5 47,5	ODP6/3-2 a,b
	47,6 47,6 47,6 47,6 47,7 47,7 47,7 47,7	ODP6/3-3 a,b,c
	47,8 47,8 47,9 47,9 47,9 48,0	ODP6/4 a,b,c,d,e,f,g
Site 963A 8H-1	63,8	ODP8/1-5
Site 963A 8H-3	66,6	ODP8/3-6

[a] Levels in meters refer to the depth below sea floor of ODP Leg 160, Site 963A.

Tab. 2. 7 Tephra layers recovered along the ODP Leg 160, Site963A; in yellow the tephra layers studied in this PhD thesis.

Core	Tephra layer	Tickness (cm)	Sample	Volcanic constituents
ODP Leg 160, Site 963A 3H-5	**ODP3/5-1**	4	ODP3/5-1 a	Light grey vesicular glass shards and rare dark scoria (Kf)
			ODP3/5-1 b	Light grey vesicular glass shards and rare dark scoria (Kf)
ODP Leg 160, Site 963A 6H-3	**ODP6/3-2**	4	ODP6/3-2 a	Rare dark scoria , rare yellow vesicular glass shards (Kf, px)
			ODP6/3-2 b	Rare dark scoria , rare yellow vesicular glass shards (Kf, px)
	ODP6/3-3	18	ODP6/3-3 a	Rare dark scoria, light pumice with tubular vesicles, brown vesicular glass shards (Kf)
			ODP6/3-3 c	Rare dark scoria, light pumice with tubular vesicles, brown vesicular glass shards (Kf)
	ODP6/3-4	26	ODP6/3-4 b	Rare dark scoria, light pumice with tubular vesicles, rare yellow vesicular glass shards (Kf)
			ODP6/3-4 c	Rare dark scoria, light pumice with tubular vesicles, rare yellow vesicular glass shards (Kf)
			ODP6/3-4 d	Rare dark scoria, light pumice with tubular vesicles, rare yellow vesicular glass shards (Kf)
			ODP6/3-4 e	Rare dark scoria, light pumice with tubular vesicles, elongate white vesicular glass shards (Kf)
			ODP6/3-4 f	Rare dark scoria, light pumice with tubular vesicles, elongate white vesicular glass shards (Kf)
			ODP6/3-4 g	Rare dark scoria, light pumice with tubular vesicles, elongate white vesicular glass shards (Kf)
ODP Leg 160, Site 963A 8H-1	**ODP8/1-5**	2		Pumice, with tubular vesicles, grey vesicular glass shards (kf, cpx)
ODP Leg 160, Site 963A 8H-3	**ODP8/3-6**	2		Pumice, with tubular vesicles, abundant grey vesicular glass shards (kf, cpx)

Tab. 2.8 Lithological characteristics of tephra sampled levels studied.

2.4 Tephras studied in this work

In Fig. 2.4 the simplified core logs is reported.

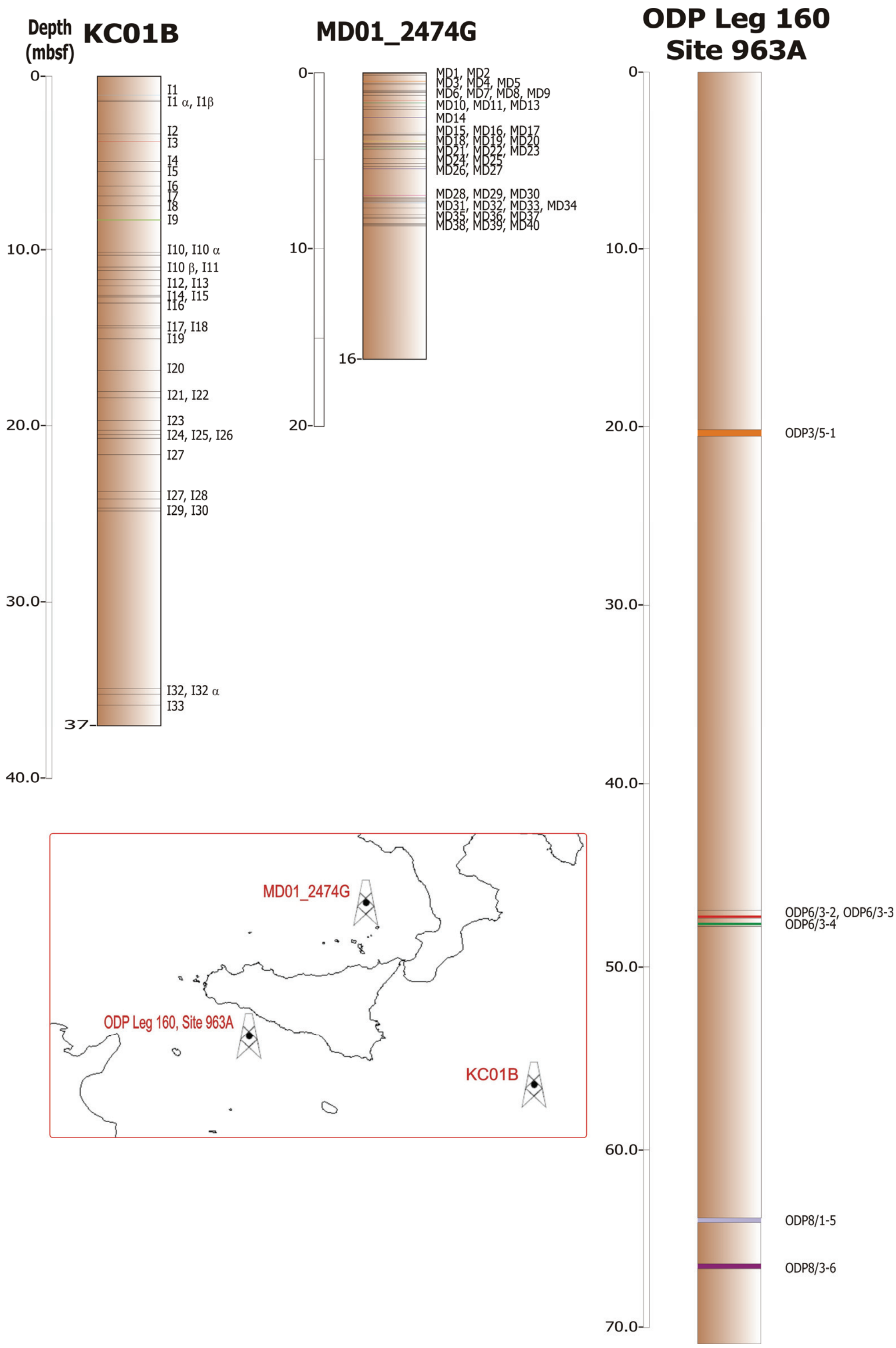

Fig. 2.4 Stratigraphic position of the studied tephras along the three records.

3 Analytical methods

3.1 Chemical analysis of tephra samples

Tephra samples consist of well-preserved pumice, scoria and glass shards. Tephra layers not visible by naked eye in the core sediments (cryptotephras) were identified by peaks of abundance of glass fragments above the background in the whole detritic material coarser than 63 μm. Each sample was observed under binocular microscope for lithological description (Tab. 2.4, 2.6, 2.8) and juvenile materials hand-picked for chemical analyses. A number of 10 to 30 shards were mounted on epoxy resin in 2.5 cm-diameter × 1.0 cm-thick slides and suitably polished. Tab. 3.1 shows the total number of tephra samples collected for chemical analysis from each sedimentary core along with the total number of points analysed on the single shards.

Tephra layers have been labelled following a progressive numbering from the younger to the older are along the studied cores. The number is preceded by MD (Marion Dufresne) for core MD01_2474G, I (Ionian Sea) for core KC01B and ODP (Ocean Drilling Project) for ODP Leg 160 Site 963A.

A total of twenty tephras were analysed from the three cores (3 tephras from core KC01B, 11 tephras from core MD01_2474G and 6 tephras from ODP Leg 160 Site 963A) and only those containing fresh juvenile material (pumices, scoriae and glass shards) were processed and analysed. The primary origin of the studied tephras was assessed by the peak abundance of the glass fraction above the lithic and crystal content; and the recognition of chemical glass populations from *n* chemical analyses (≥ 10 points).

Core	Tephra sample	Volcanic material analysed	EDS	WDS	(LA)-ICP_MS
KC01B	I1	GS		11	11
	I3	GS		15	9
	I9 c	GS		10	9
MD01_2474G	MD3 c	GS		7	
	MD10 c	GS		9	
	MD14 b	Sc		10	
	MD15 a	GS/Sc		8	
	MD15 b	GS		11	18
	MD15 c	GS		5	
	MD18 a	GS		6	6
	MD18 b	Sc		4	
	MD22 a	GS		10	
	MD22 b	GS/Sc		14	
	MD22 c	GS/Sc		15	19
	MD22 d	GS		9	7
	MD27 a	Sc		8	7
	MD27 b	GS/Sc		16	23
	MD28 a	GS		4	
	MD28 b	GS/P		19	15
	MD28 c	GS		17	
	MD33	GS/P		16	10
	MD35	GS		12	11
ODP Leg 160, Site 963A 3H-5	ODP3/5-1 a	GS		8	1
	ODP3/5-1 b	GS		8	8
ODP Leg 160, Site 963A 6H-3	ODP6/3-2 a	GS		10	10
	ODP6/3-2 b	GS		9	4
	ODP6/3-3 a	GS		11	9
	ODP6/3-3 b	GS		15	5
	ODP6/3-4 b	GS		10	
	ODP6/3-4 d	GS		9	
	ODP6/3-4 e	GS		8	
	ODP6/3-4 f	GS		8	
	ODP6/3-4 g	GS		11	
ODP Leg 160, Site 963A 8H-1	ODP8/1-5	GS	13		5
ODP Leg 160, Site 963A 8H-3	ODP8/3-6	GS	10		8

Tab. 3.1 Synopsis of the tephra samples analysed from the KC01B, MD01_2474G and ODP 160, Site 963A cores.

3.1.1 Analysis of major elements (EDS/WDS)

Major elements analysis of micro-pumices/scoria and glass shards from the tephra layers of KC01B, MD01_2474G and ODP 160 Site 963A cores 3H and 6H, were performed at the Istituto di Geologia Ambientale e Geoingegneria (CNR, Rome, Italy) with a Cameca SX50 electron microprobe equipped with five *wavelength-dispersive spectrometers*, using 15 kV accelerating voltage, 15 nA beam current, 10–15 μm beam size, and 20 s counting for peaks and 10 s for backgrounds. Instrumental calibration was done using the following standards: Jadeite for Na, Periclase for Mg, Wollastonite for Si and Ca, Rutile for Ti, Corundum for Al, Magnetite for Fe, metallic manganese for Mn, Orthoclase for K, Sylvite for Cl, Barite for S and F-phlogopite for F. A conversion from X-ray counts to oxide weight percentages (wt%) was obtained by PAP data reduction method (Pouchou & Pichoir, 1985).

Tephra layers (pumice fragments and glass shards) from Site 963 A-core 8H were analyzed by a *SEM* JEOL JSM 5310 (15 kV, ZAF Correction Routine) with *EDS* at CISAG (Centro Interdipartimentale di Servizio per Analisi Geomineralogiche) at the University of Naples Federico II. Instrument calibration was based on international mineral and glass standards.

All results of chemical analyses were recalculated to 100% on an anhydrous basis, and individual analyses with total oxide sums lower than 90 wt.% were excluded.

3.1.2 Analysis of minor and trace elements (LA-ICP-MS)

Trace element signature of individual micro-pumices/scoria and glass shards from the tephra collected throughout the KC01B, MD01_2474G and ODP 160 Site 963 A cores, were determined by laser ablation LA-ICP_MS at the I.G.G.-CNR (Pavia, Italy) laboratory. The adopted instrument combines a Nd:YAG *laser* source (Brilliant, Quantel) operating at 266 nm, and a quadrupole *ICP-MS* (Drc-e, Perkin Elmer). Analyses were carried out on spots 15/50 μm in diameter and using NIST SRM 610, BCR 2 and ^{29}Si as external and internal standards, respectively. These analytical conditions ensures an accuracy better than 20% with an associated detection limit, for the selected elements, is lower than 1 ppm.

3.2 Stable isotopes analysis

Oxygen and carbon isotope measurement on samples of MD01_2474G core were carried out on the planktonic foraminifers G. *bulloides* for a total of 154 samples collected at the frequency of 1 sample/1 cm (in the interval from 300 and 550 cm) and 1 sample/5 cm (in the other parts of the studied record (Appendix B). Samples were measured by automated continuous flow carbonate preparation GasBenchII device (Spötl & Vennemann, 2003) and a ThermoElectron Delta Plus XP mass spectrometer at the IAMC-CNR (Naples) isotope geochemistry laboratory. Acidification of samples was performed at 50°C. An internal standard (Carrara Marble with $\delta^{18}O$ = -2.43‰ versus VPDB and $\delta^{13}C$ = 2.43‰ versus VPDB) was run every 6 samples and the NBS19 international standard was measured every 30 samples. Standard deviations of carbon and oxygen isotope measures were estimated at 0.1 and 0.08‰, respectively, on the basis of ~100 repeated samples. All isotope data are reported in per mil (‰) relative to the VPDB standard.

3.3 Radiocarbon dating

The AMS ^{14}C analyses were performed on the planktonic foraminifers G. *bulloides*, G. *inflata* and G *rubber*, collected at 28, 151 and 311 cm of MD01_2474G, at the Centre for Isotopic Research on Cultural and Environmental Heritage (CIRCE) radiocarbon laboratory, Caserta (Italy) (Terrasi et al., 2007). The system is based on a tandem accelerator 9SDH-2 (built by National Electrostatics Corporation, WI, USA) with a maximum terminal voltage of 3 MV. The δ13C of each sample was also measured using an elemental analyzer (ThermoFinnigan EA 1112) coupled with an IRMS (ThermoFinnigan Deltaplus) at the Department of Environmental Science (Second University of Naples, Caserta, Italy). Radiocarbon ages were calibrated by using calibration software CalPal 2005 (Weninger et al., 2004). AMS measurements of radiocarbon abundance of carbonates are based on graphite targets. The reservoir correction ΔR (reservoir age) used for calibration is 400y (Siani et al. 2001). The calibrated age ranges are reported in years BP and referred to 2σ.

4 Results

This chapter is focused to a detailed description of the chemical analyses (Appendix C) carried out on the ash-layers from sedimentary cores KC01B, MD01_2474G, and ODP Leg 160 Site 963A.

Tephra layers were classified according to the Total Alkali (Na_2O + K_2O) / Silica diagram (TAS, Le Maitre et al., 1989), Binary plots SiO_2/K_2O wt% (Peccerillo & Taylor, 1976); and Al_2O_3/FeO_{tot} (Mc Donald, 1974). To better characterise the volcanic sources, REEs (Rare Earth Elements) were used on normalised to chondrite value (expressed in ppm) according to Boynton (1984) (Appendix D). Normalization values to primordial mantle, were used also for selected trace elements.

4.1 Tephras from the KC01B core

I1 – The tephra I1 is a thin dark layer (< 1 cm thick) characterized by altered pumices and abundant glass shards. Major element analysis display a *benmoreitic* composition (Fig. 4.1).

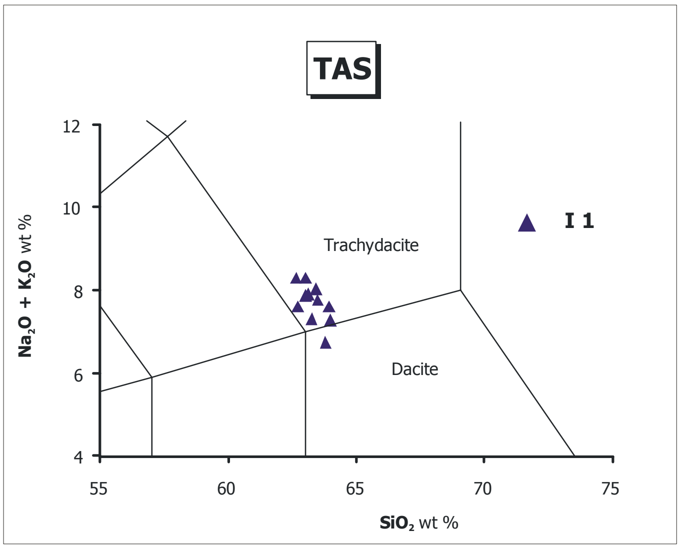

Fig. 4.1 Total alkali versus silica (TAS) diagram for the tephra I1.

The SiO_2 content ranges between 62.6 and 64.0 wt% while the Na_2O contents are remarkably correlated to K_2O concentrations (Fig. 4.2).

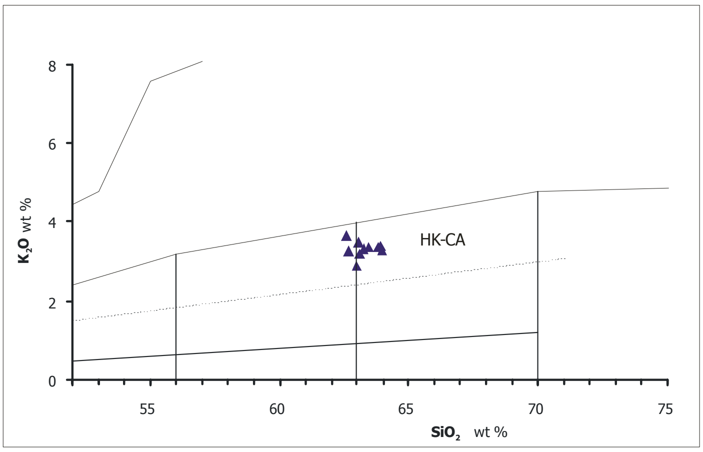

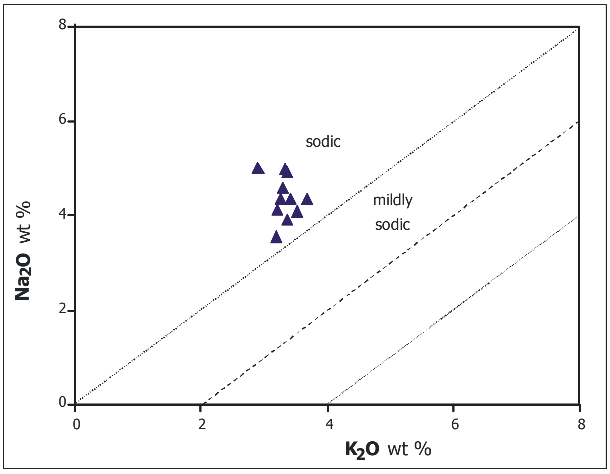

Fig. 4.2 K_2O versus SiO_2 diagram (Le Maitre et al. 1989) and Na_2O versus K_2O diagram. *HK-CA* High-K Calc-Alkaline.

Using Zr as differentiation index a continuous and moderately scattered trend for some trace elements can be observed (Fig. 4.3).

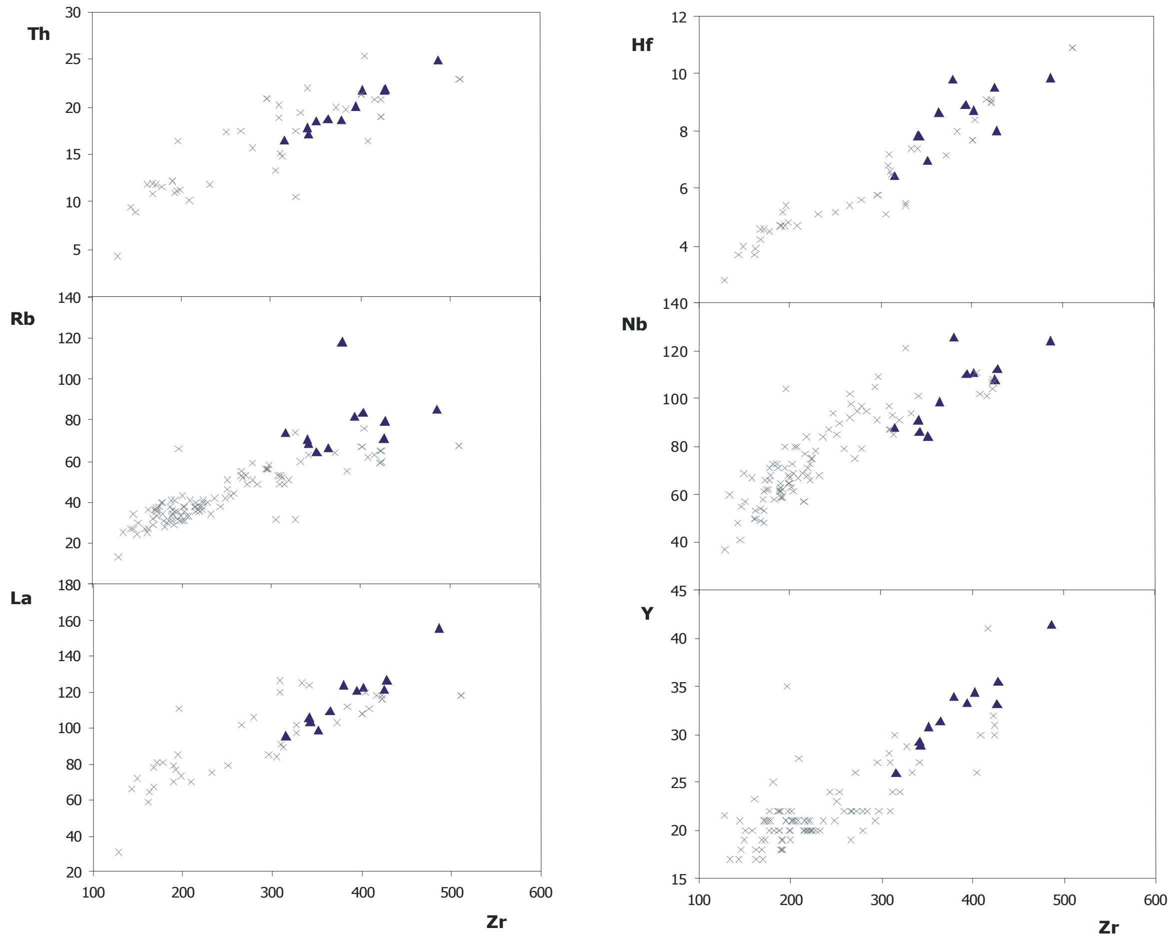

Fig. 4.3 Variation diagrams for trace elements (ppm). Symbols: blue full triangles data from this work, grey crosses for Etna on land data from the literature (D'Orazio et al., 1977, Tanguy et al., 1997; Armienti et al., 2004) used for comparison.

Incompatible elements normalised to primordial mantle composition show a marked upward convexity and small troughs of Sr and Ti. The REEs content, normalized to chondritic values, shows a progressive and homogenous fractionation from LREE to HREE ($[La/Yb]_N$ ranging between 19 and 35, Fig. 4.4).

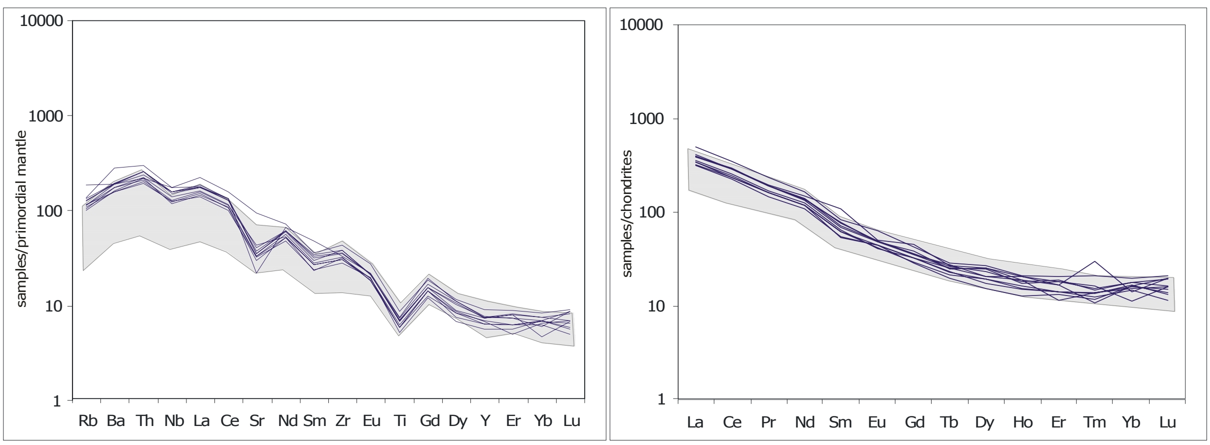

Fig. 4.4 Mantle-normalized trace elements patterns for **I1** on the left, Chondrite-normalized REE patterns on the right. Symbols: blue lines data from this work and blue filed for **Etna** on land data from literature (D'Orazio et al., 1977, Tanguy et al., 1997; Armienti et al., 2004) used for comparison.

Major and trace elements data support an Etnean provenance for the this tephra according to database reported by D'Orazio et al. (1977), Tanguy et al. (1997) and Armienti et al. (2004).

I3 – The tephra I3 is made up by altered pumices and glass shards with tubular vesicles (< 1 cm thick). The major elements show a *trachytic* composition (Fig. 4.5) of the analysed shards with variable contents of Na_2O (between 3.11 and 6.21 wt%) and K_2O (ranging between 7 and 10 wt%, Fig. 4.6).

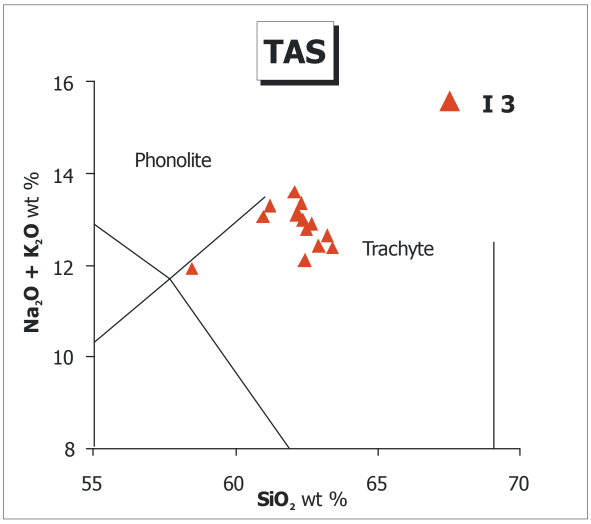

Fig. 4.5 Total alkali versus silica (TAS) diagram for the tephra I3.

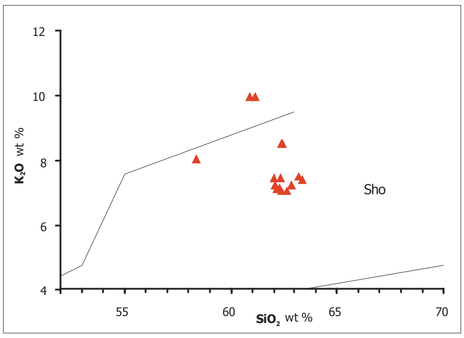

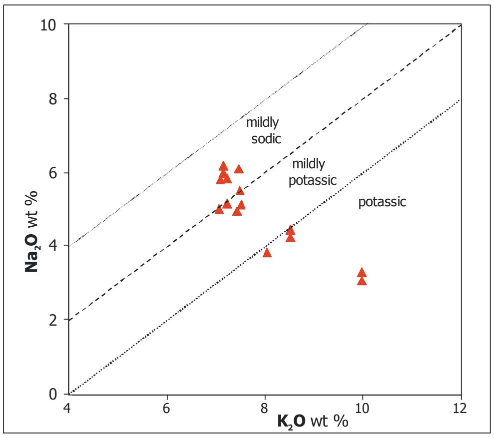

Fig. 4.6 K_2O versus SiO_2 diagram (Le Maitre et al., 1989) on the left, and Na_2O versus K_2O diagram on the right. *SHO* Shoshonite.

Trace elements and particularly REEs analysis allowed us to recognise a more "primitive" (Zr < 250 ppm) and "evolved" (Zr < 500 ppm) thachyttic composition of the studied layer (Fig. 4.7).

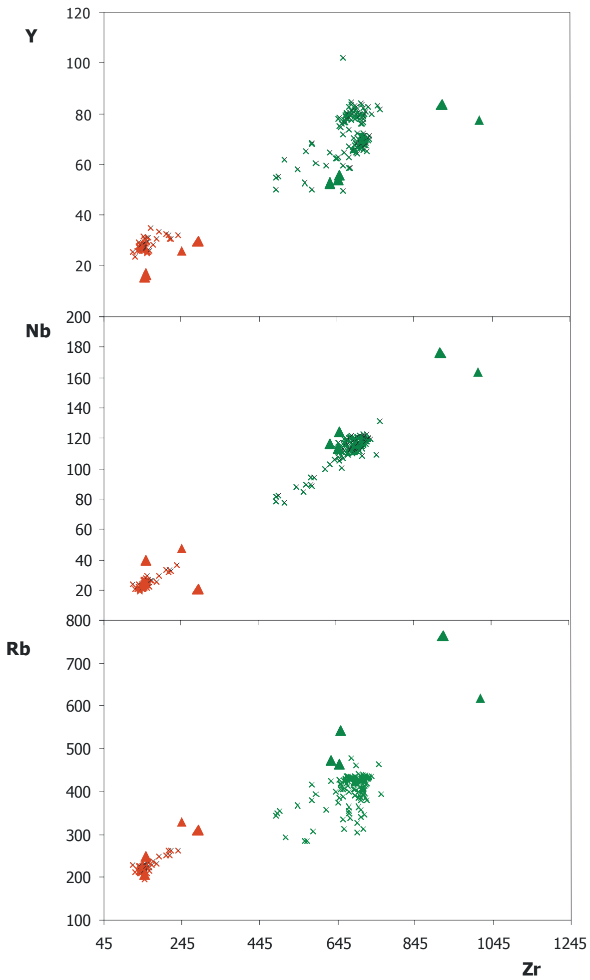

Fig. .4.7 Variation diagrams for trace elements (ppm). Symbols: red and green full triangles data from this work; red and green crosses for CI on land data from literature for comparison.

Particularly, the light rare earth elements (LREE) are strongly fractionated ($[La/Sm]_N$ (ranging between 4.3 and 6.2), while heavy rare earth elements (HREE) show an almost flat pattern ($[Gd/Yb]_N$=0.8-2.1). The Eu shows a marked trough in the "evolved" part (Eu/Eu*=0.3-0.4) whereas the "primitive" one is characterized by small negative Eu peak (Eu/Eu*=0.7–1.4) and, in few cases, even by light positive anomalies. Similar observations can be made on primitive mantle-normalized diagrams (Fig. 4.8), where points with a different degree of differentiation again show similar subparallel trends, with analysis of single shard characterized by progressively higher incompatible element abundances and deeper Ba, Sr and Ti troughs as their degree of differentiation increases (Fig. 4.8).

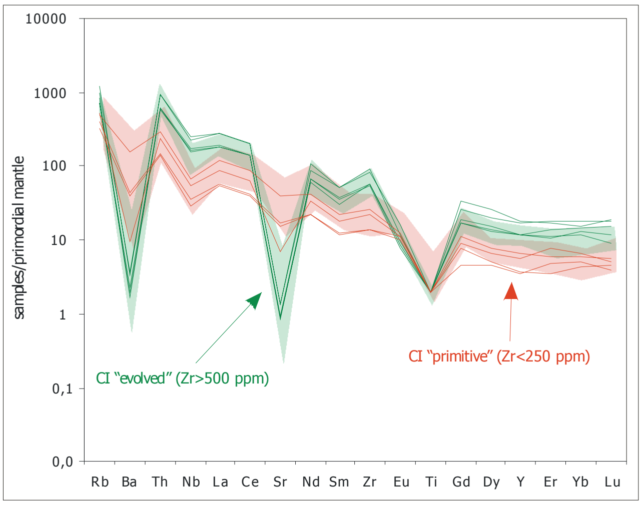

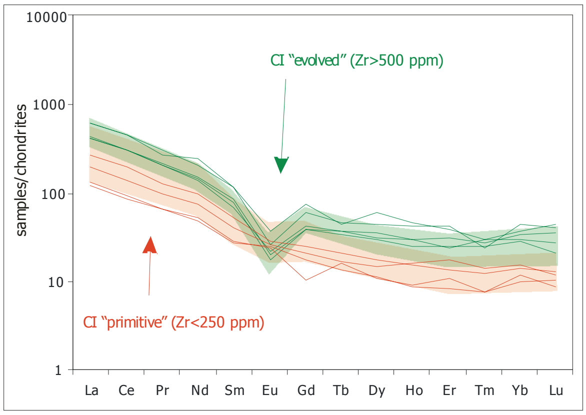

Fig. 4.8 Mantle-normalized trace elements patterns for **I3** on the left, Chondrite-normalized REE patterns on the right. Symbols: red and green lines data from this work; red and green fields for **CI** on land data from literature (Civetta et al., 1997; Pappalardo et al., 1999; Fedele et al., 2008) for comparison.

Combination of major and trace element analyses suggest a Campanian origin for the tephra I3 according to data from the literature (e.g. Civetta et al., 1997; Pappalardo et al., 1999; Fedele et al., 2008).

I9 – The tephra I9 is a thick dark brown layer (6.5 cm) mainly constituted by elongate and platy glass shards. The major elements analysis shows *thrachytic* composition with a *shoshonitic* affinity (Fig. 4.9), with a limited range of silica contents (62.1-63.2 wt%).

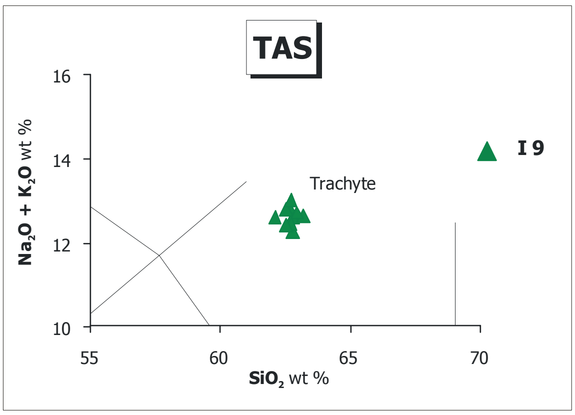

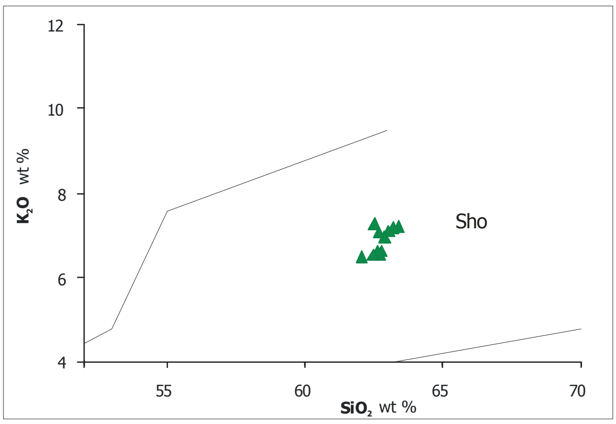

Fig. 4.9 Total alkali versus silica (TAS) diagram for the tephra I9 on the left and K_2O versus SiO_2 diagram (Le Maitre et al., 1989) on the right. *Sho* Shoshonite.

The trend of the Na_2O and Al_2O_3 is negative, while K_2O increases with to SiO_2 (Fig. 4.10).

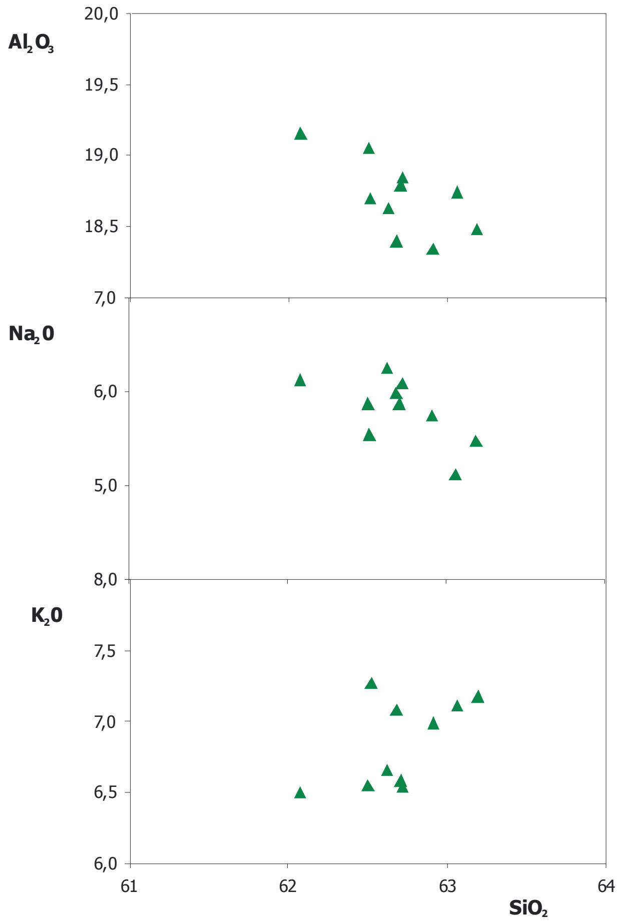

Fig. 10 Variation diagrams for major elements (wt %) versus SiO_2.

Trace elements binary plots show a positive correlation with Zr contents (e.g. Th, Nb and Y, Fig. 4.11) and indicate different degrees of evolution.

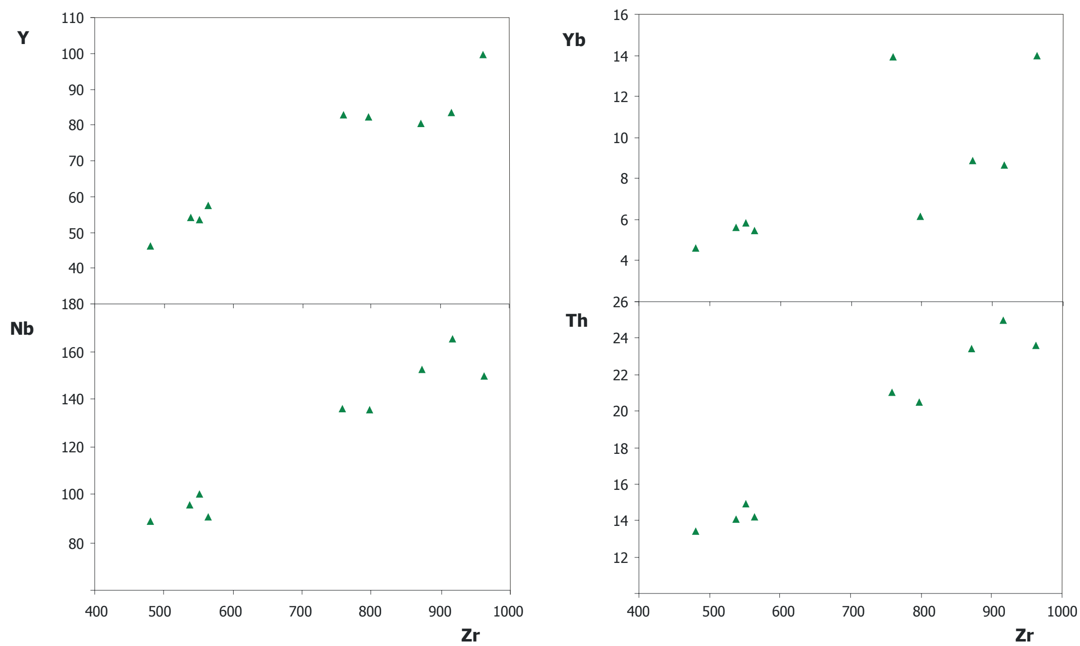

Fig. 4.11 Variation diagrams for trace elements (ppm).

Two chemical groups can be clearly distinguished: a population characterised by Zr < 600 ppm and the other one with Zr > 750 ppm, even though the REE contents normalized to chondritic values show patterns characterized by the same trend. Plot of normalised trace elements content to primitive mantle, show the typical trend of evolved rocks, similar to tephra I3, with strong negative peaks of Ba, Sr and Ti (Fig. 4.12).

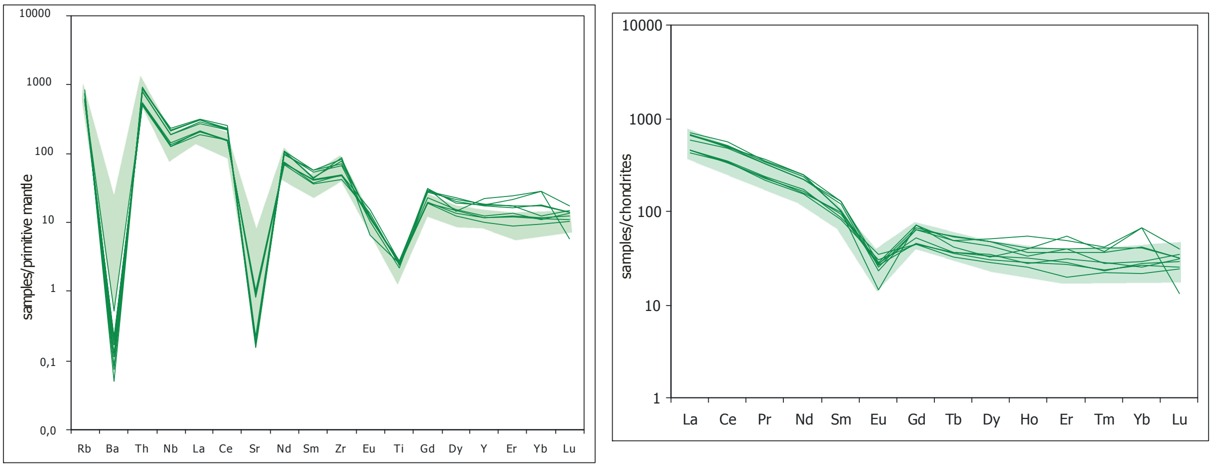

Fig. 4.12 Mantle-normalized trace elements patterns for **I9** on the left, Chondrite-normalized REE patterns on the right. Symbols: green lines data from this work; green field for **Campanian** on land data from literature (Civetta et al., 1997; Pappalardo et al., 1999; Fedele et al., 2008) for comparison.

REE normalized pattern is characterized by an evident fractionation of LREE ($[La/Sm]_N$=4.3-7.4), Eu though (Eu/Eu*=0.1-1) and a scattering and flat HREE pattern (Fig. 4.12). Distribution of major, trace and rare earth elements are typical of Campanian volcanic activity (Civetta et al., 1997; Pappalardo et al., 1999; Fedele et al., 2008).

4.2 Tephras from the MD01_2474G core

MD3 – This tephra layer represents the younger pyroclastic deposits from core MD01_2474G, recovered at 53 cm b.s.f.. It is 4 cm thick and presents abundant dark vesicular scoria and brown curvy glass shards with tubular vesicles. According to TAS diagram, it shows *latitic* composition (Fig. 4.13).

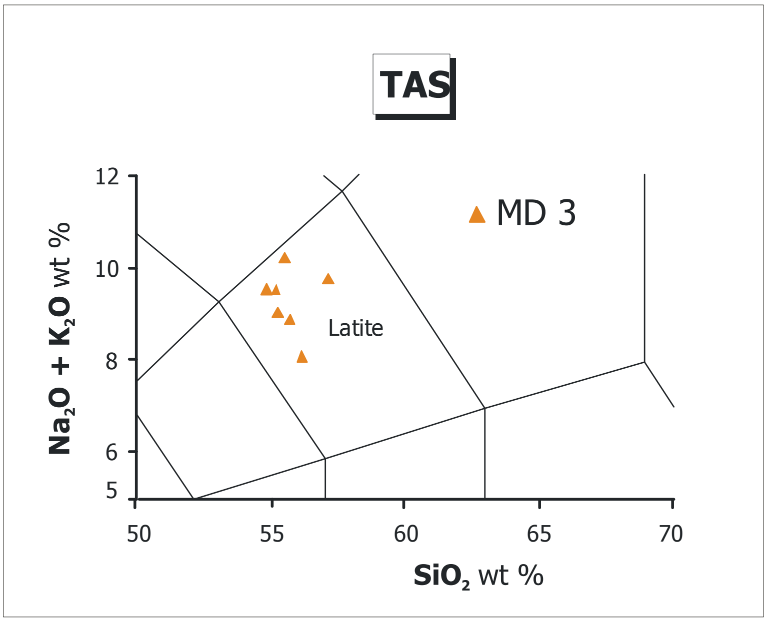

Fig. 4.13 Total alkali versus silica (TAS) diagram for the tephra **MD3**.

A negative correlation of MgO, and CaO with SiO_2 can be observed, while Al_2O_3 contents show an increasing trend with SiO_2 (Fig. 4.14).

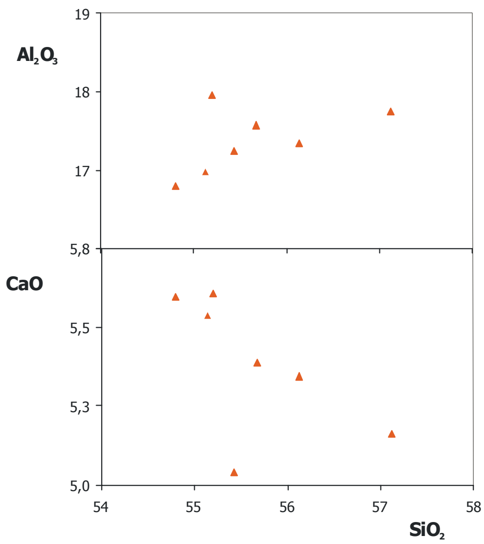

Fig. 4.14 Variation diagrams for major elements (wt %) versus SiO_2.

Major elements pattern suggests a potential origin of MD3 tephra from a Aeolian volcanic source, probably from the Vulcano island (data from De Astis et al., 1997).

MD10 - The MD10 tephra layer sampled at 176 cm b.s.f. is about 3 cm thick. It is characterized at the bottom by a dark layer (MD10c). This tephra is mainly made up of abundant dark scoria and light yellow vesicular pumices, while glass shards are rare. Chemical analyses were carried out on scoria that show a *benmoreitic* and *trachytic* composition (Fig.4.15).

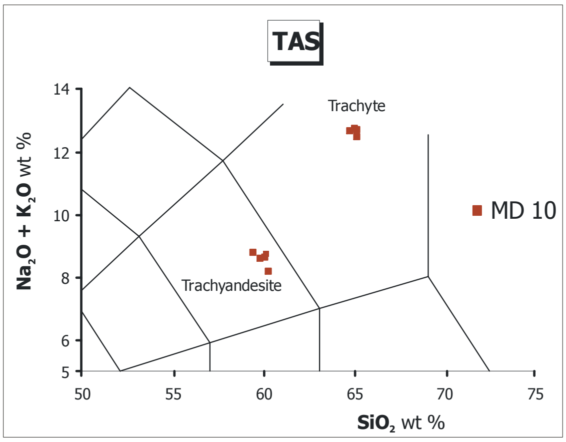

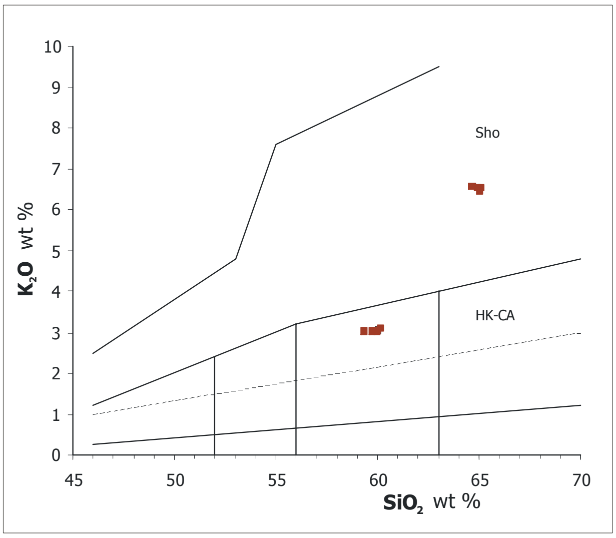

Fig. 4.15 Total alkali versus silica (TAS) diagram for the tephra **MD10** on the left and K_2O versus SiO_2 diagram (Le Maitre et al., 1989) on the right. *Sho* Shoshonite, *HK-CA* High-K Calc-Alkaline.

This different chemical signature is well clear even observing the SiO_2/K_2O diagram (Fig. 4.16) where the two populations show a HK-CA and shoshonitic affinity, respectively. The compositional gap between the two populations is confirmed by the evident differences in TiO_2, MgO, CaO, FeO, K_2O and P_2O_5 contents, while Al_3O_3, MnO and Na_2O show comparable concentrations (Fig. 4.16).

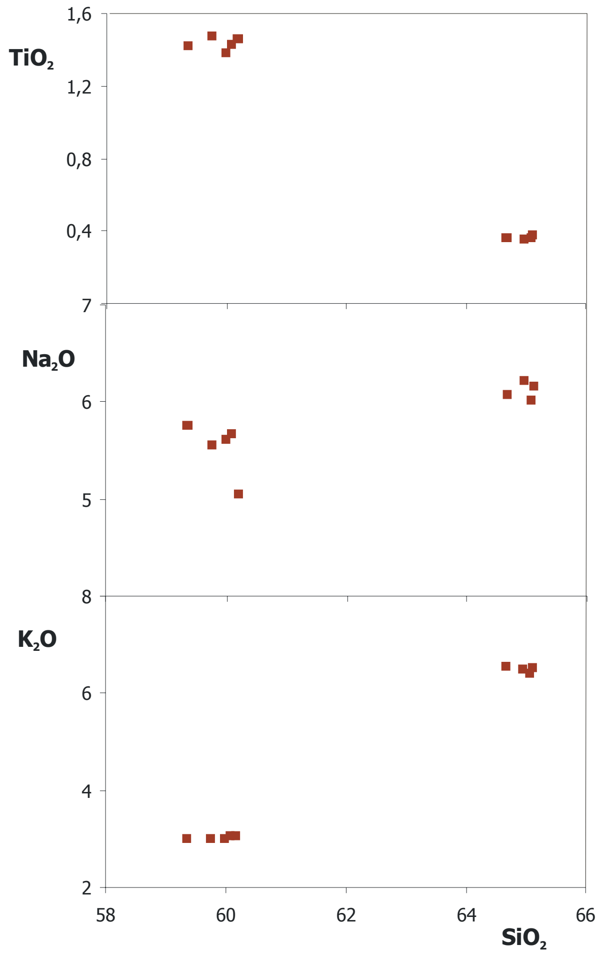

Fig. 4.16 Variation diagrams for major elements (wt %) versus SiO_2.

The bimodal chemical pattern of major elements may suggest two potential sources: Campanian (Civetta et al., 1997; Pappalardo et al., 1999) and Aeolian (e.g. D' Orazio et al., 1997).

MD11 - The MD11 layer can be considered as a crypto-tephra because not visible at naked eyes. It is 1 cm thick at 186 cm b.s.f.. It is made up of abundant dark vesicular scoria and light brown glass shards with tubular vesicles. A bimodal distribution of major elements, less evident than in tephra MD10 was observed for tephra MD11. Its chemical composition is *latitic* with some points falling into the *trachydacitic* field (Fig. 4.17).

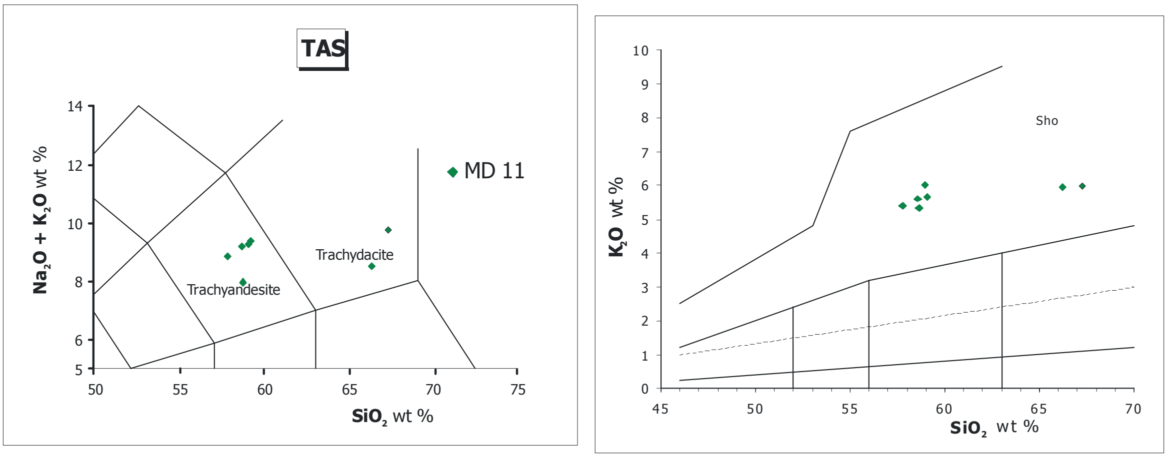

Fig. 4.17 Total alkali versus silica (TAS) diagram for the tephra **MD11** on the left and K_2O versus SiO_2 diagram (Le Maitre et al., 1989) on the right. *Sho* Shoshonite.

The results show a decreasing Al_2O_3, MgO, CaO and FeO trend related to an increase of silica content (ranging between 57.8 and 59.1 wt%, Fig. 4.18).

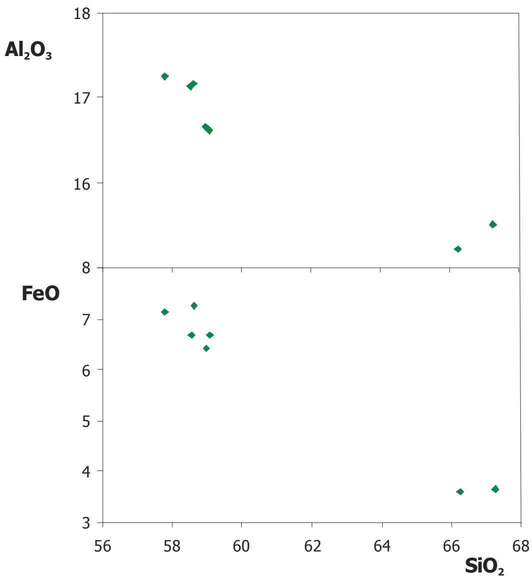

Fig. 4.18 Variation diagrams for major elements (wt %) versus SiO_2.

Available major element analyses may support an Aeolian provenance.

MD14 - The MD14 tephra layer at 260 cm b.s.f., about 2 centimetres thick is made up by dark vesicular scoria at the base and honey coloured, curvy glass shards characterising the top of the deposit, loose feldspar crystals are very abundant throughout the layer. Scoria from the middle part of the layer (MD14b) show a wide compositional range from basaltic *trachy-andesite* to *latite* and *thrachydacites* (Fig. 4.19).

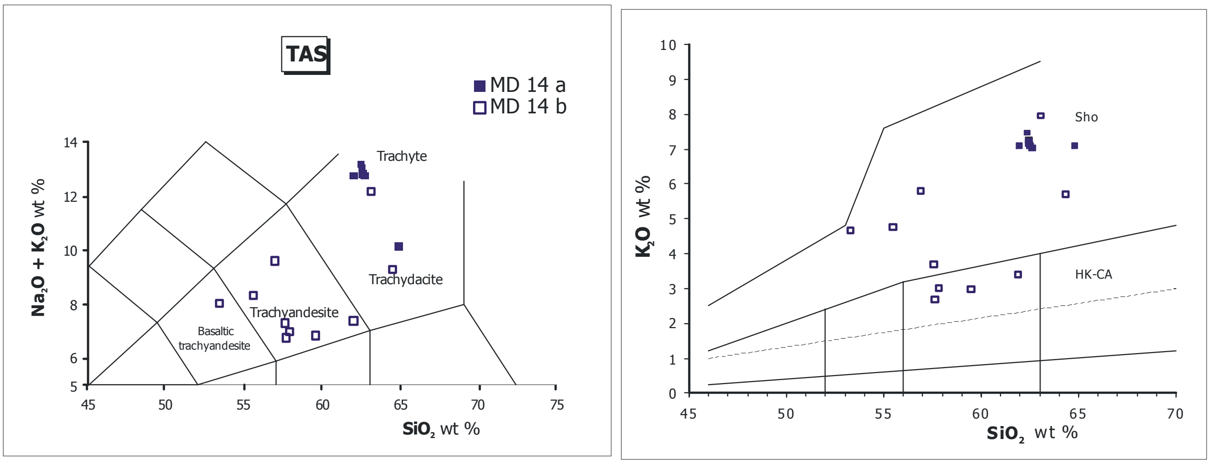

Fig. 4.19 Total alkali versus silica (TAS) diagram for the tephra **MD14** on the left and K_2O versus SiO_2 diagram (Le Maitre et al., 1989) on the right. *Sho* Shoshonite, *HK-CA* High-K Calc-Alkaline.

Glass shards from the top of MD14 (MD14a) are *trachytic* in composition. The MD14b sample shows compositional trends for TiO_2, MgO, CaO, and FeO decreasing with proportional increase of SiO_2 (Fig. 4.20). Na_2O contents evidence a not linear response to the increasing SiO_2 percentages.

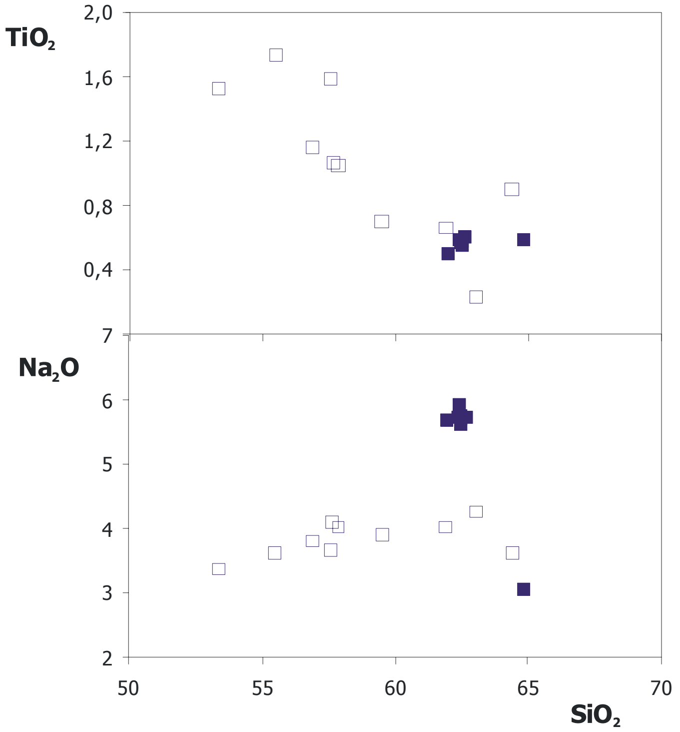

Fig. 4.20 Variation diagrams for major elements (wt %) versus SiO_2.

These petrochemical features may suggest a general link tephra MD14 with the Aeolian and Campanian activities (e.g., Gioncada et al., 2003; De Astis et al., 1997, 2000; Poly et al., 1987; Civetta et al., 1997; D' Antonio et al., 1999).

MD15 - The MD15 tephra layer at 342 cm b.s.f, 10,8 cm thick, is one of the thicker throughout the core. The bottom (MD15c) of the tephra is constituted by abundant dark scoria and glass shards (brown vesicular fragments and pumiceous shards with tubular vesicles), whereas the top and middle part is formed by abundant dark vesicular scoria and rare dark brown glass fragments. The composition of MD15 ranges from *basaltic-trachyandesite* (MD15a, b and c) to *trachyandesite* (MD15b and a) (Fig. 4.21).

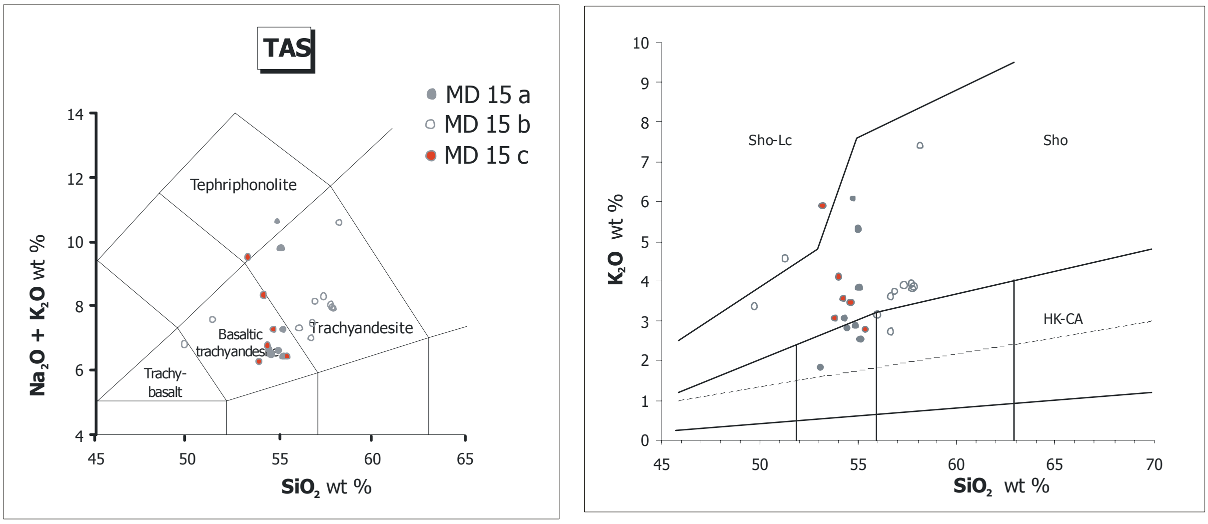

Fig. 4.21 Total alkali versus silica (TAS) diagram for the tephra MD15 on the left and K_2O versus SiO_2 diagram (Le Maitre et al., 1989) on the right. *Sho* Shoshonite, *HK-CA* High-K Calc-Alkaline.

MD15b shows relatively higher silica content, while the bottom of the layer (MD15c) is characterised by lower SiO_2 concentrations with comparable values of Na_2O and K_2O wt% (Fig.4.22).

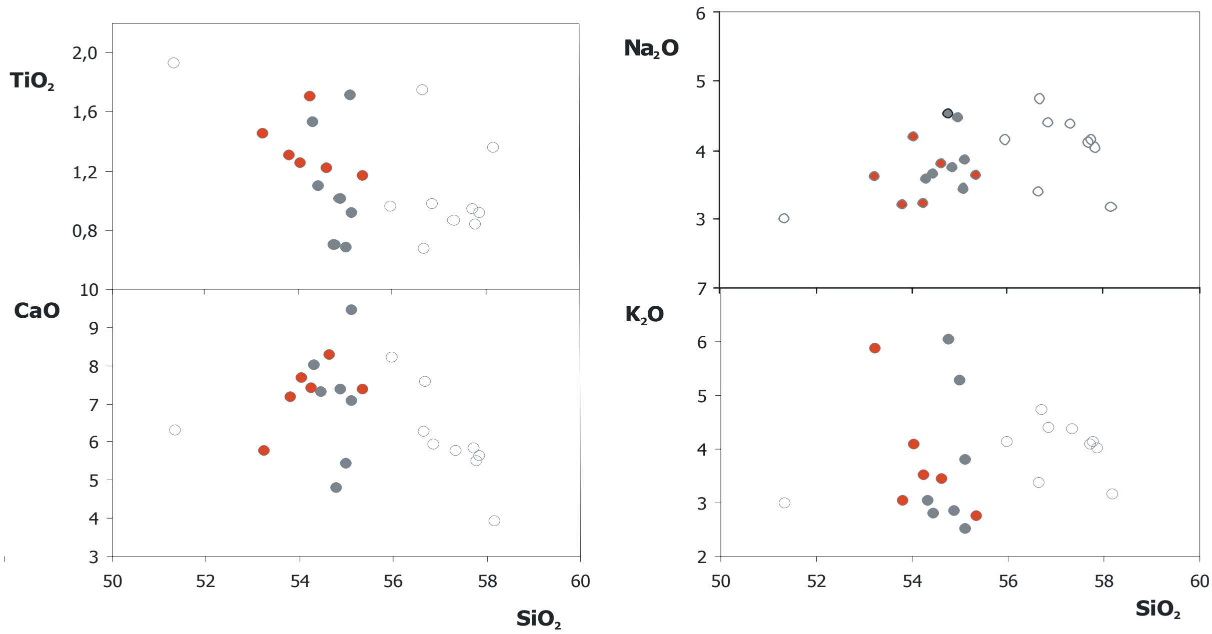

Fig. 4.22 Variation diagrams for major elements (wt %) versus SiO_2.

REE contents normalized to chondrites values evidence a generally fractionation process: enrichment in LREE ($[La/Sm]_N$=2.7-7.3) relative HREE ($[Gd/Yb]_N$=0.7-3.2) and limited negative Eu anomaly (Eu/Eu*=0.3-1.6) (Fig. 4.23).

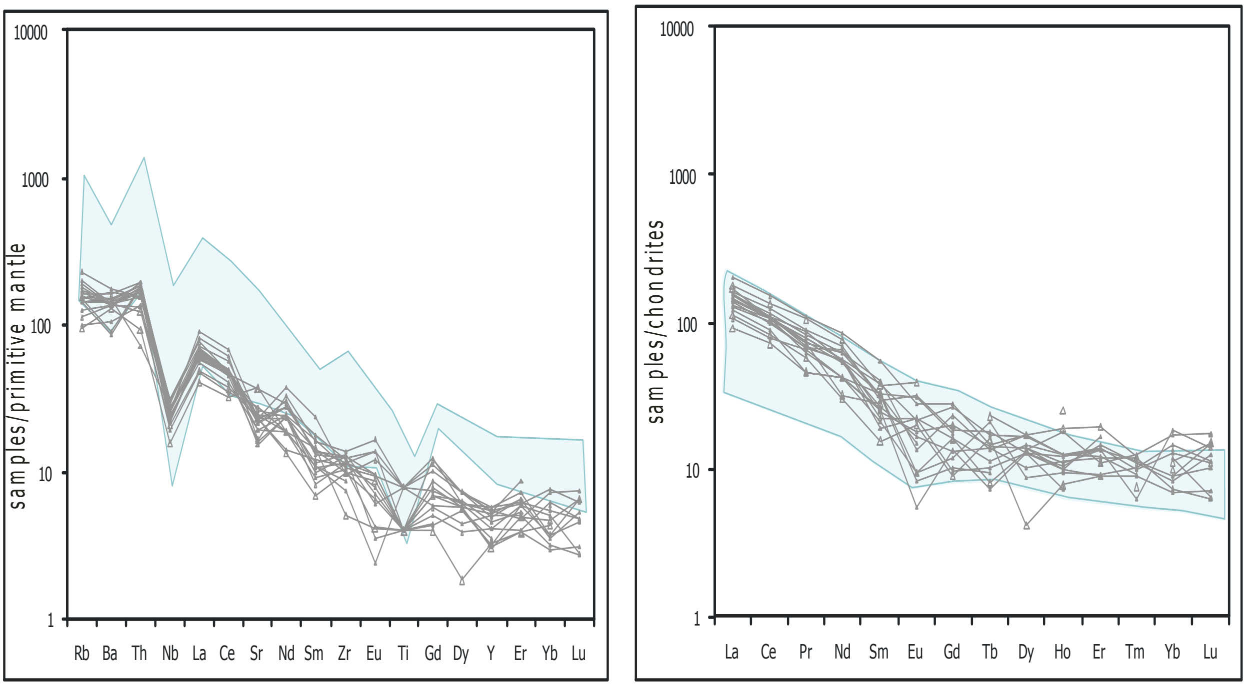

Fig. 4.23 Mantle-normalized trace elements patterns for **MD15** on the left, Chondrite-normalized REE patterns on the right. Symbols: grey lines data from this work; blue field for **Aeolian** on land data from literature (Del Moro et al., 1998; De Astis et al., 1997,2000; Gioncada et al., 2003) for comparison.

Diagram of trace elements normalized to primordial mantle (Fig. 4.24) shows an increase of Rb, Ba and Th and troughs of Nb, Sr and minor TiO_2. Zr and HREE (as Gd, Dy, Er, Yb and Lu) are characterised by scatter trends, due to analytical problems during the acquisition data.

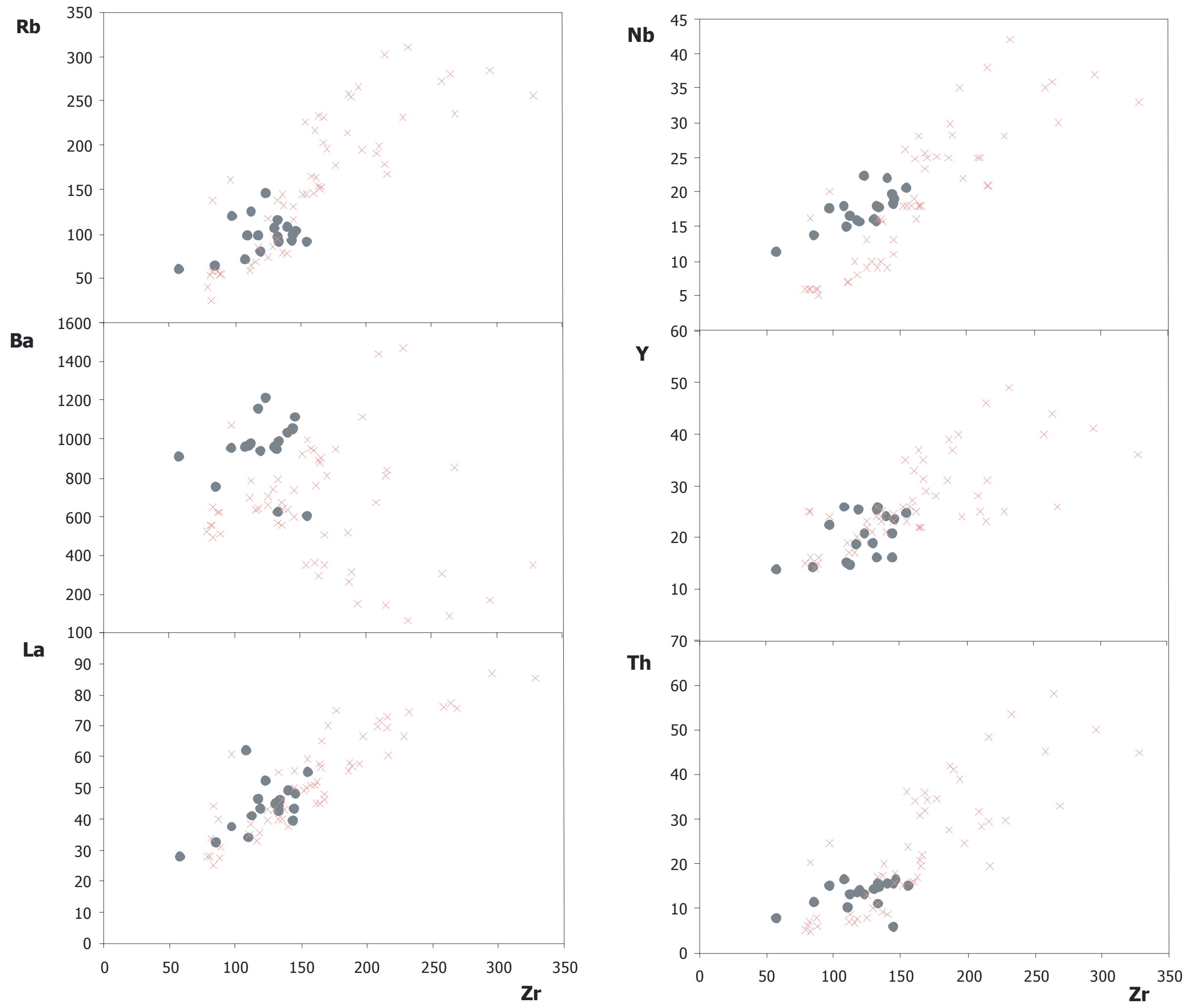

Fig. 4.24 Variation diagrams for trace elements (ppm). Symbols: grey full circles data from this work; pink crosses for Vulcano on land data from literature (Del Moro et al., 1998; De Astis et al., 1997,2000; Gioncada et al., 2003) for comparison.

These petrochemical features may suggest for tephra MD15 the Aeolian volcanic arc as a possible source area, particularly from the Vulcano island (see Del Moro et al., 1998; De Astis et al., 1997,2000; Gioncada et al., 2003 for comparable datasets).

MD18 – Crypto-tephra MD18 at 401 cm from sea floor is about 5 cm thick. The main pyroclastic components are represented by dark vesicular scoria and brown glass shards. The chemical composition of glass shards (based on three analysed points) is *basaltic-trachy-andesitic*, with shoshonitic affinity, with two points following in the *dacitic* field (Fig.4.25).

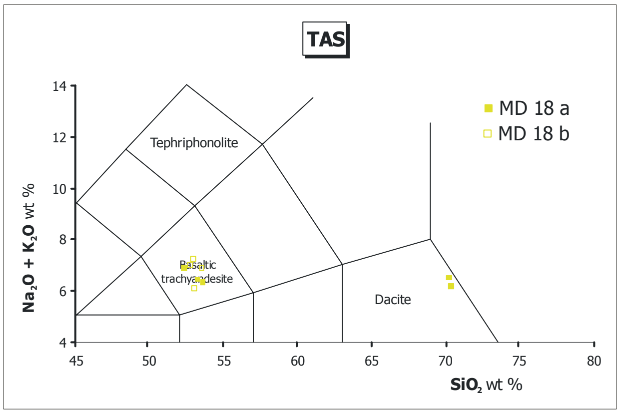

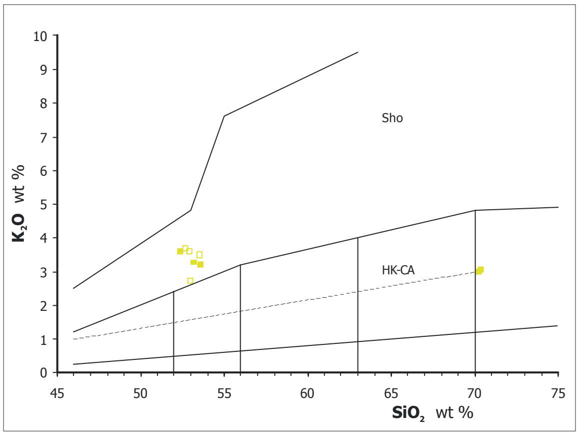

Fig. 4.25 Total alkali versus silica (TAS) diagram for the tephra MD18 on the left and K_2O versus SiO_2 diagram (Le Maitre et al., 1989) on the right. *Sho* Shoshonite, *HK-CA* High-K Calc-Alkaline.

A negative correlation of TiO_2, MgO, and CaO with SiO_2 can be observed, while Al_2O_3, NaO_2 and K_2O show comparable concentrations (Fig. 4.26).

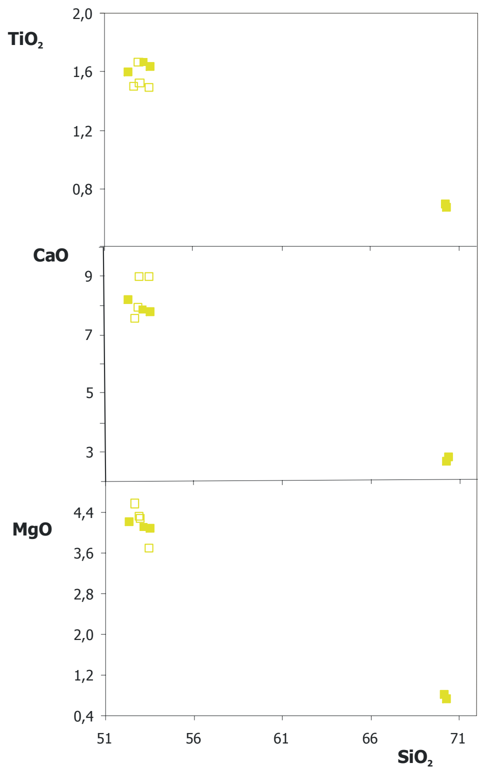

Fig. 4.26 Variation diagrams for major elements (wt %) versus SiO_2.

The trace element contents normalized to primordial mantle pattern (Fig.4.27) show similar features respect to tephra MD15: relative high Rb, Ba and Th with negative spikes of Nb, Sr and TiO_2.

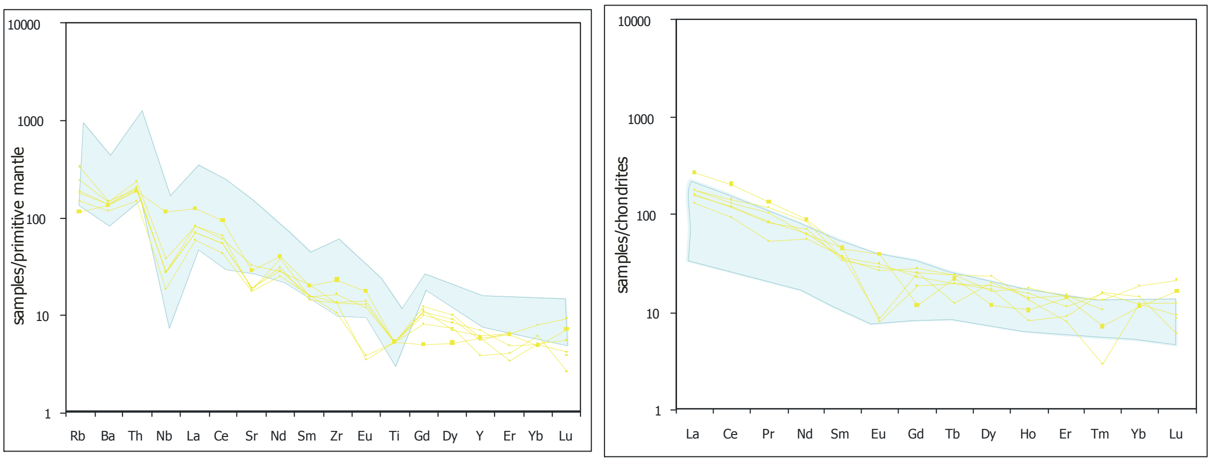

Fig. 4.27 Mantle-normalized trace elements patterns for **MD18** on the left, Chondrite-normalized REE patterns on the right. Symbols: yellow lines data from this work; blue field for **Aeolian** on land data from literature (Del Moro et al., 1998; De Astis et al., 1997,2000; Gioncada et al., 2003) for comparison.

Differently, the negative Eu anomaly is absent from the two analyses. HREE contents exhibit evident scattered trends for analytical problems (Fig. 4.28).

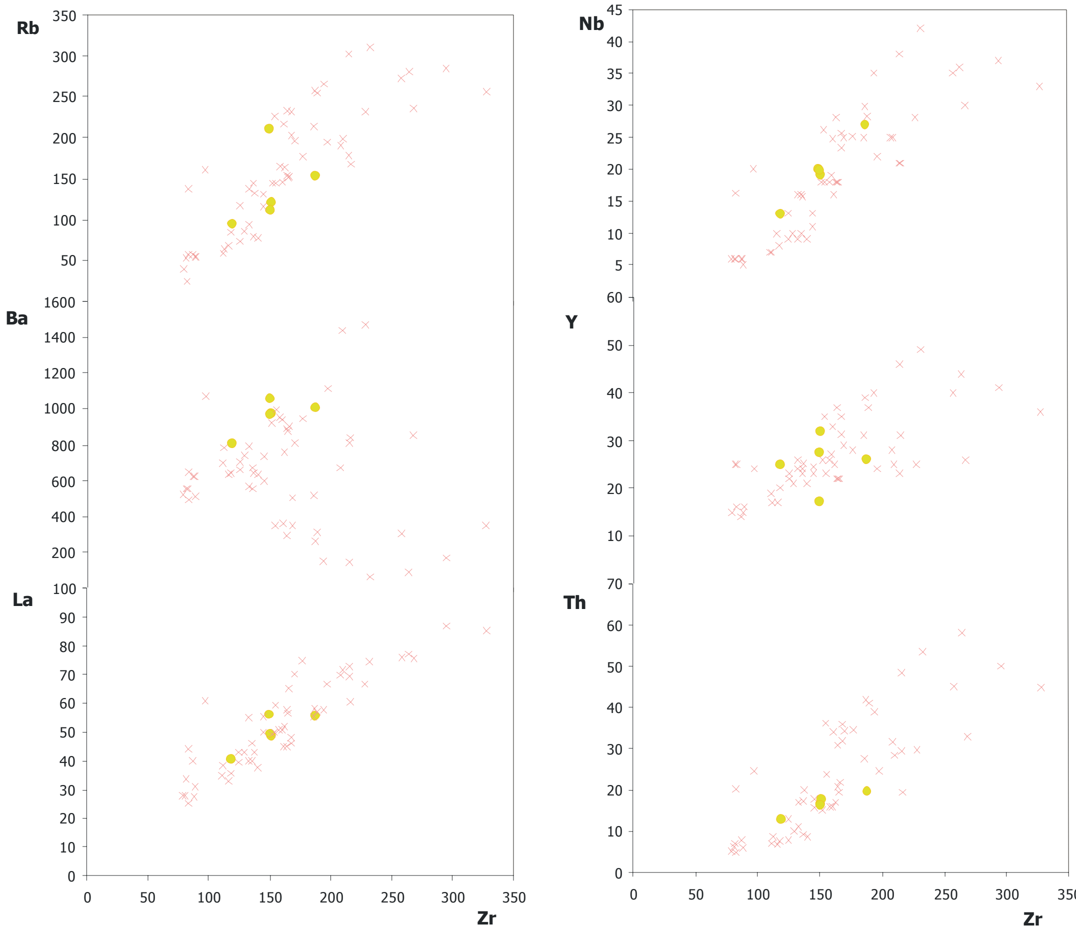

Fig. 4.28 Variation diagrams for trace elements (ppm). Symbols: yellow full circles data from this work; pink crosses for Vulcano on land data from literature (Del Moro et al., 1998; De Astis et al., 1997,2000; Gioncada et al., 2003) for comparison.

Also in this case the combined information from major and trace elements suggests an Aeolian origin (possibly from the Vulcano island) for these volcanic deposits (see Del Moro et al., 1998; De Astis et al., 1997, 2000; Gioncada et al., 2003).

MD22 - The tephra layer MD22 at 449 cm b.s.f. about 8,3 cm. It is rich of dark poorly vesiculated scoria and either light brown curvy and elongate and pumiceous shards. The chemical composition of this layer shows a wide range of variability with *sub-alkaline* affinity (HK-CA, Fig. 4.29).

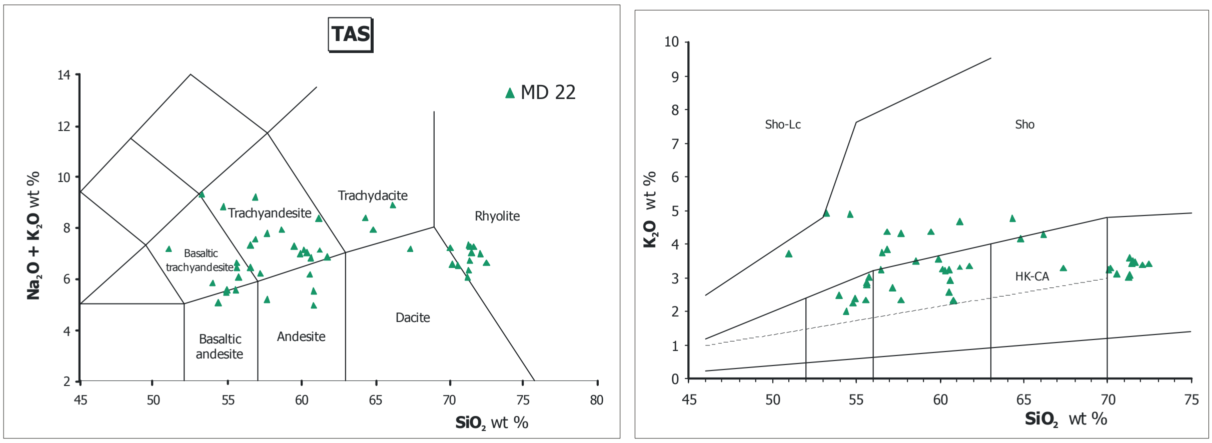

Fig. 4.29 Total alkali versus silica (TAS) diagram for the tephra MD22 on the left and K_2O versus SiO_2 diagram (Le Maitre et al., 1989) on the right. *Sho* Shoshonite, *HK-CA* High-K Calc-Alkaline.

Major elements are characterised by variable silica (ranging 51 and 72 wt%) and TiO_2 contents (0.46/1.80 wt%), while Na_2O and K_2O have similar concentrations (between 2.5 and 4.5 wt%). Generally, a negative correlation of MgO, CaO, MnO FeO and P_2O_5 with SiO_2 can be observed (Fig. 4.30).

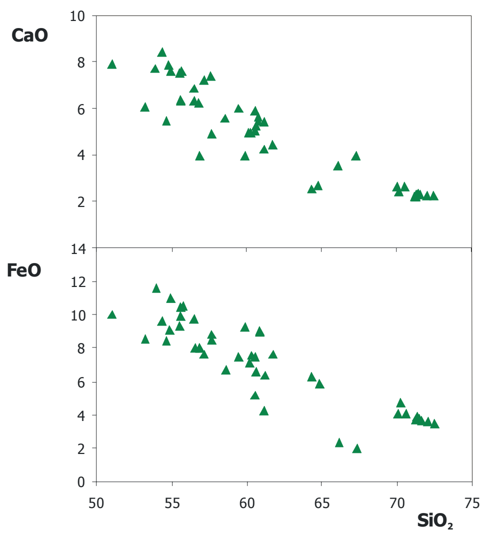

Fig. 4.30 Variation diagrams for major elements (wt %) versus SiO_2.

It is worth noting that major elements at the top and the bottom of the layer (samples MD22 a and d) are characteristic by more acid terms, whereas in the middle part the silica contents significantly decreas. Trace element contents for the tephra MD22 show high variability too and especially HREE contents show scattered trends produced during data acquisition. Particularly Rb, Nb, La and Y versus Zr show evident positive correlations (Fig. 4.31).

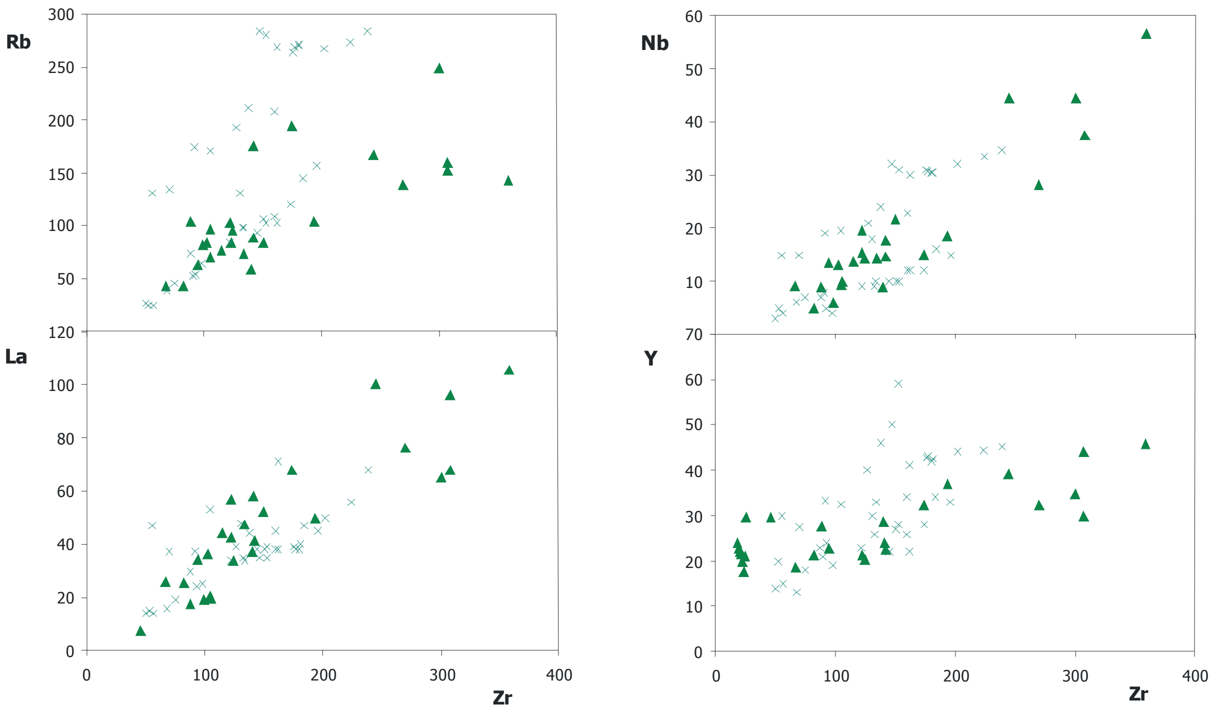

Fig. 4.31 Variation diagrams for trace elements (ppm). Symbols: green full triangles data from this work; green crosses for Lipari on land data from literature (Crisci et al., 1991; Esperanca et al., 1992; Gioncada et al., 2003) for comparison.

REE are fractionated ($[La/Yb]_N$=2.7-27.3), with light negative anomaly of Eu (Eu/Eu*=0.2-1.9), higher enrichments in LREE ($[La/Sm]_N$=1.3-10.8) relative to HREE ($[Gd/Yb]_N$=0.5-5.6) with a light increase of Tm, Yb and Lu (Fig. 4.32). Incompatible elements values normalized to primordial mantle give patterns with troughs of Nb and Sr, and positive spikes of Th, La, Nd and Gd (Fig. 4.32).

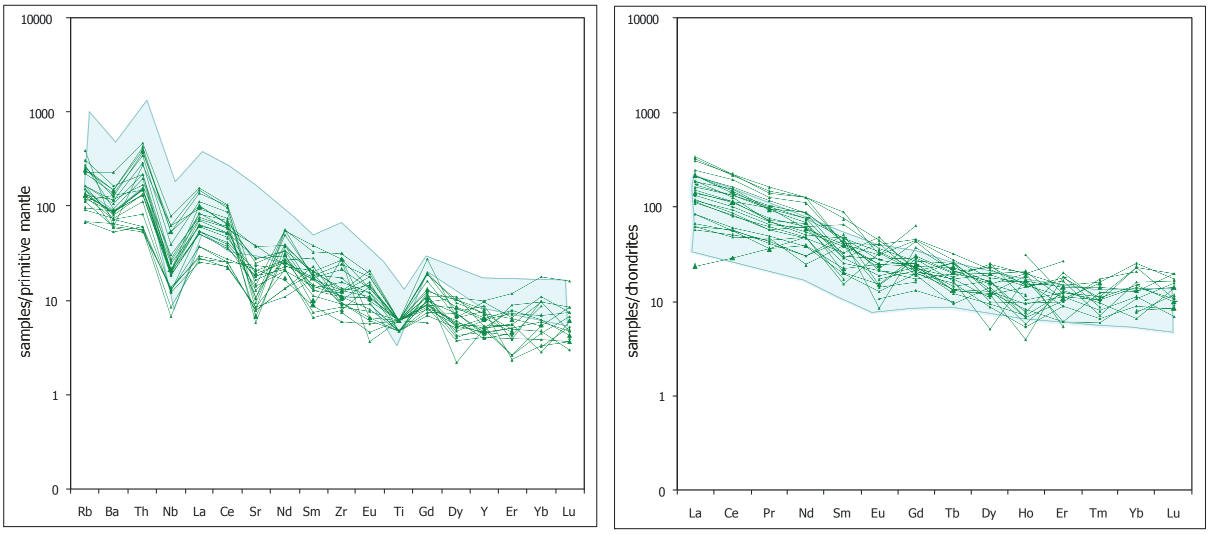

Fig. 4.32 Mantle-normalized trace elements patterns for **MD22** on the left, Chondrite-normalized REE patterns on the right. Symbols: green lines data from this work; blue field for **Lipari** on land data from literature (Crisci et al., 1991; Esperanca et al., 1992; Gioncada et al., 2003) for comparison.

The distribution patterns of trace and rare-earth elements suggest an affinity with Aeolian products and in particular with those related to volcanic activity of the Lipari island (according to Crisci et al., 1991; Esperanca et al., 1992; Gioncada et al., 2003).

MD27 – The MD27 layer at 558 cm b.s.f. is a dark layer, about 2 cm thick. This layer is characterized by abundant dark, poorly vesiculated scoria, rare dark brown glass shards and red elongate tubular pumice. Chemical analyses of scoria and glass shards display generally a *trachyandesitic composition* with few points felling within the basaltic trachyandesite field (Fig. 4.33).

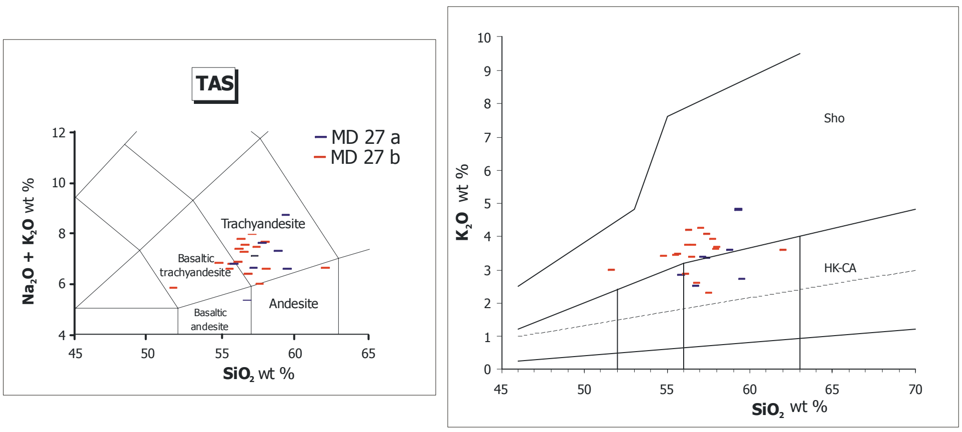

Fig .4.33 Total alkali versus silica (TAS) diagram for the tephra MD27 on the left and K_2O versus SiO_2 diagram (Le Maitre et al., 1989) on the right. *Sho* Shoshonite, *HK-CA* High-K Calc-Alkaline.

TiO_2 content always >1 wt% does not positively correlate with SiO_2, like MgO, MnO and FeO (Fig. 4.34).

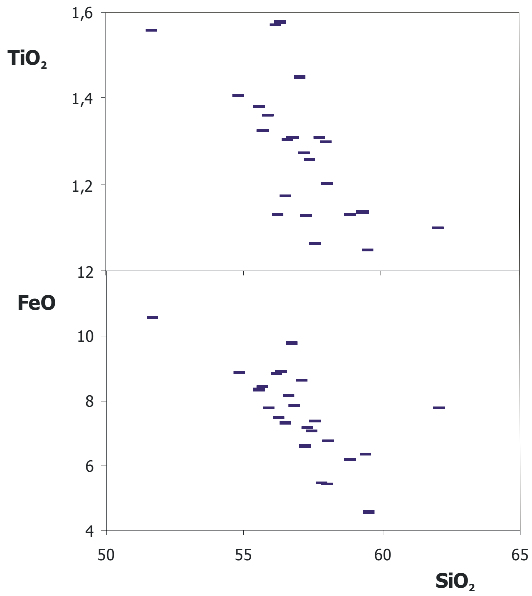

Fig. 4.34 Variation diagrams for major elements (wt %) versus SiO_2.

REE normalized values show enrichment of light REE ($[La/Sm]_N$=2.7-5.7) related to heavy REE ($[Gd/Yb]_N$=0.7-4.4) with Eu marking either a negative and positive anomaly. The diagramm of normalized trace elements contains strong negative anomalies of Nb and Sr associated to limited variability of Ba and relatively higher contents of REE (Th, La ,Eu and Gd, Fig. 4.35).

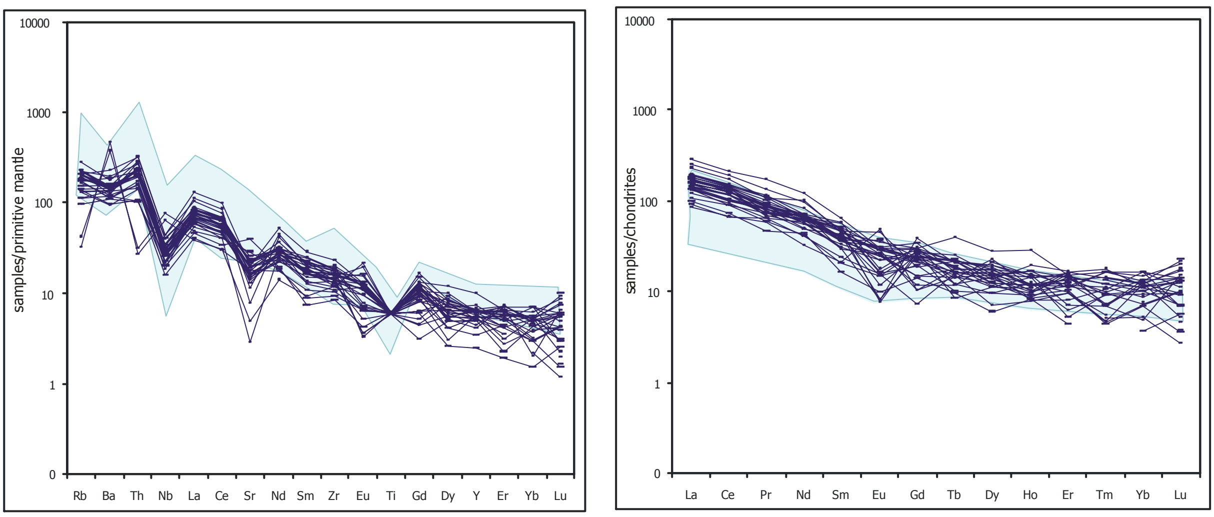

Fig. 4.35 Mantle-normalized trace elements patterns for **MD27** on the left, Chondrite-normalized REE patterns on the right. Symbols: blue lines data from this work; blue filed for **Vulcano** on land data from literature (Del Moro et al., 1998; De Astis et al., 1997,2000; Gioncada et al., 2003) for comparison.

This latter feature suggests an origin for this tephra layer from the Vulcano island (Aeolian arc) (see Del Moro et al., 1998; De Astis et al., 1997, 2000; Gioncada et al., 2003).

MD28 – The MD28 tephra at 701 cm b.s.f., 11 cm thick, consists of light bubble-wall junction shards some of them with tubular morphologies. Glass shard analyses have a *trachytic* composition with $Na_2O>K_2O$ (Fig. 4.36).

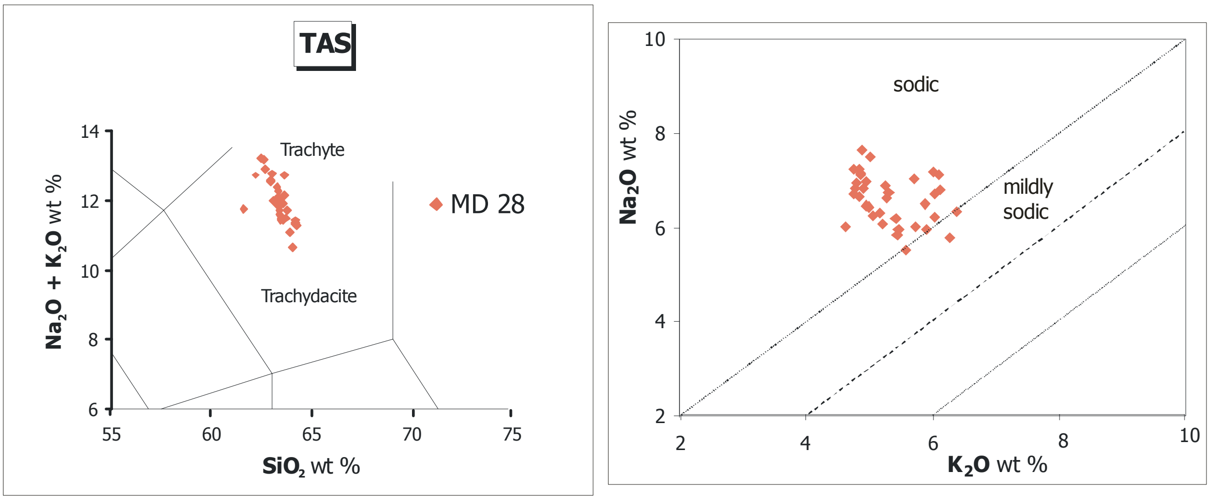

Fig. 4.36 Total alkali versus silica (TAS) diagram for the tephra MD28 on the left, and Na_2O versus K_2O diagram on the right.

Major element analyses show a moderately decrease of FeO and NaO_2 contents related to an increase of silica content (Fig. 4.37).

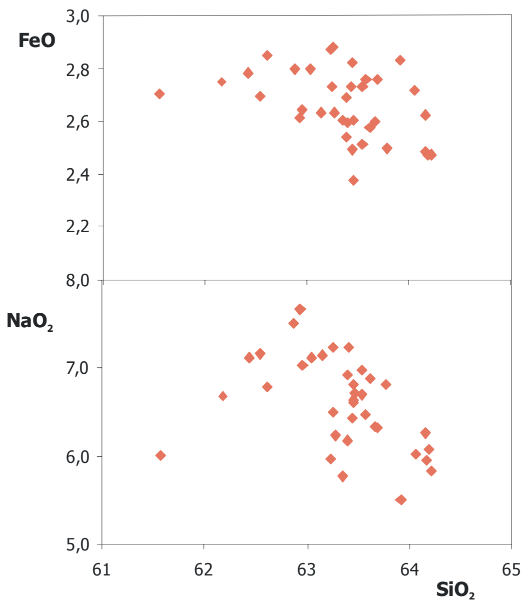

Fig. 4.37 Variation diagrams for major elements (wt %) versus SiO_2.

Trace element contents normalized to primordial mantle evidence strong negative anomalies of Ba, Sr an TiO_2 (Fig. 4.38). REE contents normalized to chondrites values (Fig 4.38) give patterns where the strong fractionation of LREE ($[La/Sm]_N$=2.3-22.3) is evident such as the trough of Eu (Eu/Eu*=0.1-0.8) which is typical in these of rocks. HREE pattern is not defined very well likely due to analytical problems during acquisition (Fig. 4.38).

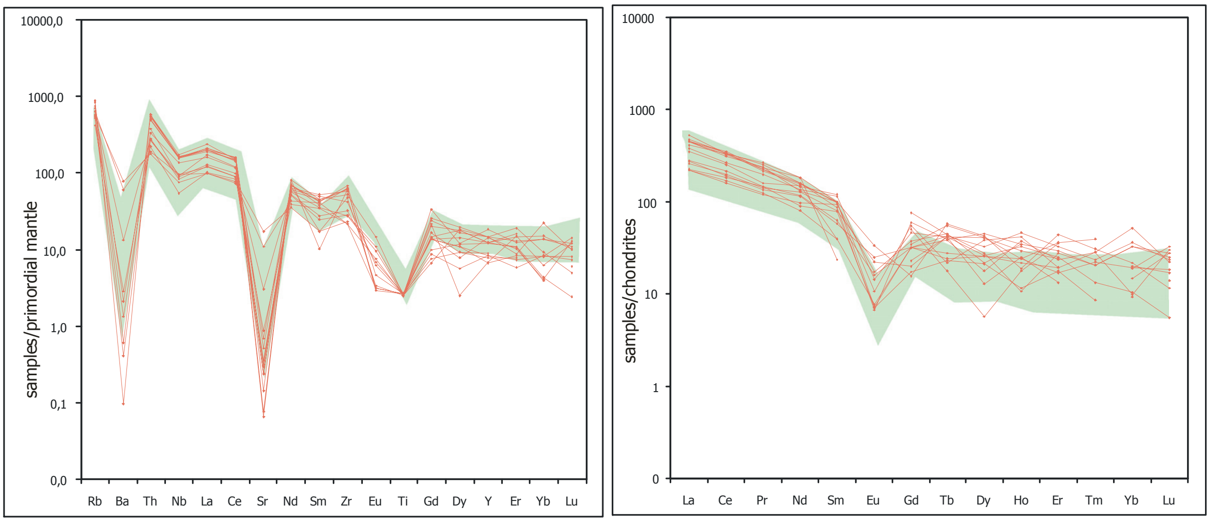

Fig. 4.38 Mantle-normalized trace elements patterns for **MD28** on the left, Chondrite-normalized REE patterns on the right. Symbols: pink lines data from this work; green field for **Campanian** on land data from literature (Civetta et al., 1997; Pappalardo et al., 1999; Fedele et al., 2008) for comparison.

All these features suggest a Campanian origin for this level and in particular allow to individuate Ischia island as the potential source of tephra MD28 (see Civetta et al., 1997; D'Antonio et al., 1999; Pappalardo et al., 1999 for comparable dataset).

MD33 – This crypto-tephra recognised at 764,5 cm b.s.f. is 1 cm thick. It was recognized through inspection of dry and sieved sediments at binocular microscope. The deposit is represented by abundant dark dense scoria, vesicular pumice and rare glass shards (beige and fragmented). Pumices and glass shards have a composition ranging from *andesitic* to *dacitic* with a sub-alkaline affinity (HK-Ca/Ca) (Fig. 4.39).

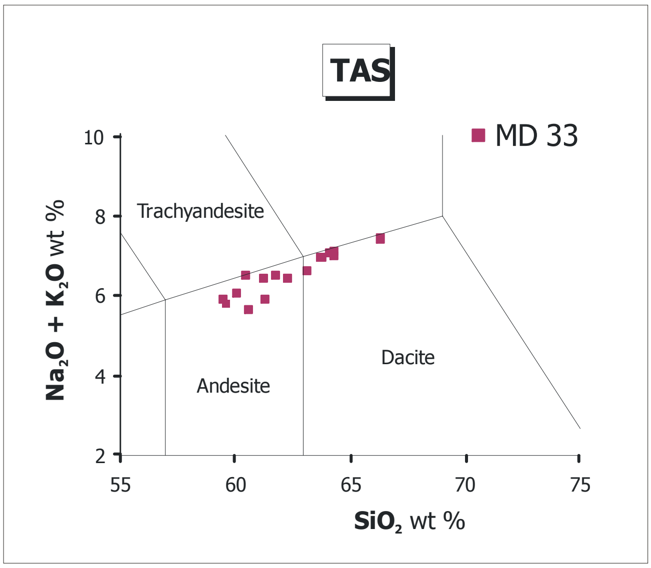

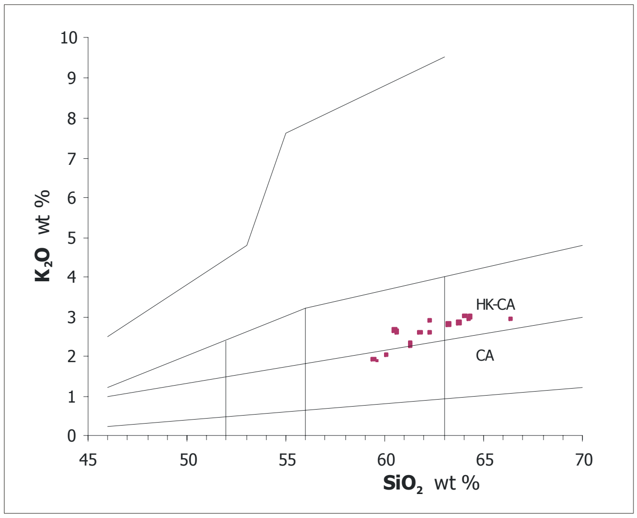

Fig. 4.39 Total alkali versus silica (TAS) diagram for the tephra MD33 on the left and K_2O versus SiO_2 diagram (Le Maitre et al., 1989) on the right. *HK-CA* High-K Calc-Alkaline, *CA* Calc-Alkaline.

Negative correlations between TiO_2 and CaO and positive correlations between K_2O and SiO_2 can be observed (Fig. 4.40).

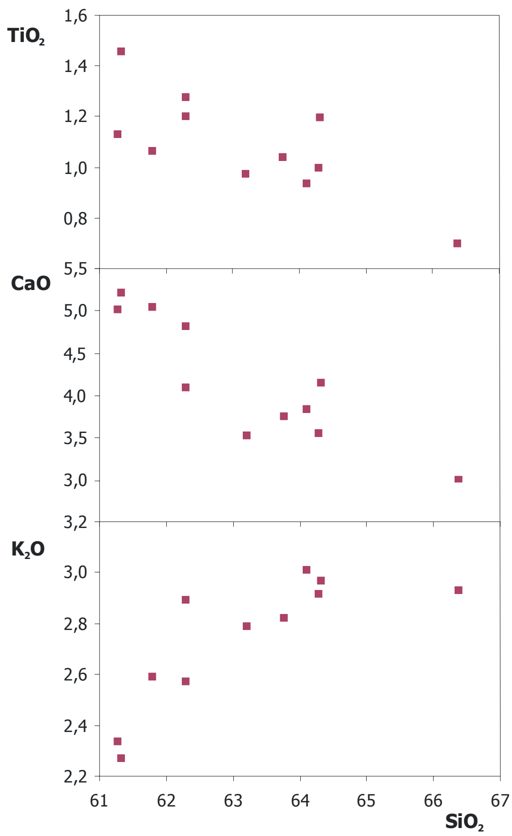

Fig. 4.40 Variation diagrams for major elements (wt %) versus SiO_2.

Trace element normalized pattern evidences troughs of Nb and TiO_2 and less evident Ba, Sr and Sm (Fig. 4.41). REE pattern is fractioned ($[La/Yb]_N$=6.5-14.4) and only two analysis show a slight negative anomaly of Eu (Fig 4.41).

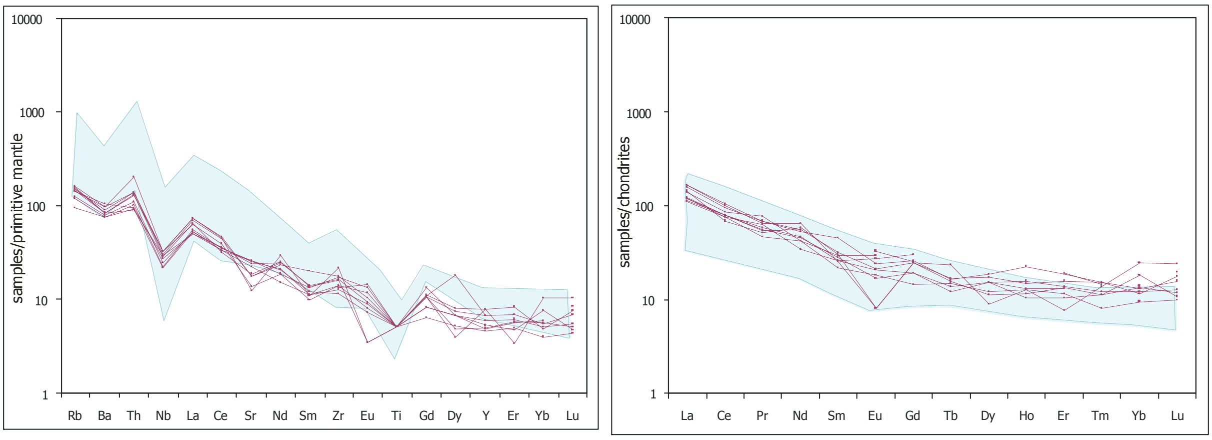

Fig. 4.41 Mantle-normalized trace elements patterns for **MD33** on the left, Chondrite-normalized REE patterns on the right. Symbols: violet lines data from this work; blue filed for **Salina** on land data from literature (Ellam et al., 1989; Francalanci et al., 1993; Gertisser & Keller 2000; Calanchi et al., 2002) for comparison.

Combined chemical features of major and trace elements indicate for this tephra an Aeolian origin with characteristics typical of the Salina and Panarea volcanic activity (see Ellam et al., 1989; Francalanci et al., 1993; Gertisser & Keller, 2000; Calanchi et al., 2002 for comparable dataset).

MD35 - The tephra MD35 at 807,5 cm b.s.f. is about 1,5 cm thck. It is made up mainly of light vesicular glass shards. The analysis of the tephra MD 35 exhibits a wide range of composition from *basaltic trachyandesites* to *trachydacites* with shoshonitic affinity (Fig. 4.42).

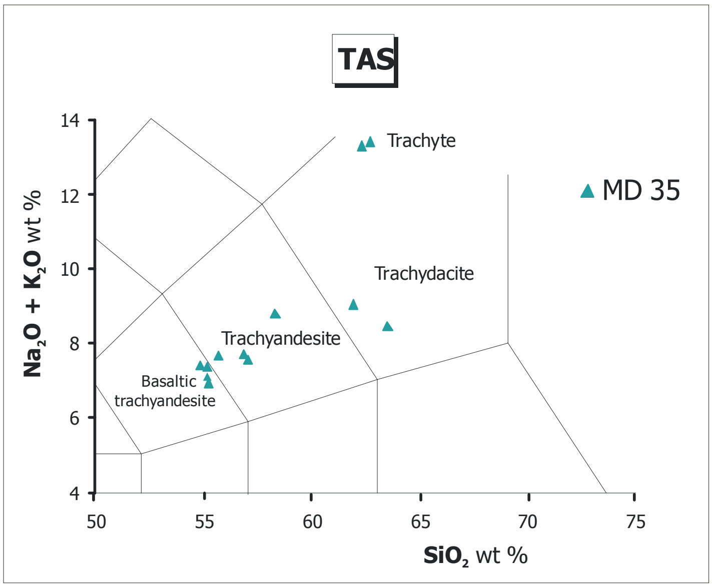

Fig. 4.42 Total alkali versus silica (TAS) diagram for the tephra MD35.

Two points fall in the trachytic field. The MgO, CaO, FeO and P_2O_5 contents show a negative correlations with SiO_2, associated to proportional increase of Na_2O (Fig. 4.43).

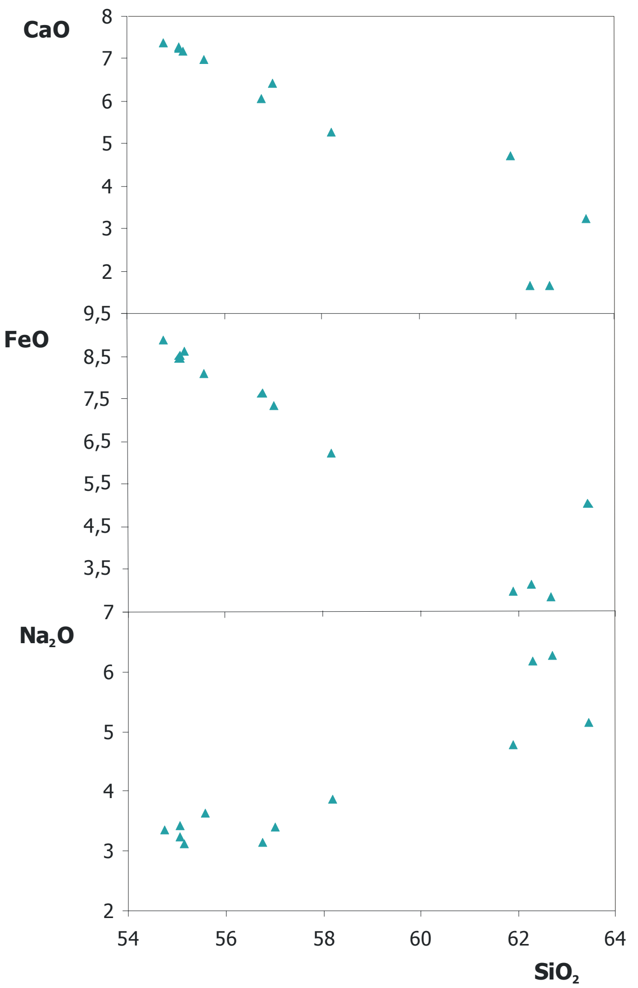

Fig. 4.43 Variation diagrams for major elements (wt %) versus SiO_2.

Trace elements normalized pattern shows a strong decrease of Ba, Sr and TiO_2 related to REE (Th, La, Ce, Nd and Gd) and Zr, with a minor negative spikes of Nb and Sm (Fig. 4.44). REEs are fractioned ($[La/Yb]_N$=7.9-34.7) even if the HREE pattern is quite scattered for analytical problems (Fig. 4.44).

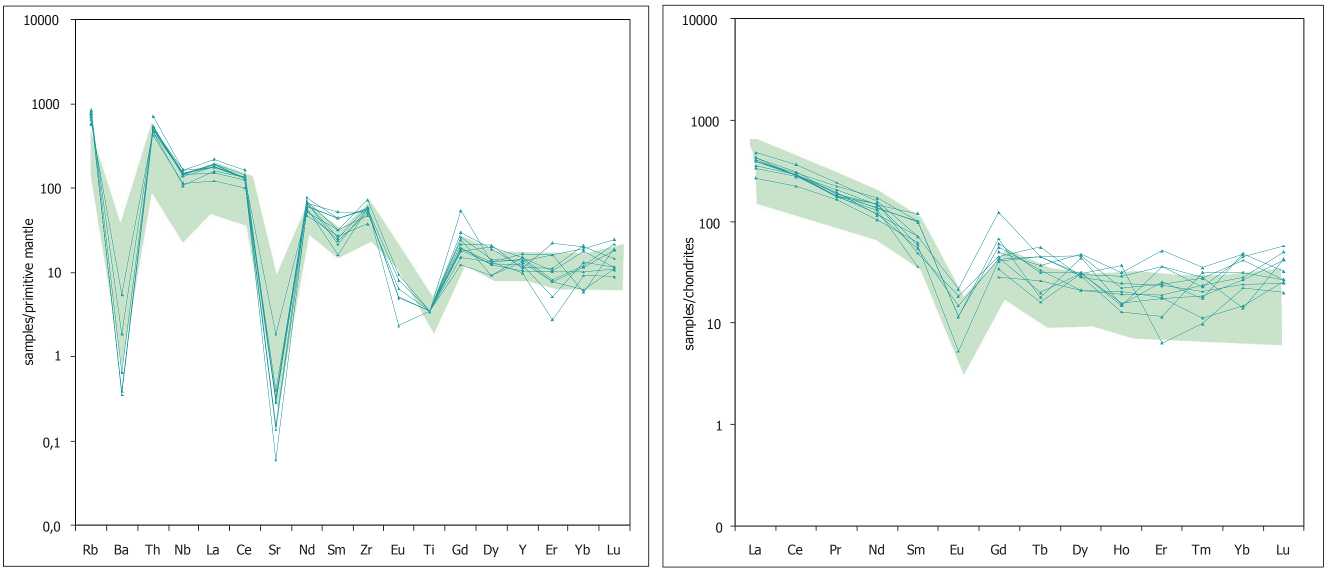

Fig. 4.44 Mantle-normalized trace elements patterns for **MD35** on the left, Chondrite-normalized REE patterns on the right. Symbols: green lines data from this work; green field for **Campanian** on land data from literature (Civetta et al., 1997; D'Antonio et al., 1999; Orsi et al., 1995; Pappalardo et al., 1999) for comparison.

Chemical features of this tephra indicate a Campanian origin (e.g. Civetta et al., 1997; D'Antonio et al., 1999; Orsi et al., 1995; Pappalardo et al., 1999).

4.3 Tephras from the ODP Leg 160 Site 963A core

Core 3H

Tephra **ODP3/5-1** (section 5, Appendix E) is a dark 4 cm thick layer recognised in core 3H. It is represented mostly by light grey glass shards. Major element analysis resulted generally in two compositions (Fig. 4.45): *rhyolitic* for the bottom sample (homogeneous SiO_2 content of 73 wt% with decreasing contents of MnO, Na_2O, K_2O and P_2O_5, Fig. 4.46) and *trachydacitic* for the top one (SiO_2 ranging between 63 and 65 wt%, associated to decreasing percentages of Al_2O_3 and MnO, Fig. 4.46). Glass shards with rhyolitic composition are characterized by a A.I.>1 (*Agpaitico Index* = $(Na_2O+K_2O)/Al_2O_3$ molar) ranging from 1.33 to 1.55. Hence, may be classified as *pantellerites* according to MacDonald classification (Fig. 4.45).

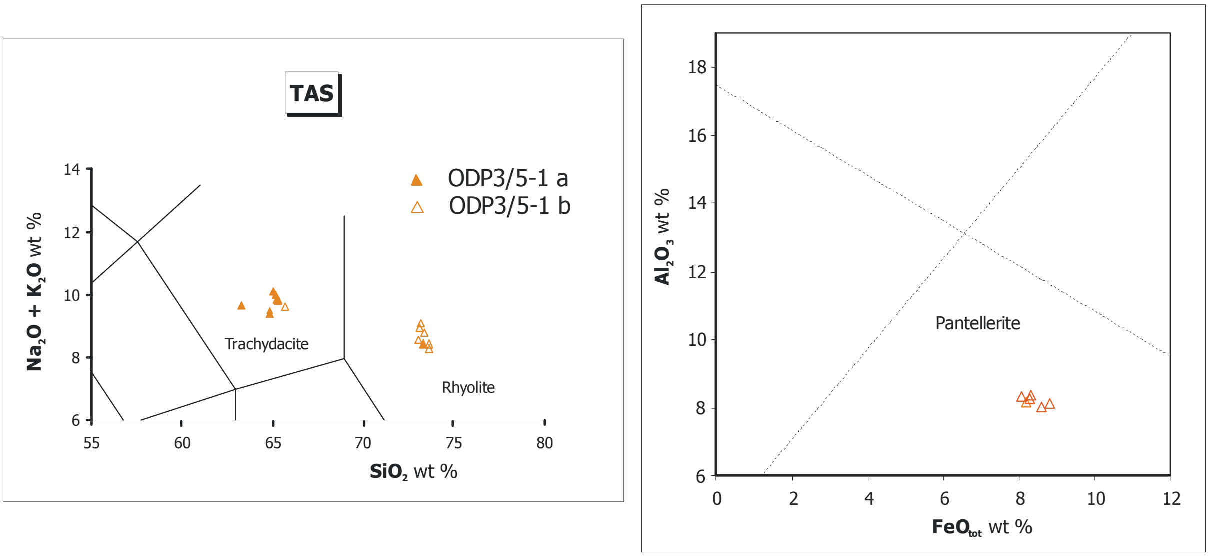

Fig. 4.45 Total alkali versus silica (TAS) diagram for the tephra ODP3/5-1 on the left and Al_2O_3 versus FeO_{tot} (wt %) according to MacDonald (1974).

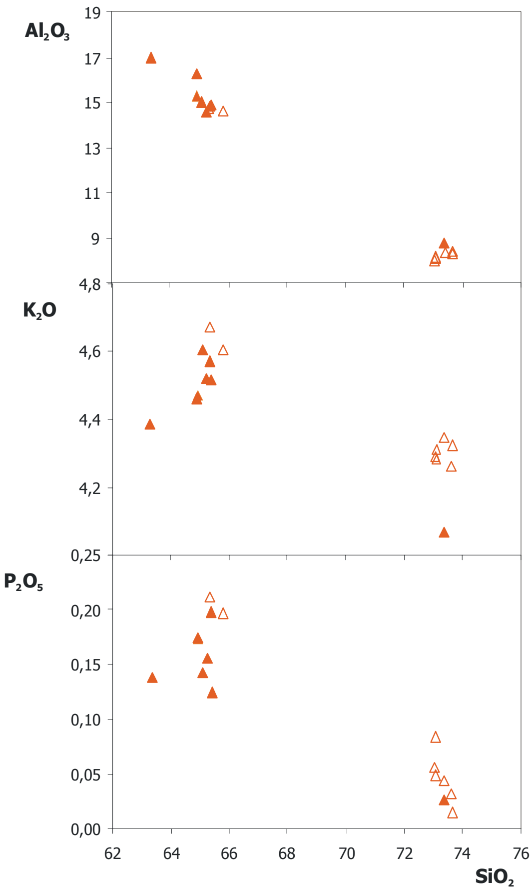

Fig. 4.46 Variation diagrams for major elements (wt %) versus SiO_2.

Pantellerites are characterized by increase of La, Ce and Y (bivariant plots vs Zr in Fig. 4.47), enrichment in LREE compared to HREE ($[La/Yb]_N$=6.6-10) and troughs of Eu (Eu/Eu*=0.4-1), Ba, Sr and TiO_2 (Fig. 4.48).

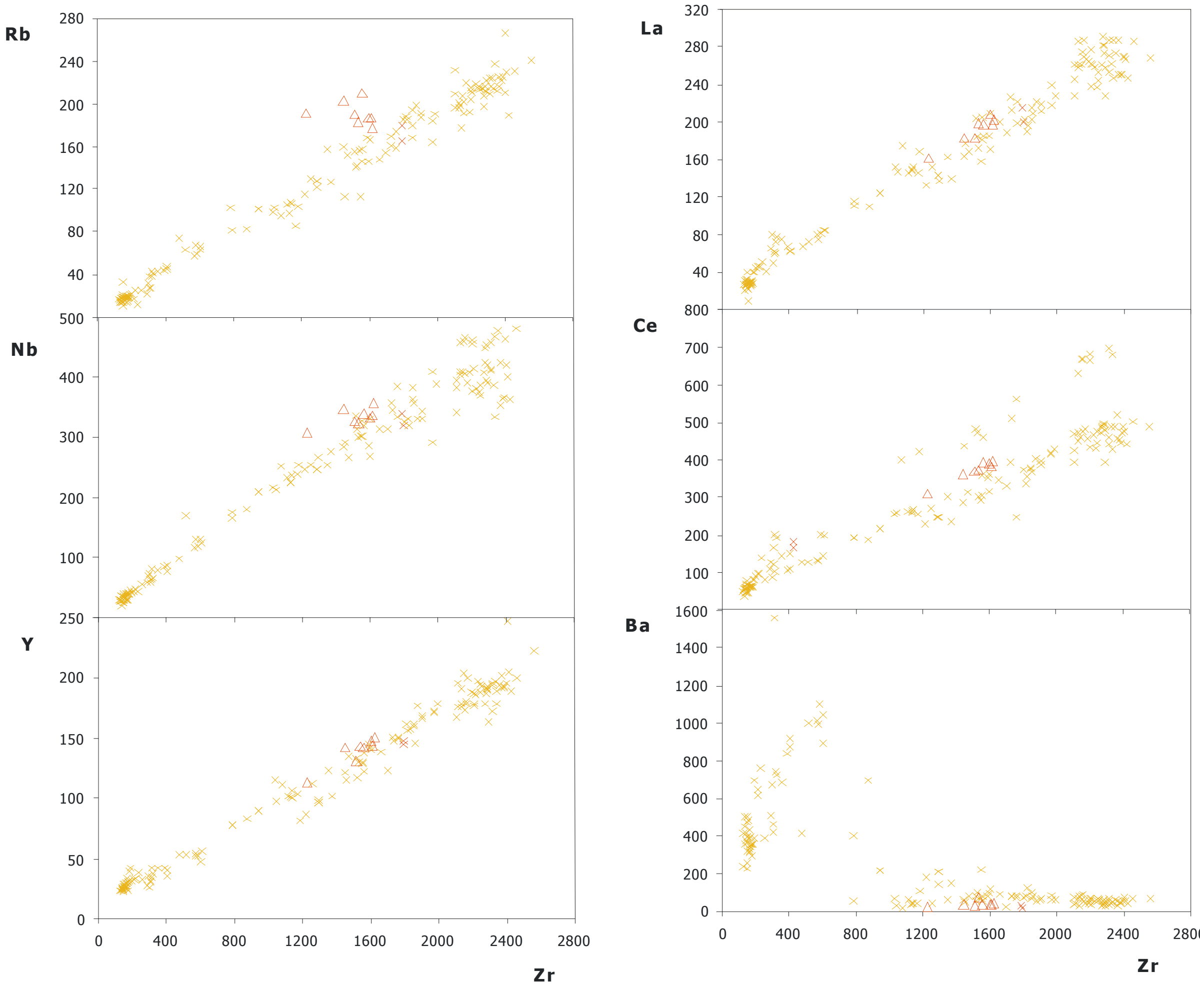

Fig. 4.47 Variation diagrams for trace elements (ppm). Symbols: open orange triangles data from this work; orange crosses for Pantelleria on land data from literature (Avanzinelli et al., 2004; Civetta et al., 1984, 1998; Esperanca et al., 1995) for comparison.

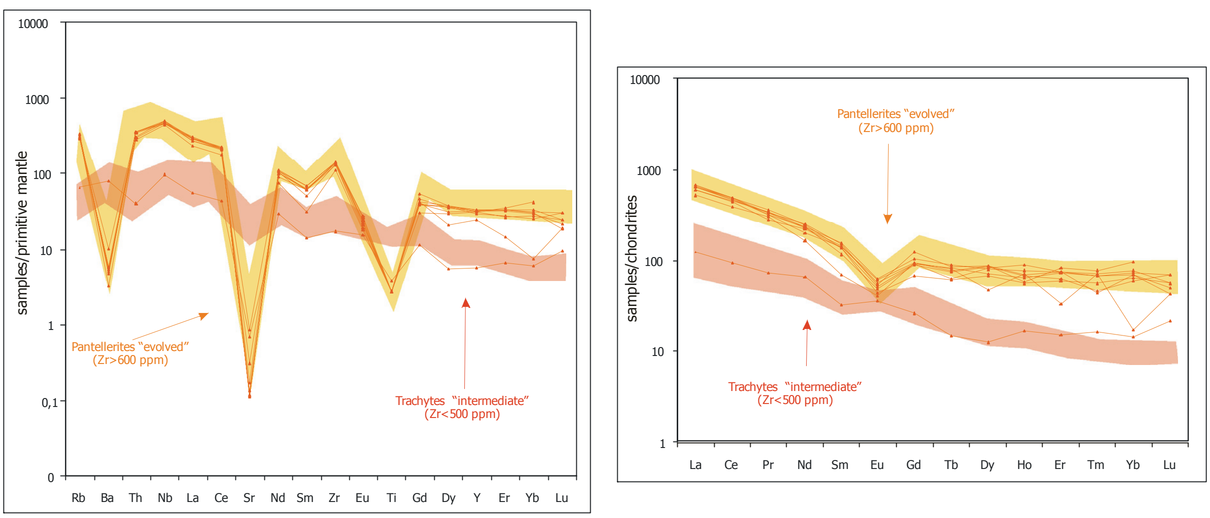

Fig. 4.48 Mantle-normalized trace elements patterns for **ODP3/5-1** on the left, Chondrite-normalized REE patterns on the right. Symbols: orange lines data from this work; orange and red fields for **Pantelleria** on land data from literature (Avanzinelli et al., 2004; Civetta et al., 1984, 1998; Esperanca et al., 1995) for comparison.

Major and trace element contents along with location of the studied core are allow us to correlate this tephra to the volcanic products of the Pantelleria island (see Avanzinelli et al., 2004; Civetta et al., 1984,1998; Esperanca et al., 1995).

Core 6H

The Core 6H is characterized by the presence of several volcanic layers (section 3, Appendix E), generally well distinguishable by naked eyes.

The **ODP6/3-2** tephra layer at 52 cm is a 4 cm thick dark lens. It consists of few dark and yellow glass shards, and loose of Kf crystals. Chemical analyses show a *trachydacitic* composition with a sodic affinity (SiO_2 ranging from 60 to 67 wt%, K_2O between 2.4 and 4.9 wt% and Na_2O between 4.7 and 6.3 wt%, Fig. 4.49).

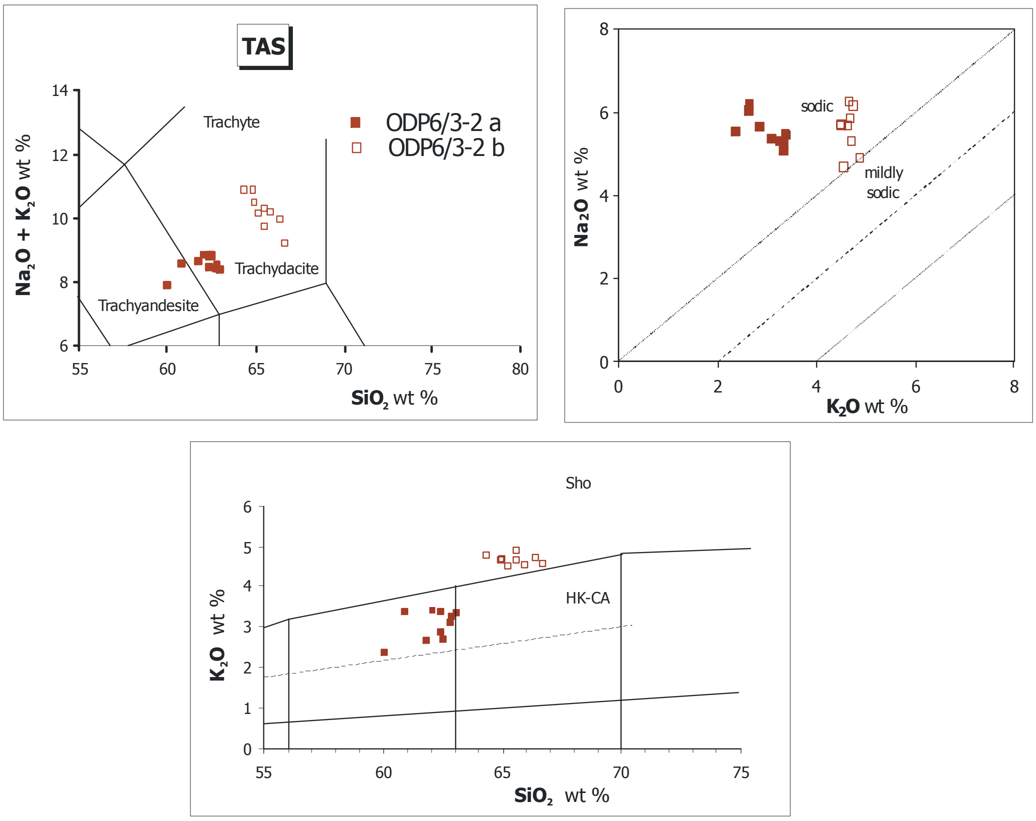

Fig. 4.49 Total alkali versus silica (TAS) diagram for the tephra **ODP6/3-2** on the right, Na_2O versus K_2O diagram on the right and below K_2O versus SiO_2 diagram (Le Maitre et al., 1989). *Sho* Shoshonite, *HK-CA* High-K Calc-Alkaline.

The top of the tephra is characterised by less acid deposits with decreasing contents of CaO (ranging from 4.7 to 3 wt%) and increasing of MgO (ranging between from 1,05 to 1.73 wt%) contents related to increase of SiO_2. The bottom deposits whereas are characterised by compared concentrations of CaO and MgO. Both deposits show decrease of Al_2O_3 contents (ranging between 20.7 and 14.7 wt%) and increase of FeO contents (Fig. 4.50).

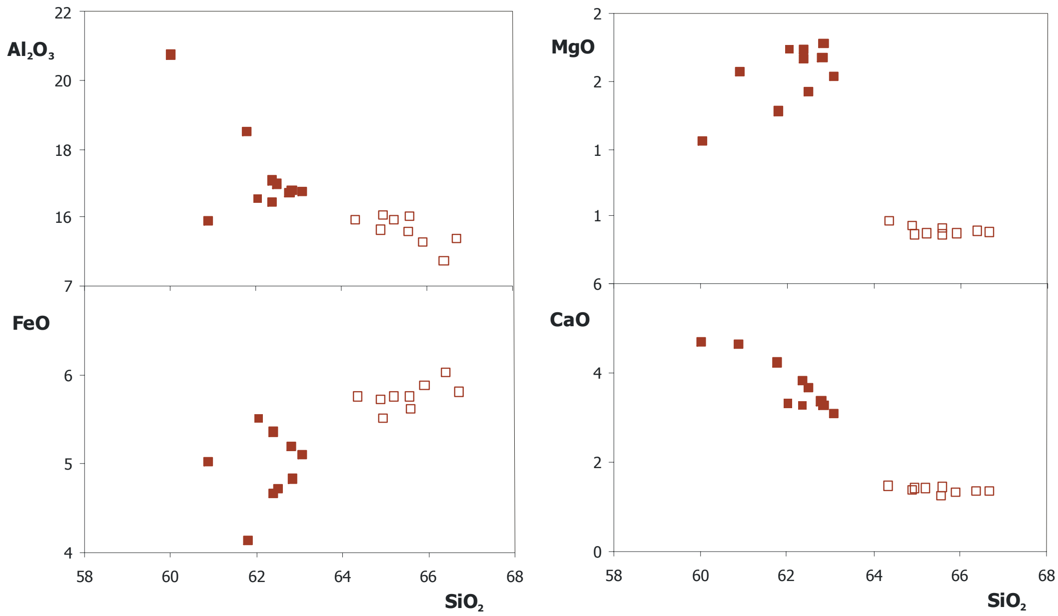

Fig. 4.50 Variation diagrams for major elements (wt %) versus SiO_2.

The trace elements content normalized to primordial mantle and REE content normalized to chondritic values give patterns that evidence the different geochemical behaviour between the top and the bottom part of the deposit (Fig. 4.51).

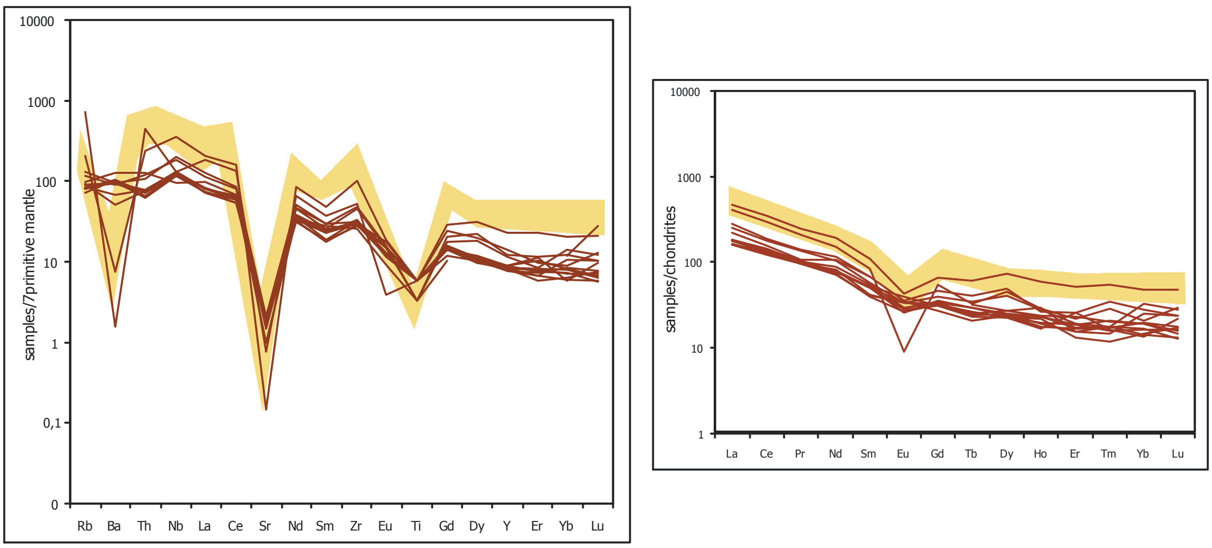

Fig. 4.51 Mantle-normalized trace elements patterns for **ODP6/3-2** on the left, Chondrite-normalized REE patterns on the right. Symbols: red lines data from this work; orange field for Pantelleria on land data from literature (Avanzinelli et al., 2004; Civetta et al., 1984, 1998; Esperanca et al., 1995) for comparison.

The chemical signature of this tephra is similar to the preceding one but shows lower silica and REEs content (Fig. 4.52).

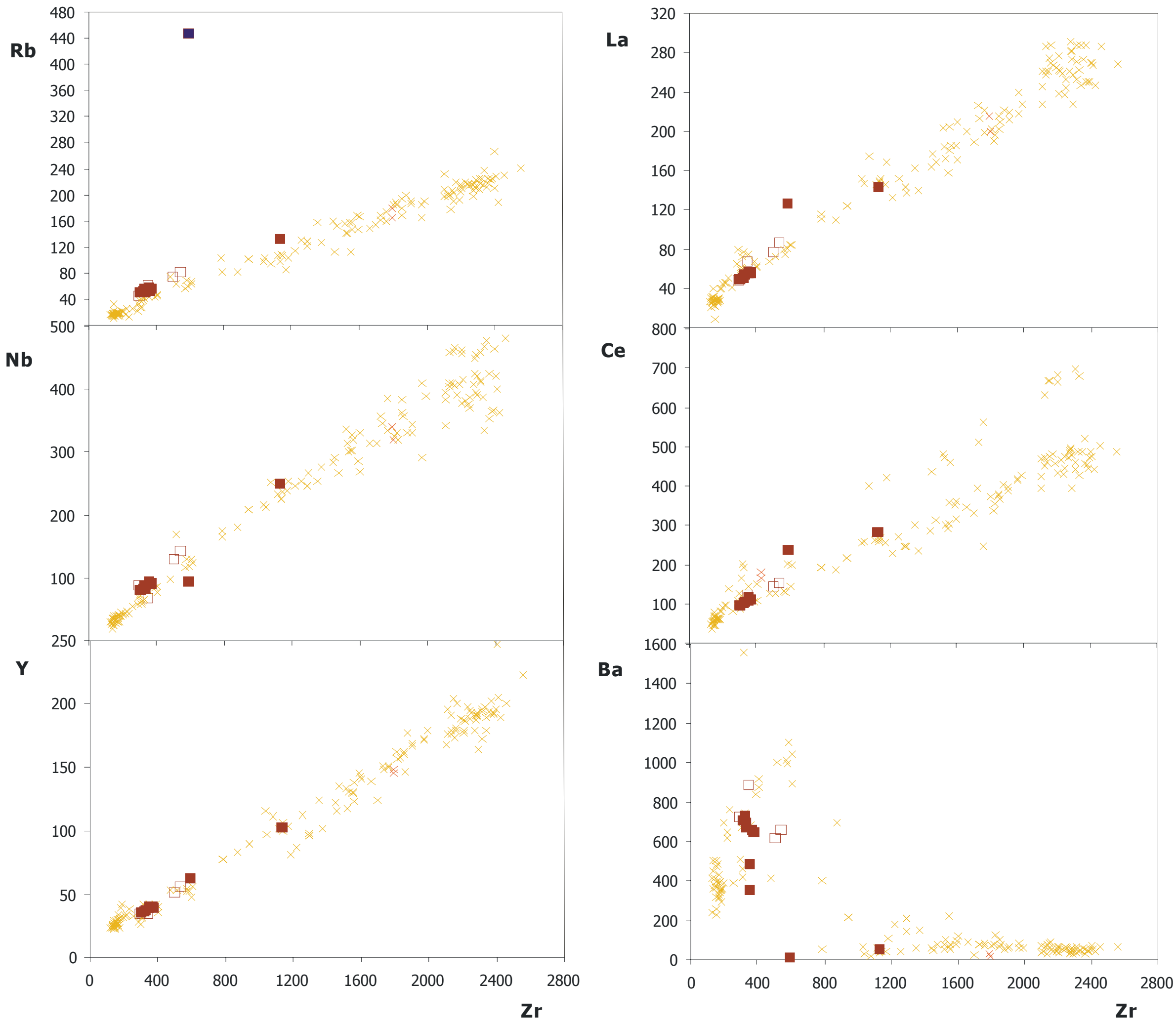

Fig. 4.52 Variation diagrams for trace elements (ppm). Symbols: red open and full squares data from this work; orange crosses for Pantelleria on land data from literature (Avanzinelli et al., 2004; Civetta et al., 1984, 1998; Esperanca et al., 1995) for comparison.

ODP6/3-3 tephra layer is characterised by dark medium-grained volcanic ash. The main volcanic constituents are light pumice with tubular vesicles, brown glass shards, and feldspar crystals. As for the previous tephra two chemical composition were recognised throughout the deposit. As for the preceding tephra two chemical composition were recognised thought the deposit. The bottom part is generally characterized by *peralkaline rhyolites* whereas the top is *trachytic*, but in this case the compositional variability of the top of the tephra is restricted related to tephra ODP6/3-2 (Fig. 4.53).

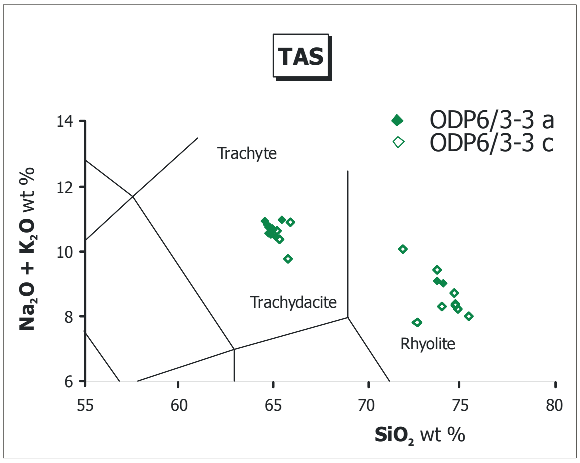

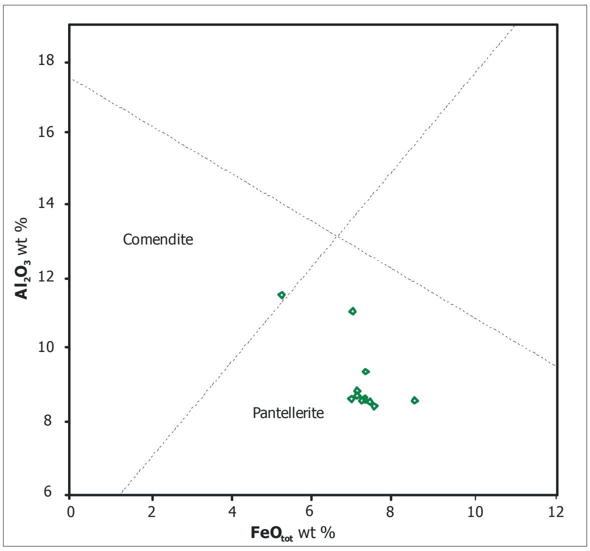

Fig. 4.53 Total alkali versus silica (TAS) diagram for the tephra ODP6/3-3 on the left and Al_2O_3 versus FeO_{tot} (wt %) according to MacDonald (1974) on the right.

At increasing SiO_2, the main feature of the normalized REE patterns are: increase of total concentration of REE, enrichment in light REE relative to heavy REE ($[La/Yb]_N$=6.9-13.8), strong development of the Eu trough (Eu/Eu*=0.3-0.9), small but progressive enrichment of the heavy REE ($[Gd/Yb]_N$=1-2.2) (Fig. 4.54). In particular, the silicic group is characterized by the increasing of REE, Rb, Th, Nb, Zr and Y, and a decreasing of Ba, Sr with increasing differentiation from trachyte to pantellerite, and a common trough of TiO_2 (Fig. 4.54).

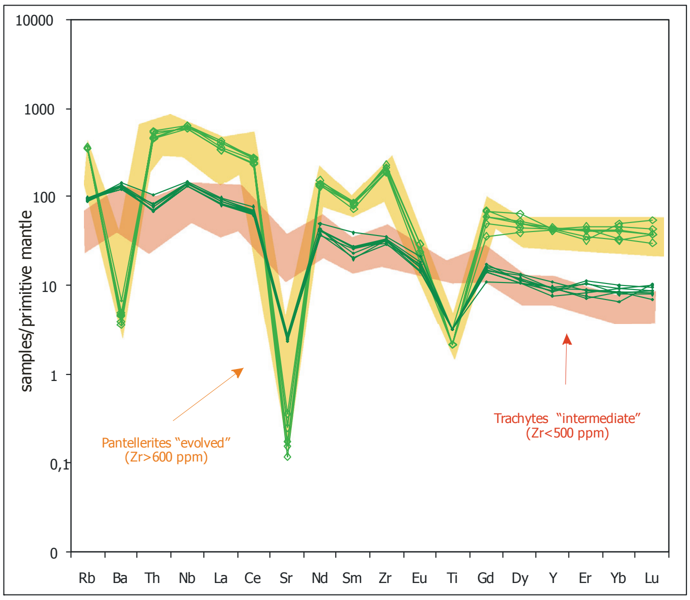

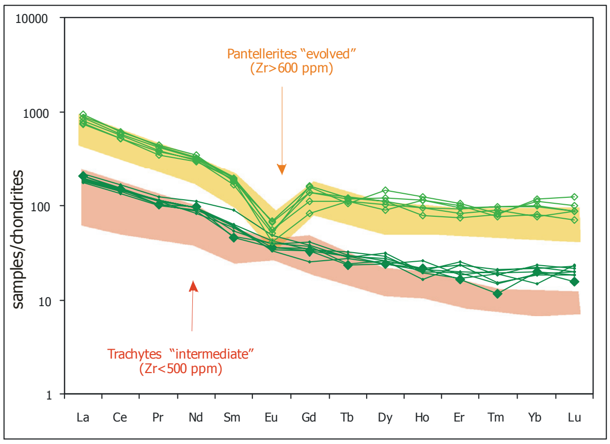

Fig. 4.54 Mantle-normalized trace elements patterns for **ODP6/3-3** on the left, Chondrite-normalized REE patterns on the right. Symbols: green lines data from this work; orange and red fields for **Pantelleria** on land data from literature (Avanzinelli et al., 2004; Civetta et al., 1984, 1998; Esperanca et al., 1995) for comparison.

All these features, along with the analysis of Rb, La, Nb, Ce, Y, Ba vs Zr (Fig. 4.55) to link this tephra to Pantelleria volcano activity (Avanzinelli et al., 2004; Civetta et al., 1984,1998; Esperanca et al., 1995).

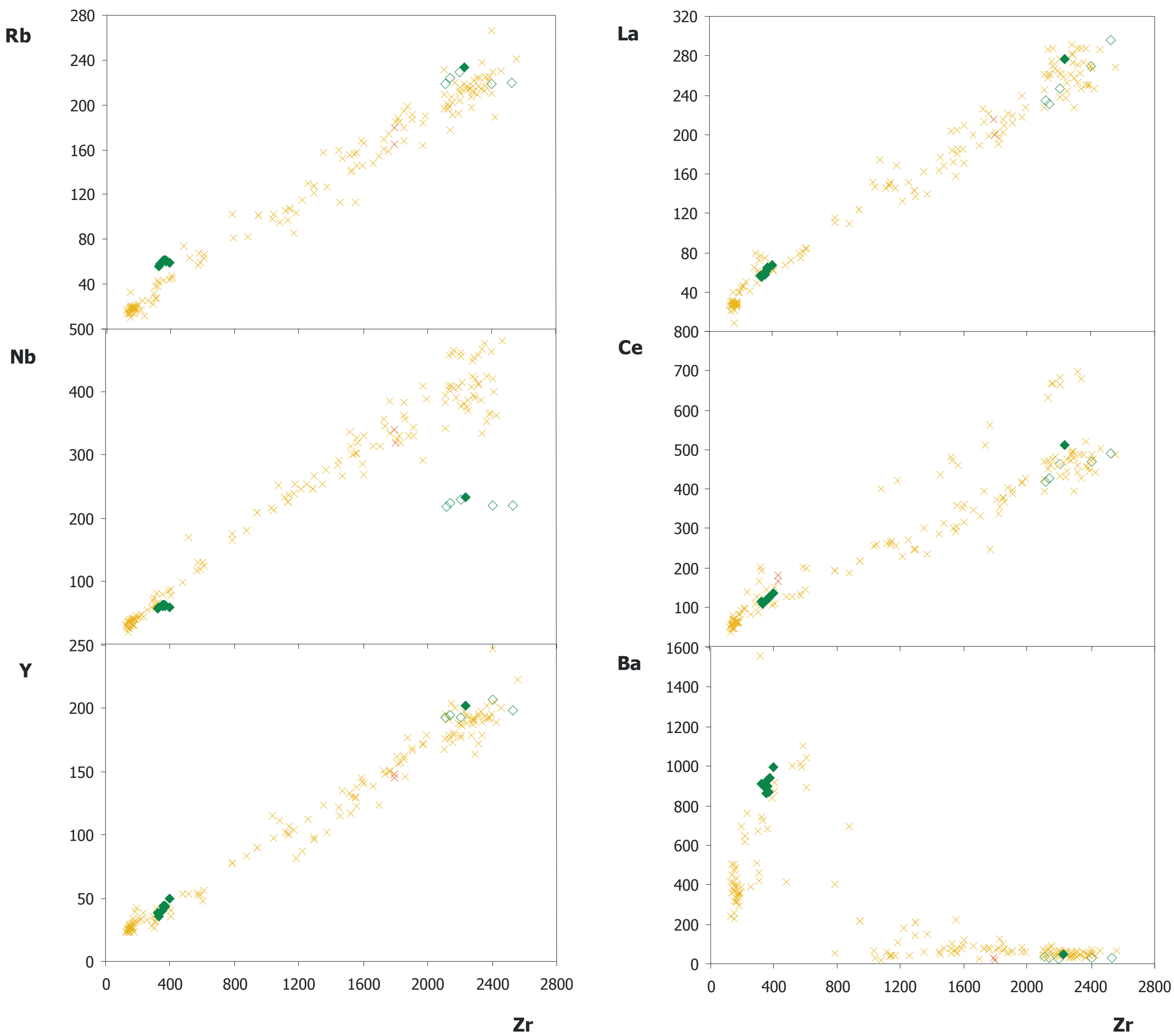

Fig. 4.55 Variation diagrams for trace elements (ppm). Symbols: open and full green rhombuses data from this work; orange and red fields for Pantelleria on land data from literature (Avanzinelli et al., 2004; Civetta et al., 1984, 1998; Esperanca et al., 1995) for comparison.

We grouped in a single layer labelled **ODP6/3-4** several volcanic components invisible by naked eyes from the 47,7 to 48 mbsf of the Site 963 A. The main volcanic elements are light-grey vesicular pumices and light elongated pumiceous glass shards. Some scoria fragments are also present. Chemical analyses indicate a *trachydacitic* and *rhyolitc* composition (Fig. 4.56).

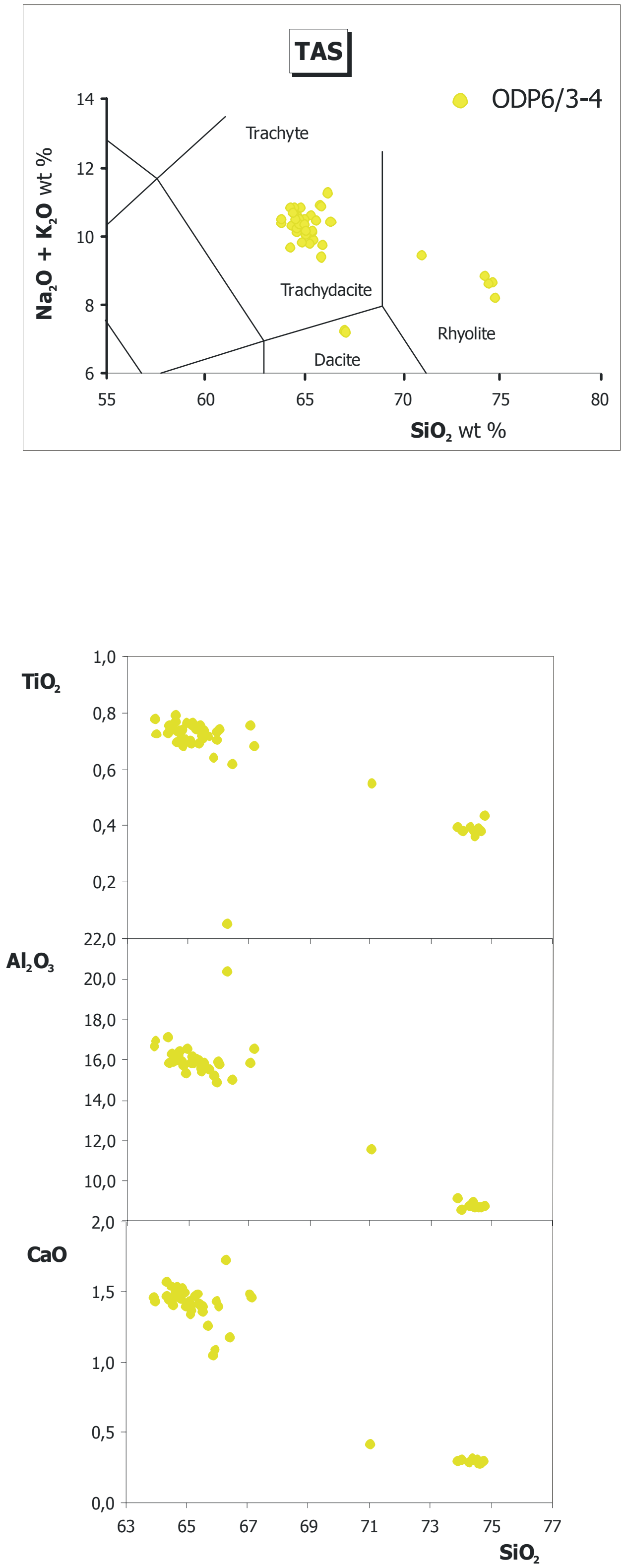

Fig. 4.56 Total alkali versus silica (TAS) diagram for the tephra ODP6/3-4 on the top and variation diagrams for major elements versus SiO_2 (wt %) below.

The great chemical affinity with the tephra layer recorded above, its heterogeneous character, suggest for these deposits a systematic post-depositional action with consequent development of mixture of the ODP6/3-3 tephra layer and not volcanoclastic sediments.

Core 8H

Throughout Core 8H two tephra layers, labelled **ODP8/1-5** and **ODP8/3-6** (section 1 and 3 respectively, Appendix E) were recognised.

The **ODP8/1-5** tephra is made up of pumices with tubular vesicles and grey glass shards. Chemical analysis show a *rhyolitic* composition with peralkaline features (A.I. between 1.1 and 1.4, Fig. 4.57).

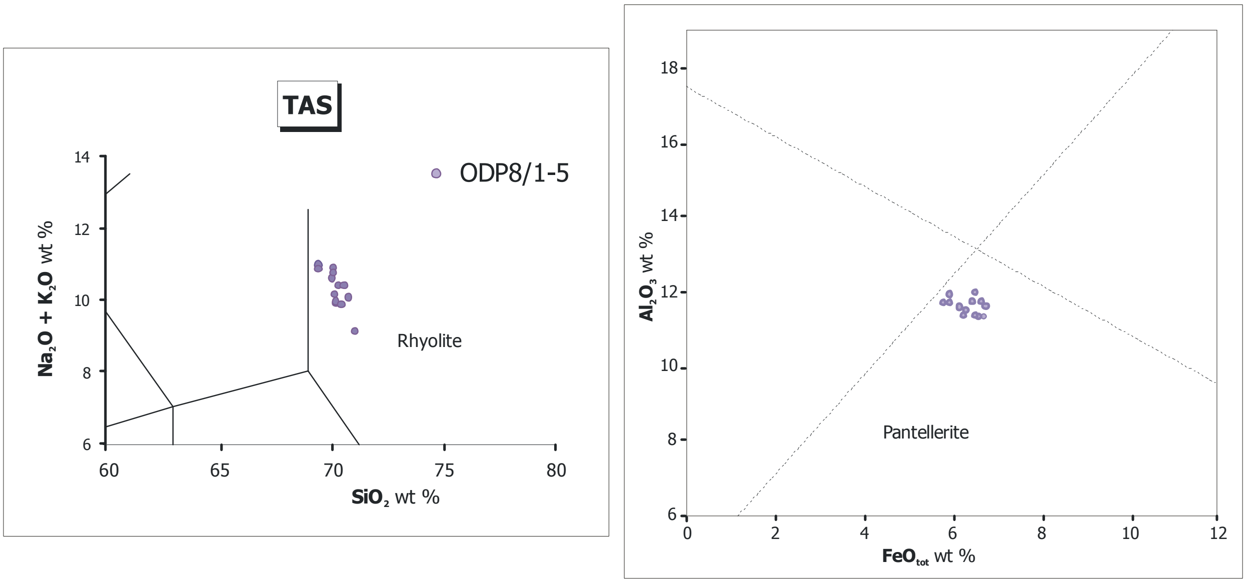

Fig. 4.57 Total alkali versus silica (TAS) diagram for the tephra ODP8/1-5 on the left and Al_2O_3 versus FeO_{tot} (wt %) according to MacDonald (1974) on the right.

Major element analyses show a light decrease of FeO and Na_2O content proportional increase of SiO_2 (Fig. 4.58).

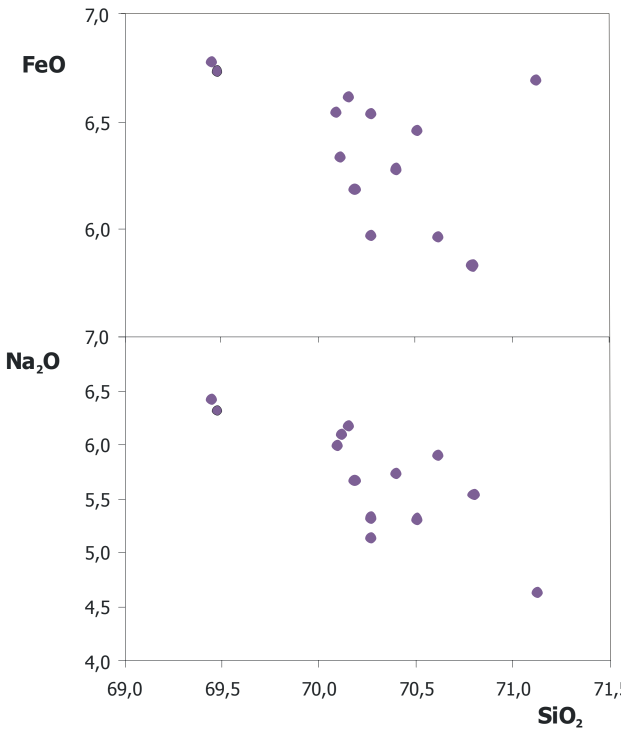

Fig. 4.58 Variation diagrams for major elements versus SiO_2 (wt %).

The trace element content normalized to primordial mantle show pattern characterized by strong decrease of Ba, Sr and TiO_2 (Fig. 4.59). REE content normalized to chondritic values give patterns that show enrichment in light REE ($[La/Sm]_N$=4-5.6) and an evident trough of Eu (Eu/Eu*=0.4-0.5) (Fig. 4.59).

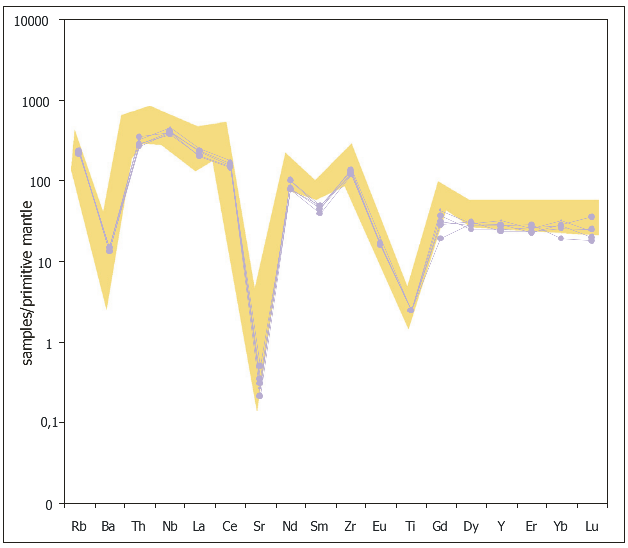

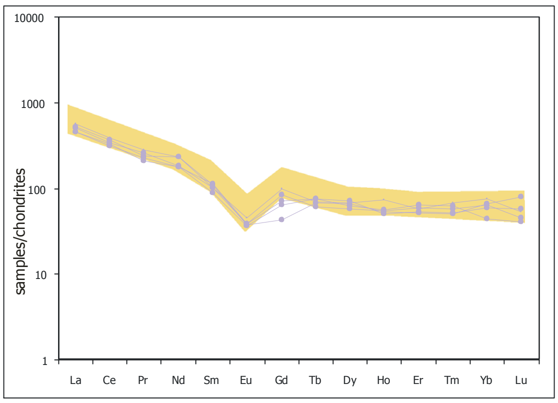

Fig. 4.59 Mantle-normalized trace elements patterns for **ODP8/1-5** on the left, Chondrite-normalized REE patterns on the right. Symbols: lilac lines data from this work; orange field for **Pantelleria** on land data from literature (Avanzinelli et al., 2004; Civetta et al., 1984,1998; Esperanca et al., 1995) for comparison.

The chemical signature of tephra ODP8/1-5 suggest an origin from Pantelleria island as also reported for other tephras at this site (e.g. Avanzinelli et al., 2004; Civetta et al., 1984, 1998; Esperanca et al., 1995).

The **ODP8/3-6** tephra is made up by pumice with tubular vesicles and abundant grey vesicular glass shards. Chemical analyses carried out on glass shards show a *trachyte* composition with peralkaline features (Fig. 4.60).

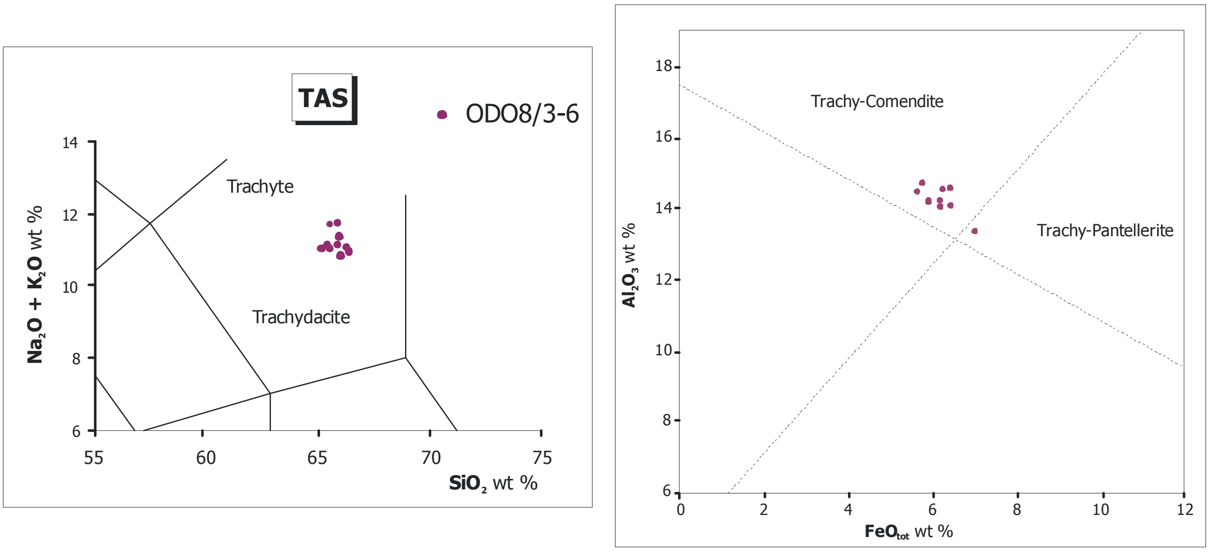

Fig. 4.60 Total alkali versus silica (TAS) diagram for the tephra ODP8/3-6 on the left and Al_2O_3 versus FeO_{tot} (wt %) according to MacDonald (1974) on the right.

Major element analyses show a light decrease of TiO_2 and CaO content proportional increase of SiO_2 (Fig. 4.61).

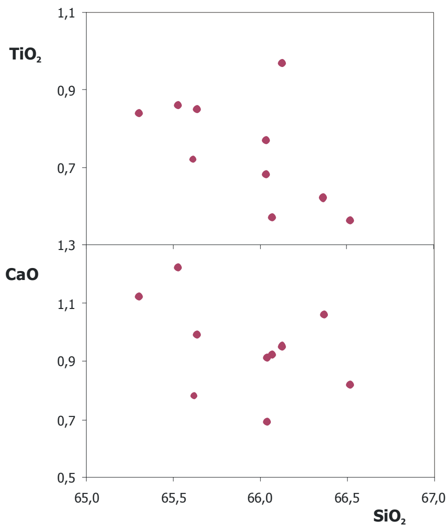

Fig. 4.61 Variation diagrams for major elements versus SiO_2 (wt %).

Trace elements contents normalized to primordial mantle give patterns with troughs of Ba, Sr and TiO_2 (Fig. 4.62), while the REE pattern shows moderate fractionation of LREE in respect to HREE ($[La/Yb]_N$=7.2-13.5) a slight trough of Eu (Eu/Eu*=0.4-0.8).

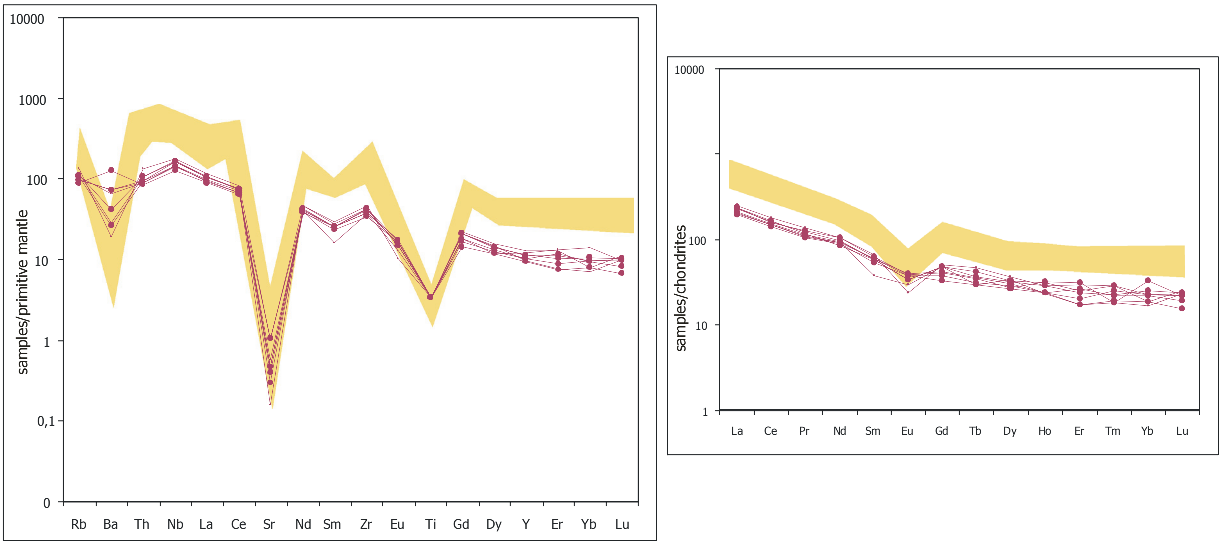

Fig. 4.62 Mantle-normalized trace elements patterns for **ODP8/3-6** on the left, Chondrite-normalized REE patterns on the right. Symbols: violet lines data from this work; orange field for **Pantelleria** on land data from literature (Avanzinelli et al., 2004; Civetta et al., 1984, 1998; Esperanca et al., 1995) for comparison.

The chemical signature of this tephra is similar to all preceding tephras and suggest an Pantelleritic origin (e.g. Avanzinelli et al., 2004; Civetta et al., 1984,1998; Esperanca et al., 1995).

5 The age models

5.1 Age model for KC01B core

A new integrated oxygen isotope chronology and sapropel-based astronomical timescale for the last 1.1 Myr of the Mediterranean basin has been recently proposed by Lourens (2004) by comparing high-resolution colour reflectance records of KC01B and KC01 cores (Calabrian Ridge, Ionian Sea) with a modified spliced high-resolution colour reflectance record of **O**cean **D**rilling **P**rogram Leg 160 Site 964 (in particular Hole A, Hole B, Hole D, Hole E and Hole F data from Emeis et al., 1996) (Fig. 1a and 1b in Lourens, 2004). Astronomical tuning of the sedimentary record is based on the $La90_{1,1}$ (Laskar, 1990) 65°N summer insolation target curve including present-day values for the tidal dissipation by the Sun and Moon and dynamical ellipticity of Earth. The age model for the S1-S12 sapropels interval resulted refined with differences in age of few thousand years compared with previous age models.The sapropel chronologies proposed for KC01B and ODP 964 follows the method described by Lourens et al. (1996). In addition to the sapropel midpoints, Langereis et al. (1997) used sapropel-related signals (on the basis of rock-magnetic and geochemical properties) for refining the age model of KC01B. The proposed ages for the sapropels (and sapropel related signals) of KC01B and ODP Site 964 are compared in Table 5.1.

Sapropel Chronology [a]							
KC01B [b]				ODP 964 [c]			
Level,[d] m	Sapropel	Si Cycle	Age $_1$, kyr	Leve,[d] ccd	Sapropel	i Cycle	Age $_2$, kyr
0.000	top		8	0.000	top		0
	S1 ?	Si2		0.691	SAP 1	2	8
	S3 ?	Si8	81				81
6.840	X, below S3			5.675	X	8	
7.805	S4	Si10	102	6.674	SAP 2	10	102
8.780	S5	Si12	124	7.470	SAP 3	12	124
11.950	S6	Si16	172	10.470	SAP 4	16	172
12.873	S7	Si18	195	11.553	SAP 5	18	195
13.460	S8	Si20	217	12.218	SAP 6	20	217
14.046	S9	Si22	240	12.868	SAP 7	22	240
15.740	S'	si26	288	14.794	Y		
16.833	S10	Si30	331	15.903	Z		
19.265	S11	Si38	407	18.860	SAP 8	38	407
21.715	S12	Si44	461	21.735	SAP 9	44	461
22.850	Sa	Si50	529	23.043	SAP 10	46	483
24.005	S*	si54	575	24.283	SAP 11	54	575
24.390	Sb	Si56	597	24.702	SAP 12	56	597
25.025	*	si58	618	25.600			
28.870	*	si74	785	29.030			
30.440	*	si82	862	30.800			
	*	si86	908 [e]				
32.455	S"	si90	955	33.060	SAP 13	90	955
32.895	Sc	Si92	976	33.577	SAP 14	92	977
33.315	*	si94	997	34.009	SAP 15	94	997
33.970	*	si96	1027	34.767	SAP 16	96	1027
	*	si98	1048 [e]				
34.933	Sd	Si100	1070	35.725	SAP 17	100	1070
	*	si102	1091 [e]				
36.000	*	si104	1111	36.656	SAP 18	102	1091
	*	si108	1144[f]				
36.950	base						
				38.212	SAP 19	104	1111

a) Age calibration points are based on revised sapropel midpoints (m) and refer to the age of their correlative 3 kyr lagged insolation maxima.
b) From Langereis et al. (1997).
c) From Emeis et al. (2000).
d) Levels in meters refer to the modified piston depths of KC01B and corrected composite depth of ODP 964 as used in Lourens (2004)
e) Levels were excluded as calibration points.

Tab. 5.1 Sapropels chronology for KC01B and ODP Leg 160, Site 964 sedimentary records proposed in Lourens (2004).

Marked by low colour reflectance values, a total of 33 tephra layers (Ionian, I1–I33) were detected throughout the KC01B core by Lourens (2004). In Tab. 5.2 the corrected composite depths and associated astronomically tuned ages are reported for tephras of KC01B and ODP Leg 160, Site 964 cores.

Tephra Chronology of KC01, KC01B and ODP Site 964						
Tephra	KC01B		KC01		ODP 964	
Ionian	Level,[a] m	Age_{new}, kyr	Level,[a] ccd	Age_{new}, kyr	Level,[a] ccd	Age_{new}, kyr
I1	1.275	16.7	2.350	16.9	1.283	17.3
I2	3.370	34.1	4.505	35.8	2.465	34.7
I3	3.835	39.1	4.950	40.0	2.706	38.3
I4	4.930	52.6	6.245	52.9	3.972	57.0
I5	5.430	59.5	6.800	58.7	4.215	60.6
I6	6.240	71.8	7.910	70.8	4.965	71.7
I7	6.840	82.8	8.930	82.8	5.675	82.8
I8	7.490	95.1	9.710	93.8	6.324	94.5
I9	8.205	110.5	10.520	108.2	6.932	108.5
I10	10.160	142.9	12.410	142.1	8.592	142.0
I11	10.760	150.8			9.247	152.4
I12	11.010	154.5			9.439	155.5
I13	11.410	161.9	13.090	161.6	9.825	161.7
I14	11.690	167.2	13.420	168.2	10.210	167.8
I15	11.930	171.6	13.590	171.6	10.576	174.3
I16	12.720	191.2	14.335	191.2	11.385	191.4
I17	14.035	238.5	15.485	239.0	12.849	238.3
I18	14.255	245.0	15.685	244.9	13.099	246.0
I19	14.975	265.9	16.335	264.1	13.889	269.9
I20	16.540	319.5	17.845	319.7	15.449	313.4
I21	17.715	358.6	18.955	357.8	16.950	357.9
I22	18.125	371.4	19.360	370.4	17.443	370.6
I23	19.645	421.7	20.900	421.9	19.456	426.7
I24	20.285	446.6	21.510	446.9	20.014	445.1
I25	20.425	452.0	21.670	453.5	20.206	451.5
I26	20.675	461.7	21.840	460.4	20.36	456.6
I27	21.585	497.0	22.745	497.5	21.552	496.0
I28	23.285	569.2	24.175	566.4	23.514	569.3
I29	24.005	596.0	24.885	595.6	24.264	595.3
I30	24.505	622.4	25.500	622.6	24.822	622.8
I31	34.865	1066.1			35.676	1066.8
I32	35.240	1082.6			36.080	1085.0
I33	36.020	1111. 8			36.666	1111.5

a) Levels in meters refer to the modified piston depths of KC01B and corrected composite depth of ODP Leg 160 Site 964 as used in Lourens 2004

Tab. 5.2 Tephra layers chronology from KC01B and ODP Leg 160 Site 964 sedimentary cores proposed by Lourens 2004.

Timing of each tephra layer was adopted by Lourens (2004) unique tool to indirectely refer tephra nomenclature reported in Keller et al., (1978).

5.2 Age model for the MD01_2474G core

Detailed stable oxygen isotope analyses performed on the planktonic species *Globigerina bulloides* combined to AMS ^{14}C radiocarbon data (3 points) and semi-quantitative analyseis of the planktonic foraminifera allowed us to define a high-resolution age model for the MD01_2474G sedimentary core. The main stratigraphic events (Holocene, Last Glacial Maximum, MIS 3 and MIS 4) were clearly identified along the $\delta^{18}O$ curve (Fig. 5.1).

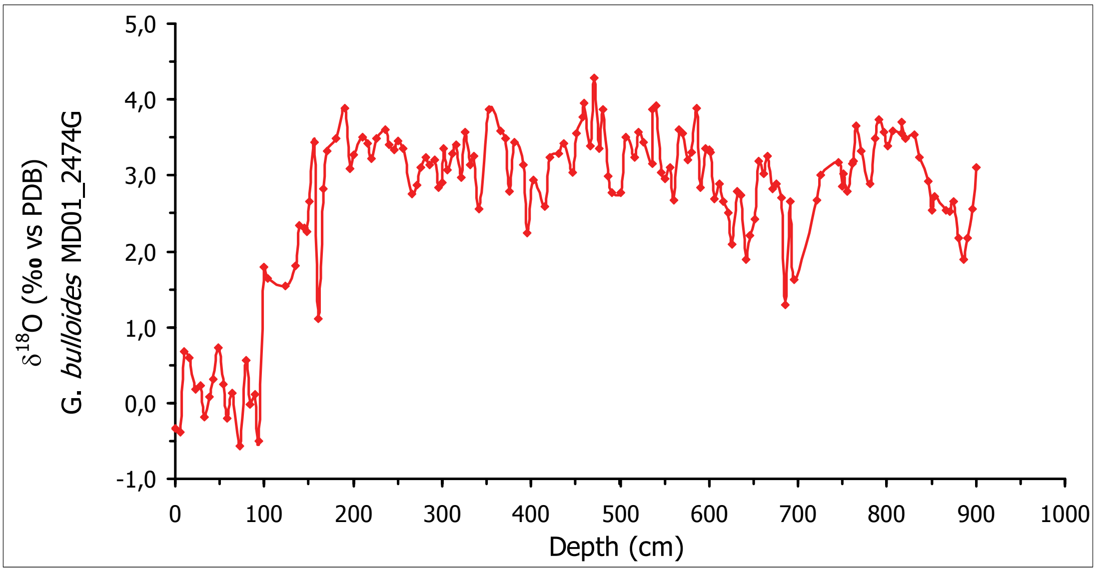

Fig. 5.1 Oxygen isotope record of G. *bulloides* from MD01_2474G sedimentary core plotted *versus* depth (cm).

Moreover, in order to achieve a higher resolution age model, this signal was compared with the oxygen isotope record of the NGRIP ice core (NGRIP members, 2004). Actually, the stratigraphic interval from about 40 and 80 kyr is characterised by the absence of reliable radiometric dating methods suitable for dating of marine sediments. Therefore, the direct comparison of marine stable isotope records with the high-resolution records of the northern ice cores, characterised by an age model based on reliable counting of the annual layering, provides an excellent climate-mediated system to date sedimentary sequences deposited during the MIS3-4 intervals. The oxygen isotopes of the planktonic foraminifers from the MD01_2474G show a remarkable similarities with the $\delta^{18}O$ record from the Greenland GRIP ice core which documents extremely rapid fluctuations in air temperature in the high northern latitudes during the last glacial–interglacial cycle (NGRIP members, 2004) (Fig. 5.2).

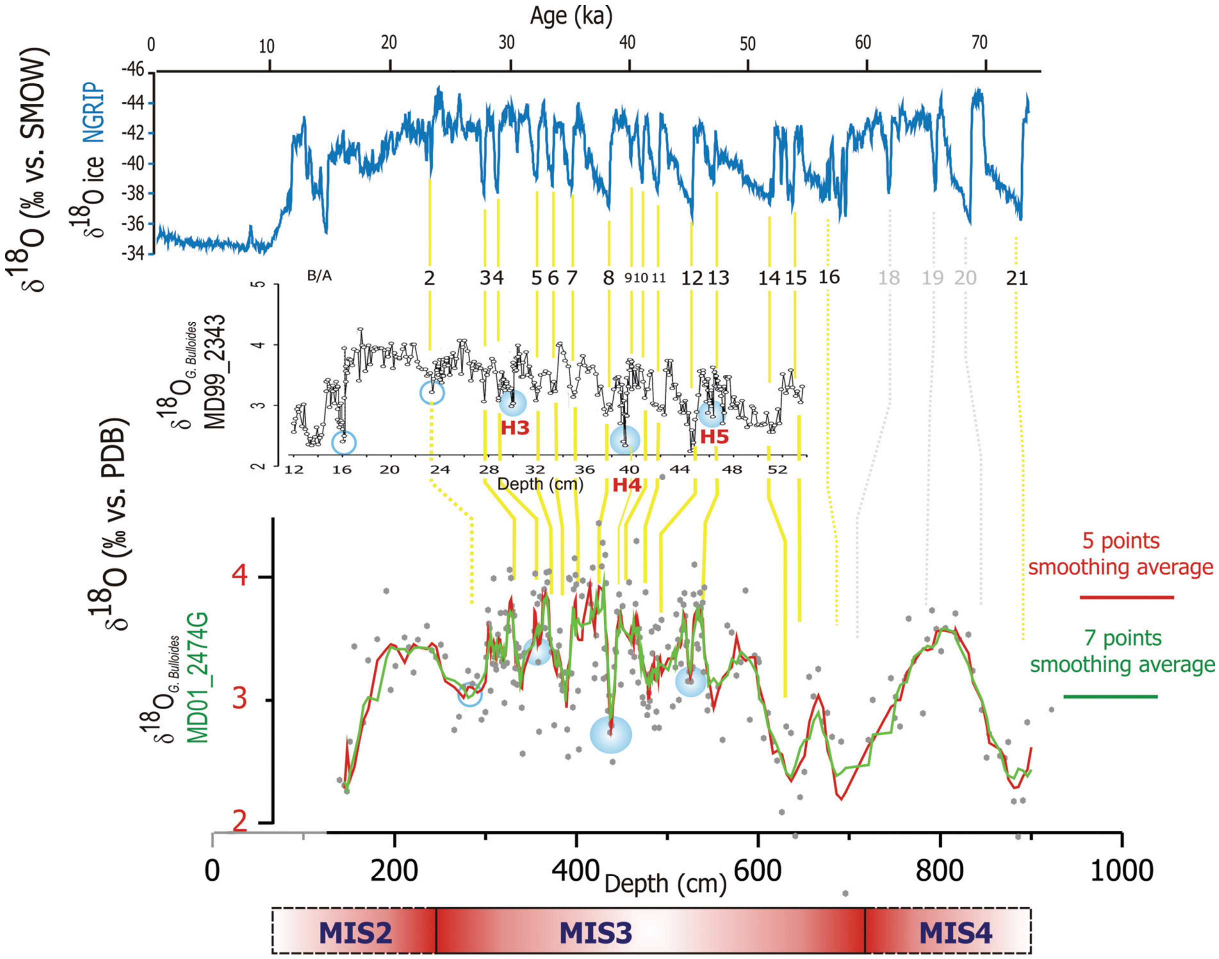

Fig. 5.2 Comparison of the oxygen isotope record of the MD01_2474G core in this study (grey full circles with red and green average lines) with the MD99-2343 (Sierro et al., 2005) and NGRIP (NGRIP members, 2004) isotope signals. Yellow lines correlate D/O interstadials and blue circles correlate Heinrich events.

Thus a peak to peak correlation of the sixteen - Dansgard-Oeschger - Interstadials (D/O) (during the MIS3 and part of the MIS4 intervals, Swenson et al. 2006) recognized at NGRIP with the synchronous abrupt planktonic $\delta^{18}O$ lightening provided the final high-resolution tuning of the studied sedimentary sequence. Four events of strong depletion in the planktonic $\delta^{18}O$ signal were recognized at ~ 12, 29, 39, and 46 kyr and correspond to the massive ice discharges known as Heinrich Events (HE) which occurred in the North Atlantic during some of the coldest stadials at the end of long-term cooling trends including several D/O oscillations as previously reported for coeval Mediterranean records (Sierro et al., 2005).

The list of the tie-points used for constructing the age-depth model is reported in Table 5.3.

Isotope Event , Radiocarbon Dating	Age (years)	Depth (cm)
AMS ^{14}C	4460	28
Base Holocene	10000	100
AMS ^{14}C	13670	151
B/A	14560	156
D/O 2	23303	296
AMS ^{14}C	25080	311
D/O 3	27736	341
D/O 4	28941	359
D/O 5	32123	376
D/O 6	33455	391
D/O 7	35147	403
D/O 8	38201	420
D/O 9	40134	449
D/O 10	41091	460
D/O 11	42486	471
D/O 12	45283	486
D/O 13	46911	506
D/O 14	51607	626
D/O 15	53497	641
D/O 16	56237	686
D/O 21	68720	886

Tab. 5.3 List of the tie-points used for constructing the age-depth model of the MD01_2474G core.

A second, third and fifth-order polynomial is needed to describe the age-depth relationship for the studied record. The first part of the age model (from 29 to 506 cm) comprise the three ^{14}C-AMS data acquired during this research and is well described by a second-order polynomial with an associated 388 yr confidence interval (blue and red lines in Fig. 5.3). Below it has been possible to identify an abrupt increase an average sedimentation rate (from 10cm/1000yr of the preceding part to 30 cm/1000 yr). Visual check of the limited from 506 to 626 cm show a good macth of data with a fifth-order polynomial curve (yellow line in Fig. 5.3). Nonetheless, the age model of this time interval results more problematic for the limited available tie points. The last part of the age model, from 626 to 886 cm, is well fitted by a second-order polynomial curve with an associated 269 yr confidence interval and an average sedimentation rate of 20cm/1000yr (blue line in Fig. 5.3). In Tab. 5.4, 5.5 and 5.6 are reported the statistical functions used for the construction of the age model for the MD01_2474G core.

					2° order polynomial						3° order polynomial			
EVENT	Age (years)	Depth (cm)	Estimated age (2° order)	Calculated error	Relevance level (α)	Standard Deviation of Population (σ)	Population	Confidence interval (±)	Estimated age (3° order)	Calculated error	Relevance level (α)	Standard Deviation of Population (σ)	Population	Confidence interval (±)
^{14}C	4460	29	5791	-1331	0,05	815	17	**388**	4856	-396	0,05	809,9	17	**385**
Base Holocene	10000	100	9514	486					9864	136				
^{14}C	13670	151	12710	960					13307	363				
B/A	14560	156	13047	1513					13644	916				
D/O 2	23303	296	24180	-877					23790	-487				
^{14}C	25080	311	25567	-487					25026	54				
D/O 3	27736	341	28455	-719					27630	106				
D/O 4	28941	359	30261	-1320					29287	-346				
D/O 5	32123	376	32016	107					30925	1198				
D/O 6	33455	391	33605	-150					32432	1023				
D/O 7	35147	403	34903	244					33683	1464				
D/O 8	38201	420	36783	1418					35527	2674				
D/O 9	40134	449	40102	32					38884	1250				
D/O 10	41091	460	41398	-307					40231	860				
D/O 11	42486	471	42715	-229					41621	865				
D/O 12	45283	486	44542	741					43588	1695				
D/O 13	46911	506	47038	-127					46345	566				

					5° order polynomial			
EVENT	Age (years)	Depth (cm)	Estimated age (5° order)	Calculated error	Relevance level (α)	Standard Deviation of Population (σ)	Population	Confidence interval (±)
^{14}C	25080	311	24963	117	0,05	827	15	**418**
D/O 3	27736	341	27618	118				
D/O 4	28941	359	29565	-624				
D/O 5	32123	376	31562	561				
D/O 6	33455	391	33400	55				
D/O 7	35147	403	34893	254				
D/O 8	38201	420	36998	1203				
D/O 9	40134	449	40432	-298				
D/O 10	41091	460	41644	-553				
D/O 11	42486	471	42790	-304				
D/O 12	45283	486	44232	1051				
D/O 13	46911	506	45916	995				
D/O 14	51607	626	50931	676				
D/O 15	53497	641	51406	2091				
D/O 16	56237	686	54175	2062				

					2° order polynomial			
EVENT	Age (years)	Depth (cm)	Estimated age (2° order)	Calculated error	Relevance level (α)	Standard Deviation of Population (σ)	Population	Confidence interval (±)
D/O 14	51607	626	51915	-308	0,05	275	4	**269**
D/O 15	53497	641	53061	436				
D/O 16	56237	686	56370	-133				
D/O 21	68720	886	68714	6				

Tab. 5.4-5.5-5.6 Schematic summary of the statistical data related to the construction of the age model for the MD01_2474G core.

Summarizing, the stable isotope, radiocarbon and bio-stratigraphy of the record implemented by detailed correlation with NGRIP ice core allowed us to define a high-resolution age model for the MD01_2474G sedimentary core from 2 kyr (top of the core) down to about 70 kyr (base of the studied sedimentary interval) (Fig. 5.3 and Fig .5.4).

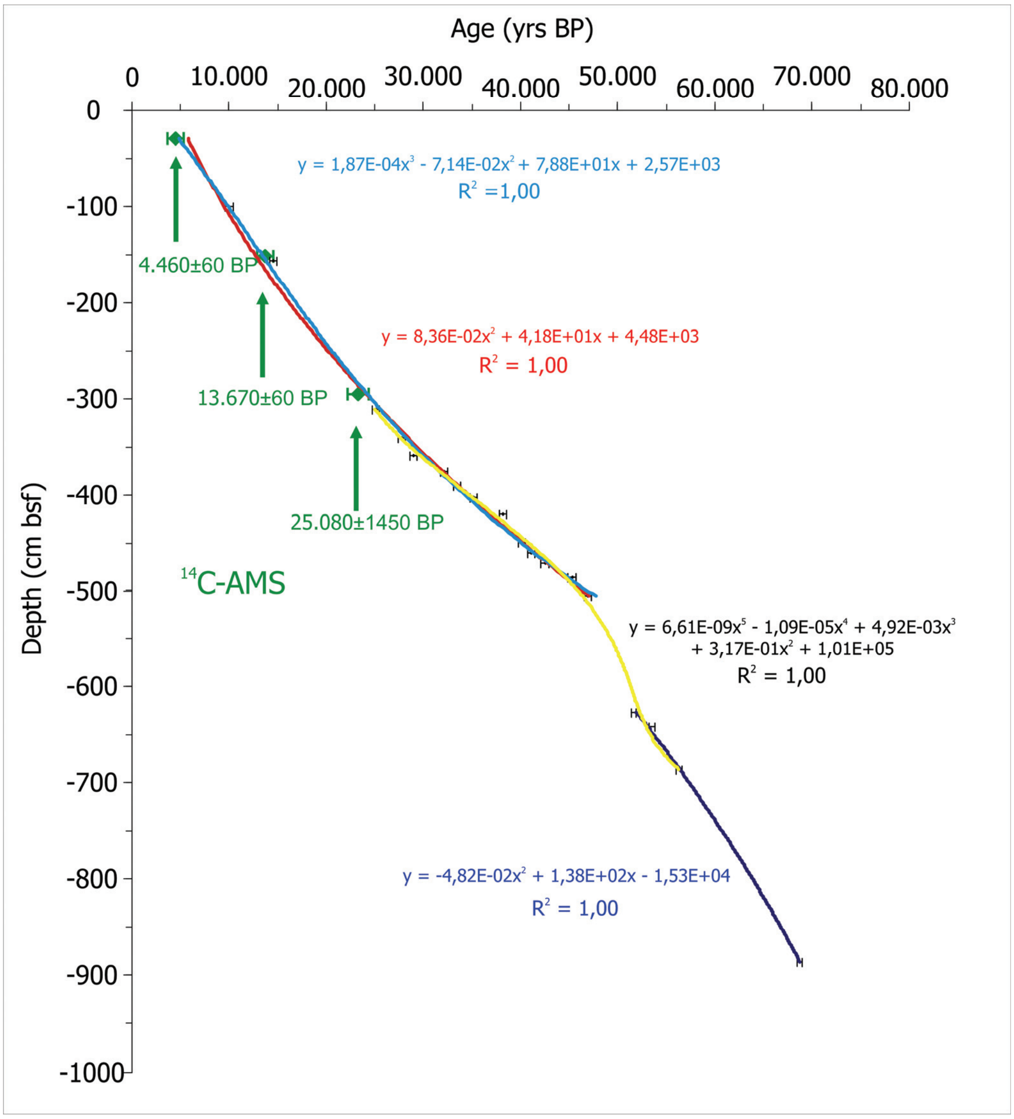

Fig. 5.3 Age model of the MD01_2474G core with three calibrate ^{14}C-AMS data, 2° (blue line) 3° (red line) and 5° (yellow line) order polynomial fitting lines with equations related.

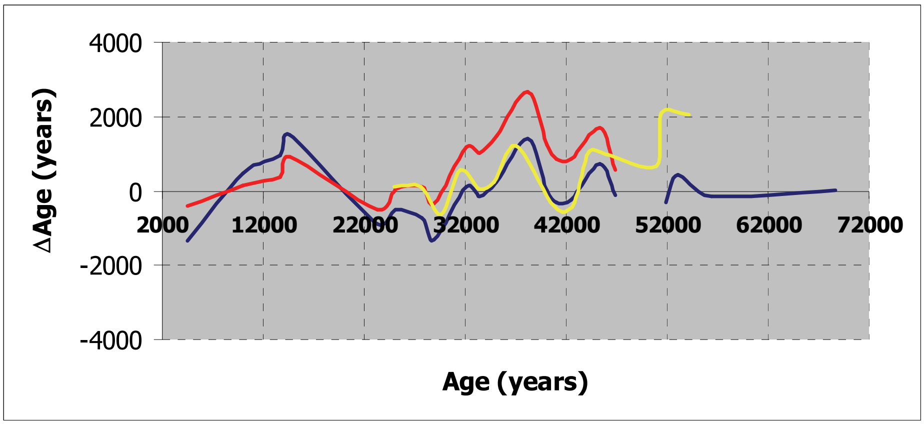

Fig. 5.4 Statistics of the error associated to the calibrated age model of the MD01_2474G record. Blue, red and yellow lines are referred to the 2°, 3° and 5° order polynomial fitting lines, respectively.

5.3 Age models for ODP Leg 160 Site 963A

Core 3H

The age model of this record is described in detail in Sprovieri et al. (*personal comunication*). Hereafter a synthesis of the results and final definition of the chronology of the studied interval is reported.

The age model of the ODP site 963A is constrained at the top by two AMS ^{14}C dates of mixed benthic and planktonic foraminifera. Radiocarbon ages have been transformed into calibrated ages by OxCal v4.0, using the Marine04 curve (Hughen et al., 2004), without any ΔR correction, since the oceanic reservoir correction seems to be suitable even in the Sicily Channel (Siani G., 2005, personal communication). The lower part of the record was tuned by a peak to peak correlation of the high abundances in the *G. ruber* curve and corresponding lows in the $\delta^{18}O_{Np}$ and $\delta^{18}O_{b}$ signals with the 17 D/O Interstadials identified in $\delta^{18}O_{NGRIP}$ curve during the MIS3/MIS4 intervals (Swensson et al., 2006) (Fig. 5.5). The Interstadial 18 was already identified and reported by Sprovieri et al. (2006). This procedure is justified by the fact that the strong link between $\delta^{18}O$ of Greenland ice cores and Mediterranean paleoceanographic proxies has been established in several papers and already exploited for age model assessing (Sprovieri et al., 2006 and references therein).

In order to create the age-depth profile for the whole record, as reference ages were considered the level characterised by the most positive isotope values from each abrupt Interstadial warming phase in the NGRIP ice core (Fig. 5.5). All reference depth levels used to establish the chronology are given in Table 5.7. In particular, the isotope record representing the 20 years means of $\delta^{18}O_{NGRIP}$ with the Greenland Ice Core Chronology GICC05 of Andersen et al. (2006) and Svenson et al. (2006) for the interval 20-42 ky was considered and the isotope signal representing the 50 years means of $\delta^{18}O_{NGRIP}$ of NGRIP members (2004) with the ss09sea chronology for the interval 42-65 ky BP2000.

In Fig. 5.6 the achieved age model is shown with the interpolating thick line reproducing a cubic spline function that ensures limited loss of amplitudes at higher frequencies and reduced bias effect (Schulz & Statteger, 1997). Based on this age model, we estimated an average (throughout the whole record) ~43±14 (1σ) and ~83±36 (1σ) years sampling resolution for the planktonic assemblage and isotope signals, respectively. Once compared to other high-resolution sedimentary records collected from the Mediterranean basin (e.g., Cacho et al., 1999; Sierro et al., 2005) such a sampling frequency is 2 to 5 times better (depending on the time intervals) and therefore offers a unique opportunity to reliably explore climate/ocean evolution of the basin at the century scale.

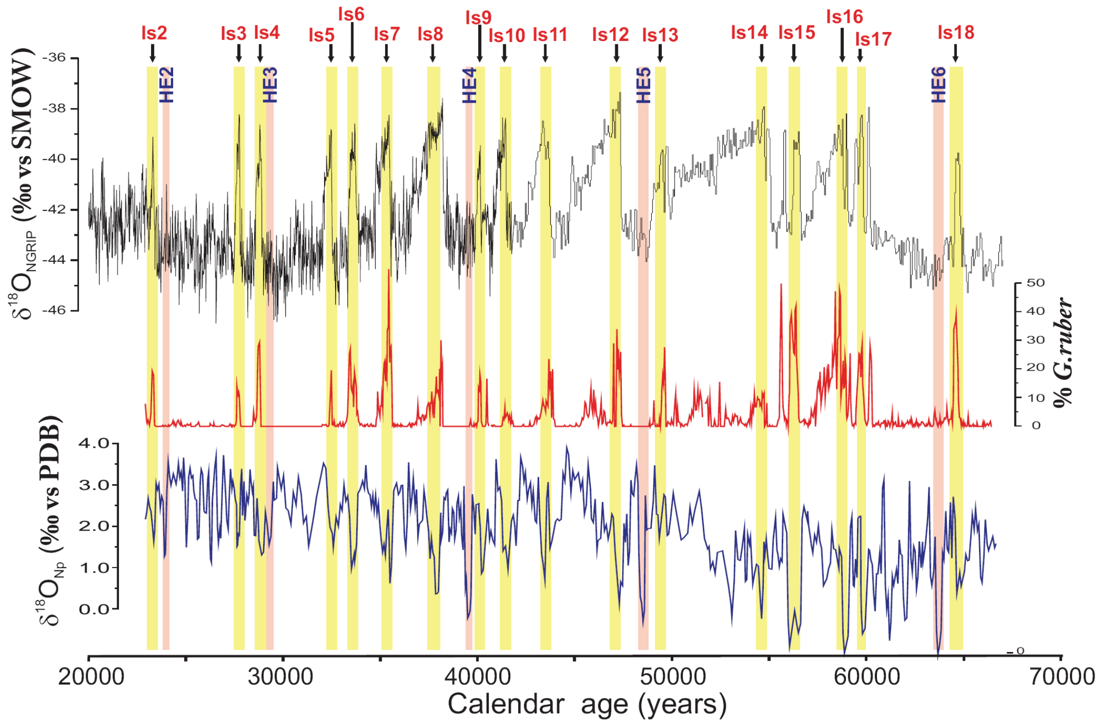

Fig. 5.5 Comparison of the oxygen isotope record and abundance curve of G. *ruber* of the ODP Leg 160, Site 963A core in this study (blue and red lines, respectively) with the NGRIP (NGRIP members, 2004) isotope signals (black lines). Yellow bands correlate D/O interstadials and the pink bands correlate Heinrich events.

Isotope Event/ Radiocarbon dating	Calendar Years	Depth (mbsf)
AMS ^{14}C	18,855±225	6,44
IS-2	23,340±298	9,68
AMS ^{14}C	23,200±650	9,88
IS-3	27,780±416	12,40
IS-4	28,900±449	13,16
IS-5	32,500±566	14,46
IS-6	33,740±606	14,88
IS-7	35,480±661	15,90
IS-8	38,220±724	17,34
IS-9	40,160±790	18,64
IS-10	41,460±817	19,24
IS-11	*43400*	*20,20*
IS-12	*47200*	*21,80*
IS-13	*49650*	*23,16*
IS-14	*54400*	*24,86*
IS-15	*56400*	*26,00*
IS-16	*58650*	*27,06*
IS-17	*59800*	*27,76*
IS-18	*64650*	*30,38*

Tab. 5.7 List of the tie-points used for constructing the age depth model of the ODP Leg 160 Site 963A core.

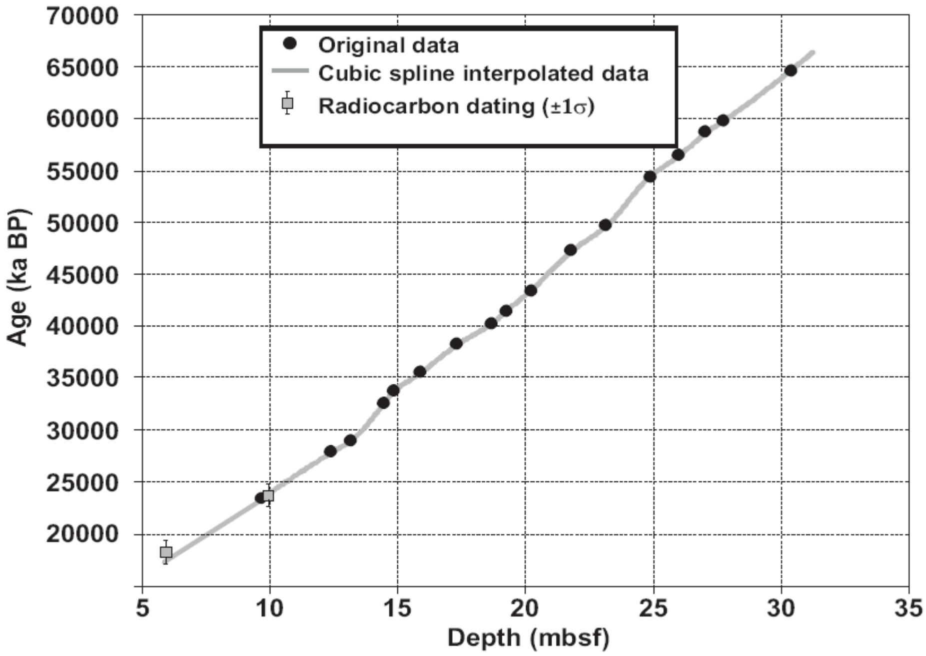

Fig. 5.6 Age model of the ODP leg 160, Site 963A core with two calibrate ^{14}C-AMS data and 5° (grey line) order polynomial fitting.

Core 6 H

Sprovieri et al. (2006) have identified and indicated millennial climatic variations in the central Mediterranean basin on base of calcareous plankton data from ODP Hole 963 A, throughout Marine Isotopic Stage (MIS) 5. In the following part briefly is described the chronological framework obtained from oxygen isotope data from ODP Leg 160 Site 963 A Core 6H.

In Sprovieri et al. (2006) only the 31.07 and 47.60 mbsf of Hole 963A, which includes MIS 5, as indicated by planktonic δ^{18}O analysis was used. The relative abundance patterns of the selected calcareous plankton taxa, benthic and planktonic δ^{18}O curves are plotted versus depth in Fig. 5.7.

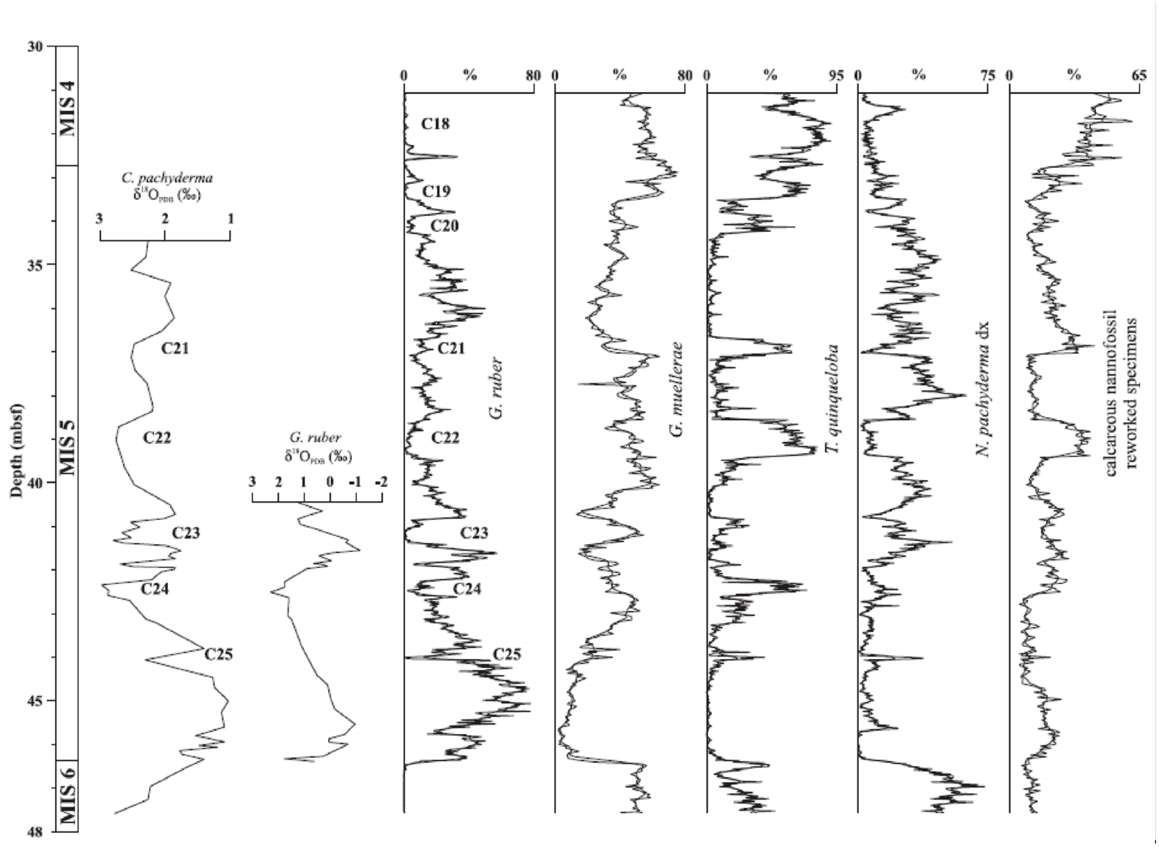

Fig. 5.7 Quantitative distribution patterns of selected planktonic species, benthic and planktonic. Oxygen isotope fluctuations at Hole 963A, all plotted versus depth (mbsf), with 5-pt moving average curves in bold. On the left, the interpreted isotope stratigraphy is shown. Identified cold (C) events, are reported on the G. *ruber* distribution pattern.

The δ^{18}O variations of benthic and planktonic foraminifera, although at relatively low resolution, parallel the trends indicated by the relative abundances of calcareous plankton taxa, what can be used to confirm that surface variations are due to either temperature or salinity, and hence climatically relevant.

The age model of Hole 963 A has been assessed on the basis of a peak to peak correlation between planktonic foraminifera paleoclimatic curve and δ^{18}O of NGRIP ice core (Fig. 5.8)

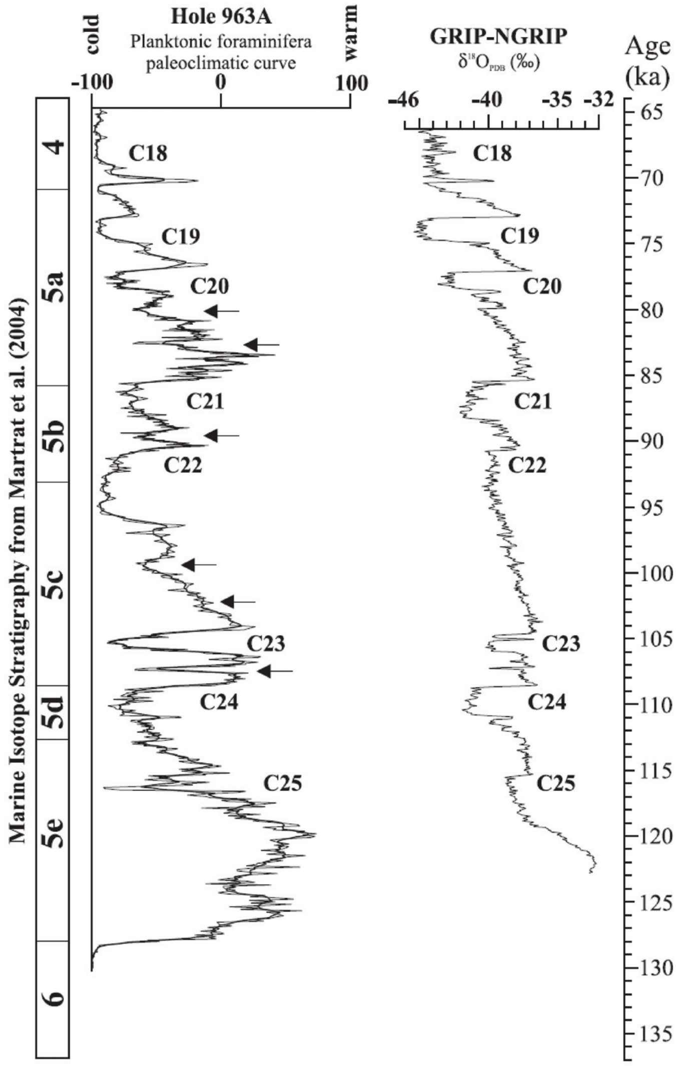

Fig 5.8 Comparison of the different Northern Hemisphere records discussed in Sprovieri et al. 2006, plotted on their own independent age model: Planktonic foraminifera paleoclimatic curve of ODP Site 963, with 5-pt average in bold (on the left); $\delta^{18}O$ of NGRIP Greenland ice core (NGRIP members, 2004) (on the right). The column on the left shows the Marine Isotopic Stratigraphy from Martrat et al. (2004). Black arrows on the left indicate possible additional cooling events.

The calibration between Site 963 A and NGRIP ice core has been carried out using as tie-points the base and top of cold events, except for C22 and C25 in which only the top has been adopted. Since Greenland ice cores suffer from stratigraphic disturbance in levels older than about 120 ka BP (Grootes et al., 1993; Bender et al., 1994; Fuchs & Leuenberger, 1996; Chappellaz et al., 1997), Sprovieri et al. 2006 have tentatively used for the boundary between MIS 6 and MIS 5 the age reported from the nearby Alboran Sea (Martrat et al., 2004). According to this chronological framework reconstruction, the quantitative analyses on planktonic foraminifera and calcareous nannofossils in ODP Hole 963 A come from samples collected every about 80 and 160 years, respectively. Numbered from C25 to C18, the cold events in ODP Hole 963 A seem to match the corresponding events of selected Northern Hemisphere records. The good match with the western Mediterranean record except for C23, whose assignment in the western Mediterranean may be too young, supports age model proposed by Sprovieri et al. 2006, and further suggests basin-wide climatic changes during MIS 5. In summary, additional millennial cold events within couplets of the labelled cold events are recognizable in the Mediterranean ODP Hole 963 A, and are indicated by arrows in Fig. 5.8. The general framework of climatic variability in the Sicily Strait is largely compatible with that of the Alboran Sea (Martrat et al., 2004; Perez-Folgado et al., 2004) but the greater resolution of the ODP 963 A records allows the identification of previously undocumented higher-frequency climate oscillations in the Mediterranean Sea. Nevertheless, adopting the Marine Isotope Stratigraphy of the Alboran Sea study (left column in Fig. 5.8), all the sub-stage boundaries are largely compatible with the climatic/environmental interpretation of calcareous plankton and stable isotopes at Site 963 A.

Core 8H

Incarbona et al. (*in preparation*) propose an high-resolution calcareous nannofossil biostratigraphic framework for the last 430 kyr, obtained from ODP 160 Site 963 A. The study show calcareous nannofossil quantitative analysis carried out between about 5.5 and 112 meters (2308 samples were analysed) below sea floor (mbsf) by observation with a polarized microscope.

The age model has been assessed through oxygen isotope data of 963 Site composite section (Howell et al., 1998). Benthic and planktonic foraminifera $\delta^{18}O$ curves have been correlated to the SPECMAP stack curve (Imbrie et al., 1984) (Fig. 5.9).

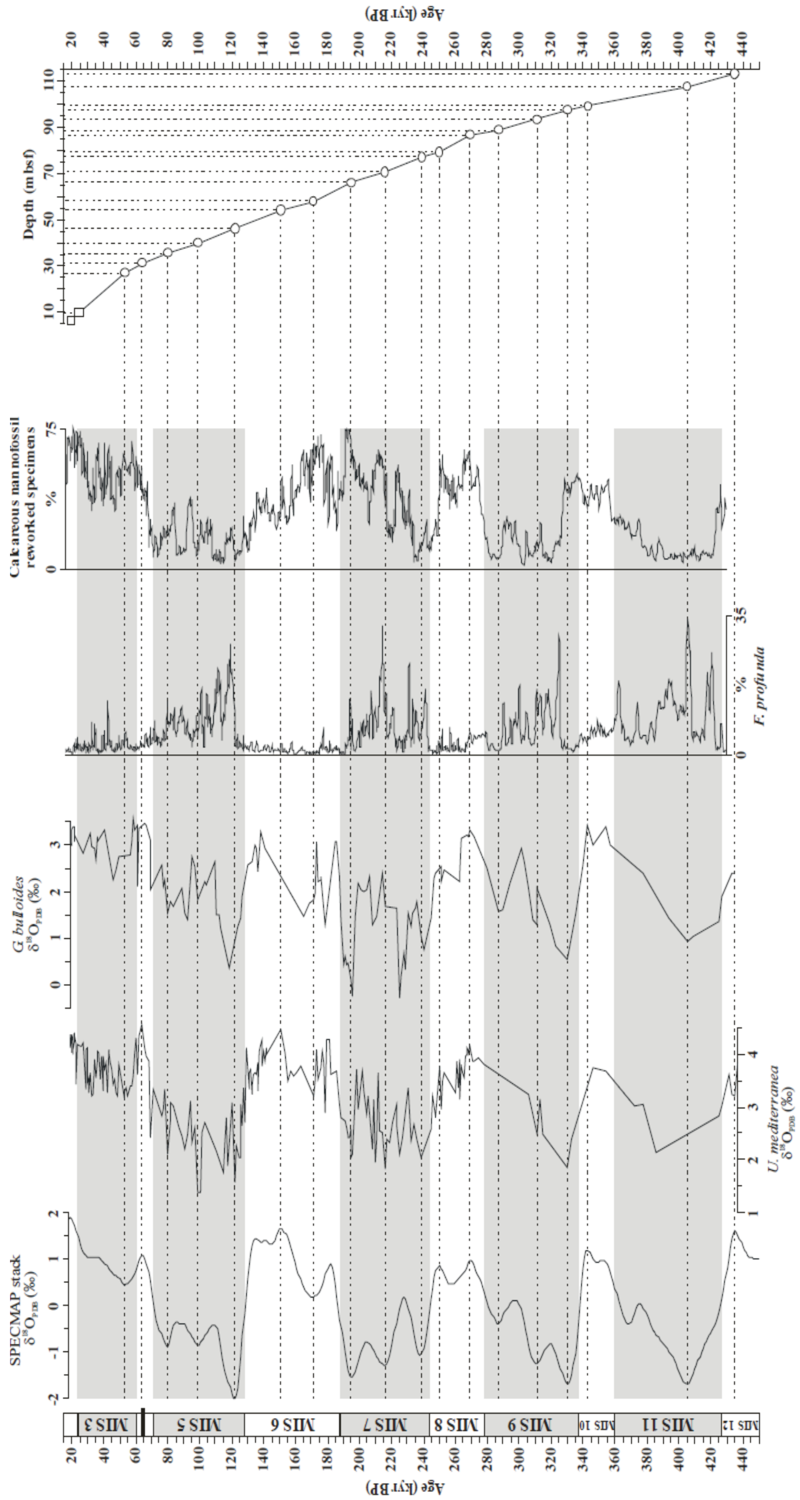

Fig. 5.9 Proxies for the stratigraphic framework assessment, plotted *versus* age (kyr BP). From the left, SPECMAP stack curve (Imbrie et al., 1984); Benthic and planktonic foraminifera $\delta^{18}O$ curves from the 963 Site composite section (Howell et al., 1998); Downcore variations of F. *profunda* and reworked calcareous nannofossils, presented as a 3-pt moving average; Age-depth plot, in which adopted tie-points are indicated as circles (correlation to the SPECMAP curve) and squares (radiocarbon calibrated ages). Grey bands mark odd Marine Isotopic Stages. Dotted lines indicate the adopted tie-points on the SPECMAP curve.

Further indication on the general validity of the chronological framework comes from *Florisphaera profunda* and reworked specimens of calcareous nannofossil (Fig. 5.9) (F. *profunda* is abundant at low- and middle-latitudes in today's oceans). In particular in the Sicily Channel the increased percentages of F. *profunda* is concomitant to light oxygen isotopic values (Fig. 5.9) and this suggest that the development of a vertical zonation in coccolithophore communities during each interglacial period, possibly tied to a deeper and stronger summer thermocline, as already observed during the Holocene and most of Marine Isotopic Stage (MIS) 5 (Sprovieri et al., 2003; Di Stefano & Incarbona, 2004). Finally, the age-*versus*-depth curve shown in Fig. 5.9 allows to estimate in 25.7 cm/kyr the mean sedimentation rate. This study demonstrates that the succession of calcareous nannofossil acme intervals is the same as that of the Atlantic Ocean. The boundaries of acme intervals fall within the same MISs for both Mediterranean and Atlantic sites and also the age estimates are strongly comparable. All the principal assemblage changes seem to be independent from climatic/environmental forcing.

5.4 The composite record

In Tab. 5.8, Tab. 5.9 and Tab. 5.10 an accurate dating of the studied tephras, collected from the three cores, is reported.

Tephra Chronology of KC01B		
Tephra	KC01B	
Ionian	Level,[a] m	Age, kyr
I1	1.275	16.7
I3	3.835	39.1
I9	8.205	110.5
a) Levels in meters refer to the modified piston depths of KC01B as used in Lourens 2004		

Tab. 5.8 Summary list of the studied tephra layers with depth and age according to Lourens (2004).

Tephra Chronology of MD01_2474G				
Tephra	Level, cm	Age [a], kyr	Age [b], kyr	Age [c], kyr
MD 3	54	7,01	6,67	
MD 10	174,5	14,33	14,90	
MD 11	186	15,16	15,68	
MD 14	260,5	21,05	21,02	
MD 15	347	29,05	28,17	
MD 18	403	34,90	33,68	
MD 22	453	40,57	39,37	
MD 27	558,5			48,97
MD 28	706	57,78		
MD 33	764,5	61,67		
MD 35	807,5	64,33		
a) Estimated age on second-order polynomial base b) Estimated age on third-order polynomial base c) Estimated age on fifth-order polynomial base				

Tab. 5.9 Summary list of the studied tephra layers with depth and estimated age from this study.

Tephra Chronology of ODP Leg 160 Site 963 A		
Tephra	Level[a], mbsf	Age, kyr
Core 3 H		
ODP3/5-1 a	20,84	42,47
ODP3/5-1 b	20,86	42,50
Core 6 H		
ODP6/3-2 a	47,52	127,41
ODP6/3-2 b	47,54	127,48
ODP6/3-3 a	47,58	127,63
ODP6/3-3 c	47,72	128,13
ODP6/3-4 a	47,74	128,20
ODP6/3-4 b	47,76	128,28
ODP6/3-4 c	47,80	128,42
ODP6/3-4 d	47,86	128,64
ODP6/3-4 e	47,90	128,78
ODP6/3-4 f	47,92	128,85
ODP6/3-4 g	47,98	128,85
Core 8 H		
ODP8/1-5	63,84	188,69
ODP8/3-6	66,56	197,73

a) Levels in meters below seea floor referto the modified piston depths of ODP Leg 160 Site 963 A as used in:
Sprovieri et al. in preparation
Sprpvieri et al. 2006
and Incarbona et al. in preparation.

Tab. 5.10 Summary list of the studied tephra layers with depth and age according to Sprovieri et al. (in preaparation), Sprovieri et al. (2006) and Incarbona et al. (in preparation).

6 Discussion

The precise and reliable age model available/achieved for the three studied cores allows one to improve the dating of the different tephras analysed throughout the cores. In Fig. 6.1 the analysed tephra layers picked up from the three sedimentary records are reported versus time considering the age models of the different cores. Details on the accuracy related to the different metodological approaches are reported in chapter 5.

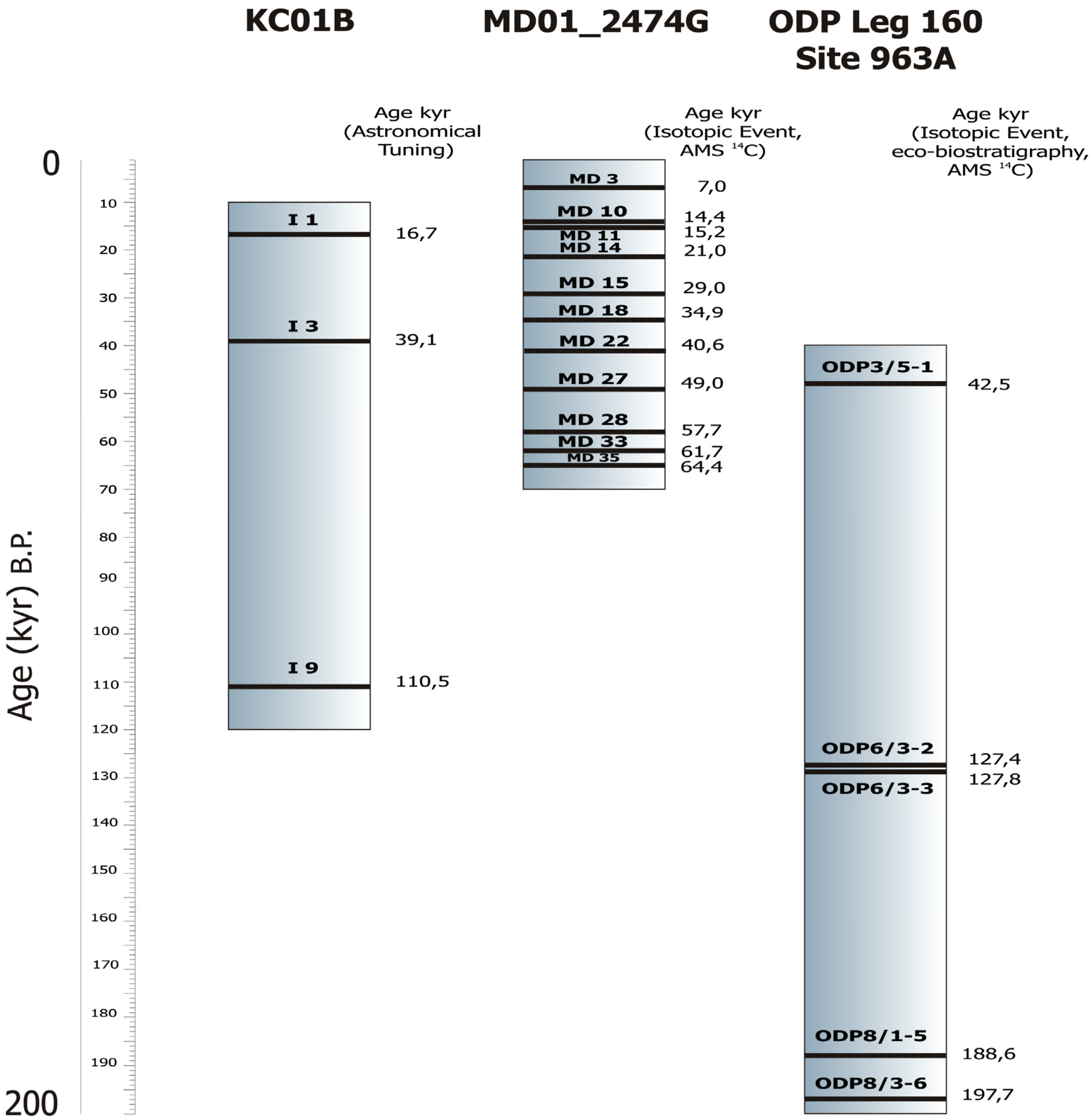

Fig. 6.1 Chronology of the tephra layers collected for the three sedimentary records.

For a sake of simplicity I preferred to discuss the tephrostratigraphy and then the tephrochronology of the available records grouping the tephra deposits for volcanic sources (Campanian, Aeolian, Etnean and Pantelleritic) and then discussing problems related to chemical attribution and then timing of the single clusters. At the end of the chapter a synthetic scheme will compare ages obtained for the studied tephra layers with those reported for the same events by Keller et al. (1978) underlying the potential of a refined tephrochronology (at least a number of events) for the Mediterranean basin.

6.1 Tephras from the Campania Plain

Two tephra deposits (**I3** and **I9**), recognised throughout the core KC01B (at 1,255 m and 8,215 m from the top, respectively), show major and trace elements patterns comparable to chemical composition of Campanian volcanic deposits.

Tephra **I3** has a very distinctive trachytic composition, that can be clearly distinguished from that of tephra produced by other sources in the Mediterranean area. It can be interpreted to represent a distal co-ignimbritic fallout deposit of the well-known CI eruption, occurred at Campi Flegrei at ~ 39 kyr B.P. (De Vivo et al., 2002; Fedele et al., 2008). The variability in the CI rock composition indicates that the CI eruption was fed by a trachytic magma chamber which included more evolved upper magma layer and a less evolved lower layer (e.g. Civetta et al., 1997). The most evolved and intermediate products are at great extend volumetrically predominant in the mid-distal area 20–80 km from the vent (Civetta et al., 1997; Pappalardo et al., 2002; Fedele et al., 2008) (green crosses in Fig. 6.2 and Fig. 6.3) while the deposits generated by the less evolved magma, extracted only during the terminal phase of the eruption, are dispersed mainly close to the source (red crosses in Fig. 6.2 and Fig. 6.3).

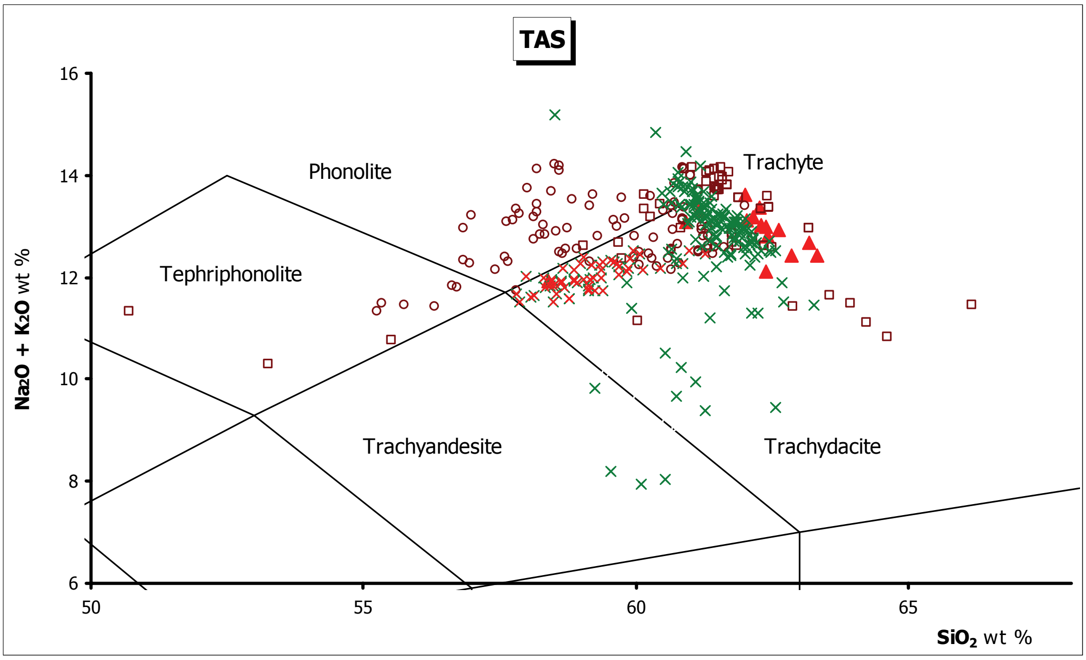

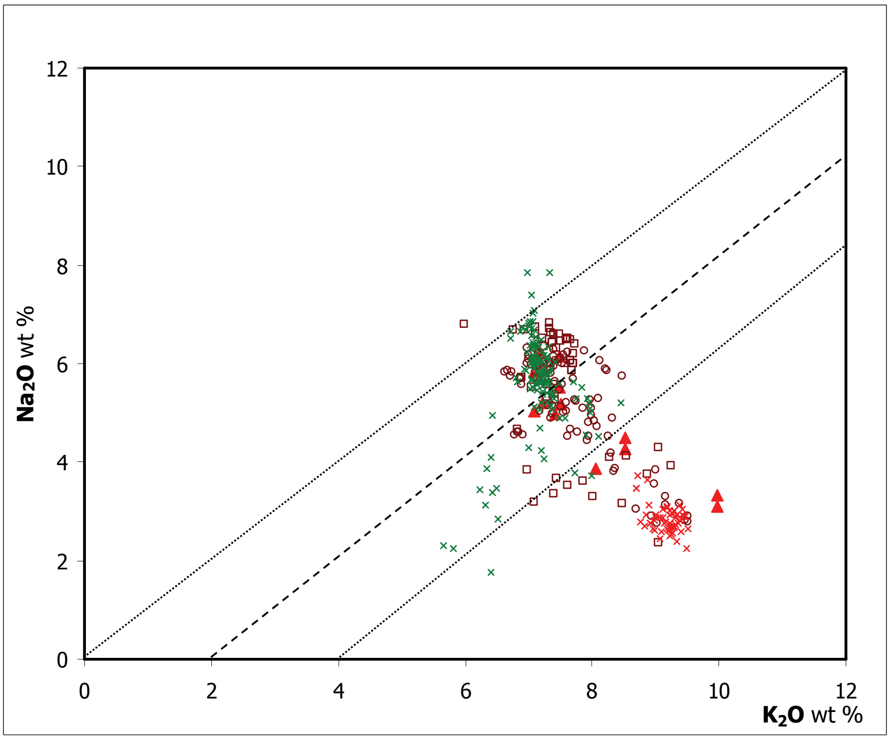

Fig. 6.2-6.3 Classification of the studied tephra **I3** (red full triangles) according to TAS (Total Alkali/Silica) diagram. Compositional range of marine **Y5** and on land deposits is shown for comparison (red open circles **CI** data [WDS] from Civetta et al., 1997; red and green crosses CI data [XRF] from Fedele et al., 2008; red open squares Y5 data from Keller et al., 1978 [XRF]; Munno & Petrosino, 2004, 2007 [EDS]; Narcisi, 1996 [EDS]; Paterne et al., 1985, 1986 [EDS]; Vezzoli, 1991 [EDS]; Vinci, 1985 [EDS]; Wulf et al., 2004 [WDS]).

The presence of a double composition is a peculiar characteristic and is considered to constitute a chemical marker to trace the CI tephra up to very distal settings. The distal deposits associated to the CI events, are known as Y-5 tephra and occur in various deep-sea sites from the Central-Eastern Mediterranean Sea (Keller et al., 1978; Munno & Petrosino, 2004/2007; Narcisi, 1996; Paterne et al., 1985, 1986; Vezzoli, 1991; Vinci, 1985; Wulf et al., 2004) (open red square in Fig. 6.2 and Fig. 6.3). Major elements of tephra I3 well correlate with marine tephra Y5 from the literature and CI deposits on land although a definitive attribution of tephra I3 to CI eruption is based on a detailed analysis the trace element patterns reported in Fig. 6.4. Actually, though the chemical database of CI on land is already detailed, chemical data of marine tephra Y5 are generally limited to the major element suite. In this context the more complete and accurate chemical analysis of tephra I3 offers a novel contribution of this research not only for a better identification of the dispersal product of the CI eruption, but also for a more complete and reliable characterization of marine deposits associated to that volcanic event.

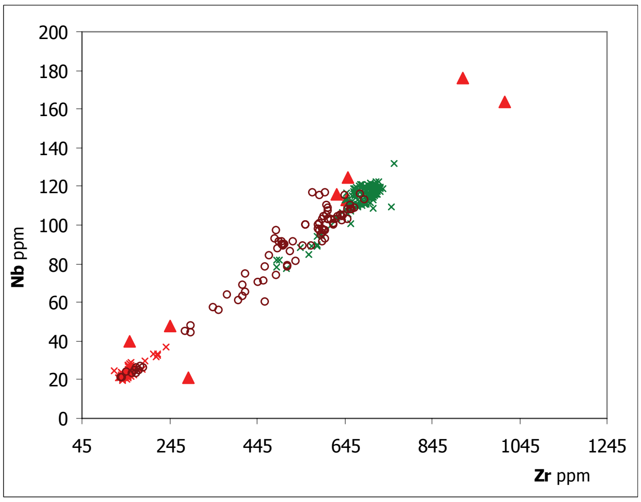

Fig. 6.4 Compositional range of the studied tephra **I3** (red full triangles). Data from on land deposits are shown for comparison (red open circles **CI** data [WDS] from Civetta et al., 1997; red and green crosses CI data [XRF] from Fedele et al., 2008).

Based on the astronomical tuning of Lourens (2004) of the KC01B core, this tephra was dated at 39,1 Kyr in excellent agreement with the available radiometric dating reported by De Vivo et al. (2002) and Fedele et al. (2008) of 39,1±0,2 kyr and 38,6±1,1 kyr respectively (Tab. 6.1).

Marine Tephra in this study			Literature								
			Paterne et al. 1986; Ton-That et al. 2001			Keller et al. 1978			Fedele et al. 2008		
Marine Tephra	**Chemical classification**	**Age kyr (Astronomical Tuning)**	**Marine Tephra**	**Chemical classification**	**Age kyr (Oxygen-isotope stratigraphy; Ar/Ar)**	**Marine Tephra**	**Chemical classification**	**Age kyr (Oxygen-isotope stratigraphy)**	**Proximal Tephra**	**Chemical classification**	**Age kyr (Ar-Ar)**
I3	Trachyte	39,1	C13	Trachyte	40±13; 41,1±2,1	Y5	Trachyte	35,0		Trachyte and Trachy fonolite	38,6±1,1

Tab. 6.1 Ages of I3 tephra following correlation with dated correlatives marine tephra and on land products.

As tephra I3, tephra **I9** has major and trace elements contents typical of the Campanian products. Based only on direct age comparison Lourens (2004) proposed a correlation of tephra I9 dated between 108 and 110 kyr B.P., with the marine tephra X6 (Keller et al., 1978) reported by several authors in different settings of the central Mediterranean (e.g. Paterne et al., 2008; Marciano et al., 2008; Munno & Petrosino, 2007; Keller et al. 1978) and dated by Keller et al. (1978) at 107 kyr. Actually, major elements content of tephra I9 in the KC01B core well compares with literature data for tephra X6 characterised by a quite homogenous trachytic composition (Fig. 6.5). In order to investigate the potential eruptive events that generated the marine tephra X6 (correlated to the studied tephra I9), the composition of marine tephra X6 and chemical data related to old volcanic products from Campanian Plain (Di Vito et al., 2008) are reported in Fig. 6.5.

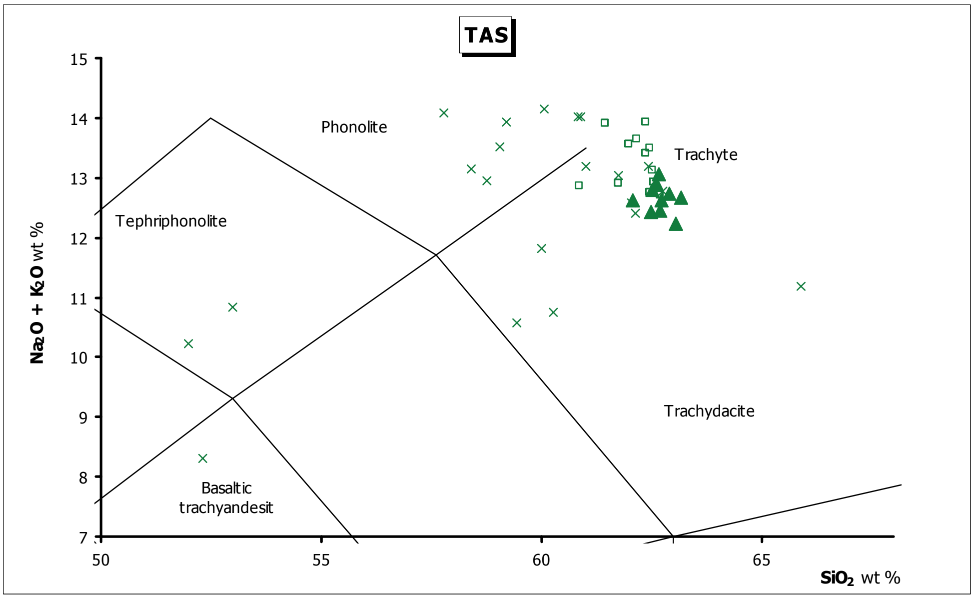

Fig. 6.5 Classification of the studied tephra **I9** (green full triangles) according to TAS (Total Alkali/Silica) diagram. Compositional range of on land deposits is shown for comparison (green crosses pre-CI data from Di Vito et al. 2008 [EDS]; green open squares X6 data from Keller et al., 1978 [XRF]; Wulf et al., 2006 [WDS]; Munno & Petrosino, 2007 [EDS]; Lucchi et al., 2008 [EDS]).

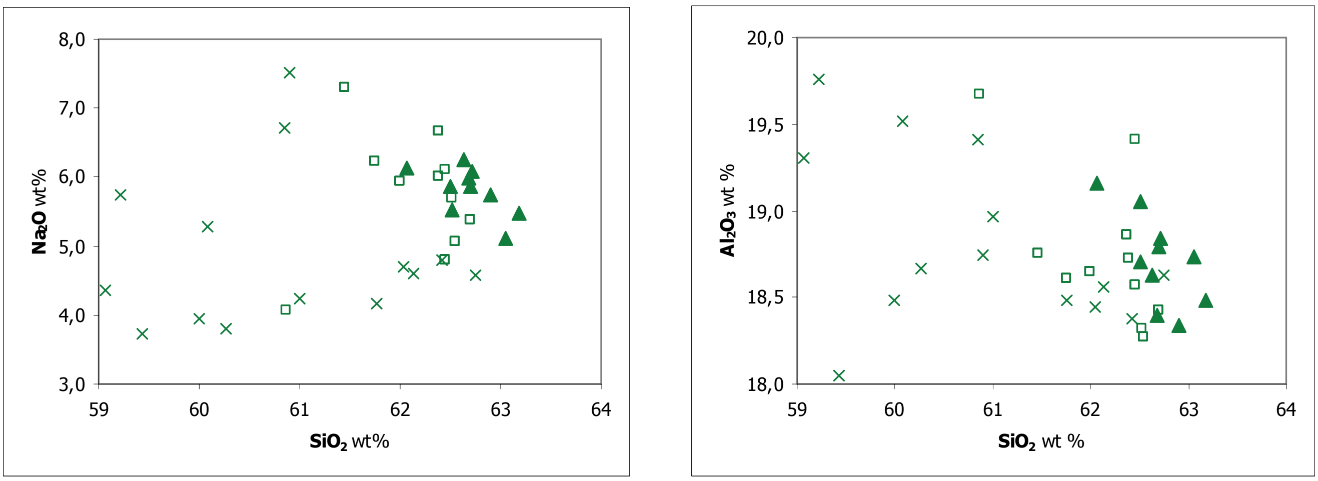

Fig. 6.6 Comparison between compositional range of the studied tephra **I9** (green full triangles), on land deposits (green crosses pre-CI data from Di Vito et al. 2008 [EDS]), and marine tephra **X6** (green open squares from Keller et al., 1978 [XRF]; Wulf et al., 2006 [WDS]; Munno & Petrosino, 2007 [EDS]; Lucchi et al., 2008 [EDS]).

As shown in Fig. 6.5 and Fig. 6.6, the correlation between marine tephra I9 and X6 is evident while the comparison with older products (< 125 kyr) of the Campanian Plain (analysed by Di Vito et al., 2008) evidence several differences. In this case, it appears most likely that the following eruptive events on land were definitively obliterated.

Marine Tephra in this study			Literature					
			Paterne et al. 2008			Keller et al. 1978		
Marine Tephra	**Chemical classification**	**Age kyr (Astronomical Tuning)**	**Marine Tephra**	**Chemical classification**	**Age kyr (Oxygen-isotope stratigraphy)**	**Marine Tephra**	**Chemical classification**	**Age kyr (Oxygen-isotope stratigraphy)**
I9	Trachyte	108,2-110,5	C31	Trachyte	108,0	X6	Trachyte	107

Tab. 6.2 Ages of I9 tephra following correlation with dated correlatives marine tephras.

Once again, based on astronomical tuning of the KC01B record, the age of tephra X6 can be definitively dated at 108-110 kyr (Tab. 6.2).

Two tephras from the MD01_2474G core (**MD28** and **MD35**), are likely sourced by the Campania Plain. Chemical composition of tephra **MD28** displays an origin from Ischia volcano and, in particular, it suggests a correlation with the Green Tuff of Monte Epomeo, the most important pyroclastic formation outcropping on the island (Vezzoli, 1991 and Brown et al., 2007) (Fig. 6.6 and Fig. 6.7).

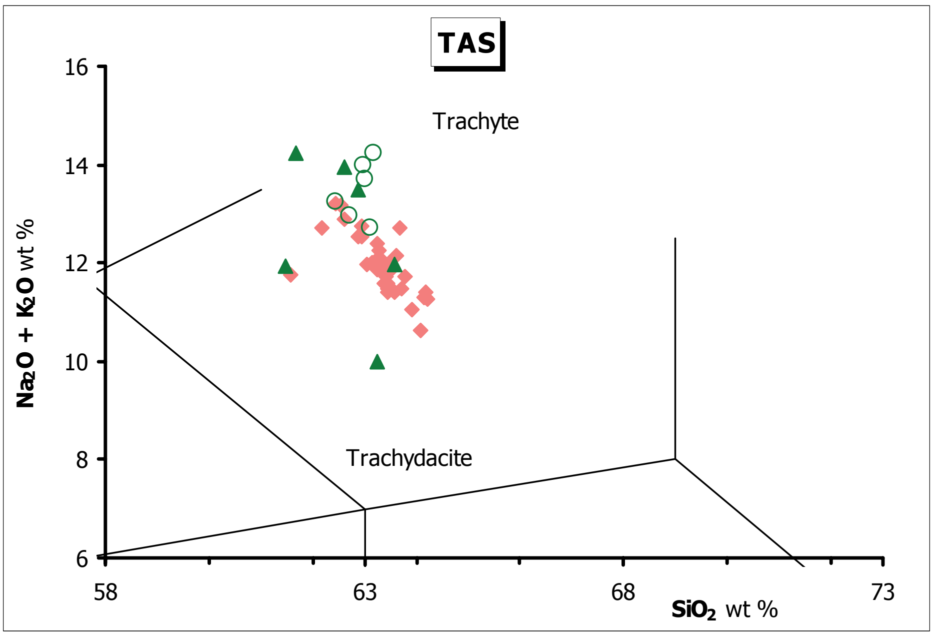

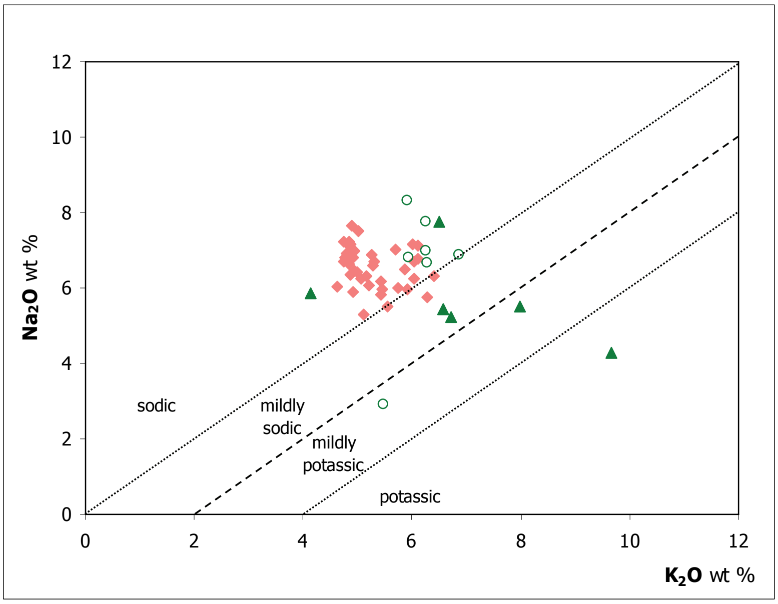

Fig. 6.6-6.7 Comparison among compositional range of the studied tephra **MD28** (pink full rhombus), on land deposits (green full triangles 35Z; data from Vezzoli 1988 [XRF]) MEGT (data from Brown et al. 2007 [XRF]), and marine tephra **Y7** (green open circles from Keller et al., 1978 [XRF]; Wulf et al., 2004 [WDS]; Narcisi 1996 [EDS]; Paterne et al., 1988 [EDS]; Lucchi et al., 2008 [EDS]).

While on land the distal products related to this formation are poorly known due to the scarce outcrops, they were found in the deep-sea sediments of the Tyrrhenian and Adriatic sea (Paterne et al., 1988; Narcisi 1996) and named Y7 by Keller et al. (1978) (Fig. 6.8 and Fig. 6.9).

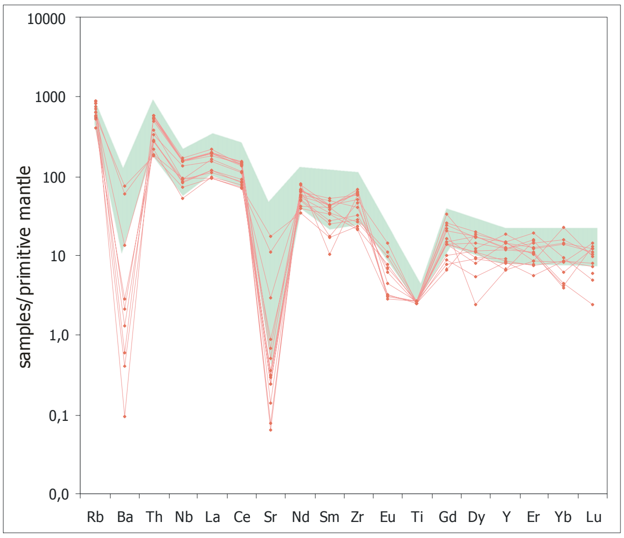

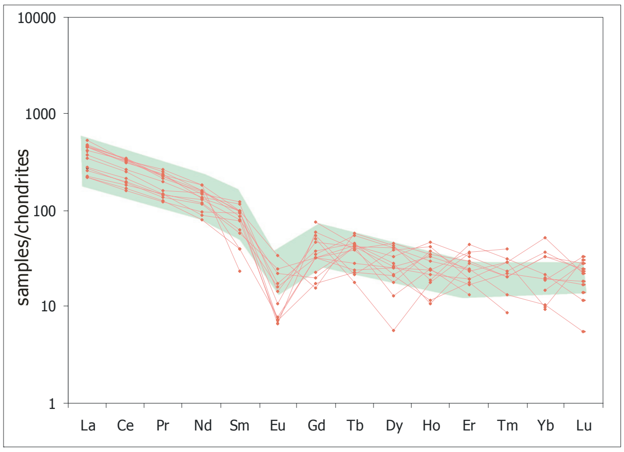

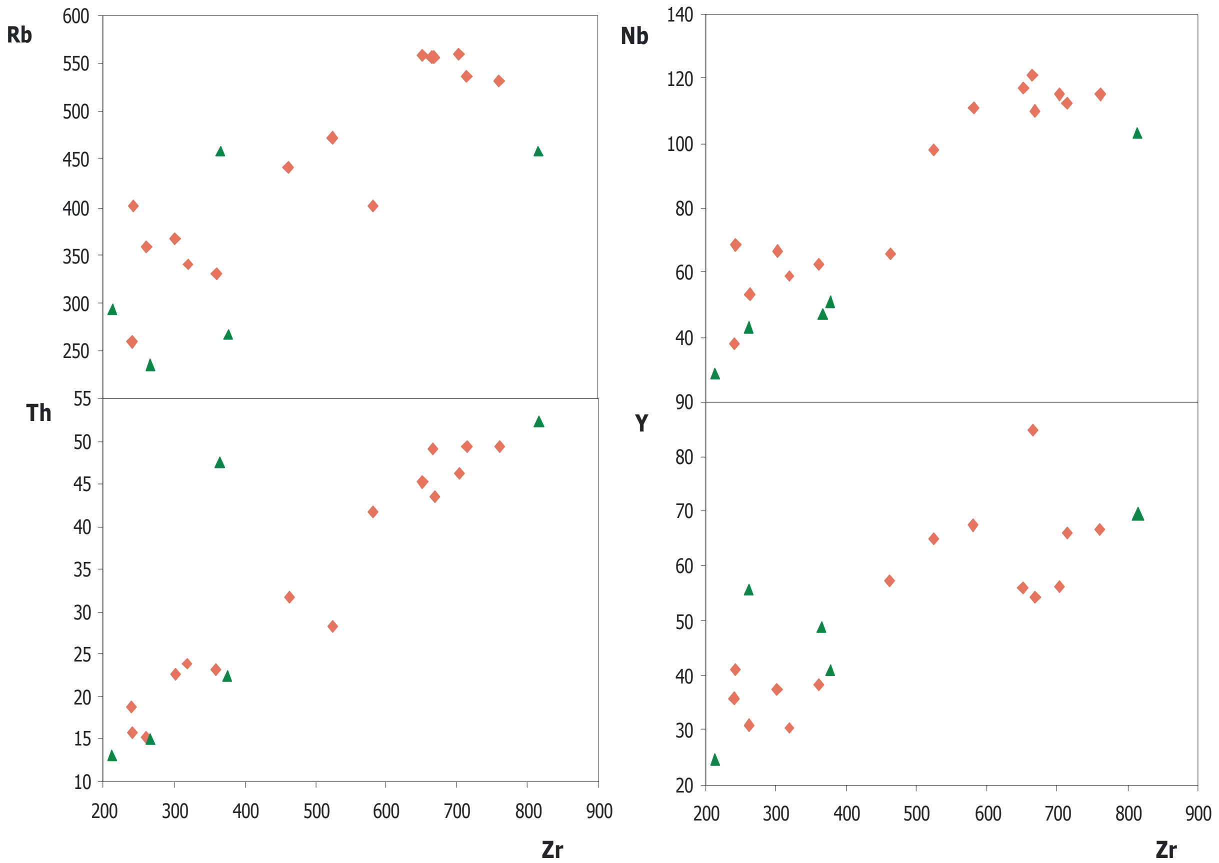

Fig. 6.8-6.9 Comparison between compositional range of the studied tephra **MD28** (pink full lines and rhombuses) and on land deposits of Monte Epomeo Green Tuff (green field and full triangles for 35Z data from Vezzoli 1988 [XRF], MEGT data from Brown et al. 2007 [ICP-MS]).

The age model of MD core locates tephra MD28 at 58 kyr. This results is in good agreement with the K/Ar dating of Monte Epomeo Green Tuff at 55,8±1,8 kyr and 56,8±2,8 reported in Gillot (1982) and Vezzoli (1988), respectively (Tab. 6.3).

Marine Tephra in this study			Literature											
			Wulf et al. 2004			Keller et al. 1978			Vezzoli 1988			Brown et al. 2007		
Marine Tephra	Chemical classification	Age kyr (^{14}C, Oxygen isotope stratigraphy)	Lacustrine Tephra	Chemical classification	Age kyr (varve)	Marine Tephra	Chemical classification	Age kyr (Oxygen-isotope stratigraphy)	Continental Tephra	Chemical classification	Age kyr (K-Ar)	Continental Tephra	Chemical classification	Age kyr (K-Ar)
MD28	Trachyte	57,8	TM19-TM20	Trachyte	56,25 and 57,57	Y7	Trachyte	50	35Z	Trachyte	50,1±1,3 / 55,8±1,8	UMEGT (intracaldera)	Trachyte	56±2,8

Tab. 6.3 Ages of MD28 tephra following correlation with dated correlatives marine tephras and on land eruption.

Tephra **MD35** has a heterogeneous composition ranging from basaltic-trachyandesite to trachyte (Fig. 6.10).

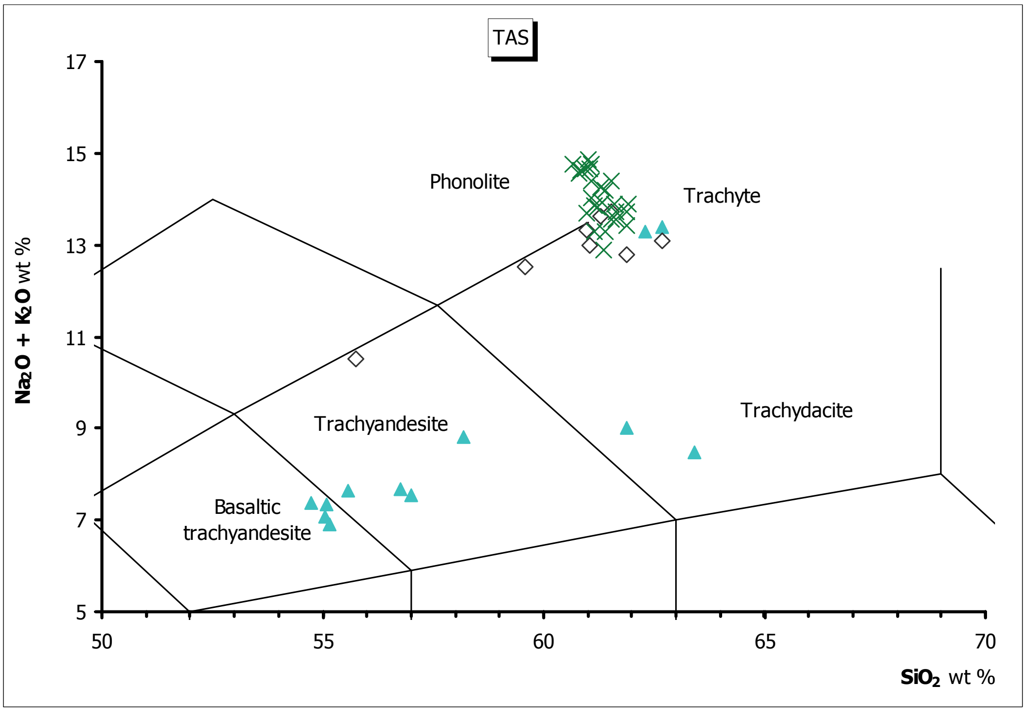

Fig. 6.10 Classification of the studied tephra **MD35** (blue full triangles) according to TAS (Total Alkali/Silica) diagram. Compositional range of marine **X2** and **pre-MEGT** on land deposits are shown for comparison (green open rhombuses X2 from Keller et al., 1978 [XRF]; Munno & Petrosino, 2007 [EDS]; Paterne et al., 1985 [EDS], Vezzoli 1991 [EDS])., green crosses pre-MEGT data from Brown et al. 2007 [XRF]).

It has been correlated with the Campania marine marker X2 of Keller et al. (1978), found in a limited number of deep-sea sediments of the Ionian and Tyrrhenian Sea (Keller et al., 1978; Paterne et al., 1985). It is difficult to correlate this tephra with a well-defined eruptive event because in the Campania area, outcrops about 50-70 kyr old are mainly characterised by pyroclastic deposits on the island of Ischia (Vezzoli, 1988 and Brown et al., 2007). As shown in Fig. 6.11 the comparison between the major element contents of tephra MD35 and land deposits related to the pre-Green Tuff volcanism of Ischia, highlights a good mach for the trachytic part, while there is a consistent part comparable with the marine tephra X2 but characterized by less silica contents probably due to alteration processes or different analytical approaches adopted.

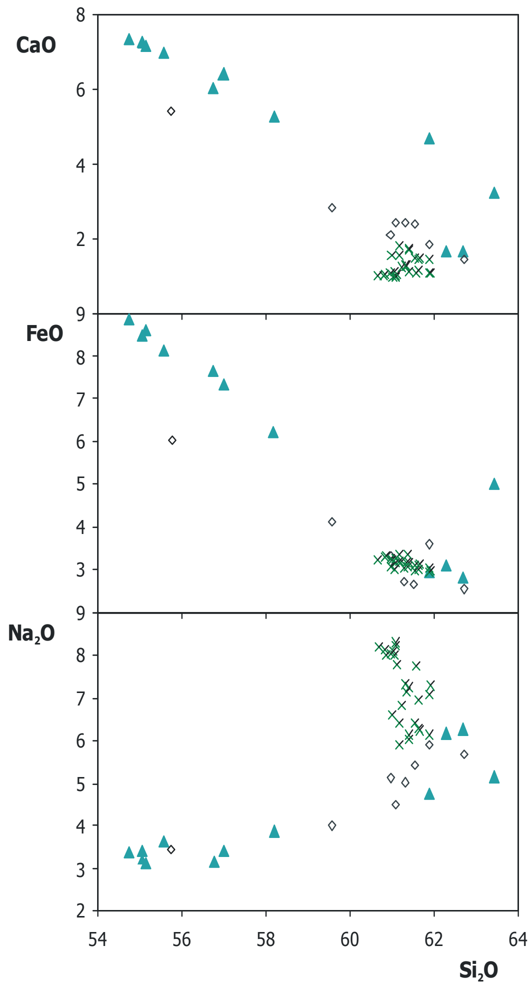

Fig. 6.11 Comparison among compositional range of the studied tephra **MD35** (blue full triangles), on land deposits (green triangles **pre-MEGT** data from Brown et al. 2007 [XRF]), and marine tephra **X2** (green open rhombuses from Keller et al., 1978 [XRF]; Munno & Petrosino, 2007 [EDS]; Paterne et al., 1985 [EDS], Vezzoli 1991 [EDS]).

However, the good compositional comparability among trace elements patterns of MD35 and those of pre-Green Tuff products, makes evident a reliable correlation between the MD tephra and the volcanic activity of the Ischia island older than 55 kyr (Fig. 6.12 and Fig .6.13).

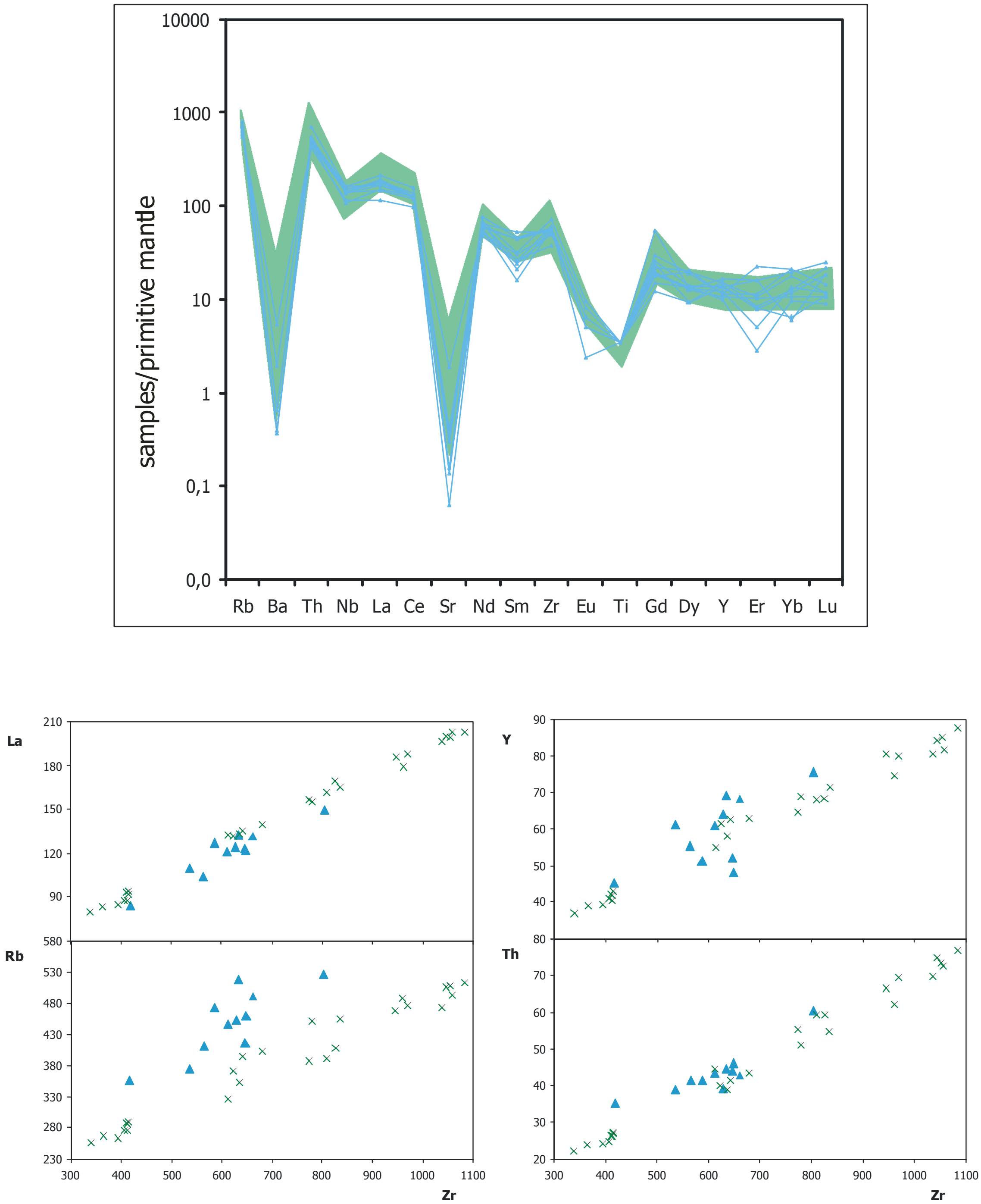

Fig. 6.12-6.13 Comparison between compositional range of the studied tephra MD35 (blue full triangles), on land deposits (green triangles and fields pre-MEGT data from Brown et al. 2007 [ICP-MS]).

In any case while the link between the marine tephra labelled X2 and MD35 is not definitively constrained by a chemical point of view tephra MD35 can be interpreted as a distal product of the older Ischia volcanism. The complete chemical and chronological characterization of MD35 then, allow to investigate this poorly known volcanic activity and then well indicate an energetic eruption occurred at ca. 64 kyr B.P. (Tab. 6.4).

Marine Tephra in this study			Literature					
			Paterne et al. 1985			Keller et al. 1978		
Marine Tephra	**Chemical classification**	**Age kyr (^{14}C, Oxygen isotope stratigraphy)**	**Marine Tephra**	**Chemical classification**	**Age kyr (Oxygen-isotope stratigraphy)**	**Marine Tephra**	**Chemical classification**	**Age kyr (Oxygen-isotope stratigraphy)**
MD35	from Basaltic-trachyandesite to Trachyte	64,3	C-22 and cm 825	Trachyte	81	X2	Trachyte	70

Tab. 6.4 Ages of MD35 tephra following correlation with dated correlatives marine tephras.

6.2 Tephras from the Aeolian arc

Seven tephras from the MD01_2474G core (**MD3**, **MD11**, **MD15**, **MD18**, **MD22**, **MD27** and **MD33**), show an Aeolian origin, exhibiting a chemical composition mainly ranging from basaltic-trachyandesite to rhyolites (high-K CA series), from andesite to dacite (CA series) and from basaltic-trachyandesite to trachyte-dacite (shoshonitic series).

The eruptive history of the Aeolian volcanoes is characterised by successive epochs of activity separated by major quiescence stages. Starting from 80 kyr, evolved CA and HK-CA andesitic to dacitic/trachytic/rhyolitic products were mainly erupted on Lipari (Tranne et al., 2002) and Salina islands (Keller, 1980) and to a lesser extent on Panarea (Lucchi et al., 2003, 2007) and Filicudi islands (Tranne et al., 2002), all resulting from effusive activity (mainly dome-forming) and associated explosive eruptions. Moreover, Stromboli (e.g Gillot & Keller, 1993; Hornig-Kjarsgaard et al., 1993) and Vulcano islands (De Astis et al., 2000) show a progressive transition from HKCA to SHO and K-alkaline mafic magmas during the last 20 kyr with recurrent high energy eruptive events.

MD3 tephra (at 54 cm of the core MD01_2474G) is dated, on the basis of the achieved age model, at 7 kyr. This tephra shows a latitic composition. Similar latitic composition marks several products of the younger volcanic activity either Campi Flegrei and Ischia island and the Vulcano island. In many cases the Campi Flegrei activity, during the time spam 10-5 kyr, produces small cones with a phreatomagmatic eruptive style (with low energy rate) and lava flows. For this reason also if there is a good mach, in terms of chemical composition, between MD3 tephra and several Campi Flegrei products younger than 10 kyr, it is difficult to assume a so distal dispersion for this ash-layers associated to low energy eruptions. At the same time an origin from Ischia island can be reasonably excluded since the unite of Piano Liguori dated at cal. 5,8 kyr B.P. (Orsi et al., 1996) and the older unite of Maisto tephra show a different trachytic composition (Fig. 6.14). Furthermore other latitic products from Ischia island, as Napolitano lava, similar to tephra MD3 can be probably excluded as primary sources due to their eruptive low energy rate (Napolitano and Trippodi laves dated < 10 kyr B.P. Vezzoli, 1988).

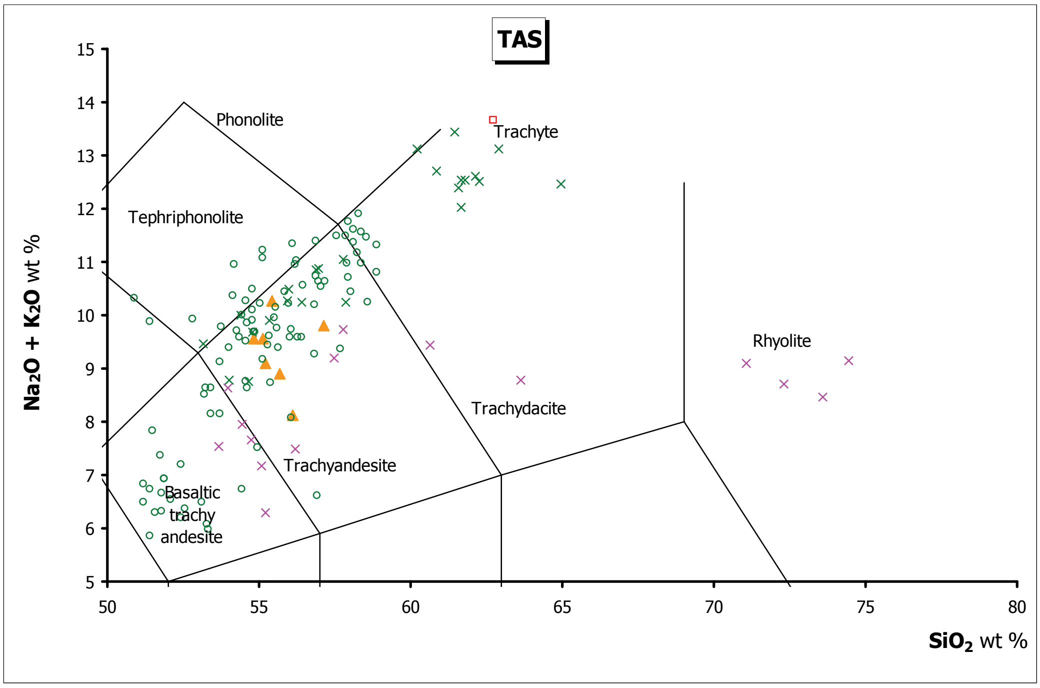

Fig. 6.14 Classification of the studied tephra **MD3** (orange full triangles) according to TAS (Total Alkali/Silica) diagram. Compositional range of marine tephra **CO**, Ischia **IV phase** and **Campi Flegrei** data on land and **GRT** is shown for comparison (red open square CO data from Paterne et al., 1988 [EDS]; green crosses IV phase data from Vezzoli, 1988 [XRF]; green open circles CF younger than 10 kyr data from Armienti 1983; Beccaluva 1991; D'Antonio 1997; Di Girolamo 1984, Ghiara et al. 1989-1990, Lustrino 2002, Rosi & Sbrana 1987; pink crosses Vulcano < 30 kyr data from De Astis et al. 2000 [XRF]; open green circles ; green crosses).

Finally, the MD3 tephra could be correlated to the products of the Vulcano island. Actually, this volcanic source shows a continuous and often high energy volcanism during the last 20 kyr (Lucchi et al. 2008 and therein references). In particular, the pyroclastic products of Piano Grotta dei Rossi Tuff formation (GRT, Lucchi et al., 2008), dated at 8,8±1,26 kyr by De Astis et al. (1997) (^{14}C age), present a latitic composition comparable with MD3 tephra. Based on the age model of the MD01_2474G core, this tephra is in agreement with the GRT available radiometric dating reported by De Astis et al. (1997) (Tab. 6.5).

Marine Tephra in this study			**Literature Lucchi et al. 2008**		
Marine Tephra	**Chemical classification**	**Age kyr (Isotopic event, AMS ^{14}C)**	**Island Tephra**	**Chemical classification**	**Age kyr (^{14}C)**
MD3	Latite	7	GRT unite	Trachy-andesite	8,8±1,26

Tab. 6.5 Ages of MD3 tephra following correlation with dated correlatives eruption on Aeolian archipelago.

Chemical composition of the tephra **MD11** (186 cm of MD core) presents a wider range from trachyandesitic to trachydacitic. The good chemical match between younger volcanic activity of Vulcano island (De Astis et al., 2000) and the MD11 tephra seems to suggest an Aeolian origin for this deposit (Fig. 6.15). This tephra is dated, on the basis of the realized age model, at 15 kyr B.P..

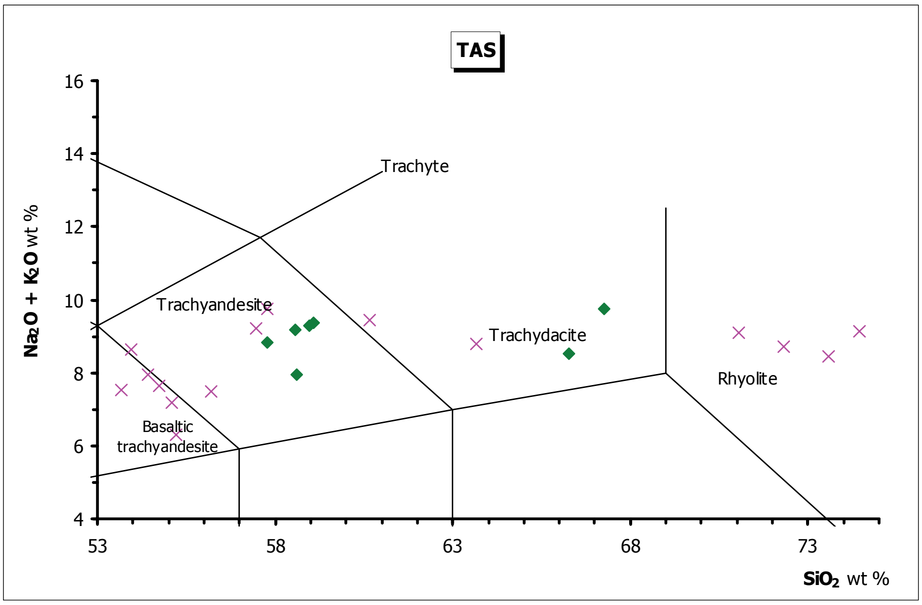

Fig. 6.15 Classification of the studied tephra **MD11** (green full rhombuses) according to TAS (Total Alkali/Silica) diagram. Compositional range of "**UBT"** is shown for comparison (pink crosses Vulcano < 30 kyr data from De Astis et al. 2000 [XRF]).

Recently, stratigraphycal studies proposed by Lucchi et al. (2008) identify the Brown Tuff formation (BT) as the major widespread volcaniclastic deposits outcropping on the Aeolian archipelago. This prominent event is characterised by voluminous and recurrent pyroclastic succession during the last 80 kyr B.P. (Lucchi et al., 2008 and references therein). In particular, the Upper Brown Tuff (UBT) unit has a chemical composition ranging from basaltic trachy-andesite to rhyolite. The age of 16,8±2 kyr B.P. (^{14}C age, Crisci et al., 1983) represents the lower chronological limit for this deposits (Tab. 6.6).

Marine Tephra in this study			**Literature Lucchi et al. 2008**		
Marine Tephra	**Chemical classification**	**Age kyr (Isotopic event, AMS ^{14}C)**	**Island Tephra**	**Chemical classification**	**Age kyr (^{14}C)**
MD11	Trachyandesite and Trachydacite	15,1	UBT unite	from Trachy-andesite to Rhyolite	from 16,8±2 to 20,3±0,7

Tab. 6.6 Age of MD11 tephra following correlation with dated correlative eruption on Aeolian archipelago.

Tephras **MD15** and tephra **MD18**, dated at ca. 29 kyr B.P. and 35 kyr B.P. respectively in MD01_2474G core, also exhibit compositional affinity with Aeolian products (seen chapter 4 and Fig. 6.16).

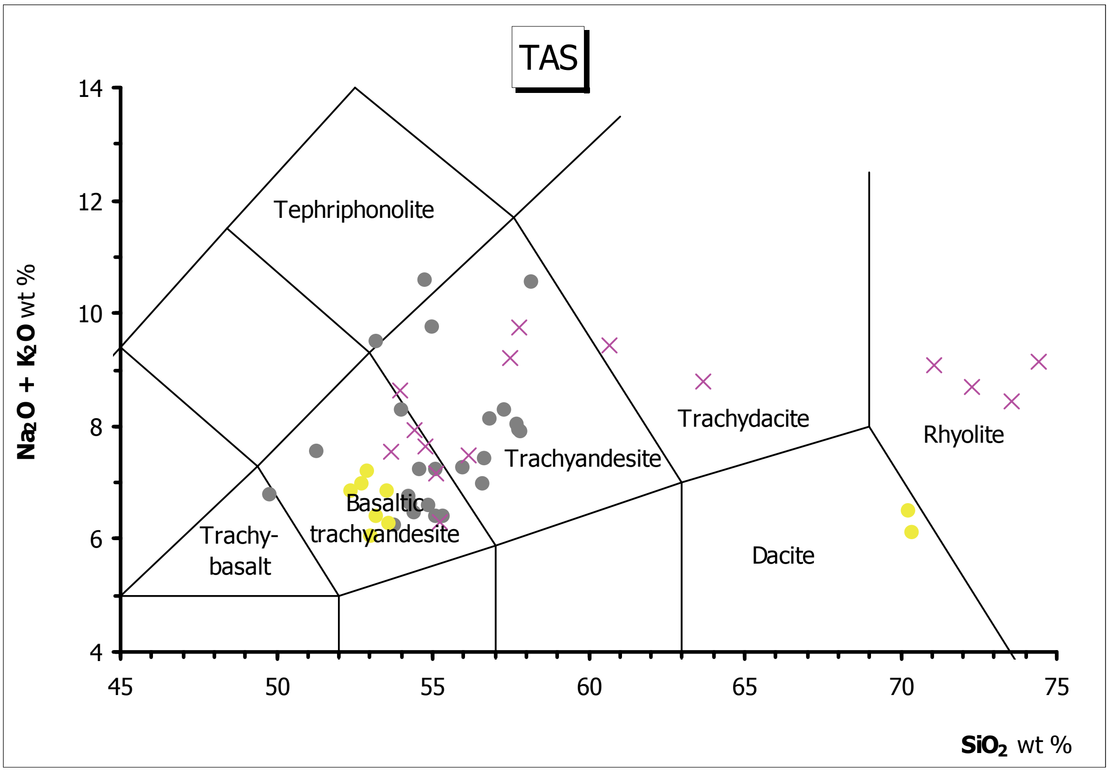

Fig. 6.16 Classification of the studied tephra **MD15** (grey full circles) and **MD18** (yellow full circles) according to TAS (Total Alkali/Silica) diagram. Compositional range of "**IBT**" is shown for comparison (pink crosses Vulcano < 30 kyr data from De Astis et al. 2000 [XRF]).

In particular, MD15 tephra comprises basaltic trachy-andesite and trachy-andesitic scoria and glass shards while MD18 is characterised by trachy-basaltic to dacitic products, both probably resulting from explosive activities that occurred at Vulcano island. Concerning the only two dacitic analysis of MD18 tephra they are much probably due to alteration processes of alkali. The correlative fallout layers (IBT) are not directly dated but attributed to the restricted time interval between ca. 20 to 56 kyr B.P. by means of stratigraphic relations with ^{14}C dated BT units and the well-known Y7 (Crisci et al., 1981, 1983).

Marine Tephra in this study			Literature Lucchi et al. 2008		
Marine Tephra	**Chemical classification**	**Age kyr (Isotopic event, AMS ^{14}C)**	**Island Tephra**	**Chemical classification**	**Age kyr (^{14}C)**
MD15	from Trachybasalt to Trachyandesite	29	IBT unite	from Trachy-basalt to Rhyolite	from 20,3±0,7 to ca. 57
MD18	from Basaltic-trachyandesite to Dacite	34,9			

Tab. 6.7 Age of the MD15 and MD18 tephras following correlation with dated correlative eruption on Aeolian archipelago.

Another tephra from MD01_2474G core that shows chemical composition close to that of the Aeolian activity is **MD22**. This tephra displays a wider compositional features from basaltic trachy-andesite to rhyolite (Fig. 6.17) and it is dated at ca. 40 kyr.

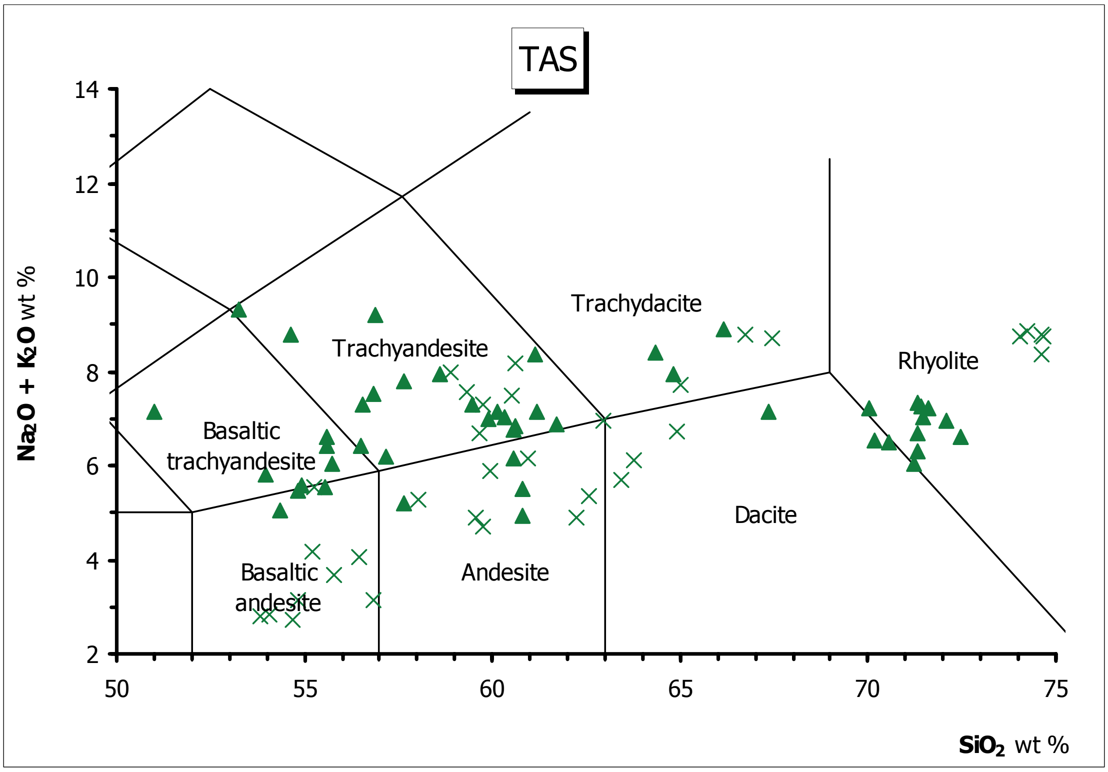

Fig. 6.17 Classification of the studied tephra **MD22** (green full triangles) according to TAS (Total Alkali/Silica) diagram. Compositional range of correlated **Lipari** on land deposits is shown for comparison (green crosses Lipari data from Gioncada et al. 2003 [XRF]).

The pyroclastic products of the explosive activity of Lipari island are widespread over the Aeolian archipelago with a characteristic HK-CA affinity. Actually, despite the voluminous and recurrent explosive activity verified by several authors on land, coeval marine tephras recovered in the Tyrrhenian Sea seem substantially absent. Therefore, tephra MD22 can be correlated with the VII cycles proposed by Gioncada et al. (2003)

incorporated in the Brown Tuff units of Lucchi et al. (2008) and in particular with the Punta del Perciato formation dated at ca. 41 kyr B.P. (Crisci et al. 1983, 1991).

Marine Tephra in this study			Literature Lucchi et al. 2008		
Marine Tephra	**Chemical classification**	**Age kyr (Isotopic event, AMS ^{14}C)**	**Island Tephra**	**Chemical classification**	**Age kyr**
MD22	from Basaltic-trachyandesite to Rhyolite	40,6	Punta del Perciato	from Andesite to Rhyolite	from 40±2,5 to 42±0,3

Tab. 6.8 Ages of MD22 tephra following correlation with dated correlative eruption of Lipari island.

As previously tephra MD15, tephra **MD27** has major and trace elements contents typical of the Aeolian volcanism and in particular of the Vulcano island (De Astis et al., 2000, see chapter 4 and Fig. 6.18). This tephra shows basaltic-trachyandesite and trachy-andesite composition and is dated at ca. 49 kyr B.P..

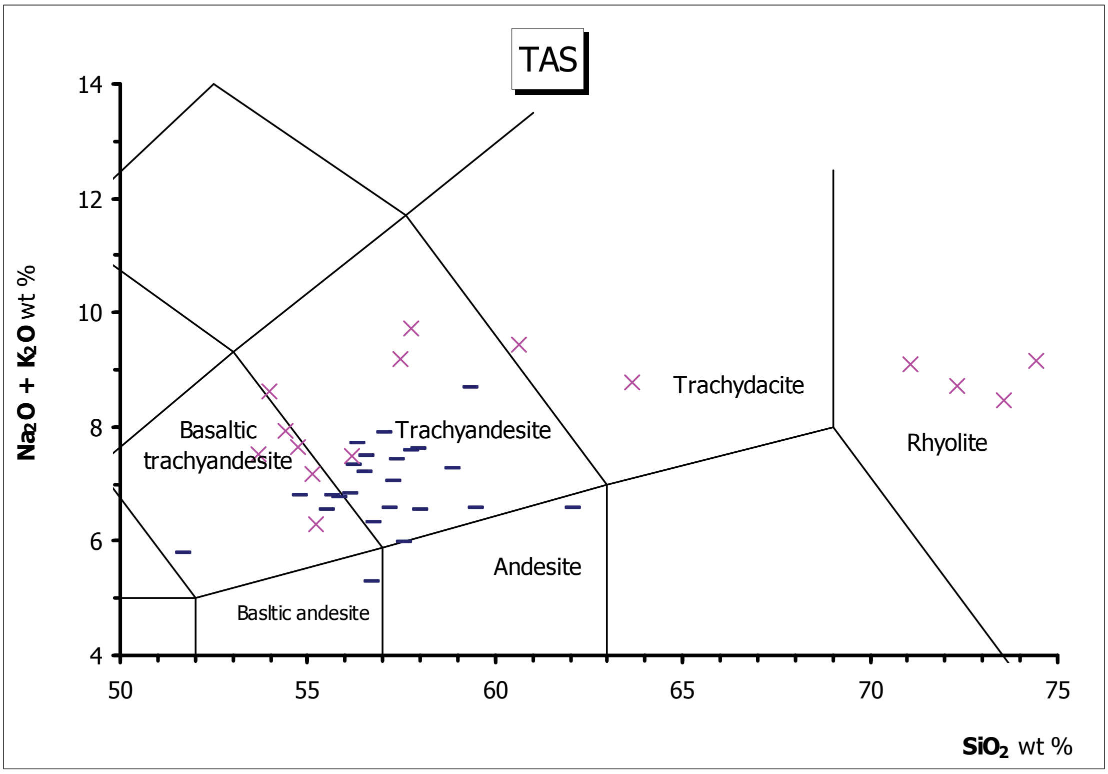

Fig. 6.18 Classification of the studied tephra **MD27** (blue bars) according to TAS (Total Alkali/Silica) diagram. Compositional range of "**IBT**" is shown for comparison (pink crosses Vulcano < 30 kyr data from De Astis et al. 2000 [XRF]).

Also in this case, the potential correlative explosive event of MD27 it is the IBT unite that, as previously mentioned, are not directly dated but attributed to the restricted time interval between ca. 20 kyr B.P. to 56 kyr B.P..

Marine Tephra in this study			Literature Lucchi et al. 2008		
Marine Tephra	**Chemical classification**	**Age kyr (Isotopic event, AMS ^{14}C)**	**Island Tephra**	**Chemical classification**	**Age kyr (^{14}C)**
MD27	Basaltic-trachyandesite and Trachyandesite	49	IBT unite	from Trachy-basalt to Rhyolite	from 20,3±0,7 to ca. 57

Tab. 6.9 Ages of MD27 tephra following correlation with dated correlative eruption on Aeolian archipelago.

Tephra **MD33** has a composition ranging from andesite to dacite, typical of the volcanic products of Salina island (e.g. Gertisser & Keller, 2000, Fig. 6.19).

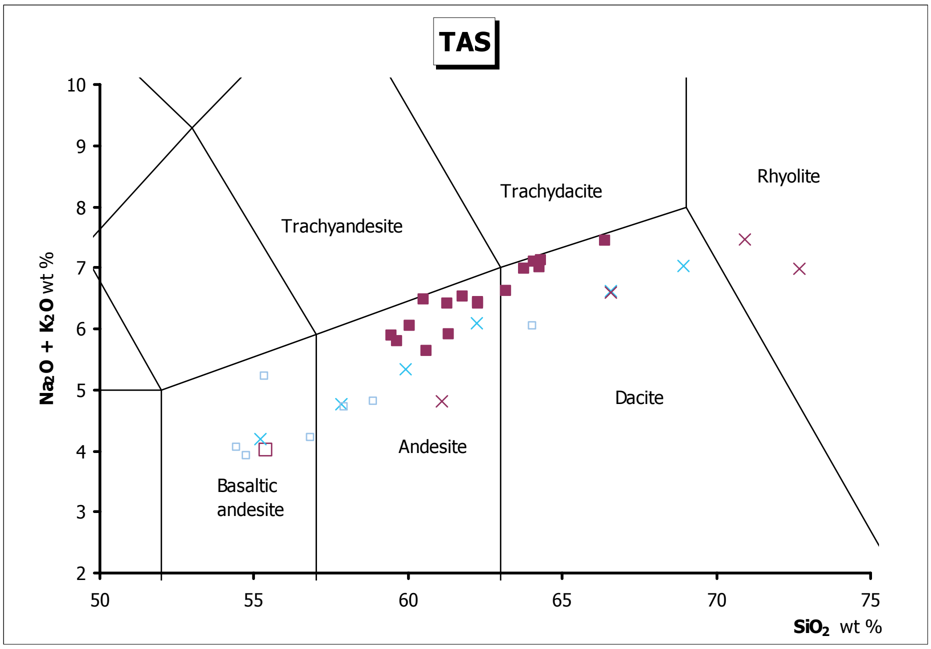

Fig. 6.19 Classification of the studied tephra **MD33** (violet full squares) according to TAS (Total Alkali/Silica) diagram. Compositional range of marine **Y8** and correlated **Salina** on land deposits are shown for comparison (violet open square from Keller et al., 1978 [XRF]; violet crosses from Paterne et al., 1988 [EDS]; blue open squares from De Rosa et al., 2003 [XRF], blue crosses from Gertisser & Keller, 2000 [XRF]).

The volcanic activity of Salina island is divided in two main cycles: the older cycle (430-127 kyr) comprises four volcanic centers (Corvo, Capo, Rivi and Fossa delle Felci) and consists in basaltic strombolian cinder with minor lava flow; the younger sequence is mainly represented by Fossa delle Felci sub-plinian and strombolian eruptions with a progressive decrease of silica content (composition from dacite to basaltic andesite) with time. Unfortunately, the volcanic history of Salina is poorly constrained by on land deposits. Marine tephra Y8 has been related to the younger activity of Salina by Keller et al. (1978). It shows a basaltic-andesite composition and it has been dated at ca. 55 kyr B.P (Keller et al., 1978). As shown in Fig.

6.19 and Fig. 6.20 the comparison between the chemical composition of MD33 and that of the younger products outcropping on Salina island presents a good match (Gertisser & Keller, 2000), except for the TiO_2 content that is considerably lower than the Salina products.

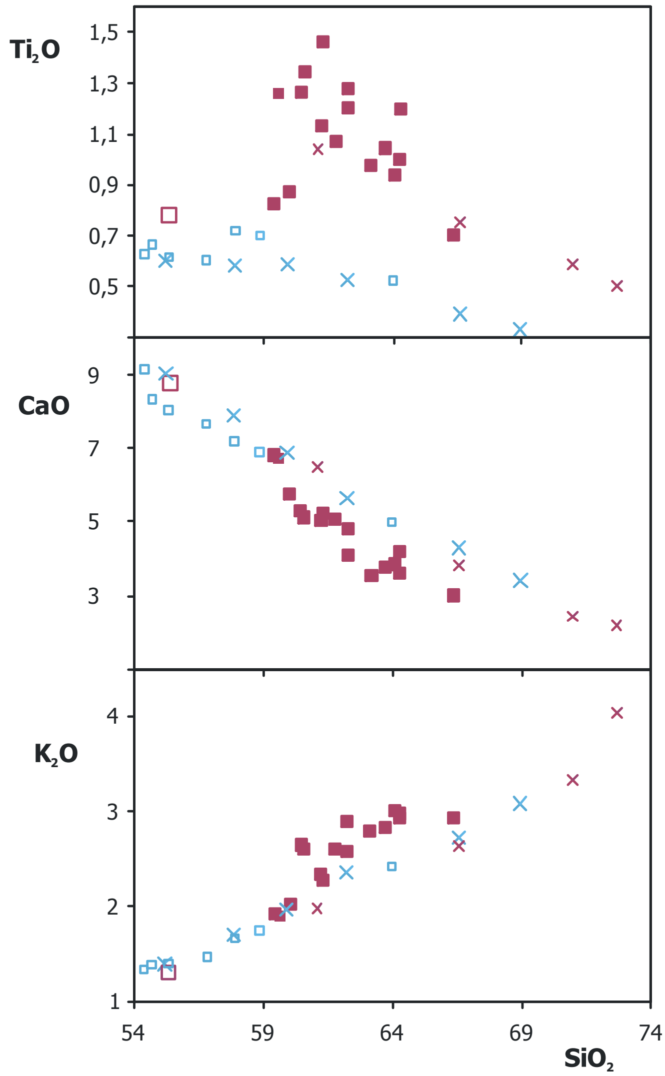

Fig. 6.20 Comparison among major elements contents of the studied tephra **MD33** (violet full squares), marine tephra **Y8** and correlated **Salina** on land deposits (violet open square from Keller et al., 1978 [XRF]; violet crosses from Paterne et al., 1988 [EDS]; blue open squares from De Rosa et al., 2003 [XRF], blue crosses from Gertisser & Keller, 2000 [XRF]).

In particular, regarding the trace elements patterns, MD33 composition compared to the available chemical analysis of the Porri eruption (Gertisser & Keller, 2000), dated at ca. 67 kyr B.P. (Gillot, 1987), represents those of the evolved distal products which are poorly known (Fig. 6.21).

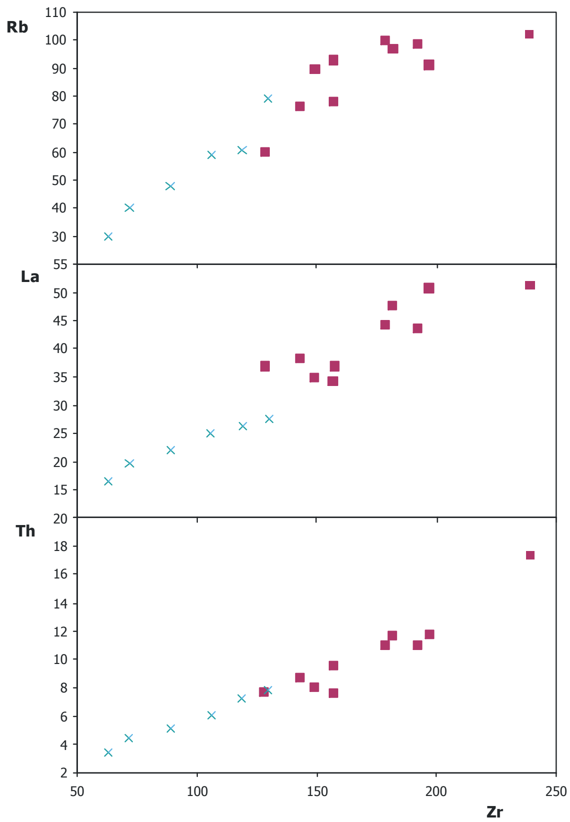

Fig. 6.21 Trace elements diagrams comparing the chemical composition of tephra MD33 and the Porri deposits on land (violet full squares for MD33; blue crosses for Porri data from Gertisser & Keller, 2000 [XRF]).

Based on these results it is possible to identify unprecedented remarkable pyroclastic events from the Salina island at ca. 61 kyr B.P.

Marine Tephra in this study			Literature					
			Keller et al. 1978			Gertisser & Keller 2000		
Marine Tephra	**Chemical classification**	**Age kyr (Isotopic event, AMS ^{14}C)**	**Marine Tephra**	**Chemical classification**	**Age kyr (Oxygen-isotope stratigraphy)**	**Continental Tephra**	**Chemical classification**	**Age kyr (K/Ar)**
MD33	Andasite and Dacite	61,7	Y8	Basaltic andesite	55	Porri	Basaltic andesite	67±8

Tab. 6.10 Ages of MD33 tephra following correlation with dated correlative marine tephra and eruption on Aeolian archipelago.

6.3 Tephras from the Etna volcano

Tephra layer **I1** from core KC01B was attributed to the explosive activity of Mount Etna. This tephra, benmoreitic in composition (recorded at 1.275 m), is dated on the basis of the astronomical tuning at 16.7 kyr B.P. (Lourens, 2004). Its chemical composition and age are comparable to those reported for the eruption of Biancavilla-Montalto, dated between 14 Kyr and 16 kyr B.P. (see chapter 1, Table 1.3), and related to the ignimbrite formation of the Ellittico caldera (De Rita et al., 1991, Coltelli et al., 2000). The marine tephra associated to this event is labeled Y1 and shows a widespread distribution in the central and Eastern Mediterranean Sea (Keller et al., 1978; Paterne et al., 1988; Vezzoli, 1991; Narcisi, 1993; Calanchi et al., 1996,1998) as well as in continental records of central and southern Italy (Narcisi 1993, 1996; Calanchi et al., 1996; Wulf et al., 2004). This broad dispersal pattern can be explained as the result of different explosive eruptions of benmoreitic composition closely spaced in time. This is in agreement with terrestrial data reported by Coltelli et al. (2000), which recognized four layers characterized by benmoreitic composition (named Unit D1 a, b and D2 a, b, dated 15.05±70 kyr below layer D2a) on the eastern slopes of Etna volcano. Comparing Unit D of Coltelli et al. (2000), I1 chemical composition shows a light major SiO_2 content (~ 63 wt % respect to ~ 59 wt % from data on land) (Fig. 6.22).

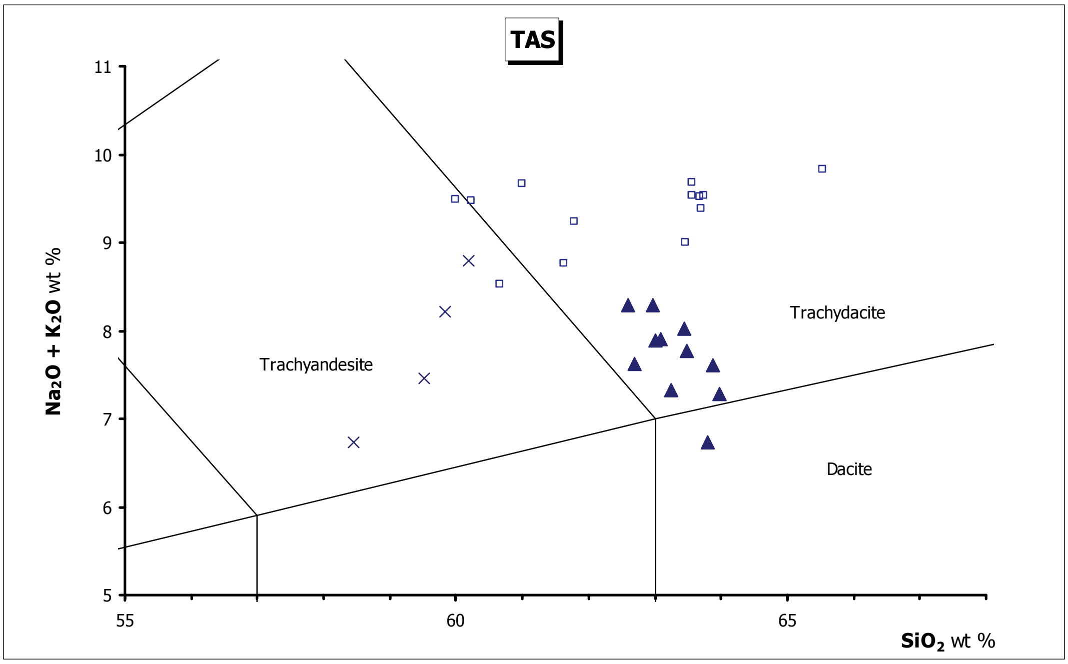

Fig. 6.22 Classification of the studied tephra **I1** (blue full triangles) according to TAS (Total Alkali/Silica) diagram. Compositional range of marine **Y1** and correlated on land deposits is shown for comparison (blue crosses Unit D data from Coltelli et al., 2000; blue open squares Y1 data from Calanchi et al., 1996; Paterne et al. 1988 [EDS]; Siani et al., 2004 [EDS], Vezzoli, 1991 [EDS]; Wulf et al., 2004 [WDS]).

On the other hand, Y1 data from literature (Calanchi et al., 1998; Siani et al., 2004 and Wulf et al., 2004) exhibit wider SiO_2 (ranging between 60 to 65 wt %) and K_2O contents comparable with those of I1 layer. Also in this case the correlation between chemical data of marine tephra and terrestrial deposits, show differences that can be explained by the potential effects of chemical alteration in the seawater or due to the preparation procedures adopted. However trace element contents (see chapter 4) definitively attribute the I1 event to Etna volcanic activity.

Tab. 6.11 shows a comparison between I1 tephra and the published data of Y1. Tephra therefore, a definitive age of 16.7 ky can be attribute to the Y1 tephra of Keller et al. (1978).

Marine Tephra in this study			Literature											
			Siani et al. 2004			Wulf et al. 2004			Keller et al. 1978			Coltelli et al. 2000		
Marine Tephra	Chemical classification	Age kyr (Astronomical Tuning)	Marine Tephra	Chemical classification	Age kyr (^{14}C)	Lacustrine Tephra	Chemical classification	Age kyr (varve)	Marine Tephra	Chemical classification	Age kyr (Oxygen-isotope stratigraphy)	Continental Tephra	Chemical classification	Age kyr (^{14}C)
I1	Benmoreite	16,7	450 cm	Trachydacite	14,65±90	TM11	Benmoreite and Trachydacite	16,44 ±82	Y1		15	Unit D	Benmoreite	15,05 ±70

Tab. 6.11 Age of the I1 tephra following correlation with dated correlatives marine, lacustrine tephra and eruption on land.

6.4 Tephras from the Pantelleria island

Five tephra layers, recovered throughout ODP Leg 160 Site 963A core (**ODP3/5-1**, **ODP6/3-2**, **ODP6/3-3**, **ODP8/1-5** and **ODP8/3-6**), can be reliably correlated to the explosive activity of the Pantelleria island. Chemical features of these tephra layers are typical of peralkaline rocks that outcrop on the Pantelleria island.

Several authors have analysed the volcanological evolution of that island into two main distinct phases separated by the Green Tuff eruption (e.g. Villari, 1974; Cornette et al., 1983; Mahood and Hildreth, 1983, 1986; Civetta et al., 1984, 1988, 1998; Orsi & Sheridan, 1984, Avanzinelli et al., 2004). However, it appears nowadays difficult to identify a clear sequence of eruptive phases because of the scarce and scattered distribution of land outcrops. The only reliable chemical databases for the Pantelleritic products related to the last 120 kyr of volcanic activity come from the studies of Mahood & Hildreth (1986) and Civetta et al. (1998)

A peralkaline ash layer (Y6), found in sediment cores from the eastern Mediterranean Sea, was attributed to Pantelleria Green Tuff with an assigned age of ~ 45 Kyr B.P., based on oxygen isotope stratigraphy by Keller et al. (1978). The comparison between tephra ODP3/5-1, the marine tephra Y6 and a number of deposits on land related to Green Tuff explosive eruption (Fig. 6.23 and Fig. 6.24) shows a good agreement, confirming the compositional recurrent and characteristic change from the base upwards (from pantelleritic to trachytic group) according to Civetta et al. (1984, 1998).

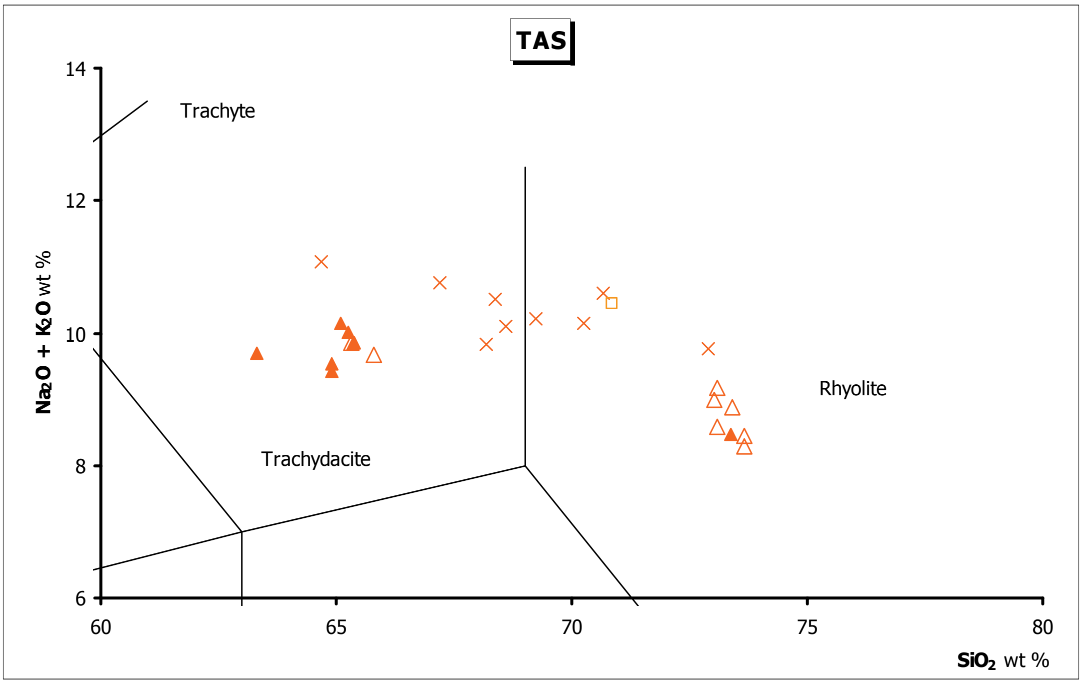

Fig. 6.23 Classification of the studied tephra **ODP3/5-1** (open and full orange triangles) according to TAS (Total Alkali/Silica) diagram. Compositional range of marine **Y6** and on land deposits are shown for comparison (orange crosses Green Tuff data from Civetta et al., 1998 [WDS] and Avanzinelli et al., 2004 [XRF, AAS]; orange open square Y6 data from Keller et al., 1978 [XRF]).

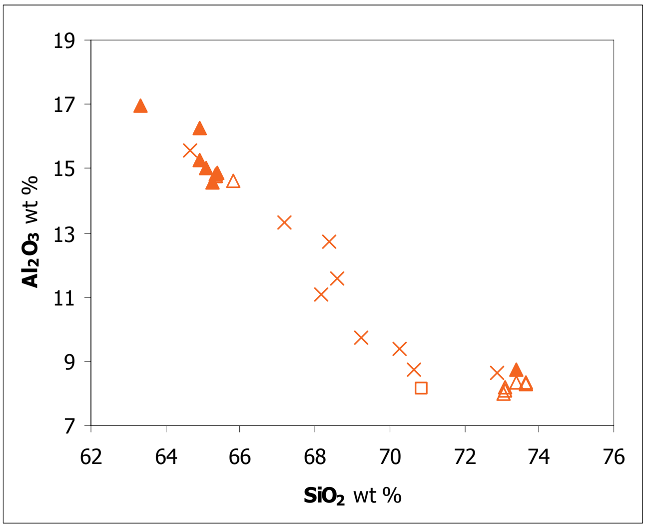

Fig. 6.24 Major elements diagrams comparing the chemical composition of tephra **ODP3/5-1** (open and full orange triangles) with on land deposits of Green Tuff from literature (orange crosses, Civetta et al., 1998 [WDS] and Avanzinelli et al., 2004 [XRF, AAS]) and for marine **Y6** from Keller et al., (1978) [XRF] (orange open square).

In terms of chronological data Mahood & Hildrecth (1986) propose an time interval from 45 to 50 kyr B.P. for the Green Tuff products based on K-Ar dating methods, while the age of ODP3/5-1 based on the age model of the core (Sprovieri et al. *personal communication*) is ~ 42 Kyr B.P.

Tephra ODP6/3-2 and tephra ODP6/3-3 also in this case exhibit a compositional affinity with pantelleritic products possibly to correlate with the older volcanic alacrity activity of Civetta et al. (1998) (Fig. 6.25).

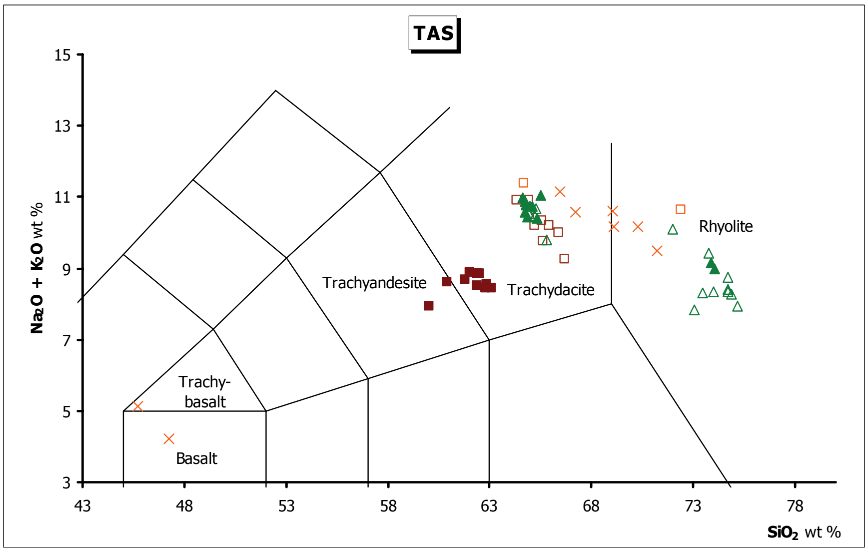

Fig. 6.25 Classification of the studied tephra **ODP6/3-2** (open and full red squares) and **ODP6/3-3** (open and full green triangles) according to TAS (Total Alkali/Silica) diagram. Compositional range of marine **P11** and on land old deposits are shown for comparison (orange crosses old data from Civetta et al., 1998 [WDS] and Avanzinelli et al., 2004 [XRF, AAS]; orange open squares P11 data from Paterne et al., 2008 [EDS]).

Paterne et al. (2008) recognised in a number of marine sedimentary cores from the Tyrrhenian and the Ionian Sea, a total of seven tephra layers related to the older volcanic activity of Pantelleria. In particular in the Ionian Sea throughout the KET8222 and KET8011 cores, four thick tephra layers (P11, P12, P13 and P14) with tephri-phonolitic, trachy-comenditic and pantelleritic composition of the glass shards, were found and dated at 131, 164, 192, 193 kyr B.P., respectively. Tephra layer P11, particularly, display a good correlation with the tephras ODP6/3-2 ODP6/3-3 even if the tephra ODP6/3-2 present at the top a trachy-andesitic composition not documented neither by Paterne et al. (2008), nor on land deposits of Civetta et al. (1998) (Fig. 6.25 and Fig. 6.26).

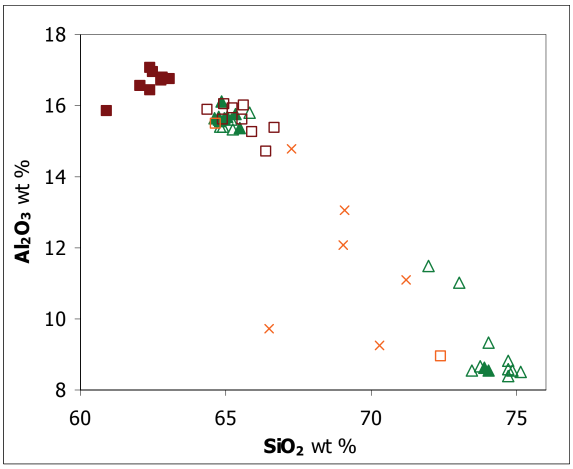

Fig. 6.26 Major elements diagrams comparing the chemical composition of tephra **ODP6/3-2** (open and full red squares) and **ODP6/3-3** (open and full green triangles) with on land deposits from literature (orange crosses, Civetta et al., 1998 [WDS] and Avanzinelli et al., 2004 [XRF, AAS]) and with the marine **P11** from Paterne et al., (2008) [EDS] (orange open square).

Tephra ODP8/1-5 can be correlated, instead with tephra composition P13 of Paterne et al. (2008) (Fig. 6.27 and Fig. 6.28). The age model for the core section allows us to definitively date these deposits at ~ 189 kyr B.P.

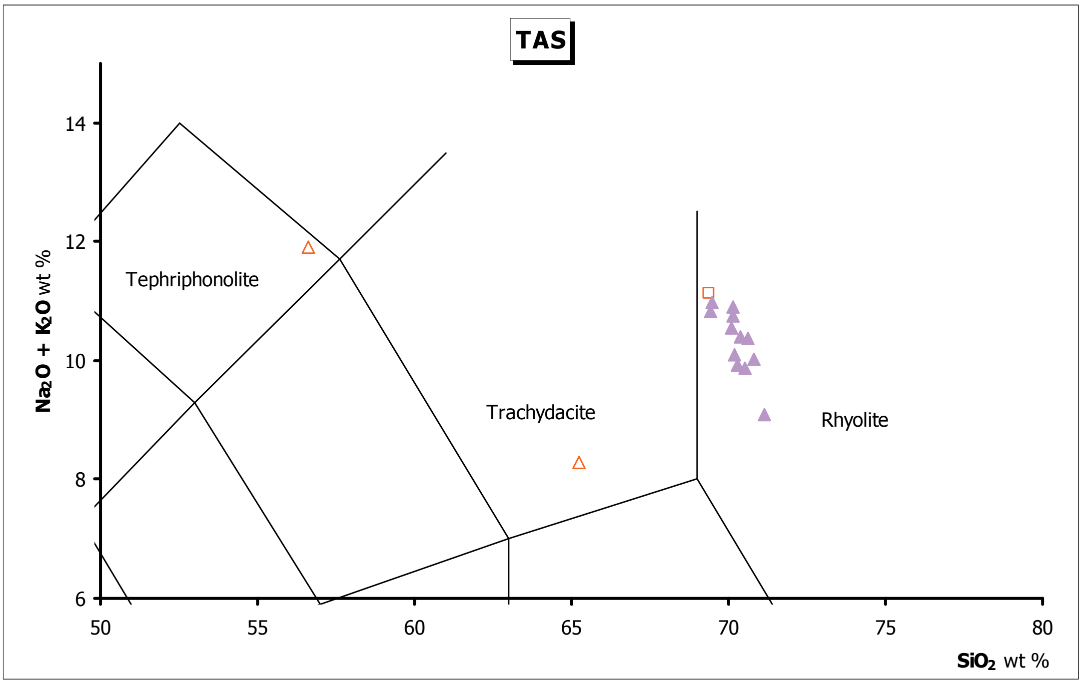

Fig. 6.27 Classification of the studied tephra **ODP8/1-5** (full lilac triangles) according to TAS (Total Alkali/Silica) diagram. Compositional range of marine **P13** and **P14** tephra (orange open square and orange open triangles, respectively) data from Paterne et al. (2008) [EDS].

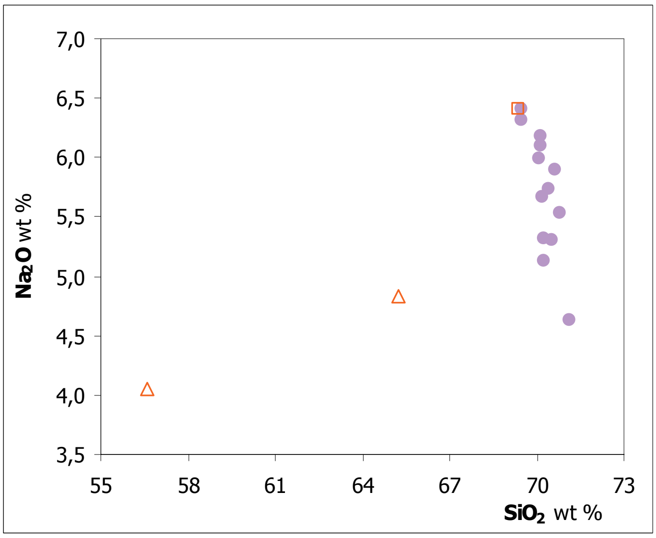

Fig. 6.28 Major elements diagrams comparing the chemical composition of the tephra **ODP8/1-5** (full lilac circles) with marine **P13** and **P14** from Paterne et al., (2008) [EDS] (orange open square and triangles, respectively).

The last and older tephra layer ODP8/3-6, recorded throughout the ODP Leg 160, Site 963A shows a chemical signature very similar to tephra P15 and or P16 dated by Paterne et al. (2008) at ~ 198 Kyr B.P. (Fig. 6.29).

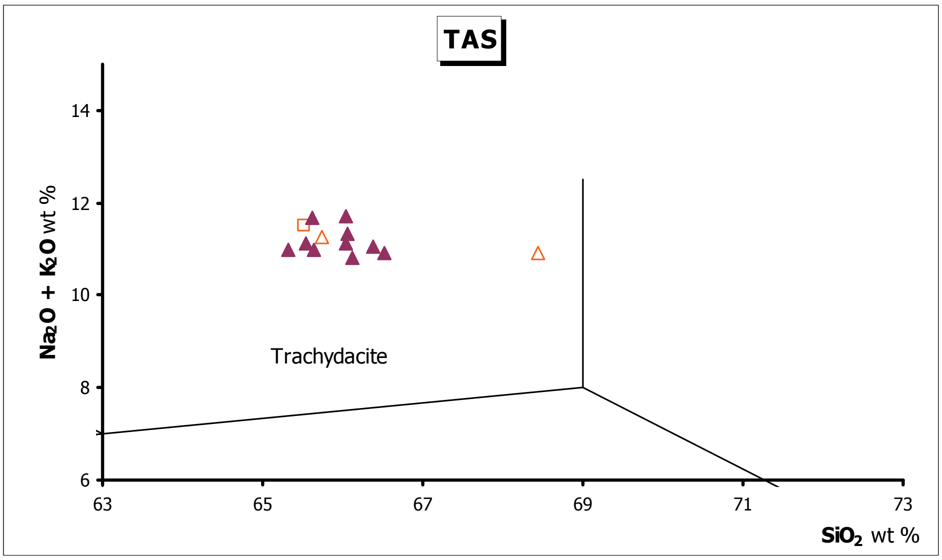

Fig. 6.29 Classification of the studied tephra **ODP8/3-6** (full violet triangles) according to TAS (Total Alkali/Silica) diagram. Compositional range of marine **P15** and **P16** (orange open square and orange open triangles respectively). Data from Paterne et al. (2008) [EDS].

Table 6.12 shows the correlation of tephra layers from ODP Leg 160 Site 963A core with the coeval events reported by Paterne et al. (2008).

Marine Tephra in this study			Literature								
			Paterne et al. 2008			Keller et al. 1978			Mahood and Hildreth 1986		
Marine Tephra	**Chemical classification**	**Age kyr (Oxygen-isotope stratigraphy, eco-biostratigraphy)**	**Marine Tephra**	**Chemical classification**	**Age kyr (Oxygen-isotope stratigraphy)**	**Marine Tephra**	**Chemical classification**	**Age kyr (Oxygen-isotope stratigraphy)**	**Continental Tephra**	**Chemical classification**	**Age kyr (K-Ar)**
ODP3/5-1	Trachy-dacite and Pantellerite	42,5				Y6		45	Green Tuff	Trachyte and Pantellerite	45-50±4
ODP6/3-2	Trachy-andesite and trachy-dacite	127,4	P11	Trachy-comendite and Pantellerite	131				Unit P		133,1±3,3
ODP6/3-3	Trachy-dacite and Pantellerite	127,8									
ODP8/1-5	Pantellerite	188,7	P13-P14	Tephriphonolite, Trachy-comendite and Pantellerite	192,5 and 193				Unit I		189,3±6
ODP8/3-6	Trachy-comendite	197,7	P15-P16	Trachy-comendite and Pantellerite	197,4 and 198				409		195±10

Tab. 6.12 Age of the tephras collected from the ODP Leg 160, Site 963A following correlation with dated correlatives marine tephras and eruptions on land.

The accurate chronology here reported for tephras associated to the Pantelleria explosive volcanic activity offered an intriguing extension of the present knowledge for the volcanic cycles during the last 200 kyr and then allowed us to verify the consistence of previous chronological data.

6.5 Tephras with uncertain attributions

Some tephras recognised throughout the MD01_2474G record are characterised by chemical compositions that do not allow to clearly recognising a source area. In particular, an evident chemical heterogeneities of these deposits suggests an origin from zoned magma chambers and/or contemporaneous different eruptions. Moreover, the closeness of these tephras suggests that effects of mixing by bioturbation may render highly improbable an attribution to volcanic sources.

In particular, two tephra layers recovered along the MD01_2474G core (MD10 and MD14) at 176 cm and 260 cm respectively, show heterogeneous chemical features. The younger tephra **MD10**, dated at ~ 14 kyr B.P., shows two distinct groups of trachyandesitic and trachytic compositions (Fig. 6.30).

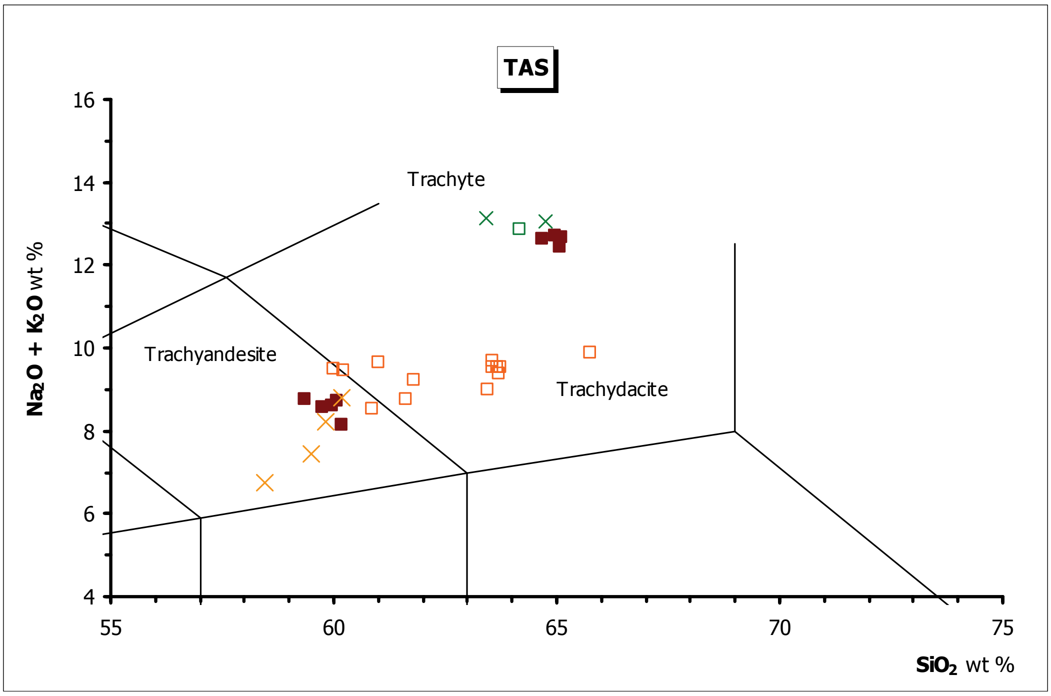

Fig. 6.30 Classification of the studied tephra **MD10** (red full squares) according to TAS (Total Alkali/Silica) diagram. Compositional range of marine **Y1, C3** and correlated on land deposits are shown for comparison (orange open squares Y1 data from Calanchi et al., 1996; Paterne et al. 1988 [EDS]; Siani et al., 2004 [EDS], Vezzoli, 1991 [EDS]; Wulf et al., 2004 [WDS]; green open square C3 data from Paterne et al. 1988 [EDS]; orange crosses Unit D data from Coltelli et al., 2000; green crosses Campotese data from Vezzoli, 1988 [XRF]).

Trachyandesitic composition group of MD10 tephra are comparable to that of the explosive activity of Mount Etna, and in particular similar to the well-known eruption of Biancavilla-Montalto dated between 14-16 kyr B.P. (Coltelli et al., 2000). At the same time the trachytic chemical group can been correlated to Campania volcanism (Fig. 6.31).

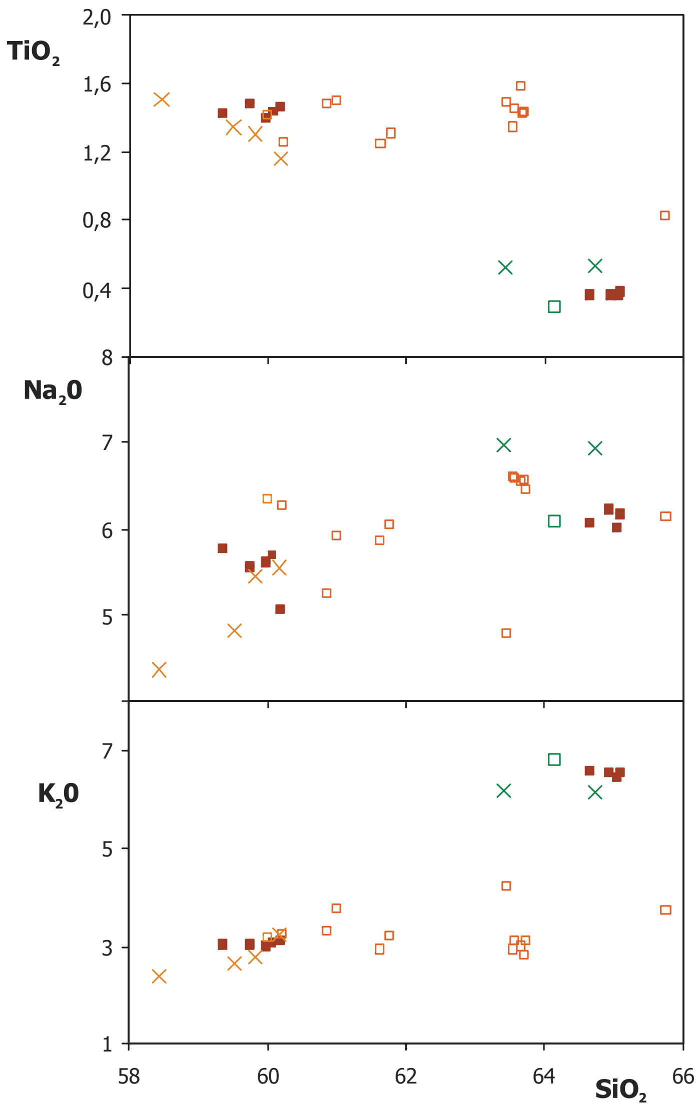

Fig. 6.31 Major elements diagrams comparing the chemical composition of the tephra **MD10** (red full squares) with that of the marine **Y1, C3** and correlated on land deposits (orange open squares Y1 data from Calanchi et al., 1996; Paterne et al. 1988 [EDS]; Siani et al., 2004 [EDS], Vezzoli, 1991 [EDS]; Wulf et al., 2004 [WDS]; green open square C3 data from Paterne et al. 1988 [EDS]; orange crosses Unit D data from Coltelli et al., 2000; green crosses Campotese data from Vezzoli, 1988 [XRF]).

Poly et al. (1989) indicate in the south-western sector of Ischia island the beginning of the construction of the Campotese volcano with a trachytic lava flows mark. Its activity continues up to 18 kyr ago with a huge explosive eruption that closed the IV phase of activity on the island (Chiesa et al., 1985 a, b and c). This event, known as "Sant' Angelo Tuff" was dated at 17,8±3,2 kyr by K/Ar (Poly et al., 1987). Marine tephra related to this explosive eruption in the Tyrrhenian Sea is also reported by Paterne et al. (1988) (tephra C-3) at 14,4 kyr B.P (interpolate age) (Tab. 6.13).

Marine Tephra in this study			Literature					
			Siani et al. 2004			**Coltelli et al. 2000**		
Marine Tephra	**Chemical classification**	**Age kyr (Isotopic event, AMS ^{14}C)**	**Marine Tephra**	**Chemical classification**	**Age kyr (^{14}C)**	**Continental Tephra**	**Chemical classification**	**Age kyr (^{14}C)**
	Benmoreite		450 cm	Trachyandesite	14,65±90	Unit D	Benmoreite	15,05 ±70
MD10		14,4	**Paterne et al. 1988**			**Vezzoli 1988**		
			Marine Tephra	**Chemical classification**	**Age kyr (Oxygen-isotope stratigraphy)**	**Continental Tephra**	**Chemical classification**	**Age kyr (K Ar)**
	Trachyte		C3	Trachyte	14,4	134	Trachyte	17,8±3,2

Tab. .6.13 Ages of MD10 tephra following correlation with dated correlatives marine tephras and eruptions on land.

As the previous tephra **MD14** tephra has an heterogeneous chemical composition: from basaltic trachyandesite to trachydacite and trachyte (Fig. 6.32).

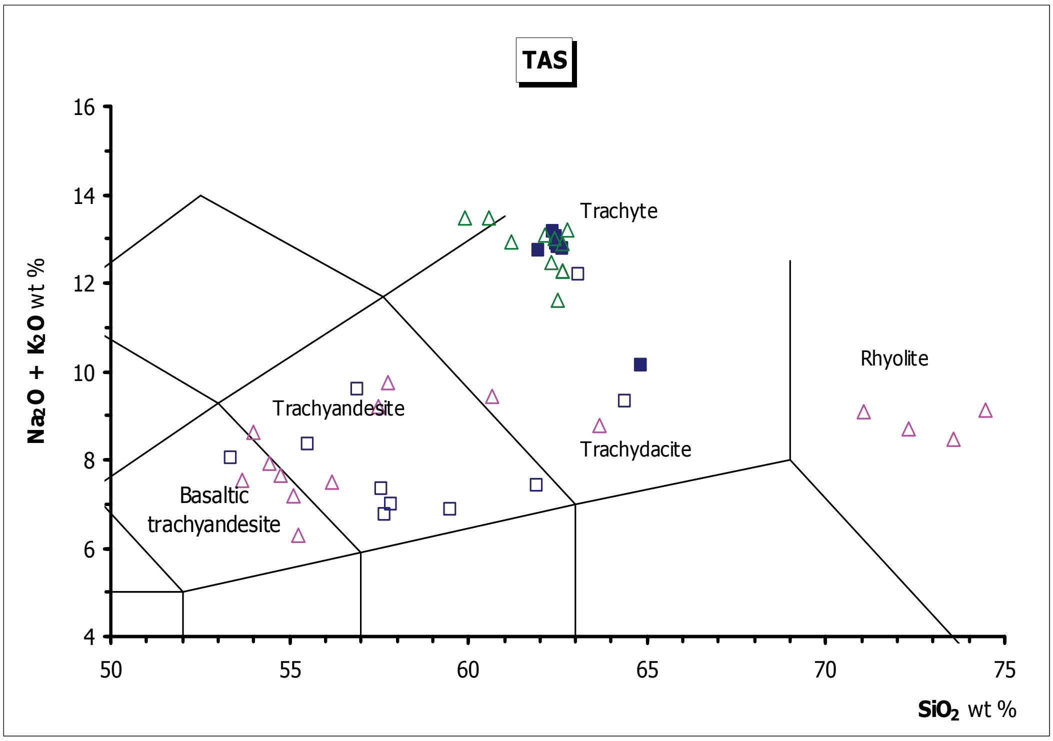

Fig. 6. 32 Classification of the studied tephra **MD14** (blue full and open squares) according to TAS (Total Alkali/Silica) diagram. Compositional range of marine **Y3** and correlated **Volcano** on land deposits is shown for comparison (green open triangles Y3 data from; Munno & Petrosino 2004, 2007 [EDS]; Paterne et al. 1988 [EDS]; Sulpizio et al., 2003 [EDS], Wulf et al., 2004 [WDS]; Keller et al., 1978 [XRF]; pink open triangles Volcano data from De Astis et al. 2000 [XRF]).

The first group is similar to that of the Intermediate Brown Tuff (IBT) unit originated by the complex Vulcano-Lipari activity. Lucchi et al. (2008) attribute to this unit an age from ca. 21 kyr to ca. 56 kyr B.P with a wider chemical composition from basalt trachy-andesite to rhyolite. Actually, the chronological limits of IBT and the subdivision between IBT and the underlying Lower Brown Tuff (extened up to 80 kyr) is marked at the top by the interbedded outcrops of the Quadrata and Spiaggia Lunga formations dated at 21,3±3,4 Kyr and 24±5 kyr B.P., respectively, and by the local contact with the Monte Epomeo Green Tuff (ca. 56 kyr old) at the base. As shown in the major element versus the silica content diagrams (Fig. 6.33) there is clear overlap between the MD14 and the IBT except for the TiO_2 contents.

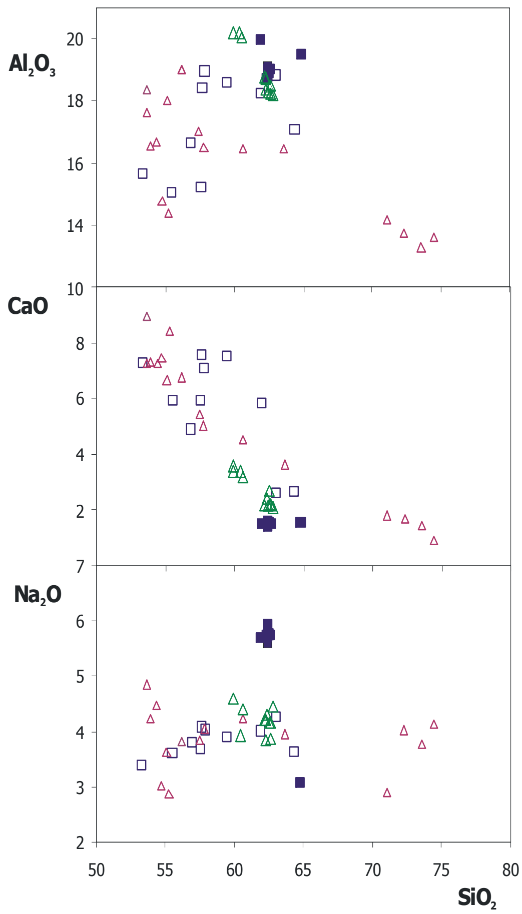

Fig. 6.33 Major elements diagrams comparing the chemical composition of the tephra MD14 with marine tephra Y3 and correlated Volcano on land deposits (green open triangles Y3 data from Munno & Petrosino 2004, 2007 [EDS]; Paterne et al. 1988 [EDS]; Sulpizio et al., 2003 [EDS], Wulf et al., 2004 [WDS]; Keller et al., 1978 [XRF]; pink open triangles Volcano data from De Astis et al. 2000 [XRF]).

At the same time the trachytic group, on chronological and chemical base, corresponds most likely to the glass chemistry of the marine Y3 tephra occurring in deep-sea cores from the Ionian Sea (Keller et al., 1978; Kraml, 1997 a and b) (Tab. 6.14). Tephra Y3 has been dated at 25,57±0,11 kyr by radiocarbon dating (Buccheri et al., 2002). The origin of Y3 is debated because related outcrops on land are scarce. For example, while Keller et al. (1978) has generically attributed it to the Campanian Province, Paterne et al. (1988), on the contrary, ascribed it to the "Campanian Ignimbrite Series".

Marine Tephra in this study			Literature					
			Paterne et al. 1988			Di Vito et al. 2008		
Marine Tephra	**Chemical classification**	**Age kyr (Isotopic event, AMS ^{14}C)**	**Marine Tephra**	**Chemical classification**	**Age kyr (Oxygen-isotope stratigraphy)**	**Continental Tephra**	**Chemical classification**	**Age kyr (^{14}C)**
MD14	Trachyte	21	C7	Trachyte	26,9	SIMP1-e	Trachyte	30,67±0,27
			Lucchi et al. 2008					
			Island Tephra	**Chemical classification**	**Age kyr (^{14}C)**			
	from Basaltic-trachyandesite to Trachydacite		IBT unite	from Basaltic-trachyandesite to Trachydacite	22,6±0,3			

Table 6.14 Ages of MD14 tephra following correlation with dated correlatives marine and on land tephras.

Finally the MD14 tephra can be interpret as originated by two coeval but distinct eruption from Campanian and Aeolian sources, and in particular the accurate age of MD14 at 21 kyr allow to grow the chronological information as regard the complex Aeolian unit correlated.

6.6 Correlation of the studied tephra layers with the Keller's tephrochronology

The last 200 kyr explosive activity of southern Italian volcanoes, the main source of tephras in the central Mediterranean basin, is relatively poorly known probably because the products of those phenomena are generally covered by most recent deposits and are not directly accessible. On the other hand, distal archives (e.g. marine successions, lacustrine records, ect) better preserve deposits related to volcanic activities far from the eruptive centres.

Most of distal marine tephra from sedimentary records in the Mediterranean are labelled with the acronyms defined by Keller et al. (1978), (e.g. zone Y, tephra layer Y-1, Y-2, Y-3 etc.) with a nomenclature system developed for deposits found in cores from the Ionian and Aegean seas. It is noteworthy to establish that the tephrostratigraphic reconstruction of those authors considered only layers visible by naked eyes. Moreover, since the studied cores were located hundreds of kilometres from the nearest volcanic sources, only the most powerful and highly dispersive eruptions (i.e. those with a consequential relevant thickness in the marine cores) were identified and correlated at regional scale.

In this paragraph, a synopsis of the tephrostratigraphic reconstruction achieved in this research work is reported along with a detailed comparison with available literature data useful to verify the potential for a refined tephrochronology of the Mediterranean basin (Fig. 6.34 and Tab. 6.15).

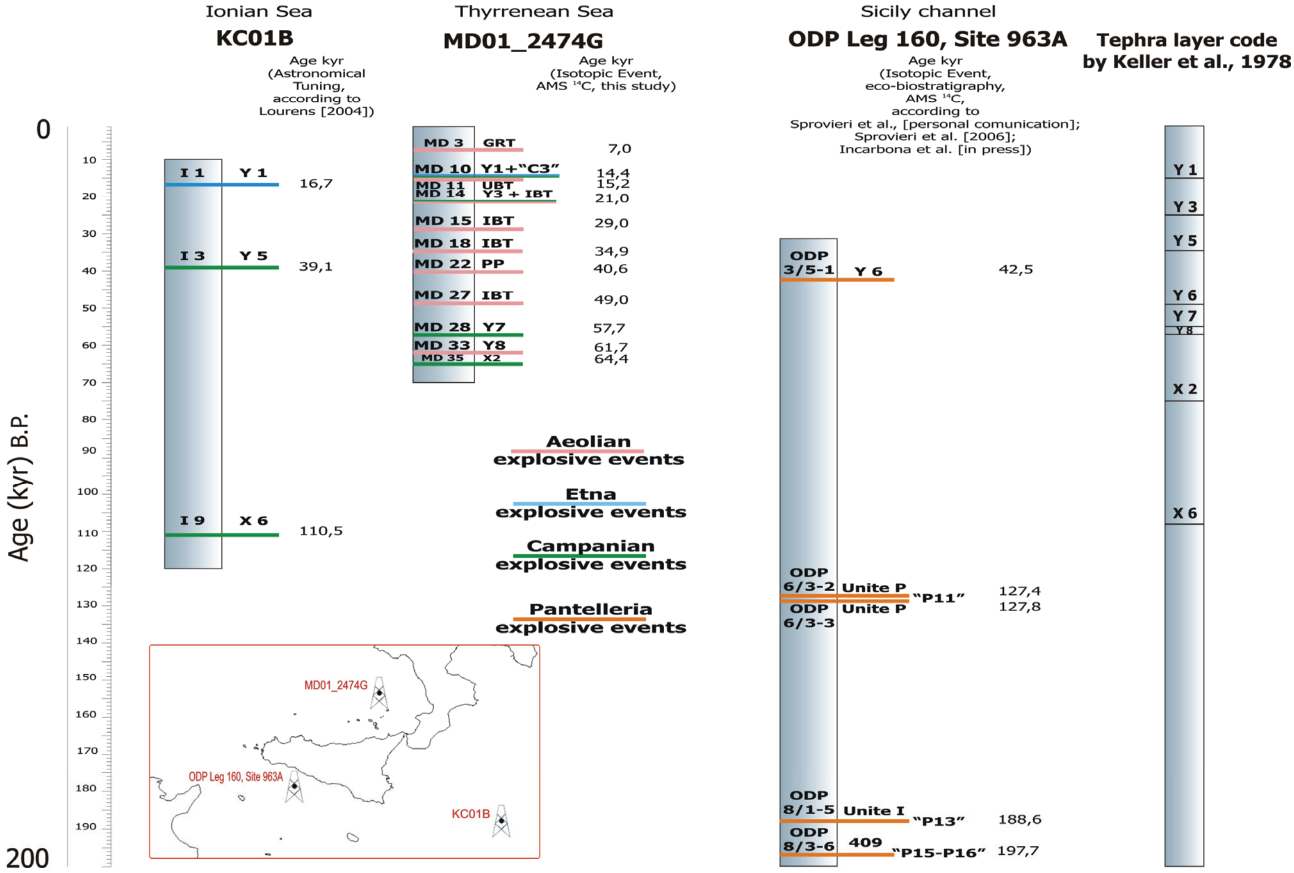

Fig. 6.34 Schematic correlation among tephra layers recognised in the three studied marine records with the potential explosive events.

The youngest tephra layer MD3, dated at 7 kyr, was correlated with an eruption from the Vulcano island. This tephra have not correspondence with marine tephras previously reported by Keller et al. (1978) and consequently the new label ***Vul1*** is proposed for that deposit.

At ca 15 kyr B.P. several authors indicate the presence, in numerous distal settings, of tephras related to the Biancavilla-Montalto ignimbrite (**Y1**). In this study, the MD10v tephra layer dated at 14,4 by isotopic event-AMS ^{14}C, and the I1 deposits dated 16,7 kyr by astronomical tuning event were correlated to that eruptive event. Particularly, differences in age proposed in this research with respect to those reported in literature may be attributed to different dating approach and we consider final age proposed as the most reliable.

The chemical signature of the MD10 tephra, with a calibrated age of 14,4 kyr, previously not recorded in sedimentary records, clearly suggests a direct influence from Ischia eruption. For this tephra a new label ***Is1*** is here proposed. The MD11 tephra was been attributed to an Aeolian explosive eruption, most likely with a limited dispersive pattern and consequently not earlier recorded in Mediterranean sedimentary records. For this tephra the new label ***Ae1*** is here proposed.

The MD14 tephra shows a chemical signature correspondent to that of the known **Y3** tephra of Keller et al. (1978), while the MD14 deposit, with a calibrated age of 21 kyr, suggests a previously not documented Aeolian volcanic source, is here labelled ***Ae2***.

The tephra layers MD15 and MD18, with ages of 29 and 34,9 ky respectively, were attributed to other Aeolian eruptive events, and labelled ***Ae3*** and ***Ae4***.

One of the most known eruptions occurred in the last 200 kyr and generally well documented in Mediterranean sedimentary records, is the Campanian Ignimbrite (**Y5**) dated at ca 39 kyr B.P. The CI products were clearly recognised in this study in the deposit I3.

The tephra MD22, dated at 40,6 ky, was correlated to an early unrecognised volcanic activity of the Lipari island. For that event a new label ***Ae5*** is proposed.

The four tephra layers MD28, MD33, MD35 and I9 were definitively correlated, on the basis of chemical signatures, to the known **Y7**, **Y8**, **X2** and **X6** of Keller et al. (1978).

Finally, chemical signatures of the four tephra layers ODP6/3-2, ODP6/3-3, ODP8/1-5 and ODP8/3-6, dated at 127,4, 127,8, 188,6, 197,7 ky respectively, were clearly correlated to sequential volcanic activity of the Pantelleria island and that here we labelled with ***Pant1***, ***Pant2***, ***Pant3*** and ***Pant4*** codes.

Tephra label	Age (kyr)	Composition	Origin	Correlation attempt	Tephra code (this study)
MD3	7,0	Latite	Aeolian		Vul1
MD10	14,4	Benmoreite + Trachyte	Etna/Campanian	Y1 +	Is1
MD11	15,2	Trachyandesite and Trachydacite	Aeolian		Ae1
I1	16,7	Benmoreite	Etna	Y1	
MD14	21,0	from Basaltic-trachyandesite to Trachydacite + Trachyte	Aeolian/Campanian	Y3 +	Ae2
MD15	29,0	from Trachybasalt to Trachyandesite	Aeolian		Ae3
MD18	34,9	from Basaltic-trachyandesite to Dacite	Aeolian		Ae4
I3	39,1	Trachyte	Campanian	Y5	
MD22	40,6	from Basaltic-trachyandesite to Rhyolite	Aeolian		Lip1
ODP3/5-1	42,5	Trachy-dacite and Pantellerite	Pantelleria	Y6	
MD27	49,0	Basaltic-trachyandesite and Trachyandesite	Aeolian		Ae5
MD28	57,7	Trachyte	Campanian	Y7	
MD33	61,7	Andasite and Dacite	Aeolian	Y8	
MD35	64,4	from Basaltic-trachyandesite to Trachyte	Campanian	X2	
I9	110,5	Trachyte	Campanian	X6	
ODP6/3-2	127,4	Trachy-andesite and trachy-dacite	Pantelleria		Pant1
ODP6/3-3	127,8	Trachy-dacite and Pantellerite	Pantelleria		Pant2
ODP8/1-5	188,6	Pantellerite	Pantelleria		Pant3
ODP8/3-6	197,7	Trachy-comendite	Pantelleria		Pant4

Tab. 6.15 Main tephra markers recognised in this work.

7 Conclusions

This research work aims give to a contribution to a more detailed tephrochronological reconstruction of the Mediterranean basin for the last 200 kyr (Fig. 7.1). A full chemical dataset (generally based on major, minor and trace element investigations) of 19 tephra layers integrated with a high-resolution age models representive innovative approach to the tephrochronology have been presented and results showed in Fig. 7.1.

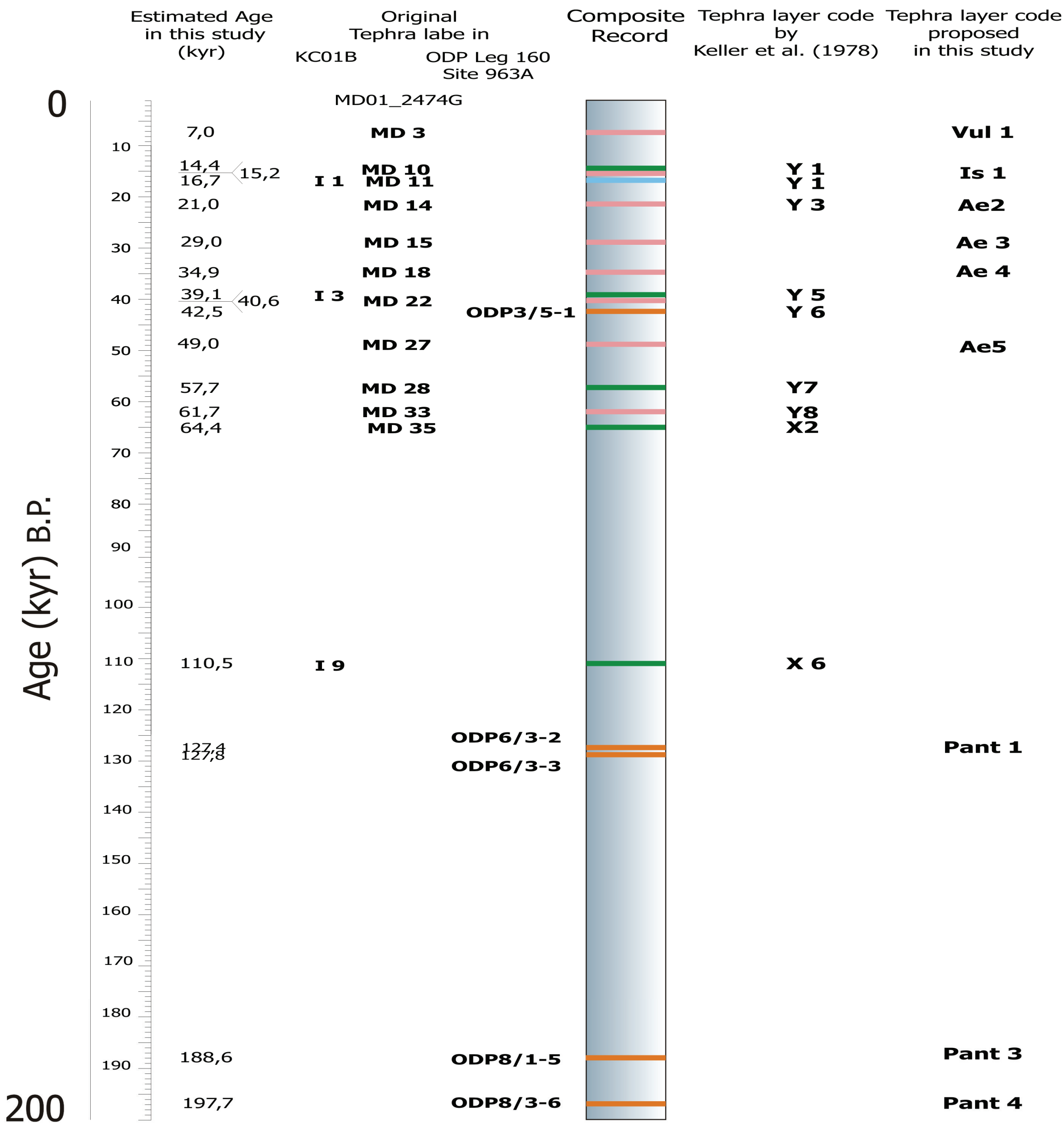

Fig. 7.1 Chronological scheme of the composite record achieved for the 7-200 kyr B.P. time interval.

Synthetically, the most significant results attained by this research are reported below:

- ✓ Generation of a high-quality chemical dataset for a number of tephra layers collected from Mediterranean records of the last 200 ky and based on WDS and LA_ICP-MS analysis of juvenile materials.
- ✓ Accurate dating of all the analysed tephra layers by adoption of high-resolution age models, based on modern stratigraphic and chronological techniques, and consequent improvement of previously reported ages of several Mediterranean late Pleistocene tephras (Tab. 7.1).

This study			**Literature**			
Tephra label	**Age (kyr BP)**	**Dating method**	**Tephra layer code by *Keller et al. (1978)***	**Age (kyr BP)**	**Dating method**	**References**
MD10	14,4	Isotopic event, AMS ^{14}C	Y1	15,05 ±0,70	^{14}C	Coltelli et al., (2000)
I1	16,7	Astronomical Tuning				
MD14	21,0	Isotopic event, AMS ^{14}C	Y3	30,67±0,27	^{14}C	Di Vito et al., (2008)
I3	39,1	Astronomical Tuning	Y5	38,6±1,1	$^{40}Ar/^{39}Ar$	Fedele et al., (2008)
ODP3/5-1	42,5	Oxygen-isotope stratigraphy, Eco-biostratigraphy	Y6	45-50±4	K/Ar	Mahood & Hildreth, (1986)
MD28	57,7	Isotopic event, AMS ^{14}C	Y7	56±2,8	K/Ar	Brown et al., (2007)
MD33	61,7	Isotopic event, AMS ^{14}C	Y8	67±8	K/Ar	Gertisser & Keller, (2000)
MD35	64,4	Isotopic event, AMS ^{14}C	X2	70	Sapropel stratigraphy	Keller et al., (1978)
I9	110,5	Astronomical Tuning	X6	107	Sapropel stratigraphy	Keller et al., (1978)

Tab. 7.1 Labels and ages of Tephra horizons from this study. Correlation with correlatives dated tephras by literature.

- ✓ Reconstructions of some steps of the volcanic activity occurred at the Aeolian arc and Pantelleria island. In particular, seven studied tephras were attributed to the volcanic activity of the Aeolian arc, and four tephras were correlated to volcanic activity of the Pantelleria island.

In some cases dating of tephras appears problematic. In particular, MD10 and I1 deposits seem clearly correlated to the Y1 event of Keller et al. (1978) but they show evident differences in ages, 14,4, 16,7 and 15,05±0,7 kyr, respectively. This chronological differences can be probably due to systematic errors associated to the different dating methods adopted for age calibration of the tephra layers (Isotopic event-AMS ^{14}C, Astronomical tuning and AMS ^{14}C, respectively) or they could be associated to different eruptive phases of the poor-documented Biancavilla-Montalto ignimbrite. Further investigations could provide definitive insights on these more complex tephrostratigraphic events.

References

- **Alley R.B.,** Clark P.U. (1999) - *The deglaciation of the Northern Hemisphere: a global perspective*. Annual Review of Earth and Planetary Sciences, 27, 149–182.
- **Allen J.R.M.,** Brandt, U., Brauer A., Hubbertens A.W., Huntley B., Keller J., Kraml M., Mackensen, A., Mingram J., Negendank J.F.W., Nowaczyk N.R., Oberhänsli, H., Watts W.A., Wulf S., Zolitschka B. (1999) - *Rapid environmental changes in southern Europe during the last glacial period***.** Nature, 400, 740–743.
- **Andersen K.K**., Ditlevsen P.D., Rasmussen S.O., Clausen H.B., Vinther B.M., Johnsen S.J. (2006) - *Retrieving a common accumulation record from Greenland ice cores for the past 1800 years*. Journal of Geophysical Research, 111, D15106.
- **Andronico D.,** Calderoni G., Cioni R., Sbrana A., Sulpizio R., Santacroce R., (1995) - *Geological map of Somma-Vesuvius volcano*. Per. Miner., 64, 77-78.
- **Andronico D & Cioni R.,** (2002) **-** *Constrating styles on Mount Vesuvius activity in the period between the Avellino and Pompei Plinian eruptions, and some implicatis for assessment of future hazards***.** Bull. Volcan., 64, 372-391.
- **Armienti P**., Francalanci L., Landi P. (2007) - *Textural effects of steady state behaviour of the Stromboli feeding system*. Journal of Volcanology and Geothermal Research, 160, 86–98.
- **Armienti P**, Tonarini S, D'Orazio M, Innocenti F. (2004) - *Genesis and evolution of Mt. Etna alkaline lavas: petrological and Sr-Nd-B isotope constraints*. Per. Mineral., 73, 29-52.
- **Armienti M.**, Barberi F., Bizourd H., Clocchiatti R., Innocenti F.,Metrich N., Rosi M., Sbrana A. (1983) - *The Phlegrean Fields: magma evolution within a shallow chamber. Explosive Volcanism*. Journal of Volcanology and Geothermal Research 17, 289-311.
- **Ascough P**., Cook G., Dugmore A. (2005) - *Methodological approaches to determining the marine radiocarbon reservoir effect*. Progress in Physical Geography, 29, 532–547.
- **Aksu A.E**., Jenner G., Hiscott R.N., İşler E.B. (2008) - Occurrence, stratigraphy and geochemistry of Late Quaternary tephra layers in the Aegean Sea and the Marmara Sea. doi:10.1016/j.margeo.2008.04.004
- **Avanzinelli R**., Bindia L., Menchettia S., Ponticelli S. (2004) - *Crystallisation and genesis of peralkaline magmas from Pantelleria Volcano, Italy: an integrated petrological and crystal-chemical study*. Lithos, 73, 41– 69.
- **Baksi A. K**., Archibald D. A., Farrar E. (1996) - *Intercalibration of $^{40}Ar/^{39}Ar$ dating standards*. Chemical Geology, 129: 307-324.
- **Bard E.,** Rostek F., Ménot-Combes G. (2004a) - *Radiocarbon calibration beyond 20,000 ^{14}C yr B.P. by means of planktonic foraminifera of the Iberian margin*. Quaternary Research, 61, 204–214.
- **Beccaluva L.**, Di Girolamo P. & Serri G. (1991). *Petrogenesis and tectonic setting of the Roman Volcanic Province*. Lithos, 26, 191-221.
- **Beccaluva L.,** Rossi P.L., Serri G. (1982) - *Neogene to Recent volcanism of the southern Tyrrhenian-Sicilian area: implications for the geodynamic evolution of the Calabrian arc*, Earth Evol Sci 3,222-238.
- **Behl R. J.,** Kennett J.P, (1996) - Brief interstadial events in the Santa Barbara basin, NE Pacific during the past 60 kyr. Nature, 379: 243-246.
- **Bender, M.,** Sowers T., Dickson M. L., Orchardo J., Grootes P., Mayewski P. and Meese. D., (1994) - *Climate correlations between Greenland and Antarctica during the past 100,000 years*, Nature 372, 663-666.
- **Bertagnini A**., Landi P., Rosi M., Vigliargio A., (1998) - *The Pomici di Base plinian eruption of Somma-Vesuvius.* JVGR, 83, 219-239.
- **Bond G. C**., R. Lotti (1995) - *Iceberg discharges into the North Atlantic on millennial time scales during the last glaciation*. Science, 267, 1005– 1010.

✓ **Bond, G.**, Broecker W. S., Johnsen S. J,. McManus J., Labeyrie L. D., Jouzel J. and Bonani G. (1993) - *Correlations between climate records from North Atlantic sediments and Greenland ice*, Nature 365, 143-147.

✓ **Bond G**., Heinrich H., Broecker W., Labeyrie L., McManus J., Andrews J., Huon S., Jantschik R., Clasen S., Simet C., Tedesco K., Klas M., Bonani G. and Ivy. S. (1992) - *Evidence for massive discharges of icebergs into the glacial northern Atlantic*. Nature, 360, 245–249.

✓ **Boynton W. V.** (1984) – *Geochemistry of the rare earth elements: meteorite studies*. In Henderson P. (ed.), Rare earth element geochemistry. Elsevier, 63-114.

✓ **Branca S.**, and Del Carlo P. (2004) - *Eruptions of Mt. Etna During the Past 3,200 Years: A Revised Compilation Integrating the Historical and Stratigraphic Records*, in Mt. Etna: Volcano observatory, Geophysical Monograph Series 143, pp. 1-27.

✓ **Broecker WS** (1994) - *Massive iceberg discharges as triggers for global climate change*. Nature, 372, 421–424.

✓ **Broecker W. S.,** G. Bond, J. F. McManus, M. Klas, E. Clark (1992) - *Origin of the northern Atlantic's Heinrich events*. Climate Dynamics, 6, 265– 273.

✓ **Brown R.J**., Orsi G., De Vita S. (2007) - *New insights into Late Pleistocene explosive volcanic activity and caldera formation on Ischia (southern Italy)*. Bulletin of Volcanology, doi:10.1007/s00445-007-0155-0.

✓ **Calanchi N.,** Peccerillo A., Tranne C.A., Lucchini F., Rossi P.L., Kempton P., barbieri W., Woo T.W. (2002) - *Petrology and geochemistry of volcanic rocks from the island of Panarea: implications for mantle evolution beneath the Aeolian island arc (southern Tyrrhenian sea)*. Journal Volcanology and Geothermal Research, 115 (3-4), 367-395.

✓ **Calanchi N.**, Dinelli E., Lucchini F., Mordenti A. (1996) - Chemostratigraphy of Late Quaternary sediments from Lake Albano and central Adriatic sea cores. In: P. Guilizzoni, F. Oldfield (eds.),Palaeoenvironmental analysis of Italian crater lakes and Adriatic sediments (PALICLAS). Mem. Ist. It. Idrobiol., 55: 247–264.

✓ **Calanchi N**., Gasparotto G., Romagnoli C. (1994) - *Glass chemistry in volcaniclastic sediments of ODP Leg 107, Site 650, sedimentary sequence: provenance and chronological implications*. Journal of Volcanology and Geothermal Research, 60, 59–85.

✓ **Calanchi N**., Cattaneo A., Dinelli E., Gasparotto G., Lucchini F., (1998) - *Tephra layers in Late Quaternary sediments of the central Adriatic Sea.* Marine Geology, 149, 191-209.

✓ **Cassignol C**., Cornette Y., David B., Gillot P. Y. (1978) - *Technologie potassium-argon*. C.E.N., Saclay. Rapp. CEA R-4802, 37 pp.

✓ **Cacho I**., Grimalt J.O., Pelejero C., Canals M., Sierro F.J., Flores J.A., Shackleton N.J. (1999) - *Dansgaard-Oeschger and Heinrich event imprints in the Alboran Sea paleotemperatures*,. Paleoceanography, 14, 698-705.

✓ **Cacho, I.**, Grimalt J. O., Sierro F. J., Shackleton N. J. and Canals M.,(2000) - *Evidence for enhanced Mediterranean thermohaline circulation during rapid climatic coolings*, Earth Planet. Sci. Lett., 183, 417– 429.

✓ **Chappellaz J.**, Blunier T., Kints S., Dällenbach A., Barnola J.M., Schwander J., Raynaud D., and Stauffer B. (1997) - *Changes in the atmospheric CH4 gradient between Greenland and Antarctica during the Holocene*. J.G.R., Vol. 102, NO. D13, 15987-15997.

✓ **Chester D.W.,** Herbette L.G., Mason R.P., Joslyn A.F., Triggle D.J., Koppel D.E. (1987) - *Diffusion of dihydropyridine calcium channel antagonists in cardiac sarcolemmal lipid multibilayers,* Biophys J;52(6):1021–1030.

✓ **Chester D.K.**, Duncan A.M., Guest J.E., Kilburn C.R.J. (1985) - *Mount Etna: The anatomy of a volcano*. Chapman and Hall London, pp. 404.

✓ **Chiesa S.**, Cornette Y., Forcella F., Gillot P.Y., Pasquare' G., Vezzoli L. (1985a) - *Carta geologica dell'isola d'Ischia*. CNR, Progetto Finalizzato Geodinamica, Roma.

✓ **Chiesa S.**, Gillot P.Y., Pasquaré G., Vezzoli L. (1985b) - *Collapse and resurgent calderic movements in a volcano-tectonic area: a new interpretation of the geological history of Ischia island.* In IAVCEI 1985 Scientific Assembly Abstracts.

✓ **Chiesa S.**, Gillot P.Y., Orsi G. (1985c). *The Citara-Serrara formation (Ischia island) - evidence for different explosive eruptions*. In IAVCEI 1985 Scientific Assembly Abstracts.

✓ **Civetta L**, D'Antonio M, Orsi G, Tilton GR (1998) - *The geochemistry of volcanic rocks from Pantelleria Island, Sicily Channel: petrogenesis and characteristics of the mantle source region*. Journal of Petrology, 39, 1453-1491.

✓ **Civetta L.**, Orsi G., Pappalardo L., Fisher R.V., Heiken G., Ort M., (1997) - *Geochemical zoning, mingling, eruptive dynamics and depositional processes — the Campanian Ignimbrite, Campi Flegrei caldera, Italy*. Journal of Volcanology and Geothermal Research, 75, 183–219.

✓ **Civetta L.**, Carluccio E., Innocenti F., Sbrana A. & Taddeucci G. (1991) – *Magma chamber evolution under the Phlegraen Field durino the last 10 ka: trace element and isotope data*, European Journal of Mineralogy 3, 415-428.

✓ **Civetta L**., Cornette Y., Gillot P.Y., Orsi G. (1988) - *The eruptive history of Pantelleria (Sicily Channel) in the last 50 ka*. Bulletin of Volcanology, 50, 47–57.

✓ **Civetta L**, Cornette Y, Crisci G, Gillot PY, Orsi G, Requejo CS (1984) - *Geology, geochronology and chemical evolution of the island of Pantelleria*. Geology Magazine, 121, 541-562.

✓ **Coltelli M**., De Carlo P., Vezzoli L. (2000) - *Stratigraphic constraints for explosive activity in the past 100 ka at Etna volcano, Italy*. International Journal of Earth Science, 89, 665–667.

✓ **Cornette Y**., Crisci G.M., Gillot P.Y., Orsi G. (1983) - *Recent volcanic history of Pantelleria: a new interpretation*. Journal of Volcanology and Geothermal Research, 17, 361–373

✓ **Corsaro R.A.** e Cristofolini R. (2000) - *Subaqueous volcanism in the Etnean area: evidence for hydromagmatic activity and regional uplift inferred from the Castle Rock of Acicastello*, J. Volc. Geoth. Res., 95, 209-225.

✓ **Crisci G.M.**, De Rosa R., Esperança S., Mazzuoli R., Sonnino M. (1991) - *Temporal evolution of a three component system: the Island of Lipari (Aeolian Arc, southern Italy)*. Bullettin Volcanology, 53, 207-221.

✓ **Crisci G**., de Fino M., La Volpe L. & Rapisardi L. (1983) - *Pleistocene ignimbrites of Monte Vulture (Basilicata, Southern Italy).* Neues Jahrbuch füer Geologie und Paläontologie Monatshefte 12: 731-746.

✓ **Crisci G.**, De Rosa, R. Lanzafame G., Mazzuoli R., Sheridan M.F. and Zuffa G.G. (1981) - *Monte Guardia sequence. A Late Pleistocene eruptive cycle on Lipari (Italy)*. Bulletin Volcanologique 44, pp. 241–255.

✓ **D'Antonio M**., Civetta L., Orsi G., Pappalardo L., Piochi M., Carandente A., de Vita S., Di Vito M. A., Isaia R. (1999) - *The present state of the magmatic system of the Campi Flegrei caldera based on a reconstruction of its behavior in the past 12 ka*. Journal of Volcanology and Geothermal Research, 91, 247-268.

✓ **D'Antonio M.**, Civetta L., Di Girolamo P. (1997) - *Heteregeneity in the mantle beneath the Campanian Region (South Italy): inferences from mafic volcanics of shoshonite suite*. J. Volcanol. Geotherm. Res., in revisione.

✓ **D'Antonio M**. and Di Girolamo P. (1994) - *Petrological and geochemical study of mafic shoshonitic volcanics from Procida-Vivara and Ventotene islands (Campanian Region, South Italy)*, Acta Volcanol 5: 69–80.

✓ **D'Orazio M**, Tonarini S, Innocenti F, Pompilio M. (1997) - *Northern Valle del Bove volcanic succession (Mt. Etna, Sicily): petrography, geochemistry and Sr-Nd isotope data*. Acta Vulcanologica, 9, 73-86.

✓ **Dalrymple G**. B. (1969). *$^{40}Ar/^{36}Ar$ analyses of historic lava flows*. Earth Planet Science Letters, 6, 47-55.

✓ **Dansgaard W.,** Johnsen S.J., Clausen H.B., Dahl-Jensen D., Gundestrup N.S., Hammer C.U., Hvidberg C.S., Steffensen J.P., Sveinbjörnsdottir, A.E., Jouzel, J., Bond, G. (1993) - *Evidence for general instability of past climate from a 250-kyr ice-core record*. Nature, 364, 218–220.

- ✓ **De Astis G.**, Piochi M., Pappalardo L. (2004) - *Procida Volcanic History: new insights in the evolution of the Phlegraean Volcanic District (Campania, Italy)*, Bull Volcanol 66:622–641.
- ✓ **De Astis G.**, Peccerillo A., Kempton P.D., La Volpe L., Wu T.W. (2000) - *Transition from calc-alkaline to potassium-rich magmatism in subduction environments: geochemical and Sr, Nd, Pb isotopic constraints from the island of Vulcano (Aeolian arc)*. Contrib Mineral Petrol, 139, 684-703.
- ✓ **De Astis G.**, La Volpe L., Peccerillo A., Civetta L. (1997) - *Volcanological and petrological evolution of Vulcano island (Aeolian arc, southern Tyrrhenian Sea)*. Journal Geophysical Research, 102, 8021-8050.
- ✓ **Deino A.L.**, Orsi G., de Vita S., Piochi M. (2004) - *The age of the Neapolitan Yellow Tuff caldera-forming eruption (Campi Flegrei caldera — Italy) assessed by $^{40}Ar/^{39}Ar$ dating method*. Journal of Volcanology and Geothermal Research, 133, 157–170.
- ✓ **Delibrias G.**, Guillier M.T., Labeyrie, J. (1986) - *Gif natural radiocarbon measurements X*. Radiocarbon, 28, 9-68.
- ✓ **Del Moro A.**, Gioncada A., Pinarelli L., Sbrana A., Joron J. L. (1998) - *Sr, Nd, and Pb isotope evidence for open system evolution at Vulcano, Aeolian Arc, Italy*. Lithos, 43, 81–106.
- ✓ **Dekkers M. J.**, Langereis C. G., Vriend S. P., Van Santvoort P. J. M., De Lange G. J. (1994) – *Fuzzy c-means cluster analysis of early diagenetic affects on natural remanent magnetisation acquisition in a 1.1 Myr piston core from the central Mediterranean*. Physical Earth Planetary International, 85, 155-171.
- ✓ **De Rita D.**, Frazzetta G., Romano R. (1991) - *The Biancavilla–Montalto ignimbrite (Etna, Sicily)*. Bulletin of Volcanology, 53, 121–131.
- ✓ **De Rosa R.** and Sheridan M.F. (1983) - *Evidence for magma mixing in the surge deposits of the Monte Guardia sequence, Lipari*, J. Volcanol. Geotherm. Res. 17, pp. 313–328.
- ✓ **de Vita S.**, Orsi G., Civetta L., Carandente A., D'Antonio M., Deino A., di Cesare T., Di Vito M.A., Fisher R.V., Isaia R., Marotta E., Necco A., Ort M., Pappalardo L., Piochi M., Southon J. (1999) - *The Agnano–Monte Spina eruption _4100 years BP/ in the restless Campi Flegrei caldera (Italy)*. Journal of Volcanology and Geothermal Research 91, 269–301.
- ✓ **De Vivo B.**, Rolandi G., Gans P.B., Calvert A., Bohrson W.A., Spera F.J., Belkin H.E. (2002) - *New constraints on the pyroclastic eruptive history of the Campanian volcanic Plain (Italy).* Mineralogy and Petrology, 73, 47–65.
- ✓ **De Vivo B.** Rolandi G. Gans P.B. Calvert A. Bohrson W.A. Spera F.J. and Belkin H.E. (2001) - *New constraints on the pyroclastic eruptive history of the Campanian volcanic Plain (Italy)*. Min. Petr. 73, pp. 47–65.
- ✓ **Di Girolamo P.**, Ghiara M.R., Lirer L., Munno R., Rolandi G. and Stanzione D. (1984) - *Vulcanologia e petrologia dei Campi Flegrei*. Boll. Soc. Geol. It., 103: 349-413.
- ✓ **Di Stefano E.** and Incarbona A. (2004) - *High resolution paleoenvironmental reconstruction of the ODP-963D Hole (Sicily Channel) during the last deglaciation, based on calcareous nannofossils*. Marine Micropaleontology 52, pp. 241–254.
- ✓ **Di Vito M.A.**, Isaia R., Orsi G., Southon J., de Vita S., D'Antonio M., Pappalardo L., Piochi M., (1999) - *Volcanism and deformation since 12,000 years at the Campi Flegrei (Italy).* J. Volcanol. Geotherm. Res. 91, 221–246.
- ✓ **Di Vito M.A.**, Sulpizio R., Zanchetta G., D'Orazio M. (2008) - *The late Pleistocene pyroclastic deposits of the Campanian Plain: New insights into the explosive activity of Neapolitan volcanoes*. Journal Volcanology Geothermal Research, doi:10.1016/j.jvolgeores.2007.11.019
- ✓ **Ellam R.M.,** Hawkesworth C.J., Menzies M.A., Rogers N.W. (1989) - *The volcanism of southern Italy: role of subduction and the relationships between potassic and sodic alkaline magmatism*. Journal Geophysical Research, 94, 4589-4601.
- ✓ **Emeis K.-C.**, Sakamoto T., Wehausen R., Brumsack H.-J. (2000) - *The sapropel record of the eastern Mediterranean Sea—Results of Ocean Drilling Program Leg 160*. Palaeogeography Palaeoclimatology Palaeoecology 158(3 –4), 371– 395.

✓ **Emeis K. C**., Robertson A. H. F., Richter C. et al. (1996) – *Site 963. Proceedings ODP, Initial Report 160*. College Station, TX (Ocean Drilling Program), 55-84.

✓ **EPICA** community members (2006) - *One-to-one coupling of glacial climate variability in Greenland and Antarctica*, Nature, 444, 195–198,.

✓ **Eriksen U**., Friedrich W.L., Buchardt B., Tauber H., Thomson M.S. (1990) - *The Stronghyle Caldera: geological, paleontological and stable isotope evidence from radiocarbondated stromatolites from Santorini.* In: Hardy, D.A., Keller, J., Galanopoulos, V.P., Flemming, N.C., Druitt, T.H. (Eds.), Thera and the Aegean World III. Santorini, Greece, 139–150.

✓ **Esperança S**, Crisci GM (1995) - *The island of Pantelleria: a case for the development of DMM-HIMU isotopic compositions in a long-lived extensional setting*. Earth Planetary Science Letters, 136, 167-182.

✓ **Esperança S**, Crisci GM, De Rosa R, Mazzuoli R (1992) - *The role of the crust in the magmatic evolution of the Island of Lipari (Aeolian Islands, Italy)*. Contrib Mineral Petrol, 112, 450-562.

✓ **Fedele L**., Scarpati C. Lanphere M., Melluso L. Morra V. Perrotta A. Ricci G. (2008) - *The Breccia Museo formation, Campi Flegrei, southern Italy: geochronology, chemostratigraphy and relationship with the Campanian Ignimbrite eruption*". Bulletin of Volcanology DOI 10.1007/s00445-008-0197-y.

✓ **Federman A.N**. & Carey S.N. (1980) - *Electron microprobe correlation of tephra layers from Eastern Mediterranean abyssal sediments and the Island of Santorini*. Quaternary Research, 13, 160–171.

✓ **Francalanci L**., Avanzinelli R., Tommasini S., Heuman A. (2007) - *A west-east geochemical and isotopic traverse along the volcanism of the Aeolian Island arc, southern Tyrrhenian Sea, Italy: Inferences on mantle source processes.* Geological Society of America Special Paper 418.

✓ **Francalanci L.**, Tommasini S., Conticelli S. (2004) - *The volcanic activity of Stromboli in the 1906–1998 period: mineralogical, geochemical and isotope data relevant to the understanding of Strombolian activity*, J Volcanol Geotherm Res 131: 179–211.

✓ **Francalanci L**., Taylor S.R., McCulloch M.T., Woodhead J. (1993) - *Geochemical and isotopic variations in the calc-alkaline rocks of Aeolian Arc (Southern Italy): constraints on the magma genesis*. Contrib Mineral Petrol, 113, 300-313.

✓ **Frigola, J.**, Moreno A., Cacho I., Canals M., Sierro F.J., Flores J.A., Grimalt J.O. (2007) - *Evidences of abrupt changes in Western Mediterranean deep water circulation during the last 50 kyr: a high resolution marine record from the Balearic Sea*, Quaternary International, 181.

✓ **Fuchs A.**, and Leuenberger M.C. (1996) - *δ^{18}O of atmospheric oxygen measured on the GRIP ice core document stratagraphic disturbances in the lowest 10% of the core*. Geophysical Research Letters 9:1049-1052.

✓ **Gertisser R**. and Keller J. (2000) - *From basalt to dacite: origin and evolution of the calcalkaline series of Salina, Aeolian Arc, Italy*. Contrib Mineral Petrol, 139, 607-626.

✓ **Gillot P.Y**., Kieffer G. and Romano R, (1994) - *The evolution of Mount Etna in the light of potassium-argon dating*, Acta Vulcanologica 5: 81-87.

✓ **Gillot P.Y.** and Keller J. (1993) - *Radiochronological dating of Stromboli*. Acta Vulcanol. 3, pp. 69–77.

✓ **Gillot, P.Y.**, (1987) - *Histoire volcanique des Iles Eoliennes: arc insulaire ou complexe orogénique annullaire?* Doc. Trav. I.G.A.L., 11, 35-42.

✓ **Gillot P.Y**. and Cornette Y. (1986) - *The Cassignol technique for K-Ar dating, precision and accuracy: examples from the late Pleistocene to recent volcanics from southern Italy.* Chemical Geology, 59: 205-222.

✓ **Gillot P.Y**. (1984) - *Datations par la méthode du potassium-argon des roches volcaniques récentes (Pleistocene et Holocene). Contribution à l'étude chronostratigraphique et magmatique des provinces volcaniques de Campanie, des îles Eoliennes, de Pantelleria (Italie du Sud) et de la Réunion (Océan Indien*). Thesis Dr. Paris-Sud, Paris, 249 pp.

✓ **Gillot P.Y.,** Chiesa S., Pasquare G., Vezzoli L. (1982) - *<33000 yr K/Ar dating of the volcano-tectonic horst of the isle of Ischia, Gulf of Naples*. Nature 229-242.

✓ **Gioncada A.**, Mazzuoli R., Bisson M., Pareschi M.T. (2003) - *Petrology of volcanic products younger than 42 ka on the Lipari-Vulcano complex (Aeolian Islands, Italy): an example of volcanism controlled by tectonics*. Journal Volcanology Geothermal Research, 122, 191-220.

Grousset, P. E., Labeyrie L., Sinko J. A., Cremer M., Bond G., Duprat J., Cortijo E. and Huon S., (1993) - *Patterns of ice-rafted detritus in the glacial North Atlantic (40-55°N)*, Paleoceanography, 8, 175–192.

✓ **Heinrich H.** (1988) - *Origin and consequences of cyclic ice rafting in the northeast Atlantic Ocean during the past 130,000 years*. Quaternary Research, 29, 143– 152

✓ **Hilgen F.J**., Abdul-Aziz H., Krijgsmenn W., Raffi I., Turco E. (2003) – *Integrated stratigraphy and astronomical tuning of Serravallian and lower Tortonian at Monte dei Corvi (middle-upper Miocene, northen Italy).* Palaeogeography Palaeoclimatology Palaeoecology, 3178, 1-36, doi: 10.1016/S0031-0182(03)00505-4.

✓ **Hilgen F.J.,** Aziz H.A., Krijgsman W., Langereis C.G., Lourens L.J., Meulenkamp J.E., Raffi I., Steenbrink J., Turco E., and van Vugt N., (1999) - *Present status of the astronomical (polarity) time-scale for the Mediterranean Late Neogene*. In Shackleton N.J., McCave I.N., and Graham P.W. (Eds.), *Astronomical (Milankovitch) Calibration of the Geological Time-Scale*. Philos. Trans. R. Soc., Ser. A., 357(1757):1931–1947. doi:10.1098/rsta.1999.0408

✓ **Hilgen F.J**., Krijgsman W., Langereis C.G., Lorens L.J., Santarelli A. Zachariasse W.J. (1995) - *Extending the astronomical (polarity) time scale into the Miocene*. Earth and Planetary Science Letters, 136, 495-510.

✓ **Howell M.W.**, Thunell R.C., Di Stefano E., Sprovieri R., Tappa E.J. and Sakamoto T. (1998) - Stable isotope chronology and paleoceanographic history of Sites 963 and 964, Eastern Mediterranean Sea, Proc. ODP Sci. Res. 160, pp. 167–180.

✓ **Hornig-Kjarsgaard I.**, Keller J., Koberski U., Stadlbauer E., Francalanci L., and Lenhart R. (1993) - *Geology, stratigraphy and volcanologic evolution of the Stromboli volcano, Aeolian islands, Italy*. Acta Vulcanol. 3, pp. 79–89.

✓ **Hughen K**., Lehman S., Southon J., Overpeck J., Marchal O., Herring C., Turnbull J. (2004) - *14C activity and global carbon cycle changes over the past 50,000 years*. Science, 303, 202–207.

✓ **Imbrie J.**, Hays J.D., McIntyre A., Mix A.C., Morley J.J., Pisias N.G., Prell W.L., and Shackleton N.J. (1984) - *The orbital theory of Pleistocene climate: Support from a revised chronology of the marine d18O record*. In "Milankovitch and Climate." (A. Berger, J. Imbrie, J. Hays, G. J. Kukla, and E. Saltzman, Eds.), pp. 269-305. D. Reidel, Boston.

✓ **Incarbona A**., Di Stefano E., Sprovieri R., Bonomo S., Censi P., Dinarès-Turell J., Spoto, S. (2008) - *Vertical structure variability of the water column and Paleoproductivity reconstruction in the Central-Western Mediterranean during the Late Pleistocene*. Marine Micropaleontology, Elsevier, Amsterdam, in press.

✓ **Ivanov A.V**., Boven A.A., Brandt S.B., Rasskazov S.V. (2002) – *Achievement and limitations of the K-Ar and $^{40}Ar/^{39}Ar$ methods: what's in it for dating the quaternary sedimentary deposits?.* International Symposium-Speciation in Ancient Lakes, September, 2002.

Johnsen, S., Clausen H., Dansgaard W, Fuhrer K., Gundestrup N., Hammer C., Iversen P., Jouzel J., Stauffer B. and Steffensen. J., (1992) - *Irregular glacial interstadials recorded in a new Greenland ice core,* Nature 359, 311-313.

✓ **Laj** C., Kissel C., Mazaud A., Channell J.E.T., Beer J. (2000) - *North Atlantic paleointensity stack since 75 ka (NAPIS-75) and the duration of the Lashamp event*. Phil. Trans. Roy. Soc. A 358 10009–101025.

✓ **Langereis C. G**., Dekkers M. J., De Lange G. J., Paterne M., Van Santvoort P. J. M. (1997) - *Magnetostratigraphy and astronomical calibration of the last 1.1 Myr from an eastern Mediterranean piston core and dating of short events in the Brunhes*. Geophysical Journal International 129, 75– 94.

✓ **Laskar J**. (1990) - *The chaotic motion of the solar system: A numerical estimate of the size of the chaotic zones*. Icarus 88, 266–291.

✓ **Le Bas M.J**., Le Maitre R.W., Streckeisen A & Zanettin P., (1986) - *A chemical classification of volcanic rocks based on the Total Alkali-Silica diagram*. Journal of Petrology, 27, 745-750.

✓ **Le Maitre R.W.**, Bateman P., Dudek A., Keller J., Lameyre J., Le Bas M.J., Sabine P.A., Schmid R., Sorensen H., Streckeisen A., Woolley A.R. & Zanettin B. (1989) - *A Classification of Igneous Rocks and Glossary of Terms: Recommendations of the International Union of Geological Sciences Subcommission on the Systematics of Igneous Rock*s. Oxford: Blackwell Scientific.

✓ **Limburg E.M**., Varekamp J.C. (1991) - *Young pumice deposits on Nisyros, Greece*. Bull. Volcanol. 54 (1), 68–77.

✓ **Lourens L.J.** (2004) – *Revised tuning of Ocena Drilling Program Site 964 and KC01B (Mediterranean) and imp0licetions for the δ18O, tephra, calcareous nannofossil, and geomagnetic reversal chronologies of the past 1.1 Myr.* Paleoceanography, 19, 3010, doi: 10.1029/2003PA000997.

✓ **Lourens L.J**., Antonarakou A., Hilgen F.J., Van Hoof A.A.M., Vergnaud-Grazzini C. Zachariasse, W.J. (1996) - *Evaluation of the Plio-Pleistocene astronomical timescale*. Paleoceanography, 11(4), 391-413.

✓ **Lucchi F**., Tranne C.A., De Astis G., Keller J., Losito R., Morche W. (2008) - *Stratigraphy and significance of Brown Tuffs on the Aeolian Islands (southern Italy)*. Journal of Volcanology and Geothermal Research (2008), DOI:10.1016/j.jvolgeores.2007.11.006.

✓ **Lucchi F.**, Tranne C.A., Calanchi N. and Rossi P.L. (2007) - *Late Quaternary deformation history of the volcanic edifice of Panarea, Aeolian Arc, Italy*. Bull. Volcanol. 69, 239-257.

✓ **Lucchi F.**, Tranne C.A., Calanchi N., Keller J. and Rossi P.L. (2003) - *Geological map of Panarea and minor islets (Aeolian Islands)*. University of Bologna, University of Freiburg and INGV, L.A.C. Firenze.

✓ **Kanenoka I.**, (1980)- *Rare gas isotopes and mass fractionation: an implication of gas transport into or from a magma.* Earth Planet. Sci. Lett., 48, 284-292.

✓ **Keller J,** (1982) - *Mediterranean Island Arcs*, In: Thorpe R S (ed) Andesites, New York: John Wiley Sons, p 307-326.

✓ **Keller J**., (1980) - *Prehistoric pumice tephra on Aegean islands.- Acta 2nd International Scientific Congress on the Volcano of Thera "Thera and the Aegean World"*, Athens, pp. 49-56.

✓ **Keller J**., Ryan W.B.F., Ninkovich D., Altherr R. (1978) - *Explosive volcanic activity in the Mediterranean over the past 200,000 yrs as recorded in deep-sea sediments.* Geological Society Am. Bulletin 89, 591–604.

✓ **Kotilainen A.**, Shackleton N.J., (1995) - *Rapid climate variability in the North Pacific Ocean during the past 95,000 years.* Nature, 377: 323-326.

✓ **Kraml M**., Keller J., Henjes-Kunst F. (1998) - *Tephrochronologische Zeitmarken für jung-quartäre Sedimente des Mittelmeeres*. Abstract, Geo-Berlin '98. Berlin, Germany, pp. 96.

✓ **Kraml M.** (1997a) - *Laser $^{40}Ar/^{39}Ar$-datierungen an distalen marinen tephren des jung-quartären mediterranean vulkanismus (Ionisches Meer, Meteor-Fahrt 25/4).* Ph.D. Thesis, Albert-Ludwigs-Universität Freiburg, Germany, pp. 216.

✓ **Kraml M.,** Keller J., Henjes-Kunst F. (1997b) - *Dating of Upper Quaternary deep sea sediments from the Ionian Sea (Eastern Mediterranean) with laser $^{40}Ar/^{39}Ar$ analyses on prominent tephra layers*. EUG 97, Terra Nova 9. Abstract Supplement 1, 406.

✓ **Kraml M.,** Keller J., Wijbrans J.R. (1996) - *First $^{40}Ar/^{39}Ar$ laser fusion dates for Upper Quaternary deep-sea tephra layers of the Ionian Sea*. DMG 96, Kiel. Abstracts.

✓ **Mahood G.A** & Hildreth W. (1986) - *Geology of the peralkaline volcano at Pantelleria, Strait of Sicily*. Bulletin of Volcanology 48: 143-172.

✓ **Mahood, G.A.** & Baker D.R. (1986) - *"Experimental constraints on depths of fractionation of mildly alkalic basalts and associated felsic rocks: Pantelleria, Strait of Sicily.*" Contributions to Mineralogy and Petrology 93: 251-264.

✓ **Mahood G.A** & Hildreth W. (1983) - *Nested calderas and trapdoor uplift at Pantelleria, Strait of Sicily*. Geology 11: 103-106.

✓ **Mangerud J**., Gulliksen S. (1975) - *Apparent radiocarbon ages of recent marine shells from Norway, Spitzbergen and Arctic Canada*. Quaternary Research, 5, 263–273.

- ✓ **Marciano R.**, Munno R., Petrosino P., Santangelo, N., Santo A. and Villa I. (2008) - *Late quaternary tephra layers along the Cilento coastline (southern Italy).* Journal of Volcanology and Geothermal Research Vol. 177, Issue 1, 227-243.
- ✓ **Margari V**., Pyle D., Bryant C., Gibbard P.L. (2007) - *Mediterranean tephra Stratigraphy revisited: results from a long terrestrial sequence on Lesvos Island, Greece*. Journal Volcanology Geothermal Research, 163, 34–54.
- ✓ **Martrat B.,** Grimald J.O., Lopez-Martinez C., Cacho I., Sierro F.J., Flores J.A., Zahn R., Canals M., Curtis J.H., Hodell D.A. (2004) - *Abrupt temperature changes in the Western Mediterranean over the past 250,000 years*. Science, 306, 1762–1765.
- ✓ **Mayewski P. A.** Twickler M. S., Whitlow S. I., Meeker L. D., Yang Q., Thomas J, Kreutz K., Grootes P., Morse D., Steig E. and Waddington E. D., (1996) - *Climate change during the Last Deglaciation in Antarctica*, Science, 272: 1636-1638.
- ✓ **McCoy F.W**., Cornell W. (1980) - *Volcanoclastic sediments in the Tyrrhenian basin*. In: Kastens, K.A., Mascle, J. et al., Eds., Proceedings of the Ocean Drilling Program, Scientific results 107, 291–305.
- ✓ **McCoy F.W.,** (1981) - *Areal distribution, redeposition and mixing of tephra within deep-sea sediments of the Eastern Mediterranean sea*. In: Self S., Sparks R.S.J. (Eds.), Tephra studies, Nato Advanced Study Institutes Series C75 Reidel, Dordrecht, 245-254.
- ✓ **MacDonald R.** (1974) - *Nomenclature and Petrochemistry of the Peralkaline Oversaturated Extrusive Rocks*. Bulletin of Volcanology, 38, 498-516.
- ✓ **Morche W.** (1988) – *Tephrochronologie der Äolischen Inseln*. Unpublished Dr. thesis, University of Friburg, 238 pp.
- ✓ **Munno R.** and Petrosino P. (2007) - *The late Quaternary tephrostratigraphical record of the San Gregorio Magno basin (southern Italy)*, J. Quat. Sci 22 (3), pp. 247–266.
- ✓ **Munno R.** and Petrosino, P. (2004) - *New constraints on the occurrence of Y-3 upper pleistocene tephra marker layer in the tyrrhenian sea*, Il Quaternario. Ital, J. Quat. Sci. 17, pp. 11–20.
- ✓ **Narcisi B.** and Vezzoli L. (1999) - *Quaternary stratigraphy of distal tephra layers in the Mediterranean—an overview.* Global and Planetary Change 21, pp. 31–50.
- ✓ **Narcisi B**. (1996) - *Tephrochronology of a late Quaternary lacustrine record from the Monticchio maar (Vulture volcano, Southern Italy)*. Quaternary Science Review, 15, 155–165.
- ✓ **Narcisi B.** (1993) - *Segnalazione di un livello piroclastico di provenienza etnea nell'area del Fucino (Italia Centrale)*. Il Quaternario 6, pp. 87–92.
- ✓ **N**orth **A**tlantic **I**ce **C**ore **P**roject **M**embers (2004) - *High-resolution record of Northern Hemisphere climate extending into the last interglacial period*. Nature, 431, 147–151.
- ✓ **Orsi G**., de Vita S., Di Vito M. (1996) - *The restless, resurgent Campi Flegrei nested caldera (Italy): constraints on its evolution and configuration*. Journal of Volcanology and Geothermal Research 74, 179–214.
- ✓ **Orsi G.,** Civetta L., D'Antonio M., Di Girolamo P., Piochi M. (1995) - *Step-filling and development of a zoned magma chamber: the Neapolitan Yellow Tuff case history*. Journal Volcanology Geothermal Research, 67, 291–312.
- ✓ **Orsi, G.** and Sheridan M.F. (1984) - "*The Green Tuff of Pantelleria: rheoignimbrite or rheomorphic fall?*" Bulletin Volcanologique 47: 611-626.
- ✓ **Pappalardo L**., Civetta L., de Vita S., Di Vito M.A., Orsi G., Carandente A., Fisher R.V. (2002) - *Timing of magma extraction during the Campanian Ignimbrite eruption (Campi Flegrei Caldera)*. Journal of Volcanology and Geothermal Research, 114, 479–497.
- ✓ **Pappalardo L**., Civetta L., D'Antonio M., Deino M., Di Vito M.A., Orsi G., Carandente A., de Vita S., Isaia R., Piochi, M. (1999) - *Chemical and Sr isotopical evolution of the Phlegrean magmatic system before the Campanian Ignimbrite and the Neapolitan Yellow Tuff eruptions*. Journal of Volcanology and Geothermal Research, 91(2-4), 141–166.

- ✓ **Paterne M**., Guichard F., Duplessy J.C., Siani G., Sulpizion R., Labeyrie J. (2008) - *A 90,000–200,000 yrs marine tephra record of Italian volcanic activity in the Central Mediterranean Sea*. Journal Volcanology Geothermal Ressearch, doi:10.1016/j.jvolgeores.2007.11.028.
- ✓ **Paterne M**., Labeyrie J., Guichard F., Mazaud A., Maitre F. (1990) - *Fluctuations of the Campanian explosive volcanic activity (south Italy) during the past 190,000 years, as determined by marine tephrochronology*. Earth and Planetary Science Letters, 98, 166–174.
- ✓ **Paterne M.,** Guichard F. & Labeyrie J., (1988) - *Explosive activity of the south Italian volcanoes during the past 80.000 years as determined by marine tephrochronology*. JVGR, 34, 153-172.
- ✓ **Paterne M.,** Guichard F., Labeyrie J., Gillot P.Y., Duplessy J.C., (1986) - *Tyrrhenian Sea tephrochronology of the oxigen isotope record for the past 60.000 years*. Marine Geology, 72, 259-285.
- ✓ **Paterne M.** (1985) - *Reconstruction de l'activitè esplosive des volcans de l'Italie du sud par téphrochronologie marine*. Thése, Università Paris XI, Orsay, France.
- ✓ **Peccerillo A.** (2005) - *Plio-Quaternary volcanism in Italy. Petrology, Geochemistry, Geodynamics*. Springer, Heidelberg, 365 pp.
- ✓ **Peccerillo A.** & Taylor S. R. (1976) - *Geochemistry of Eocene calc-alkaline volcanic rocks from the Kastamonu area, Northern Turkey*. Contributions to Mineralogy and Petrology, 58, 63–81.
- ✓ **Pe-Piper G.**, Piper D.J.W. (2002) – *The igneous rocks of Greece*. Gebrüder Borntraeger, Berlin, 573 pp.
- ✓ **Pérez-Folgado M.**, Sierro F.J., Flores J.A., Grimalt J O., Zahn R. (2004) - *Paleoclimatic variations in foraminifer assemblages from the Alboran Sea (Western Mediterranean) during the last 150 ka in ODP Site 977*. Marine Geology 212, 113–131.
- ✓ **Perini G.,** Francalanci L., Davison G.P., Conticelli S. (2004) - *Evolution and Genesis of Magmas from Vico Volcano, Central Italy: Multiple Differentiation Pathways and Variable Parental Magmas.* Journal of Petrology, vol. 45(1), 139-182.
- ✓ **Pichler H**. & Friederich W. (1976) - *Radiocarbon dates of the Santorini volcanics*. Nature 262, 373–374.
- ✓ **Pollard A.M**., Blockley S.P.E., Ward K.R. (2003) - *Chemical alteration of tephra in the depositional environment: theoretical stability modelling*. Journal of Quaternary Science, 18, 385–394.
- ✓ **Poli S.**, Chiesa S., Gillot P.Y., Guichard F., Vezzoli L. (1989) - *Time dimension in the geochemical approach and hazard estimation of a volcanic area: the Isle of Ischia case (Italy)*. J Volcanol Geother Res., 36, 327-335.
- ✓ **Poli S.,** Chiesa S., Gillot P.Y., Gregnanin A., Guichard F. (1987) - *Chemistry versus time in the volcanic complex of Ischia (Gulf of Naples, Italy): evidence of successive magmatic cycles*. Contributions to Mineralogy and Petrology, 95, 322–335.
- ✓ **Porter S.C.**, An Z.S., (1995) - *Correlation between climate events in the North Atlantic and China during the last glaciation*, Nature, 375: 305-308.
- ✓ **Pouchou J.L.** & Pichoir. F. (1985) - *"PAP" (φ-ρ-Z) correction procedure for improved quantitative microanalysis. Microbeam Analysis*. In: Armstrong, J. T. (Editor). San Francisco Press, pp. 104-106.
- ✓ **Rasmussen S.O.,** Andersen K.K., Svensson A.M. et al. (2006) - *A new Greenland ice core chronology for the last glacial termination*. Journal of Geophysical Research, 111, DO6102, doi:10.1029/2005JD006079, 16pp.
- ✓ **Reimer P.J**., et al. (2004) - *IntCal04 terrestrial radiocarbon age calibration, 0–26 cal kyr BP*. Radiocarbon, 46, 1029–1058.
- ✓ **Reimer P.J**., Reimer R.W. (2001) - *A marine reservoir correction database and on-line interface*. Radiocarbon, 43, 461–464.
- ✓ **Rehren T.** (1988) - *Geochemie und Petrologie von Nisyros (östliche Ägäis).* PhD thesis. University of Freiburg.

✓ **Renne P. R**., Swisher C. C., Deino A. L., Karner D. B., Owens T. L., DePaolo D. J., (1998) - *Intercalibration of standards, absolute ages and uncertainties in 40Ar/39Ar dating.* Chemical Geology, 145, 117-152.

✓ **Rosi M.**, Sbrana A. (1987) - *Phlegraean Fields*. CNR Quaderni della Ricerca Scientifica 114, vol.9, pp.175.

✓ **Rossignol-Strick M**., Paterne M. (1999) – *A synthetic pollen record of the eastern Mediterranean sapropels of the last 1 Ma: implications for the time-scale and formation of sapropels*. Marine Geology, 153, 221-237.

✓ **Ruddiman, W. F.** (1977) - *Late Quaternary deposition of ice-rafted sand in the sub-polar North Atlantic (40–60 N),* Geological Society of America Bulletin 88, 1813–1827.

✓ **Santacroce R**., Rosi M., Cristofolini R., La Volpe L., Orsi G. (2003) - *Italian active volcanoes*. Episodes, 26(3), 27–34.

✓ **Santacroce R.** (1987) - *Somma-Vesuvius*, Quaderni De La Ricerca Scientifica, CNR, Rome, Italy.

✓ **Schulz H.,** von Rad U., Erlenkeuser H., (1998) - *Correlation between Arabian Sea and Greenland climate oscillations of the past 110,000 years*. Nature, 393(6680): 54-57.

✓ **Schulz M.** and Statteger K. (1997) - *Spectrum: spectral analysis of unevenly spaced paleoclimatic time series*. Computers & Geosciences, 23(9), 929-945.

✓ **Shackleton N.J**., Crowhurst S., Hagelberg T., Pisias N.G., Schneider D.A. (1995) - *A new late Neogene time scale: application to leg 138 sites*. Proceedings of the Ocean Drilling Program, Scientific Results, 138, 73-91.

✓ **Siani G.**, Sulpizio R., Paterne M., Sbrana A. (2004) – *Tephrostratigraphy study for the last 18.000 ^{14}C years in a deep-sea sediment sequence of the South Adriatic*. Quaternary Science Reviews, 23, 2485-2500.

✓ **Siani G.,** Paterne M., Michel E., Sulpizio R., Sbrana A., Arnold M., Haddad G. (2001) - *Mediterranean Sea surface radiocarbon reservoir age changes since the last glacial maximum*. Science, 294, 1917–1920.

✓ **Sierro F.J.**, Hodell D. A., Curtis J. H., Flores J. A., Reguera I., Colmenero-Hidalgo E., Barcena M. A., Grimalt J. O., Cacho I., Frigola J., Canals M. (2005) - *Impact of iceberg melting on Mediterranean thermohaline circulation during Heinrich events*. Paleoceanography, 20, PA2019, doi:10.1029/2004PA001051.

✓ **Spötl C.** and Vennemann T.W. (2003) - *Continuous-flow isotope ratio mass spectrometric analysis of carbonate minerals*. Rapid Commun. Mass Spectrom. 17 , pp. 1004–1006.

✓ **Sprovieri R.**, Di Stefano E., Incarbona A., Gargano M. E. (2003) - *A high-resolution of the last deglaciation in the Sicily Channel based on foraminiferal and calcareous nannofossil quantitative distribution*. Palaeogeography, Palaeoclimatology, Palaeoecology 202, 119-142.

✓ **Sprovieri R**., Di Stefano E., Incarbona A., Oppo D. W. (2006) – *Suborbital climate variability during Marine Isotopic Stage 5 in the central Mediterranean basin: evidence from calcareous plankton record.* Quaternary Science Reviews, 25, 2332-2342.

✓ **Siani G.,** Sulpizio R., Paterne M., Sbrana A. (2004) - *Tephrostratigraphy study for the last 18,000 14C years in a deep-sea sediment sequence for the South Adriatic*. Quaternary Science Reviews, 23, 2485–2500.

✓ **Smith P.E.,** York D., Chen Y., Evensen N.M. (1996) - *Single crystal ^{40}Ar–^{39}Ar dating of a late Quaternary paroxysm on Kos, Greece: concordance of terrestrial and marine ages*. Geophys. Res. Lett. 23 (21), 3047–3050.

✓ **Stuiver M**., Reimer P. J., Braziunas T. F. (1998). *High precision radiocarbon age calibration for terrestrial and marine samples.* Radiocarbon, 40, 1127-1151.

✓ **Sulpizio R**., Zanchetta G., Paterne M., Siani G., (2003) - *A review of tephrostratigraphy in central and southern Italy during the last 65 ka*. Il Quaternario 16, 91–108.

✓ **Sun S. -s.** and McDonough W. F. (1989) – *Chemical and isotopic systematics of oceanic basalts: implications for mantle composition and processes.* Geological Society of London, special publications 42, 313-345.

- ✓ **Svensson A.**, Andersen K.K., Bigler M., Clausen H. B., Dahl-Jensen D., Davies S.M., Johnsen S.J., Muscheler R., Rasmussen S.O., Rothlisberger R., Steffensen J.P., Vinther B.M. (2006) - *The Greenland Ice Core Chronology 15–42 kyr. Part 2: comparison to other records*. Quaternary Science Reviews, 25, 3258–3267.
- ✓ **Tanguy JC**, Condomines M, Kieffer G. (1997) - *Evolution of Mount Etna magma: constraints on the present feeding system and eruptive mechanism*. Journal Volcanology Geothermal Research, 75, 221-250.
- ✓ **Telford R.J**., Heegaard E., Birks H.J.B., (2004a) - *All age-depth models are wrong: but how badly?.* Quaternary Science Reviews, 23, 1–5.
- ✓ **Telford R.J**., Heegaard E., Birks H.J.B. (2004b) - *The intercept is a poor estimate of a calibrated radiocarbon age*. The Holocene, 14, 296–298.
- ✓ **Terrasi F**., Rogalla D., De Cesare N., D'Onofrio A., Lubritto C., Marzaioli F., Passariello I., Rubino M., Sabbarese C., Casa G., Calmieri A., Gialanella, L., Imbriani G., Roca V., Romano M., Sundquist M., Loger R. (2007) - *A new AMS facility in Caserta (Italy)*. Nucl. Instrum. Methods Phys. Res., B Beam Interact. Mater. Atoms 259, 14–17.
- ✓ **Thunell R**., Federman A., Sparks R.S.J., Williams D. (1979) - *The age and volcanologic significance of the Y-5 ash layer in the Mediterranean*. Quaternary Research, 12, 241–253.
- ✓ **Tranne, C.A.**, Lucchi F., Calanchi N., Rossi P.L., Campanella T., Sardella A. (2002b) - *Geological map of the island of Filicudi (Aeolian Islands):* University of Bologna and INGV, printed by L.A.C., Firenze.
- ✓ **Turney C.S.M.,** Blockley S.P.E., Lowe J.J., Wulf S., Branch N.P., Masrtolorenzo G., Swindle G., Nathan R., Pollard A.M. (2008) – *Geochemical characterization of Quaternary tephras from the Campanian Province, Italy.* Quaternary International 178, 288-305.
- ✓ **Turney C.S.M.,** Lowe J.J., Davies S.M., Hall V., Lowe D.J., Wastegård S., Hoek W.Z., Alloway SCOTAV and Intimate Members (2004) - *Tephrochronology of Last Termination Sequences in Europe: a protocol for improved analytical precision and robust correlation procedures (a joint SCOTAV-INTIMATE proposal)*. Journal Quaternary Science, 19, 111–120.
- ✓ **Van Santvoort P. J. M.**, De Lange G. J., Langereis C. G., Dekkers M. J. (1997) - *Geochemical and paleomagnetic evidence for the occurrence of "missing" sapropels in eastern Mediterranean sediments*. Paleoceanography, 12(6), 773– 786.
- ✓ **Vezzoli L.** (1991) - *Tephra layers in Bannock Basin (Eastern Mediterranean)*. Marine Geology, 100, 21–34.
- ✓ **Vezzoli L**. (1988) - *Island of Ischia*. CNR Quaderni Ricerca Scientifica, 114-133.
- ✓ **Villari L.** (1974) - *The Island of Pantelleria*. Bull. Volc., 38, 3, 680-724.
- ✓ **Villemant B.** (1988) - *Trace element evolution in the Phlegrean Fields (Central Italy): fractional crystallization and selective enrichment*. Contrib. Mineral. Petrol., 98, 169–183.
- ✓ **Vinci A.** (1985) - *Distribution and chemical composition of tephra layers from Eastern Mediterranean abyssal sediments*. Marine Geology, 64, 143–155.
- ✓ **Voelker A.H.L**., Sarnthein M., Grootes P.M., Erlenkauser H., Laj C., Mazaud A., Nadeau M-J., Schleicher M. (1998) - *Correlation of marine ^{14}C ages from the Nordic seas with the GISP2 isotope record: implications for radiocarbon calibration beyond 25 ka BP*. Radiocarbon, 40, 517–534.
- ✓ **Wagner B**., Sulpizio R., Zanchetta G., Wulf S., Wessels M., Daut G., Nowaczyk N. - *The last 40 ka tephrostratigraphic record of Lake Ohrid, Albania and Macedonia: a very distal archive for ash dispersal from Italian volcanoes*. doi:10.1016/j.jvolgeores.2007.08.018.
- ✓ **Watts** W.A., Allen J.R.M., Huntley B. (1996) - *Vegetation history and palaeoclimate of the last glacial period at Lago Grande di Monticchio, southern Italy*. Quaternary Science Reviews 15, 133–153.
- ✓ **Weninger B.,** Jöris O., Danzeglocke U. (2004). *Calpal—the Cologne radiocarbon CALibration and PALeoclimate research package.* (http://www.calpal.de).

✓ **Wulf S.**, Kraml M., Brauer A., Keller J., Negendank J.F.W. (2004) - *Tephrochronology of the 100 ka lacustrine sediment record of Lago Grande di Monticchio (southern Italy).* Quaternary International, 122, 7–30.

APPENDIX A

ARM profile of the MD01_2474G core and correlation result tephra layers

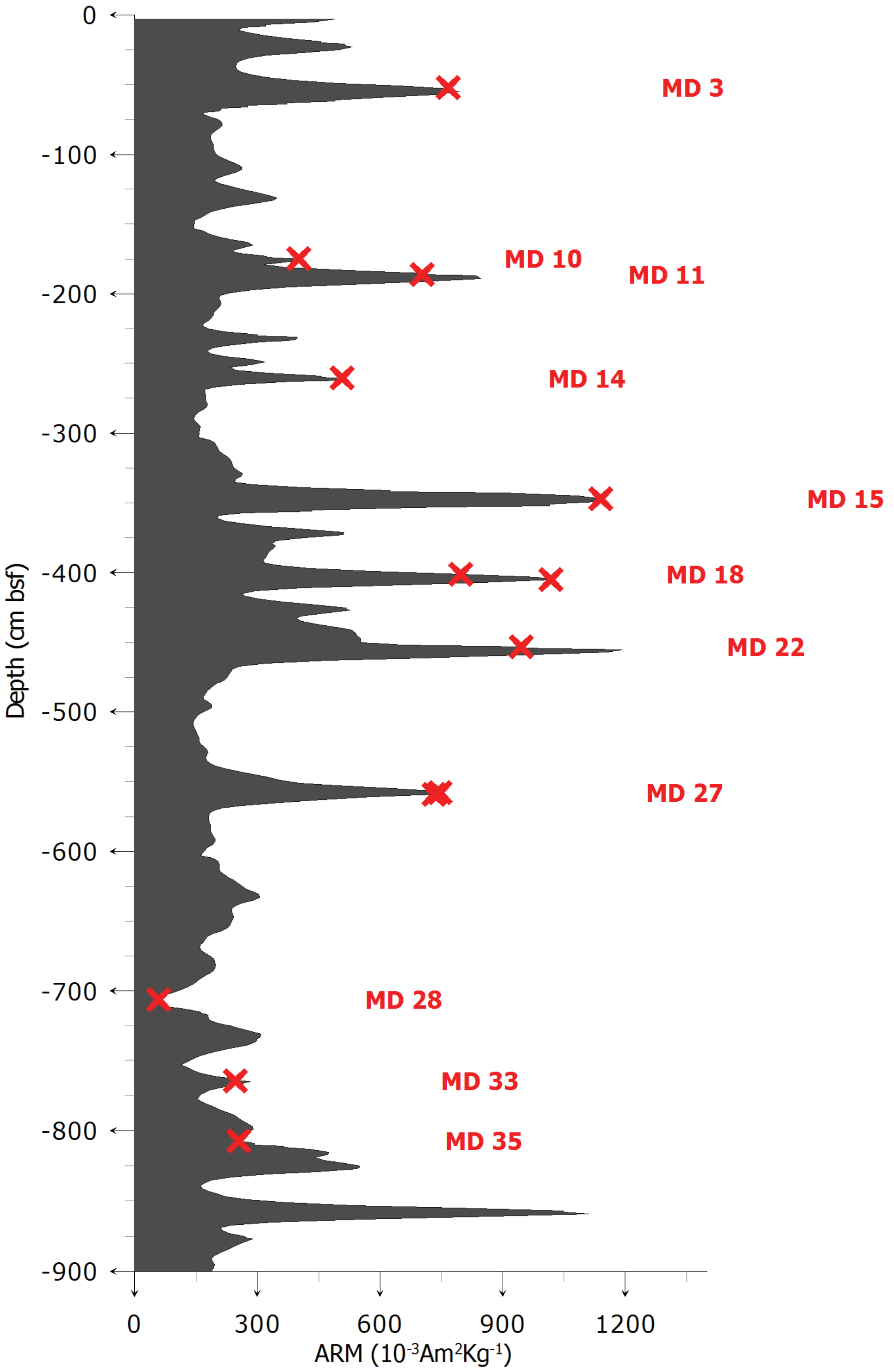

APPENDIX B

Oxygen isotopes from the MD01_2474G core

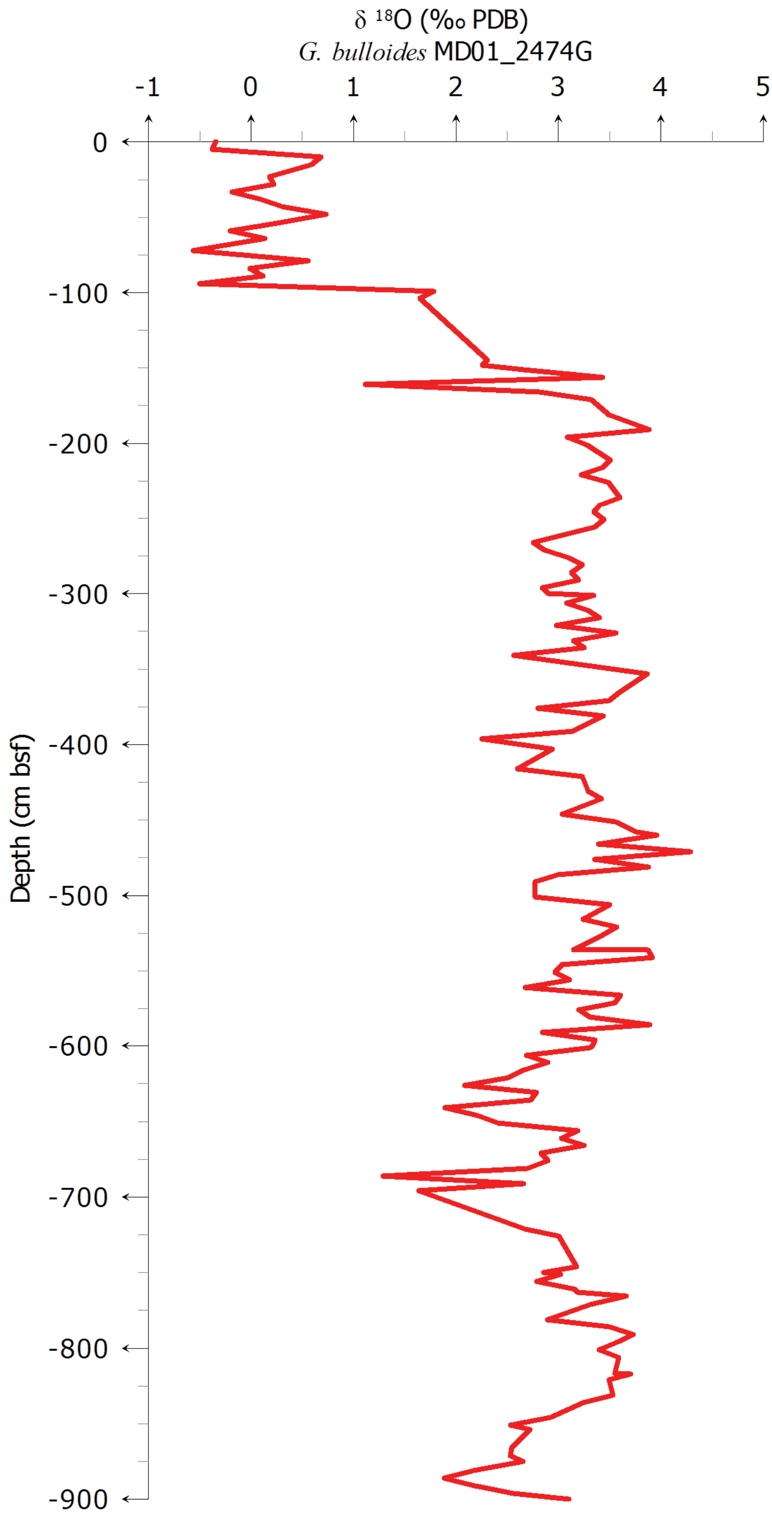

APPENDIX C

Chemical analysis of tephras from KC01B core

Major (wt. %) and trace (ppm) element composition of the tephra layers. All analysis recalculated water-free to 100. Tephra components: GS=glass shards, SC=scoria, P=pumice. Chemistry: DAC= dacite, TRA= thrachyte, BEN= benmoreite.

Tephra layer	I 1										
Sample											
Material	GS										
Classification	DAC	BEN									
SiO_2	63,8	63,0	63,1	63,2	62,6	63,4	64,0	63,0	62,7	63,9	63,5
TiO_2	1,42	1,43	1,29	1,37	1,47	1,36	1,47	1,28	1,46	1,41	1,37
Al_2O_3	16,9	16,9	17,8	16,5	16,3	16,7	16,9	16,5	16,7	16,1	16,7
FeO	5,27	4,94	4,27	5,38	5,58	5,36	5,05	5,55	5,15	5,40	4,96
MnO	0,21	0,20	0,22	0,21	0,21	0,23	0,25	0,22	0,23	0,20	0,29
MgO	1,77	1,66	1,19	1,77	1,70	1,55	1,59	1,68	1,73	1,71	1,66
CaO	3,57	3,19	3,95	3,69	3,36	3,03	3,19	3,44	3,68	3,34	3,40
Na_2O	3,56	4,93	5,01	4,12	4,97	4,35	3,92	4,59	4,10	4,35	4,36
K_2O	3,18	3,36	2,89	3,21	3,32	3,68	3,36	3,30	3,51	3,26	3,40
P_2O_5	0,37	0,41	0,29	0,45	0,45	0,36	0,34	0,43	0,76	0,38	0,42
Tot.	98,0	97,5	99,0	96,8	98,3	99,2	98,3	97,9	98,3	99,0	97,9
Alkali	6,7	8,3	7,9	7,3	8,3	8,0	7,3	7,9	7,6	7,6	7,8

Tephra layer	I 1										
Sample											
Li	23,2	41,3	18,2	25,3	32,0	12,9	29,7	22,8	18,0	17,3	11,6
Sc	8,4	17,4	13,0	13,3	12,2	11,3	7,4	9,7	11,1	8,3	11,5
V	55,7	79,8	69,6	65,9	61,8	60,4	73,7	59,8	65,2	52,8	55,0
Cr	< d.l.	< d.l.	< d.l.	< d.l.	< d.l.	< d.l.	33,6	< d.l.	< d.l.	< d.l.	< d.l.
Co	4,3	6,4	4,1	5,2	3,8	5,0	2,9	4,2	3,1	3,7	4,4
Rb	68,7	85,6	81,8	79,8	71,3	64,5	118,5	70,8	83,7	73,8	66,4
Sr	629	1991	860	738	751	700	473	893	788	682	710
Y	29	41	33	35	33	31	34	29	34	26	31
Zr	342	486	394	427	426	351	379	341	402	315	364
Nb	86	124	110	113	108	85	126	91	111	88	99
Cs	1,7	2,4	2,5	2,6	1,8	1,7	3,4	1,6	2,0	1,9	1,8
Ba	1084	1973	1324	1354	1337	1138	1335	1221	1351	1081	1220
La	103	155	121	127	121	99	124	106	123	96	110
Ce	190	277	229	233	237	192	234	197	229	180	205
Pr	20	29	23	23	23	20	24	20	23	18	20
Nd	70	98	84	80	82	71	89	72	84	65	75
Sm	12	16	14	13	15	10	21	12	15	11	13
Eu	3,2	4,6	3,7	3,5	3,6	3,3	3,7	3,1	3,6	3,3	3,0
Gd	8,4	11,0	9,2	9,9	9,3	8,4	11,6	7,5	9,3	7,3	8,4
Tb	1,1	1,4	1,2	1,2	1,3	1,2	1,3	1,0	1,2	0,9	1,1
Dy	5,6	8,6	7,9	8,2	6,6	6,5	8,2	6,1	7,5	5,0	6,2
Ho	1,1	1,5	1,2	1,4	1,5	1,3	1,3	1,1	1,3	0,9	1,2
Er	3,0	4,3	3,9	3,5	3,8	2,4	3,5	3,0	3,9	2,8	3,0
Tm	0,4	0,7	0,5	0,4	0,5	0,4	1,0	0,4	0,5	0,4	0,4
Yb	3,3	4,2	3,7	3,5	2,3	3,3	3,0	3,1	3,7	3,4	3,5
Lu	0,5	0,7	0,5	0,6	0,5	0,5	0,6	0,4	0,6	0,4	0,4
Hf	7,8	9,9	8,9	8,0	9,5	7,0	9,8	7,9	8,7	6,5	8,7
Ta	4,1	6,1	5,4	5,1	5,3	4,1	5,6	4,5	5,3	4,2	4,7
Pb	33	1667	44	50	20	46	1733	18	21	489	17
Th	17	25	20	22	22	19	19	18	22	17	19
U	5,6	7,7	6,2	6,5	6,8	5,4	7,7	5,8	6,8	4,9	6,0
Eu/Eu*	1,0	1,1	1,0	0,9	0,9	1,1	0,7	1,0	0,9	1,1	0,9
$(La/Yb)_N$	21	25	22	25	35	20	28	23	22	19	21
$(La/Sm)_N$	5,4	6,1	5,4	6,0	5,0	6,0	3,6	5,5	5,2	5,7	5,5
$(Gd/Yb)_N$	2,0	2,1	2,0	2,3	3,2	2,1	3,1	2,0	2,0	1,7	2,0

Tephra layer / Sample	I 3														
Material	GS														
Classification	TRA														
SiO_2	62,4	63,3	62,6	62,8	62,4	62,3	63,2	62,3	62,0	62,4	60,9	62,0	61,2	58,4	62,2
TiO_2	0,39	0,42	0,44	0,42	0,36	0,40	0,33	0,43	0,43	0,44	0,37	0,44	0,40	0,55	0,49
Al_2O_3	18,2	18,5	18,7	18,4	18,3	18,6	18,1	18,7	18,9	19,8	18,2	18,5	18,0	19,2	18,8
FeO	2,94	2,69	3,05	2,95	3,07	2,94	2,85	3,01	3,05	3,00	3,53	3,00	3,49	4,51	2,93
MnO	0,16	0,23	0,20	0,22	0,18	0,25	0,11	0,31	0,27	0,24	0,08	0,19	0,12	0,21	0,24
MgO	0,58	0,44	0,35	0,56	0,56	0,39	0,52	0,34	0,38	0,34	0,82	0,36	0,77	1,21	0,37
CaO	2,25	1,88	1,75	2,11	2,24	1,72	2,12	1,78	1,81	1,67	2,86	1,87	2,61	3,78	1,78
Na_2O	4,48	4,99	5,83	5,20	4,28	6,21	5,17	5,53	5,86	5,03	3,11	6,13	3,34	3,87	6,01
K_2O	8,52	7,43	7,09	7,23	8,53	7,17	7,51	7,49	7,24	7,09	9,98	7,48	9,98	8,06	7,16
P_2O_5	0,10	0,06	0,00	0,05	0,08	0,02	0,11	0,11	0,04	0,01	0,17	0,03	0,15	0,22	0,02
Tot.	96,9	97,6	96,9	97,8	90,7	94,4	96,6	98,7	98,5	99,5	92,9	94,9	95,1	95,4	98,5
Alkali	13,0	12,4	12,9	12,4	12,8	13,4	12,7	13,0	13,1	12,1	13,1	13,6	13,3	11,9	13,2

Tephra layer / Sample	I 3								
Li	112	83	43	81	86	34	18	22	53
Sc	7,7	4,2	4,5	3,3	3,9	5,2	3,7	4,9	< d.l.
V	22	14	31	13	17	92	41	46	20
Cr	40	< d.l.	< d.l.	< d.l.	< d.l.	4,8	< d.l.	< d.l.	< d.l.
Co	< d.l.	1,0	1,3	0,8	1,1	6,6	2,5	2,7	6,3
Rb	619	472	332	464	545	310	207	248	765
Sr	28	18	143	19	20	818	326	352	29
Y	78	53	26	54	55	30	16	17	84
Zr	1013	627	247	649	652	287	151	155	915
Nb	164	116	40	113	124	48	21	25	176
Cs	44	35	14	36	40	16	9	9	57
Ba	26	13	66	16	12	1108	282	306	24
La	194	127	60	129	132	81	38	40	189
Ce	366	243	114	244	253	157	69	76	368
Pr	37	24	12	25	26	16	8	8	33
Nd	120	88	45	82	91	57	31	29	145
Sm	22	15	8	13	17	10	5	5	22
Eu	1,9	1,3	1,9	1,6	1,5	2,1	1,7	1,8	2,7
Gd	15	10	6	11	10	7	3	5	20
Tb	2,2	1,6	0,8	1,8	1,7	1,0	0,8	0,6	2,1
Dy	15	10	5	11	10	6	3	4	19
Ho	3,0	1,8	1,2	2,2	2,2	1,1	0,6	0,6	3,3
Er	8,7	5,4	3,8	5,1	6,5	2,8	2,3	1,7	8,2
Tm	0,8	0,8	0,5	0,9	0,9	0,4	0,2	0,3	1,0
Yb	9,2	6,0	3,3	6,2	7,1	3,0	2,5	2,1	7,6
Lu	1,3	0,7	0,4	0,9	1,1	0,4	0,3	0,3	1,4
Hf	20	15	7	14	15	6	3	4	21
Ta	9,4	5,4	2,3	5,5	6,2	2,5	0,7	1,4	10,4
Pb	129	74	87	79	84	51	44	42	364
Th	80	50	20	52	53	25	12	13	80
U	28	18	7	19	21	8	3	4	27
Eu/Eu*	0,3	0,3	0,9	0,4	0,3	0,8	1,4	1,1	0,4
$(La/Yb)_N$	14	14	12	14	12	18	10	13	17
$(La/Sm)_N$	5,4	5,2	4,9	6,2	5,0	5,1	4,3	4,8	5,3
$(Gd/Yb)_N$	1,4	1,3	1,3	1,4	1,2	1,8	0,9	1,8	2,1

Tephra layer	I 9														
Sample	I 9 c														
Material	GS														
Classification	TRA														
SiO_2	62,7	63,1	63,4	63,5	63,6	62,7	63,2	63,1	62,7	62,6	62,5	62,9	62,7	62,1	62,5
TiO_2	0,45	0,45	0,47	0,52	0,40	0,43	0,39	0,45	0,49	0,50	0,49	0,48	0,40	0,55	0,47
Al_2O_3	19,2	19,5	19,7	19,6	19,6	18,8	18,5	18,7	18,8	18,6	18,7	18,3	18,4	19,2	19,1
FeO	2,79	2,90	2,80	3,25	2,87	1,64	1,71	1,81	1,65	1,68	1,82	1,77	1,79	1,74	1,66
MnO	0,22	0,25	0,30	0,37	0,19	0,34	0,45	0,41	0,38	0,31	0,42	0,42	0,43	0,34	0,38
MgO	0,42	0,45	0,45	0,37	0,45	3,07	2,84	2,94	3,08	3,07	3,04	3,05	2,90	3,17	3,10
CaO	1,75	1,83	1,72	1,73	1,77	0,29	0,26	0,26	0,36	0,29	0,20	0,21	0,23	0,33	0,33
Na_2O	4,91	4,03	4,00	4,18	3,82	6,08	5,48	5,11	5,87	6,25	5,53	5,74	5,98	6,13	5,87
K_2O	7,39	7,38	7,21	6,39	7,26	6,54	7,18	7,12	6,58	6,65	7,27	6,99	7,08	6,50	6,55
P_2O_5	0,12	0,09	0,03	0,02	0,04	0,05	0,03	0,10	0,09	0,00	0,01	0,10	0,11	0,01	0,09
Tot.	98,9	97,6	98,4	96,5	95,8	94,8	94,9	97,4	95,1	96,5	95,1	95,0	95,4	94,5	94,7
Alkali	12,3	11,4	11,2	10,6	11,1	12,6	12,7	12,2	12,5	12,9	12,8	12,7	13,1	12,6	12,4

Tephra layer	I 9								
Sample	I 9 c								
Li	85	143	69	104	57	84	51	116	116
Sc	3,9	3,5	3,9	1,5	1,6	4,0	1,8	< d.l.	2,8
V	23	15	25	11	25	24	13	10	13
Cr	< d.l.	< d.l.	< d.l.	< d.l.	< d.l.	< d.l.	< d.l.	< d.l.	< d.l.
Co	1,8	1,0	0,5	0,4	0,9	1,4	1,4	<1.25	1,6
Rb	394	523	382	458	391	352	441	366	469
Sr	19	4	21	3	19	18	5	3	4
Y	54	83	57	82	53	46	100	83	80
Zr	538	916	564	798	551	481	962	759	872
Nb	96	165	90	136	100	88	150	136	153
Cs	28	46	28	40	28	25	39	26	41
Ba	1,4	0,4	3,7	0,9	1,2	1,5	< d.l.	< d.l.	0,5
La	142	214	144	203	144	131	209	185	208
Ce	280	447	266	400	280	278	398	385	416
Pr	28	43	28	39	29	27	44	40	41
Nd	100	148	96	131	104	93	148	134	143
Sm	18	25	19	25	17	16	20	24	20
Eu	1,9	1,9	2,1	2,1	2,6	2,3	1,1	1,7	2,0
Gd	12	17	14	19	11	11	19	17	17
Tb	1,7	2,6	1,7	2,3	1,8	1,5	2,0	2,4	2,5
Dy	9,7	15,4	11,3	14,1	11,0	9,2	10,7	16,6	15,3
Ho	2,1	3,0	2,0	2,4	2,3	1,9	2,8	4,0	2,6
Er	5,8	8,3	6,5	8,3	6,0	4,3	11,7	10,4	7,7
Tm	0,8	1,3	0,9	0,9	0,7	0,7	1,2	1,4	1,2
Yb	5,6	8,7	5,4	6,2	5,9	4,6	14,0	13,9	8,9
Lu	0,8	1,0	1,0	1,1	0,9	0,8	1,3	0,4	1,0
Hf	11	19	11	17	11	10	22	16	18
Ta	4,7	7,6	4,3	6,6	4,8	3,9	7,2	4,9	7,5
Pb	79	157	211	242	284	76	137	382	169
Th	45	74	45	66	46	41	78	67	73
U	14	25	14	21	15	13	24	21	23
Eu/Eu*	0,4	0,3	0,4	0,3	0,6	0,5	0,2	0,3	0,3
$(La/Yb)_N$	17	17	18	22	17	19	10	9	16
$(La/Sm)_N$	4,9	5,3	4,8	5,1	5,5	5,1	6,7	4,9	6,6
$(Gd/Yb)_N$	1,7	1,6	2,0	2,5	1,6	2,0	1,1	1,0	1,6

Chemical analysis of tephras from the MD01_2474G core

Major (wt. %) and trace (ppm) element composition of the tephra layers. All analysis recalculated water-free to 100. Tephra components: GS=glass shards, SC=scoria, P=pumice. Chemistry: BAS-AND= basaltic-andesite, AND= andesite, DAC= dacite, RHY= rhyolite, PAN=Pantellerite, TRA-BAS=trachy-basalt, BAS-TRA-AND=basaltic-trachy-andesite, TRA-AND=trachy-andesite, TRA-DAC= trachy-dacite, TRA= thrachyte, TEPHRY-PHO=tephry-phonolite, LAT=latite, MUG=mugearite , SHO=shoshonite.

Tephra layer	**MD3**						
Sample	**MD3 c**						
Material	**GS**						
Classification	**LAT**						
SiO_2	55,1	54,8	55,4	57,1	55,2	56,1	55,7
TiO_2	1,20	1,26	1,27	1,15	1,23	1,37	1,28
Al_2O_3	17,0	16,8	17,2	17,7	18,0	17,3	17,6
FeO	7,98	8,26	7,27	5,76	7,51	7,92	7,71
MnO	0,14	0,14	0,15	0,15	0,18	0,14	0,21
MgO	2,56	2,68	2,38	2,28	2,48	2,77	2,39
CaO	5,54	5,60	5,04	5,16	5,61	5,34	5,39
Na_2O	3,09	3,23	3,28	3,32	2,80	2,09	2,88
K_2O	6,46	6,33	6,99	6,48	6,29	6,04	6,03
P_2O_5	0,90	0,91	0,93	0,85	0,73	0,87	0,86
Tot.	96,8	94,7	97,4	99,8	99,2	92,3	97,9
Alkali	9,6	9,6	10,3	9,8	9,1	8,1	8,9

Tephra layer	**MD10**								
Sample	**MD10 c**								
Material	**GS**								
Classification	**MUG**	**TRA**				**MUG**			
SiO_2	60,1	65,1	64,7	65,1	65,0	59,7	60,0	59,4	60,2
TiO_2	1,43	0,38	0,36	0,36	0,36	1,48	1,39	1,42	1,46
Al_2O_3	17,1	17,4	17,8	17,8	17,6	17,8	17,0	17,5	17,5
FeO	5,61	2,58	2,60	2,46	2,55	5,49	5,62	5,71	5,66
MnO	0,22	0,23	0,26	0,23	0,25	0,25	0,21	0,18	0,19
MgO	2,07	0,22	0,20	0,22	0,19	2,04	2,17	2,21	2,14
CaO	4,17	1,36	1,50	1,45	1,39	4,11	4,38	4,32	4,27
Na_2O	5,68	6,16	6,07	6,02	6,22	5,56	5,61	5,75	5,06
K_2O	3,05	6,52	6,56	6,43	6,51	3,00	3,00	3,01	3,08
P_2O_5	0,58	0,00	0,00	0,02	0,04	0,56	0,61	0,56	0,48
Tot.	97,7	93,6	91,9	94,8	92,4	98,0	97,8	93,6	97,2
Alkali	8,7	12,7	12,6	12,4	12,7	8,6	8,6	8,8	8,1

Tephra layer	MD11						
Sample							
Material	GS						
Classification	TRA-DAC	SHO	TRA-DAC	SHO			
SiO_2	67,3	57,8	66,3	58,6	59,1	59,0	58,6
TiO_2	0,41	1,05	0,43	1,05	1,23	1,18	1,14
Al_2O_3	15,5	17,2	15,2	17,2	16,6	16,7	17,1
FeO	3,65	7,12	3,61	7,26	6,69	6,40	6,67
MnO	0,06	0,10	0,11	0,17	0,10	0,19	0,26
MgO	0,70	2,28	0,70	2,33	2,02	2,09	2,10
CaO	1,88	4,84	3,24	4,82	4,15	4,39	4,29
Na_2O	3,79	3,46	2,57	2,62	3,73	3,29	3,58
K_2O	5,97	5,38	5,94	5,32	5,65	5,99	5,59
P_2O_5	0,80	0,73	1,93	0,62	0,74	0,84	0,68
Tot.	97,1	97,2	97,9	96,1	95,6	96,8	98,6
Alkali	9,8	8,8	8,5	7,9	9,4	9,3	9,2

Tephra layer	MD14								MD14									
Sample	MD14 a								MD14 b									
Material	GS								SC									
Classification	TRA				TRA-DAC	TRA			TRA	TRA-AND					TRA-DAC	BAS-TRA-AND	TRA-AND	
SiO_2	62,5	61,9	62,4	62,5	64,8	62,4	62,7	62,5	63,1	57,9	55,5	57,6	57,7	59,5	64,4	53,4	61,9	56,9
TiO_2	0,58	0,50	0,57	0,58	0,59	0,58	0,60	0,56	0,23	1,05	1,73	1,58	1,07	0,70	0,91	1,53	0,67	1,17
Al_2O_3	19,1	20,0	19,0	18,8	19,5	18,7	19,0	18,9	18,8	18,9	15,0	15,2	18,4	18,6	17,1	15,7	18,2	16,6
FeO	2,74	2,56	2,81	3,00	2,65	2,77	2,71	2,91	1,71	6,16	9,82	9,10	5,87	4,45	4,53	9,75	3,96	7,54
MnO	0,13	0,18	0,13	0,17	0,14	0,12	0,13	0,17	0,07	0,11	0,24	0,23	0,14	0,15	0,16	0,24	0,06	0,23
MgO	0,55	0,50	0,51	0,50	0,51	0,57	0,55	0,56	0,72	1,32	2,56	2,47	2,13	1,81	0,45	3,15	1,46	1,95
CaO	1,48	1,48	1,38	1,54	1,56	1,59	1,51	1,53	2,57	7,04	5,92	5,91	7,54	7,51	2,63	7,27	5,81	4,88
Na_2O	5,61	5,67	5,92	5,70	3,07	5,73	5,73	5,75	4,26	4,02	3,61	3,67	4,09	3,90	3,61	3,37	4,01	3,81
K_2O	7,22	7,07	7,14	7,19	7,07	7,43	7,03	7,06	7,93	2,99	4,74	3,66	2,69	2,96	5,69	4,65	3,39	5,78
P_2O_5	0,11	0,12	0,09	0,07	0,12	0,12	0,08	0,05	0,60	0,51	0,84	0,63	0,41	0,44	0,55	1,03	0,49	1,13
Tot.	96,9	95,0	96,3	93,8	95,0	97,5	97,6	95,1	100,2	100,3	98,1	99,4	99,4	99,4	94,9	98,4	99,1	97,7
Alkali	12,8	12,7	13,1	12,9	10,1	13,2	12,8	12,8	12,2	7,0	8,3	7,3	6,8	6,9	9,3	8,0	7,4	9,6

Tephra layer	MD15						
Sample	MD15 a						
Material	GS					SC	
Classification	TEPHRY-PHO	BAS-TRA-AND	TEPHRY-PHO	BAS-TRA-AND			TRA-AND
SiO_2	54,8	54,9	55,0	54,4	55,1	54,3	55,1
TiO_2	0,70	1,02	0,68	1,10	0,92	1,53	1,72
Al_2O_3	17,9	19,2	19,5	19,8	20,2	16,4	15,7
FeO	8,19	7,29	6,97	7,18	5,09	9,33	9,50
MnO	0,20	0,15	0,16	0,14	0,11	0,28	0,21
MgO	2,11	2,98	1,84	2,95	2,22	2,97	2,74
CaO	4,81	7,40	5,44	7,31	9,46	8,04	7,09
Na_2O	4,53	3,74	4,46	3,65	3,87	3,57	3,43
K_2O	6,06	2,86	5,30	2,81	2,52	3,05	3,81
P_2O_5	0,78	0,51	0,69	0,61	0,48	0,55	0,71
Tot.	98,3	97,4	97,8	98,7	96,2	97,8	96,5
Alkali	10,6	6,6	9,8	6,5	6,4	6,6	7,2

Tephra layer	MD15										
Sample	MD15 b										
Material	GS										
Classification	TRA-AND						BAS-TRA-AND	TRA-AND			TRA-BAS
SiO_2	57,3	56,9	57,8	57,8	57,7	56,7	56,6	58,2	56,0	51,3	49,8
TiO_2	0,87	0,98	0,92	0,85	0,95	0,68	1,75	1,36	0,96	1,93	2,73
Al_2O_3	18,2	17,8	18,0	19,3	17,9	20,7	14,6	18,9	20,4	16,6	17,0
FeO	6,44	6,72	6,68	5,93	6,44	4,77	9,65	5,01	4,90	12,09	15,33
MnO	0,32	0,21	0,15	0,22	0,19	0,15	0,17	0,05	0,16	0,26	0,22
MgO	2,34	2,76	2,31	2,08	2,41	1,59	3,18	1,02	1,60	3,08	1,91
CaO	5,77	5,94	5,66	5,50	5,85	7,59	6,28	3,94	8,22	6,31	5,76
Na_2O	4,38	4,40	4,03	4,14	4,10	4,73	3,39	3,18	4,15	2,99	3,42
K_2O	3,89	3,71	3,85	3,80	3,91	2,70	3,59	7,38	3,12	4,57	3,36
P_2O_5	0,46	0,61	0,54	0,42	0,55	0,36	0,79	1,06	0,53	0,87	0,44
Tot.	90,5	92,2	96,7	94,1	94,8	92,7	97,2	97,7	98,2	97,8	98,5
Alkali	8,3	8,1	7,9	7,9	8,0	7,4	7,0	10,6	7,3	7,6	6,8

Tephra layer	MD15					
Sample	MD15 c					
Material	GS					
Classification	BAS-TRA-AND					TEPHRY-PHO
SiO_2	54,6	54,2	54,0	53,8	55,3	53,2
TiO_2	1,22	1,70	1,25	1,31	1,17	1,45
Al_2O_3	17,0	15,8	16,4	17,1	18,2	16,9
FeO	7,39	10,15	7,52	9,31	7,03	8,91
MnO	0,25	0,27	0,23	0,26	0,18	0,27
MgO	3,33	3,17	3,64	4,23	3,56	3,01
CaO	8,29	7,42	7,68	7,19	7,37	5,79
Na_2O	3,79	3,22	4,19	3,21	3,63	3,62
K_2O	3,44	3,52	4,10	3,04	2,77	5,89
P_2O_5	0,69	0,55	0,96	0,56	0,70	0,91
Tot.	97,8	95,8	94,5	97,8	98,0	98,1
Alkali	7,2	6,7	8,3	6,2	6,4	9,5

Tephra layer	MD15																
Sample	**MD15 b**																
Li	< d.l.	13	23	< d.l.	44	< d.l.	45	49	24	21	< d.l.	8	< d.l.	< d.l.	18	< d.l.	20
Be	< d.l.	< d.l.	6,8	< d.l.	73,7	< d.l.	102,7	< d.l.	13,0	< d.l.	< d.l.	12,8	< d.l.	95,5	< d.l.	< d.l.	< d.l.
Sc	11	14	6	18		37	19	20	11	12	< d.l.	22	37	15	21	< d.l.	15
V	114	190	94	112	83	117	86	86	95	95	87	232	301	142	341	139	201
Cr	< d.l.	< d.l.	< d.l.	104	242	< d.l.	< d.l.	< d.l.	< d.l.	< d.l.	< d.l.	< d.l.	< d.l.	< d.l.	< d.l.	< d.l.	< d.l.
Co	8,8	14,9	10,0	9,4	8,0	17,3	4,6	7,7	8,0	9,9	6,3	22,0	15,5	22,0	10,6	14,7	16,8
Ni	< d.l.	< d.l.	< d.l.	< d.l.	21,2	< d.l.	< d.l.	13,5	3,7	< d.l.	< d.l.	< d.l.	9,5	51,3	< d.l.	< d.l.	< d.l.
Zn	44	84	72	< d.l.	< d.l.	< d.l.	< d.l.	45	67	82	< d.l.	89	86	58	90	161	153
Rb	60	108	106	126	121	145	115	98	103	99	92	80	97	71	92	64	91
Sr	794	448	408	451	406	494	341	517	494	550	764	521	322	491	355	575	490
Y	14	24	19	15	22	21	16	19	24	21	16	25	25	26	25	14	26
Zr	57	140	130	113	97	123	132	118	146	145	144	119	133	108	155	85	134
Nb	11	22	16	17	18	22	18	16	19	18	20	16	16	18	21	14	18
Cs	3,1	5,4	5,7	5,1	5,6	7,5	7,0	6,9	5,8	5,0	6,4	4,7	4,6	2,7	3,7	4,2	4,6
Ba	910	1036	957	980	949	1215	944	1155	1117	1054	1057	939	622	959	603	752	992
La	28	49	45	41	38	52	43	47	48	43	39	43	44	62	55	33	46
Ce	57	99	84	85	72	84	80	84	87	86	82	84	87	120	109	62	91
Pr	5,6	10,9	9,6	8,8	5,6	8,8	8,1	7,5	9,0	10,4	8,3	9,5	8,5	13,0	12,9	8,0	10,0
Nd	25	42	34	37	25	19	33	25	32	33	39	34	32	50	46	25	37
Sm	6,5	5,8	4,8	6,3	5,0	5,4	3,7	4,1	5,2	4,4	6,2	7,4	6,4	10,6	7,2	4,9	7,9
Eu	0,7	2,3	1,3	1,1	< d.l.	< d.l.	1,6	0,7	1,2	1,6	0,6	1,6	2,3	2,1	2,8	0,4	1,0
Gd	4,1	4,8	5,2	< d.l.	7,2	5,2	2,6	3,1	3,4	4,1	2,7	6,9	4,5	7,3	< d.l.	3,5	6,0
Tb	0,4	0,9	0,7	< d.l.	0,7	< d.l.	0,5	1,0	0,7	0,5	0,5	0,8	< d.l.	< d.l.	1,1	0,4	0,7
Dy	4,3	4,2	4,5	4,1	5,4	< d.l.	4,1	2,8	3,3	4,8	< d.l.	5,4	4,4	4,5	5,5	4,2	5,4
Ho	< d.l.	0,8	0,8	0,9	< d.l.	1,8	0,5	0,7	0,8	0,9	< d.l.	0,9	1,3	0,7	1,4	0,7	0,9
Er	2,4	3,2	2,9	2,8	3,1	< d.l.	< d.l.	2,0	2,5	2,6	< d.l.	2,9	2,3	3,5	4,2	1,9	3,0
Tm	< d.l.	0,4	0,4	< d.l.	< d.l.	0,3	< d.l.	0,3	0,4	0,3	< d.l.	0,2	0,4	< d.l.	0,4	0,3	0,3
Yb	2,4	1,8	1,9	2,5	< d.l.	< d.l.	< d.l.	3,1	1,6	< d.l.	2,9	3,8	3,6	1,9	< d.l.	1,5	2,7
Lu	0,5	0,4	0,3	0,2	0,4	< d.l.	< d.l.	0,4	0,2	0,6	< d.l.	0,5	0,6	0,5	< d.l.	0,2	0,4
Hf	3,6	2,2	3,4	1,3	< d.l.	3,8	5,8	2,3	3,8	4,0	4,3	2,5	2,2	2,6	5,2	1,5	4,0
Ta	0,3	0,8	0,7	0,7	< d.l.	1,3	< d.l.	1,0	1,1	1,1	1,1	0,8	0,7	1,1	1,3	0,5	0,9
Pb	15	25	31	30	23	36	42	20	24	23	50	19	16	44	16	20	21
Th	8,0	15,8	14,3	13,2	15,0	13,2	11,2	13,4	16,6	15,8	6,1	14,0	15,6	16,4	15,1	11,5	14,7
U	2,6	4,6	4,0	5,0	5,5	4,4	4,0	3,9	4,4	3,7	3,5	3,8	4,1	5,6	6,0	3,0	4,5
Eu/Eu*	0,4	1,4	0,8		0,0	0,0	1,6	0,6	0,9	1,2	0,5	0,7	1,3	0,7		0,3	0,4
$(La/Yb)_N$	8,0	18,9	16,2	11,0				10,1	20,5		9,2	7,7	8,2	22,4		15,1	11,4
$(La/Sm)_N$	2,7	5,4	5,9	4,1	4,8	6,1	7,3	7,1	5,8		4,0	3,7	4,3	3,7	4,8	4,2	3,7
$(Gd/Yb)_N$	1,4	2,2	2,2	0,0				0,8	1,8		0,8	1,5	1,0	3,2		2,0	1,8

Tephra layer	MD18									
Sample	MD18 a						MD18 b			
Material	GS						SC			
Classification	BAS-TRA-AND		DAC	BAS-TRA-AND	TEPHRY-PHO	DAC	BAS-TRA-AND			
SiO_2	53,2	52,4	70,3	53,6	54,4	70,4	52,7	53,0	53,5	52,9
TiO_2	1,67	1,59	0,69	1,63	0,75	0,67	1,49	1,52	1,48	1,66
Al_2O_3	15,4	16,1	14,8	15,0	17,3	15,0	15,2	15,4	15,6	15,0
FeO	10,61	9,78	4,12	10,73	8,46	4,06	10,68	9,76	8,95	10,08
MnO	0,15	0,19	0,16	0,26	0,26	0,19	0,30	0,29	0,23	0,16
MgO	4,09	4,20	0,81	4,09	2,44	0,74	4,57	4,27	3,69	4,33
CaO	7,83	8,17	2,59	7,76	5,28	2,75	7,51	8,97	8,96	7,91
Na_2O	3,13	3,29	3,50	3,04	4,46	3,07	3,32	3,33	3,38	3,65
K_2O	3,26	3,56	2,98	3,21	5,87	3,05	3,65	2,71	3,47	3,56
P_2O_5	0,64	0,76	0,11	0,67	0,80	0,16	0,55	0,76	0,71	0,72
Tot.	97,4	91,7	92,7	97,1	95,0	94,8	96,6	96,4	98,7	97,7
Alkali	6,4	6,8	6,5	6,3	10,3	6,1	7,0	6,0	6,9	7,2

Tephra layer	MD18					
Sample	MD18 a					
Li	< d.l.	39,0	23,7	17,1	< d.l.	18,5
Be	< d.l.	< d.l.	< d.l.	< d.l.	< d.l.	< d.l.
Sc	21	27	22	27	28	22
V	67	138	443	425	343	379
Cr	< d.l.	< d.l.	< d.l.	< d.l.	< d.l.	< d.l.
Co	6,8	21,5	29,1	28,6	31,1	24,9
Ni	15		13	16	< d.l.	9
Zn	101	45	111	105	103	54
Rb	72	211	121	112	154	96
Sr	602	704	403	395	377	366
Y	26	17	32	28	26	25
Zr	258	149	151	150	187	119
Nb	81	20	19	20	27	13
Cs	0,6	6,1	5,9	5,5	5,9	6,2
Ba	945	1058	979	970	1011	812
La	84	56	49	49	56	41
Ce	166	107	97	97	117	77
Pr	17	13	10	10	15	7
Nd	53	38	39	42	51	34
Sm	8,9	9,2	7,1	6,5	7,0	7,2
Eu	2,9	0,6	2,4	2,2	2,0	0,6
Gd	3,0	4,9	5,9	6,6	7,3	6,5
Tb	1,1	1,0	1,0	1,1	1,1	0,6
Dy	3,8	5,5	6,1	5,2	7,5	6,6
Ho	0,8	0,6	1,1	1,3	1,0	1,0
Er	3,0	1,9	2,4	3,1	1,7	3,2
Tm	0,2	0,5	0,5	0,4	0,1	0,3
Yb	2,4	3,0	2,5	3,9	2,6	< d.l.
Lu	0,5	0,2	0,3	0,7	0,4	0,3
Hf	4,4	2,3	4,0	3,6	2,5	3,4
Ta	3,2	1,3	1,1	1,0	0,9	1,1
Pb	17	27	27	22	47	27
Th	16	17	18	16	20	13
U	5,2	5,2	4,9	4,6	6,9	3,5
Eu/Eu*		0,3	1,1	1,0	0,9	0,3
$(La/Yb)_N$	24	13	13	9	15	
$(La/Sm)_N$		3,9	4,4	4,8	5,1	3,6
$(Gd/Yb)_N$		1,3	1,9	1,4	2,3	

Tephra layer	MD22																						
Sample	MD22 a										MD22 b												
Material	GS										SC						GS						
Classification	TRA-AND		RHY		TRA-AND	BAS-TRA-AND	RHY				TRA-AND		TRA-DAC	TRA-AND	DAC	BAS-TRA-AND	AND	RHY	TRA-AND		BAS-AND	TRA-AND	DAC
SiO_2	61,2	59,9	71,3	71,5	56,5	53,9	70,0	71,4	71,6	72,1	58,6	57,2	66,2	59,5	67,3	55,7	57,7	72,5	56,8	56,5	54,9	60,6	70,6
TiO_2	1,06	1,26	0,57	0,56	1,51	1,39	0,71	0,65	0,54	0,61	1,18	1,40	0,48	1,16	0,48	1,79	1,21	0,56	1,29	1,31	1,39	0,82	0,77
Al_2O_3	16,5	13,8	13,8	13,9	14,6	14,9	14,3	13,8	13,9	13,7	17,6	17,4	17,9	14,4	18,6	13,4	15,5	13,9	16,9	17,2	15,0	18,7	14,5
FeO	6,35	9,32	3,78	3,78	9,78	11,58	4,03	3,79	3,63	3,56	6,70	7,65	2,31	7,53	1,98	10,54	8,50	3,42	8,03	8,06	11,04	5,15	4,03
MnO	0,21	0,27	0,13	0,21	0,24	0,18	0,18	0,16	0,13	0,15	0,20	0,15	0,05	0,16	0,07	0,26	0,18	0,09	0,23	0,18	0,26	0,12	0,14
MgO	1,74	3,98	0,64	0,62	3,48	4,03	0,81	0,60	0,64	0,62	1,60	2,28	0,56	3,35	0,30	4,08	3,97	0,63	2,49	2,43	3,71	1,33	0,75
CaO	5,42	3,93	2,29	2,33	6,84	7,73	2,62	2,28	2,29	2,24	5,59	7,26	3,55	5,99	3,96	7,60	7,38	2,25	6,24	6,35	7,63	5,90	2,62
Na_2O	3,79	3,41	3,73	3,51	3,18	3,32	3,98	3,78	3,74	3,56	4,43	3,50	4,60	2,92	3,84	3,04	2,85	3,19	3,68	3,56	3,16	4,19	3,40
K_2O	3,34	3,57	3,59	3,50	3,25	2,49	3,24	3,45	3,48	3,40	3,51	2,70	4,28	4,37	3,30	3,02	2,33	3,42	3,84	3,74	2,40	2,59	3,11
P_2O_5	0,45	0,55	0,13	0,10	0,60	0,44	0,14	0,09	0,05	0,07	0,58	0,45	0,10	0,62	0,18	0,55	0,46	0,10	0,47	0,58	0,46	0,59	0,15
Tot.	97,7	97,9	92,5	93,2	95,3	94,9	93,1	93,1	92,2	92,8	100,3	99,4	99,5	99,7	98,3	97,7	99,5	93,7	98,9	99,5	98,9	99,6	95,5
Alkali	7,1	7,0	7,3	7,0	6,4	5,8	7,2	7,2	7,2	7,0	7,9	6,2	8,9	7,3	7,1	6,1	5,2	6,6	7,5	7,3	5,6	6,8	6,5

Tephra layer	MD22																								
Sample	MD22 c															MD22 d									
Material	GS									SC						GS									
Classification	BAS-AND			TRA-AND			AND	TRA-AND			TRA-DAC	TRA-AND			TRA-DAC	TRA-AND	DAC			AND		BAS-TRA-AND		TRA-AND	
SiO_2	55,5	54,8	54,4	51,0	60,1	61,7	60,6	60,6	53,2	57,7	61,2	56,9	64,3	60,3	64,8	71,3	71,2	70,2	60,8	60,8	55,6	55,6	71,3	54,6
TiO_2	1,47	1,33	1,35	1,59	1,41	1,49	1,41	1,25	0,73	1,09	1,22	1,04	1,50	1,44	1,54	0,61	0,63	0,46	1,30	1,32	1,81	1,80	0,59	0,89
Al_2O_3	16,0	15,9	15,4	17,4	16,4	14,9	16,5	17,1	18,5	16,7	18,5	19,0	14,9	16,8	14,9	14,6	15,3	14,8	15,1	15,3	15,4	16,0	14,9	18,5
FeO	9,36	9,11	9,60	10,00	7,09	7,62	7,48	6,55	8,56	8,85	4,26	8,03	6,33	7,56	5,85	3,78	3,74	4,71	8,93	9,03	10,49	9,93	3,94	8,44
MnO	0,20	0,21	0,29	0,24	0,19	0,22	0,13	0,16	0,17	0,23	0,06	0,15	0,17	0,16	0,18	0,12	0,14	0,20	0,20	0,20	0,25	0,15	0,06	0,21
MgO	3,94	4,74	5,01	3,87	2,18	2,07	2,22	1,83	2,69	2,28	1,37	0,97	1,26	1,35	1,48	0,59	0,63	0,57	2,42	2,44	3,09	3,04	0,62	2,27
CaO	7,52	7,86	8,43	7,89	4,94	4,41	5,05	5,25	6,03	4,91	4,26	3,96	2,54	4,95	2,67	2,18	2,19	2,45	5,46	5,64	6,35	6,36	2,21	5,47
Na_2O	3,22	3,22	3,05	3,42	3,86	3,51	2,90	3,91	4,37	3,48	3,67	4,82	3,64	3,82	3,78	3,62	3,01	3,25	3,16	2,61	3,61	3,75	3,22	3,91
K_2O	2,33	2,26	2,00	3,73	3,27	3,36	3,24	2,92	4,94	4,31	4,69	4,38	4,76	3,20	4,15	3,08	3,03	3,29	2,34	2,31	2,80	2,87	3,09	4,88
P_2O_5	0,41	0,57	0,46	0,83	0,49	0,71	0,55	0,41	0,82	0,51	0,86	0,75	0,59	0,44	0,61	0,08	0,13	0,11	0,30	0,33	0,60	0,51	0,08	0,81
Tot.	98,2	99,3	99,1	98,8	97,2	99,6	97,4	98,3	99,2	98,9	96,6	96,0	94,3	95,1	96,3	94,8	92,9	94,8	98,0	97,3	98,2	98,7	94,0	97,5
Alkali	5,6	5,5	5,0	7,2	7,1	6,9	6,1	6,8	9,3	7,8	8,4	9,2	8,4	7,0	7,9	6,7	6,0	6,5	5,5	4,9	6,4	6,6	6,3	8,8

Tephra layer	MD22																								
Sample	**MD22 c**																		**MD22 d**						
Li	< d.l.	< d.l.	8,6	20,9	14,2	14,0	< d.l.	20,7	< d.l.	12,8	17,8	< d.l.	< d.l.	16,9	< d.l.	8,7	< d.l.	< d.l.	< d.l.	< d.l.	54,4	41,7	< d.l.	< d.l.	20,7
Be	< d.l.	< d.l.	< d.l.	59,8	< d.l.	< d.l.	< d.l.	< d.l.	< d.l.	< d.l.	18,8	< d.l.	57,3	< d.l.	< d.l.	< d.l.	< d.l.	< d.l.	< d.l.	< d.l.	< d.l.	< d.l.	< d.l.	< d.l.	12,4
Sc	31	52	28	15	18	14	24	39	16	10	12	21	33	14	< d.l.	24	9	< d.l.	< d.l.	18		38	12	10	20
V	352	315	318	173	352	215	< d.l.	367	161	112	192	362	293	159	61	156	150	194	< d.l.	14	11	294	274	338	336
Cr	99	< d.l.	< d.l.	< d.l.	< d.l.	< d.l.	66	< d.l.	< d.l.	< d.l.	< d.l.	< d.l.	< d.l.	95	< d.l.	< d.l.	63	< d.l.	< d.l.	< d.l.	< d.l.	< d.l.	< d.l.	< d.l.	32
Co	23	25	28	11	22	12	< d.l.	25	10	6	16	17	19	18	4	6	17	12	5	5	1	20	10	51	28
Ni	19	48	25	< d.l.	< d.l.	< d.l.	< d.l.	< d.l.	< d.l.	< d.l.	3	14	< d.l.	< d.l.	< d.l.	< d.l.	9	< d.l.	< d.l.	< d.l.	< d.l.	< d.l.	< d.l.	27	27
Zn	50	148	93	78	43	81	110	95	40	52	128	99	60	123	71	91	59	221	147	68	58	73	99	303	132
Rb	84	43	43	95	63	104	104	58	89	143	193	249	167	175	152	160	139	74	96	70	82	103	84	77	84
Sr	402	498	450	304	385	223	181	377	345	313	780	121	224	812	142	171	202	591	179	166	165	516	447	271	578
Y	21	21	18	20	23	37	28	29	23	46	32	35	39	24	30	44	32	24	23	22	21	20	18	21	30
Zr	123	82	67	125	95	194	88	140	142	359	174	300	245	142	307	308	270	134	106	105	99	122	103	115	150
Nb	15	5	9	15	14	19	9	9	18	56	15	44	44	15	37	37	28	14	10	9	6	20	13	14	22
Cs	3,9	1,0	1,9	5,5	3,4	6,4	3,6	2,9	4,4	8,4	5,6	12,5	7,8	4,2	10,0	9,4	8,0	2,9	2,1	1,4	2,3	5,3	3,0	3,7	3,7
Ba	625	466	370	566	629	739	497	524	593	1602	1157	423	905	666	1028	1015	980	907	414	426	497	811	618	605	817
La	43	26	26	34	35	50	17	37	41	106	68	65	100	58	68	96	76	48	19	21	19	57	36	44	52
Ce	92	45	48	66	63	106	41	69	81	182	114	131	173	102	118	180	157	91	39	45	46	126	75	89	108
Pr	12	4	6	7	7	12	5	7	9	19	13	14	18	9	11	17	15	9	6	5	5	12	8	9	12
Nd	35	29	22	28	29	53	29	38	31	76	51	51	75	32	42	75	66	40	15	18	18	45	36	37	45
Sm	7,8	< d.l.	3,9	6,4	3,3	8,2	3,0	6,5	9,2	14,6	5,9	8,9	7,8	7,4	4,0	17,1	8,1	5,6	7,5	10,0	8,7	5,6	4,9	12,6	9,1
Eu	1,8	0,8	0,9	< d.l.	1,3	1,7	2,4	3,5	2,5	3,3	2,1	0,6	2,3	1,8	1,1	2,3	3,0	3,0	1,0	1,1	1,6	1,4	1,6	2,6	2,0
Gd	6,5	3,4	5,1	5,3	5,6	11,3	5,3	5,3	5,8	5,8	7,4	9,5	11,7	6,5	7,8	16,5	11,7	4,8	4,2	7,3	4,4	6,0	4,9	6,8	6,1
Tb	0,6	0,5	0,7	0,6	1,2	1,0	0,8	0,8	0,6	0,9	0,9	1,0	1,3	< d.l.	1,0	< d.l.	1,5	1,2	< d.l.	0,8	0,9	0,7	0,5	1,2	0,6
Dy	3,9		2,8	4,1	4,3	7,5	3,6	6,1	3,0	7,8	7,6	4,9	5,7	8,0	6,3	4,9	7,0	4,0	3,7	1,7	5,3	5,3	4,5	3,2	3,8
Ho	1,3	2,2	0,4	0,7	0,4	1,4	< d.l.	1,0	0,5	1,4	1,1	0,8	1,2	0,7	1,5	1,4	1,1	0,6	0,3	1,2	0,6	0,5	0,5	0,7	1,0
Er	< d.l.	2,4	1,9	2,4	2,7	1,1	< d.l.	3,5	2,6	5,6	2,4	< d.l.	1,8	2,6	2,2	3,1	3,1	1,3	3,8	1,3	4,3	< d.l.	2,2	2,1	3,7
Tm	0,4	< d.l.	0,2	0,3	0,3	< d.l.	< d.l.	0,2	0,4	< d.l.	0,3	< d.l.	< d.l.	0,3	0,5	0,5	< d.l.	0,2	0,3	0,4	0,3	< d.l.	< d.l.	0,6	0,4
Yb	< d.l.	< d.l.	1,9	2,9	1,4	1,6	< d.l.	3,4	4,8	8,7	2,4	1,6	4,9	< d.l.	< d.l.	5,3	2,7	2,2	< d.l.	2,6	4,8	< d.l.	< d.l.	4,3	3,1
Lu	0,3	0,5	0,3	0,4	0,4	0,3	< d.l.	0,5	0,6	1,2	0,2	0,4	< d.l.	0,4	0,3	0,6	0,6	0,5	0,3	< d.l.	0,4	0,6	< d.l.	< d.l.	0,3
Hf	7,2	2,8	2,8	6,6	1,5	4,5	4,3	3,4	6,1	6,6	4,6	5,4	9,5	3,7	4,5	4,6	8,2	3,9	4,0	4,3	4,0	3,4	1,8	1,1	4,5
Ta	0,8	1,3	0,4	0,7	0,6	1,0	< d.l.	1,0	0,9	3,1	1,1	3,0	2,3	1,2	3,0	1,6	1,5	1,0	0,3	1,5	0,4	< d.l.	1,0	0,9	0,8
Pb	18	13	10	18	17	19	5	13	13	31	25	23	27	25	27	31	24	21	17	15	13	24	11	27	20
Th	13	5	5	12	11	19	7	10	13	39	18	24	32	17	33	36	29	12	5	5	5	25	12	12	14
U	3,0	0,4	1,8	3,0	2,3	4,3	1,6	3,8	3,0	11,1	5,0	5,5	9,9	5,2	9,9	8,7	7,6	4,3	2,1	2,0	1,8	8,5	3,3	4,6	3,9
Eu/Eu*	0,8		0,6	0,0	0,9	0,5	1,9	1,8	1,0	1,1	0,9	0,2	0,7	0,8	0,6	0,4	0,9	1,8	0,6	0,4	0,8	0,7	1,0	0,9	0,8
$(La/Yb)_N$			9,4	7,9	16,8	20,5		7,4	5,8	8,2	19,5	27,3	13,8			12,3	19,3	14,3		5,3	2,7			6,9	11,3
$(La/Sm)_N$	3,5		4,2	3,4	6,6	3,8	3,7	3,6	2,8	4,6	7,2	4,6	8,1	5,0	10,8	3,5	5,9	5,3	1,6	1,3	1,4	6,4	4,6	2,2	3,6
$(Gd/Yb)_N$			2,2	1,5	3,2	5,6		1,3	1,0	0,5	2,5	4,8	1,9			2,5	3,6	1,7		2,2	0,7			1,3	1,6

Tephra layer	MD27																							
Sample	MD27 a								MD27 b															
Material	SC								GS								SC							
Classification	TRA-AND				BAS-AND	TRA-AND										BAS-TRA-AND	TRA-AND			AND	BAS-TRA-AND	TRA-AND	BAS-TRA-AND	BAS-TRA-AND
SiO_2	57,3	57,2	57,8	58,8	56,7	59,5	59,3	55,9	57,0	57,4	56,2	58,0	56,5	56,6	55,5	54,8	58,0	56,3	55,7	62,1	56,1	57,6	51,7	56,8
TiO_2	1,13	1,27	1,31	1,13	1,66	1,05	1,14	1,36	1,45	1,26	1,13	1,20	1,17	1,31	1,38	1,41	1,30	1,58	1,32	1,10	1,57	1,06	1,56	1,31
Al_2O_3	18,0	17,9	18,4	17,3	12,3	18,0	17,7	17,6	16,2	17,9	17,4	19,3	18,5	17,3	17,7	17,2	17,5	16,0	17,6	13,2	15,6	19,3	15,9	17,6
FeO	7,17	6,60	5,47	6,17	9,77	4,57	6,33	7,77	8,64	7,07	7,48	6,76	7,33	8,15	8,34	8,87	5,43	8,90	8,41	7,78	8,85	7,35	10,57	7,86
MnO	0,15	0,10	0,14	0,15	0,15	0,13	0,12	0,13	0,24	0,18	0,19	0,09	0,13	0,29	0,22	0,24	0,14	0,25	0,13	0,19	0,26	0,16	0,26	0,16
MgO	2,75	2,35	1,67	2,20	5,14	2,19	1,50	3,36	2,54	2,32	3,22	1,95	2,14	2,44	3,26	3,48	2,47	2,80	2,64	3,63	3,09	1,54	4,01	3,14
CaO	5,95	7,32	7,15	6,37	8,57	7,54	4,62	6,60	5,40	5,89	6,35	5,62	6,41	5,84	6,45	6,61	7,06	5,80	7,01	4,87	7,01	6,80	9,71	6,37
Na_2O	3,81	3,22	3,71	3,74	2,84	3,89	3,92	3,96	3,68	3,41	3,64	2,90	3,88	3,82	3,15	3,42	4,03	3,56	3,35	3,05	4,01	3,74	2,86	3,77
K_2O	3,25	3,36	3,88	3,55	2,46	2,67	4,76	2,81	4,23	4,02	3,70	3,64	3,34	3,69	3,41	3,38	3,57	4,16	3,44	3,54	2,83	2,24	2,95	2,56
P_2O_5	0,57	0,73	0,57	0,54	0,34	0,43	0,55	0,51	0,60	0,55	0,63	0,49	0,54	0,57	0,59	0,61	0,54	0,61	0,48	0,54	0,60	0,28	0,52	0,43
Tot.	99,6	95,6	97,8	98,8	98,3	98,2	98,1	98,5	97,8	97,1	99,6	91,9	99,5	98,3	99,4	99,7	98,3	98,8	97,7	97,0	98,0	98,4	98,4	98,4
Alkali	7,1	6,6	7,6	7,3	5,3	6,6	8,7	6,8	7,9	7,4	7,3	6,5	7,2	7,5	6,6	6,8	7,6	7,7	6,8	6,6	6,8	6,0	5,8	6,3

Tephra layer	MD27																													
Sample	MD27 a							MD27 b																						
Li	20	< d.l.	23	14	< d.l.	< d.l.	< d.l.	< d.l.	20	< d.l.	17	21	35	15	16	38	35	13	15	22	27	7	< d.l.	14	12	< d.l.	19	15	< d.l.	8
Be	< d.l.	< d.l.	4,3	< d.l.	35,8	< d.l.	< d.l.	40,6	40,1	< d.l.	< d.l.	< d.l.	< d.l.	< d.l.	22,0	< d.l.	< d.l.	65,9	< d.l.	20,0	< d.l.	< d.l.	39,6	< d.l.	6,7	< d.l.	< d.l.	< d.l.	< d.l.	7,2
Sc	13	< d.l.	25	14	19	< d.l.	14	16	< d.l.	< d.l.	20	15	19	22	15	17	8	21	10	20	7	14	20	15	19	18	24	13	8	19
V	208	175	324	233	399	202	237	18	< d.l.	132	114	284	258	252	278	307	213	394	46	307	153	216	186	401	315	304	301	224	168	345
Cr	< d.l.	< d.l.	45	< d.l.	< d.l.	76	65	111	< d.l.	71	< d.l.	< d.l.	< d.l.	166	< d.l.	< d.l.	< d.l.	< d.l.	< d.l.	< d.l.	< d.l.	31	< d.l.	< d.l.	< d.l.	< d.l.	< d.l.	184	< d.l.	25
Co	13	19	19	14	21	17	16	6	< d.l.	7	12	15	22	20	18	26	16	34	20	22	12	17	16	20	16	24	23	11	11	21
Ni	< d.l.	13	6	< d.l.	< d.l.	19	< d.l.	< d.l.	9	< d.l.	< d.l.	< d.l.	< d.l.	15	< d.l.	< d.l.	< d.l.	48	6	10	<3.04	14	37	<2.36	7	27	11	< d.l.	12	14
Zn	44	124	80	39	87	74	78	95	79	51	66	77	72	107	61	97	56	79	120	93	53	101	93	101	102	105	63	111	60	85
Rb	118	142	105	112	110	88	71	27	20	179	145	118	131	119	131	146	128	83	133	83	71	89	81	132	143	112	113	97	61	131
Sr	398	461	332	320	295	377	316	61	103	240	304	415	374	334	343	278	424	477	165	352	853	472	413	420	459	481	504	542	608	445
Y	23	24	30	28	30	22	19	28	23	28	28	25	26	23	31	27	26	21	34	28	11	29	24	45	31	28	24	23	15	29
Zr	144	208	156	153	152	115	142	173	133	223	201	157	157	164	171	212	158	119	198	132	95	197	178	261	188	183	164	134	105	182
Nb	16	28	16	19	19	11	19	55	46	31	22	19	21	18	22	29	21	13	23	15	14	24	24	31	25	20	19	21	18	22
Cs	5,2	6,6	5,8	5,4	5,8	4,7	5,1	0,5	0,3	11,1	7,3	5,6	6,3	4,8	6,6	6,6	5,6	4,7	7,2	4,2	3,3	6,5	8,4	6,0	7,9	5,0	6,5	4,1	1,3	5,9
Ba	1026	1376	861	791	790	661	925	2613	3270	1243	1056	970	1005	969	964	1017	1002	932	869	646	840	1012	949	1602	1003	1285	1119	1094	777	1069
La	46	59	42	41	40	28	44	33	27	72	51	48	48	44	52	59	47	51	77	37	31	57	50	88	60	54	50	55	41	57
Ce	95	122	84	81	86	53	84	73	54	137	110	92	102	91	113	118	103	105	154	76	59	114	99	174	123	110	99	101	72	114
Pr	9	14	10	10	10	8	9	9	7	13	11	8	9	10	10	14	10	8	16	8	6	11	11	21	14	11	11	10	7	12
Nd	36	43	38	39	33	24	30	37	19	61	39	32	43	30	36	39	34	43	57	34	26	42	42	71	50	43	38	40	25	40
Sm	7,1	11,3	7,5	9,7	5,8	4,8	8,4	9,0	4,1	8,9	10,8	8,2	7,3	6,6	10,1	9,4	8,1	5,6	9,2	6,0	3,2	10,0	7,2	12,6	8,8	7,6	7,2	7,7	4,0	7,8
Eu	1,9	1,3	1,6	1,2	0,6	1,1	0,9	3,3	3,6	2,1	2,1	2,1	1,8	1,8	2,2	1,9	0,6	1,9	0,6	1,6	0,7	1,2	2,3	2,2	2,6	2,3	2,7	1,1	1,1	2,1
Gd	3,9	8,0	6,4	4,9	9,8	1,9	6,8	4,8	2,7	6,2	2,7	7,5	5,4	3,8	5,9	3,1	6,4	5,6	6,9	7,4	3,6	7,0	6,1	7,9	7,8	8,9	6,3	7,1	5,1	5,7
Tb	0,7	0,6	1,1	< d.l.	1,0	0,8	0,9	1,0	0,7	0,7	0,8	0,8	0,7	0,8	< d.l.	0,6	0,8	0,8	1,2	1,0	0,5	0,9	0,6	1,9	1,0	0,8	1,0	0,4	0,5	1,1
Dy	4,8	4,6	5,7	4,8	6,2	3,6	3,8	6,3	4,1	7,3	5,5	< d.l.	2,3	5,7	4,8	6,8	5,2	4,4	5,0	4,3	1,9	4,0	3,1	8,9	6,0	5,1	4,0	3,6	3,1	4,8
Ho	0,6	0,6	1,1	0,9	1,1	0,8	0,7	1,0	0,6	0,8	0,9	0,7	0,6	0,8	0,8	1,1	0,7	1,4	1,2	0,7	0,6	0,9	0,9	2,0	0,8	1,0	0,9	1,0	0,6	1,2
Er	1,7	2,7	2,5	2,0	3,0	< d.l.	3,3	3,4	2,0	2,8	2,8	2,5	2,0	< d.l.	< d.l.	1,5	3,4	3,5	2,3	3,0	0,9	2,4	1,3	3,2	3,4	3,1	2,6	1,1	2,2	3,0
Tm	0,3	< d.l.	0,4	0,2	0,2	0,4	< d.l.	0,2	0,1	0,3	0,5	0,3	0,2	0,3	0,2	0,2	0,5	< d.l.	0,5	0,4	< d.l.	0,5	0,3	0,5	0,6	0,4	0,2	0,3	0,1	0,3
Yb	< d.l.	1,6	1,8	2,5	2,4	2,3	3,5	1,0	1,5	2,8	2,6	1,5		3,4	1,1	2,6	2,6	2,4	2,7	2,1	0,8	3,5	1,9	3,1	2,4	2,4	2,7	2,1	1,5	< d.l.
Lu	0,1		0,4	0,6	0,4	0,3	0,2	0,5	0,3	0,5	0,2	0,3	0,1	0,4	0,1	0,5	0,3	< d.l.	0,7	0,4	0,2	0,4	0,3	0,6	0,5	0,4	0,2	0,2	0,1	0,7
Hf	4,1	7,7	3,3	3,2	2,3	1,8	4,6	3,1	3,4	8,1	5,1	3,6	3,9	3,5	5,0	4,0	4,9	1,3	3,7	3,4	2,1	3,6	4,5	5,4	6,2	4,0	3,4	1,9	3,0	4,1
Ta	1,3	0,9	0,6	1,2	0,8	0,5	1,0	2,8	2,8	1,1	1,3	1,5	0,9	0,5	1,2	1,1	0,4	1,3	1,6	0,6	0,2	1,5	1,3	1,6	1,2	1,5	1,2	1,1	0,7	1,0
Pb	25	20	17	16	19	10	23	3	3	36	23	29	22	24	30	27	25	22	22	14	13	23	25	30	24	24	22	17	9	33
Th	19	22	13	15	14	9	18	3	2	28	24	18	20	18	20	20	16	12	24	12	9	20	20	27	21	19	17	17	9	19
U	6,1	5,7	4,0	3,7	3,5	2,8	5,4	0,8	1,0	6,9	6,7	5,4	4,4	6,7	5,1	7,4	4,9	3,8	6,0	3,6	2,3	5,9	6,1	6,8	5,9	6,9	4,6	6,1	2,7	5,1
Eu/Eu*	1,1	0,4	0,7	0,5	0,2	1,2	0,3			0,9	1,2	0,8	0,9	1,1	0,9	1,1	0,3	1,1	0,2	0,7		0,4	1,1	0,7	1,0	0,8	1,2	0,4		1,0
$(La/Yb)_N$		25,1	15,5	11,1	11,3	8,4	8,6			17,5	13,3	21,1		8,8	32,6	15,3	12,5	14,5	19,6	11,9		11,1	17,3	19,4	16,7	15,3	12,2	17,5		
$(La/Sm)_N$	4,0	3,3	3,6	2,7	4,4	3,7	3,3			5,1	3,0	3,7	4,1	4,3	3,3	4,0	3,7	5,7	5,3	3,9		3,6	4,4	4,4	4,3	4,4	4,3	4,5		4,6
$(Gd/Yb)_N$		4,1	2,8	1,6	3,3	0,7	1,6			1,8	0,8	4,0		0,9	4,4	1,0	2,0	1,9	2,1	2,8		1,6	2,5	2,1	2,6	3,0	1,8	2,7		

Tephra layer	MD28																						
Sample	MD28 a				MD28 b																		
Material	GS				GS								P										
Classification	TRA																						
SiO_2	62,2	61,6	63,3	63,4	63,5	64,2	63,0	64,1	63,9	63,5	63,4	63,8	63,4	63,4	63,5	63,1	63,5	63,0	62,5	62,6	63,3	62,4	63,7
TiO_2	0,55	0,61	0,60	0,53	0,58	0,52	0,58	0,57	0,43	0,54	0,57	0,56	0,58	0,59	0,59	0,48	0,60	0,54	0,60	0,51	0,64	0,59	0,56
Al_2O_3	19,9	21,6	19,1	19,5	19,7	19,5	19,9	20,4	19,7	20,5	19,7	19,6	20,0	20,2	19,9	20,1	19,7	19,4	19,4	19,5	19,4	19,2	18,7
FeO	2,75	2,70	2,88	2,61	2,51	2,48	2,80	2,72	2,83	2,38	2,60	2,50	2,69	2,73	2,73	2,64	2,82	2,64	2,69	2,85	2,63	2,79	2,60
MnO	0,25	0,24	0,26	0,27	0,20	0,28	0,29	0,27	0,09	0,24	0,36	0,23	0,23	0,30	0,36	0,26	0,34	0,33	0,27	0,30	0,23	0,30	0,19
MgO	0,33	0,35	0,37	0,44	0,36	0,40	0,30	0,33	0,54	0,36	0,33	0,40	0,33	0,27	0,32	0,33	0,41	0,31	0,31	0,30	0,33	0,34	0,38
CaO	1,19	1,08	1,15	1,20	1,10	1,24	1,05	0,99	1,30	1,03	1,02	1,19	1,00	1,05	1,03	1,04	1,04	1,06	1,04	1,01	1,15	1,11	1,11
Na_2O	6,69	6,01	6,50	5,77	6,97	6,26	7,12	6,02	5,50	6,64	7,23	6,80	6,93	6,42	6,69	7,14	6,81	7,03	7,16	6,78	6,23	7,12	6,33
K_2O	6,04	5,73	5,88	6,27	4,95	5,06	4,85	4,62	5,56	4,84	4,76	4,91	4,80	4,98	4,76	4,87	4,77	5,71	6,00	6,11	6,04	6,10	6,39
P_2O_5	0,08	0,07	0,01	0,09	0,07	0,09	0,03	0,00	0,08	0,06	0,02	0,06	0,03	0,06	0,06	0,01	0,04	0,05	0,00	0,00	0,05	0,00	0,03
Tot.	89,4	93,7	93,9	90,7	96,4	97,0	94,9	96,0	95,4	94,5	95,6	98,8	94,1	93,7	94,5	94,5	94,7	95,4	93,1	93,4	93,5	95,4	97,9
Alkali	12,7	11,7	12,4	12,0	11,9	11,3	12,0	10,6	11,1	11,5	12,0	11,7	11,7	11,4	11,4	12,0	11,6	12,7	13,2	12,9	12,3	13,2	12,7

Tephra layer	MD28												
Sample	MD28 c												
Material	GS												
Classification	TRA												
SiO_2	64,2	64,2	63,6	63,3	63,2	63,7	64,2	62,9	62,9	63,4	63,5	63,6	63,5
TiO_2	0,53	0,53	0,52	0,54	0,52	0,60	0,48	0,52	0,59	0,55	0,55	0,55	0,71
Al_2O_3	19,4	19,6	19,3	19,7	19,3	19,5	19,3	19,9	19,5	20,0	19,6	20,1	19,7
FeO	2,47	2,47	2,58	2,73	2,87	2,76	2,62	2,61	2,80	2,54	2,61	2,76	2,49
MnO	0,22	0,22	0,21	0,34	0,16	0,29	0,12	0,18	0,31	0,23	0,19	0,23	0,24
MgO	0,46	0,38	0,38	0,31	0,53	0,38	0,48	0,29	0,33	0,38	0,36	0,33	0,34
CaO	1,29	1,16	1,18	1,00	1,43	1,29	1,29	0,95	1,02	1,23	1,12	1,00	1,10
Na_2O	5,83	6,08	6,88	7,22	5,96	6,32	5,95	7,66	7,51	6,18	6,71	6,47	6,61
K_2O	5,42	5,21	5,26	4,85	5,91	5,17	5,45	4,88	5,02	5,42	5,30	4,94	5,28
P_2O_5	0,12	0,13	0,06	0,06	0,10	0,03	0,12	0,03	0,06	0,04	0,09	0,01	0,04
Tot.	98,4	93,2	98,6	95,6	96,6	96,1	97,5	97,0	95,3	95,5	98,3	93,8	95,3
Alkali	11,3	11,3	12,1	12,1	11,9	11,5	11,4	12,5	12,5	11,6	12,0	11,4	11,9

Tephra layer	MD28													
Sample	MD28 b													
Li	55	73	57	14	58	26	75	< d.l.	< d.l.	46	38	102	81	< d.l.
Be	< d.l.	78	< d.l.	< d.l.	< d.l.	15	41	< d.l.	< d.l.	73	< d.l.	< d.l.	41	< d.l.
Sc	< d.l.	< d.l.	< d.l.	8,7	7,1	4,5	12,6	< d.l.	16,0	< d.l.	15,1	< d.l.	17,6	19,2
V	47	25	< d.l.	37	26	28	17	51	19	40	13	32	< d.l.	36
Cr	< d.l.	< d.l.	< d.l.	< d.l.	39,0	< d.l.	< d.l.	< d.l.	< d.l.	< d.l.	< d.l.	123,7	< d.l.	131,7
Co	1,4	< d.l.	3,6	2,0	2,9	1,1	1,4	28,6	< d.l.	5,3	2,6	< d.l.	< d.l.	< d.l.
Ni	< d.l.	13,3	29,3	< d.l.	< d.l.	< d.l.	14,0	< d.l.	12,8	< d.l.	< d.l.	< d.l.	< d.l.	< d.l.
Zn	< d.l.	527,3	161,7	105,9	145,1	72,7	172,5	< d.l.	48,8	137,1	< d.l.	137,3	< d.l.	129,0
Rb	341	559	557	259	536	331	531	402	472	441	367	400	558	556
Sr	7,4	3,0	6,2	18,6	14,6	5,1	10,8	230,7	5,0	6,6	63,1	1,6	< d.l.	1,4
Y	30	56	54	36	66	38	67	41	65	57	37	67	56	85
Zr	319	703	669	240	713	360	761	242	525	462	301	581	651	665
Nb	59	115	110	38	112	62	115	68	98	66	66	111	117	121
Cs	20	34	38	11	30	17	32	25	23	21	19	23	40	39
Ba	9,2	< d.l.	< d.l.	19,9	4,2	2,8	0,7	417,4	14,9	< d.l.	93,7	< d.l.	< d.l.	< d.l.
La	84	143	140	69	144	86	138	67	109	117	81	129	140	161
Ce	155	276	251	146	275	172	282	129	205	212	159	270	258	264
Pr	16	26	29	18	31	18	28	15	19	24	17	33	27	28
Nd	68	91	78	54	95	70	95	57	89	81	76	109	88	110
Sm	11	19	20	15	17	12	19	18	8	22	15	20	24	5
Eu	1,8	0,5	< d.l.	0,5	0,5	1,2	0,8	1,3	0,6	1,1	1,6	2,4	< d.l.	< d.l.
Gd	8,2	8,1	6,0	4,5	15,2	8,2	14,2	9,8	8,3	12,0	5,2	4,0	8,8	19,8
Tb	1,2	2,0	2,0	1,1	1,8	1,3	1,0	2,1	1,8	2,0	2,0	2,7	2,6	2,1
Dy	8,1	10,5	8,5	6,8	14,6	8,1	12,3	6,9	5,8	13,0	4,1	13,7	12,9	8,9
Ho	1,5	3,3	2,3	0,8	2,5	1,7	3,0	2,5	2,7	2,1	1,8	1,3	1,8	0,8
Er	4,1	6,9	5,2	3,7	6,1	3,5	4,1	< d.l.	5,0	5,1	2,8	9,2	7,6	5,9
Tm	< d.l.	0,8	0,4	0,3	0,7	0,7	0,9	< d.l.	0,9	< d.l.	< d.l.	1,0	1,3	0,7
Yb	4,0	7,5	2,2	< d.l.	6,8	4,0	10,9	< d.l.	2,0	1,9	4,2	4,6	< d.l.	6,8
Lu	1,1	0,8	0,2	0,5	0,9	0,6	0,7	< d.l.	1,0	< d.l.	0,5	0,4	< d.l.	0,8
Hf	8,7	10,8	17,0	4,2	15,4	7,8	13,5	5,0	6,9	7,4	6,5	15,9	14,4	12,9
Ta	3,3	5,0	5,6	2,8	6,0	3,1	5,2	1,2	4,5	7,6	2,8	4,2	5,9	6,8
Pb	43	53	68	38	72	42	73	76	60	51	49	55	64	58
Th	24	46	43	19	49	23	49	16	28	32	23	42	45	49
U	7,1	18,2	15,9	5,7	15,3	7,8	16,8	9,3	11,1	10,1	5,9	11,7	13,3	18,0
Eu/Eu*	0,6	0,1		0,2	0,1	0,4	0,1	0,3	0,2	0,2	0,5	0,8		
$(La/Yb)_N$	14	13	44		14	14	8		36	41	13	19		16
$(La/Sm)_N$	4,8	4,6	4,5	2,9	5,4	4,4	4,6	2,3	9,0	3,3	3,3	4,1	3,7	22,3
$(Gd/Yb)_N$	1,7	0,9	2,2		1,8	1,6	1,0		3,3	5,0	1,0	0,7		2,4

Tephra layer	MD33															
Sample																
Material	P								GS							
Classification	AND				DAC		AND			DAC	AND		DAC		AND	DAC
SiO_2	59,6	60,5	62,3	61,8	64,1	64,3	61,3	60,6	59,4	66,4	61,3	62,3	64,3	63,2	60,1	63,8
TiO_2	1,26	1,26	1,20	1,07	0,94	1,19	1,46	1,35	0,82	0,70	1,13	1,28	1,00	0,98	0,87	1,04
Al_2O_3	17,4	15,4	15,6	14,6	16,6	15,9	15,0	14,4	19,8	17,6	17,5	15,2	16,3	16,4	18,5	16,5
FeO	7,06	7,82	6,74	6,99	5,89	5,40	8,32	8,57	5,09	3,91	6,46	7,72	5,82	6,42	6,11	5,75
MnO	0,18	0,12	0,18	0,18	0,16	0,11	0,26	0,26	0,15	0,12	0,13	0,19	0,16	0,17	0,13	0,23
MgO	1,58	2,68	2,31	3,33	1,08	1,27	2,03	3,59	1,77	0,70	1,55	2,33	1,53	2,22	2,28	1,67
CaO	6,71	5,25	4,82	5,05	3,85	4,15	5,22	5,09	6,78	3,01	5,01	4,10	3,56	3,54	5,74	3,76
Na_2O	3,91	3,85	3,85	3,93	4,08	4,15	3,63	3,02	3,96	4,50	4,08	3,55	4,08	3,84	4,02	4,16
K_2O	1,88	2,64	2,57	2,59	3,01	2,97	2,27	2,60	1,92	2,93	2,34	2,89	2,92	2,79	2,03	2,82
P_2O_5	0,41	0,47	0,40	0,43	0,30	0,53	0,47	0,54	0,30	0,20	0,54	0,48	0,38	0,40	0,31	0,33
Tot.	100,5	98,4	98,8	98,8	98,2	99,0	99,9	98,6	100,3	100,4	99,1	100,5	99,0	94,8	99,5	99,5
Alkali	5,8	6,5	6,4	6,5	7,1	7,1	5,9	5,6	5,9	7,4	6,4	6,4	7,0	6,6	6,1	7,0

Tephra layer	MD33								
Sample									
Li	< d.l.	27,8	18,7	21,5	< d.l.	13,1	13,4	13,4	5,1
Be	< d.l.	47,2	< d.l.	16,7	< d.l.	< d.l.	< d.l.	11,2	< d.l.
Sc	15,0	11,9	31,2	16,5	< d.l.	20,7	21,1	18,6	24,9
V	92	45	113	70	28	174	193	166	260
Cr	< d.l.	74,8	121,2	< d.l.	< d.l.	20,4	< d.l.	< d.l.	24,9
Co	11	6	14	5	4	11	13	12	19
Ni	20	< d.l.	25	< d.l.	9	1	7	4	5
Zn	396	60	56	28	111	120	87	66	83
Rb	102	99	93	78	89	96	91	76	60
Sr	261	402	474	558	503	378	374	535	545
Y	36	23	22	21	30	30	36	27	25
Zr	239	179	157	157	149	182	197	143	129
Nb	23	20	21	17	20	21	23	16	15
Cs	2,9	2,7	1,3	1,9	< d.l.	1,8	1,6	1,6	1,2
Ba	678	596	585	565	742	620	671	523	530
La	51	44	34	37	35	48	51	38	37
Ce	81	56	60	60	64	77	83	63	63
Pr	7,9	6,2	7,7	5,7	6,5	8,5	8,4	7,0	6,8
Nd	39	35	20	25	33	33	31	28	28
Sm	4,9	6,0	5,0	4,3	< d.l.	6,3	9,0	5,0	5,4
Eu	0,6	0,6	2,0	1,3	2,4	1,6	1,7	1,5	1,2
Gd	6,4	6,3	7,8	3,8	6,6	6,4	6,7	4,9	4,9
Tb	1,1	0,8	< d.l.	0,7	< d.l.	0,8	0,8	0,7	0,6
Dy	2,9	3,6	5,0	3,9	13,5	5,5	6,0	4,9	4,9
Ho	0,9	0,8	1,0	0,9	< d.l.	1,1	1,6	1,1	0,8
Er	1,6	2,8	2,8	2,4	< d.l.	3,3	4,0	2,9	2,2
Tm	0,5	0,4	< d.l.	0,3	< d.l.	0,5	0,5	0,4	0,4
Yb	5,1	2,8	2,9	2,0	2,0	2,7	2,4	2,5	3,8
Lu	0,8	0,4	< d.l.	0,3	< d.l.	0,5	0,6	0,4	0,4
Hf	3,6	4,0	1,9	2,8	4,2	5,2	6,1	3,5	2,8
Ta	2,0	0,8	1,1	1,0	0,6	1,1	1,1	1,0	0,7
Pb	78	11	12	8	17	10	9	8	7
Th	17	11	8	10	8	12	12	9	8
U	3,1	3,9	2,0	2,6	4,2	2,7	3,3	2,5	2,3
Eu/Eu*	0,3	0,3	1,0	1,0		0,7	0,7	0,9	0,7
$(La/Yb)_N$	6,8	10,6	7,9	12,6	11,6	11,9	14,4	10,1	6,5
$(La/Sm)_N$	6,6	4,6	4,3	5,4		4,8	3,6	4,8	4,3
$(Gd/Yb)_N$	1,0	1,8	2,2	1,5	2,6	1,9	2,3	1,6	1,0

Tephra layer / Sample	MD35											
Material	GS											
Classification	BAS-TRA-AND	TRA-DAC	TRA-AND	BAS-TRA-AND	TRA-AND	BAS-TRA-AND	TRA	TRA-DAC	TRA	TRA-AND	BAS-TRA-AND	
SiO_2	55,1	63,4	56,8	55,2	57,0	54,7	62,3	61,9	62,7	58,2	55,6	55,1
TiO_2	0,84	1,29	0,81	0,87	0,77	0,76	0,45	0,33	0,46	0,72	0,79	0,83
Al_2O_3	17,4	16,4	17,4	17,2	17,6	16,9	18,6	19,9	18,4	18,0	17,2	17,1
FeO	8,52	5,00	7,65	8,61	7,34	8,87	3,13	2,96	2,82	6,23	8,11	8,46
MnO	0,26	0,24	0,21	0,28	0,22	0,23	0,18	0,13	0,22	0,20	0,11	0,20
MgO	3,22	1,48	2,86	3,36	2,68	3,27	0,38	0,96	0,32	2,17	3,10	3,21
CaO	7,25	3,24	6,06	7,19	6,42	7,37	1,67	4,70	1,65	5,26	6,98	7,29
Na_2O	3,23	5,15	3,15	3,13	3,41	3,37	6,18	4,77	6,28	3,88	3,64	3,43
K_2O	3,85	3,32	4,53	3,79	4,14	4,02	7,11	4,25	7,12	4,92	4,02	3,91
P_2O_5	0,39	0,43	0,52	0,37	0,39	0,46	0,06	0,12	0,04	0,43	0,44	0,46
Tot.	98,2	98,7	97,5	98,6	98,2	97,2	97,1	97,5	95,8	97,3	97,2	97,3
Alkali	7,1	8,5	7,7	6,9	7,5	7,4	13,3	9,0	13,4	8,8	7,7	7,3

Tephra layer / Sample	MD35										
Li	55	44	67	36	41	116	108	47	31	33	< d.l.
Be	< d.l.	< d.l.	< d.l.	< d.l.	57	< d.l.	< d.l.	< d.l.	49	< d.l.	183
Sc	18	< d.l.	< d.l.	< d.l.	< d.l.	< d.l.	< d.l.	8	< d.l.	7	< d.l.
V	< d.l.	11,5	< d.l.	< d.l.	< d.l.	8,7	13,2	16,9	16,6	27,0	23,7
Cr	< d.l.	< d.l.	212,7	< d.l.	113,4	< d.l.	< d.l.	< d.l.	92,6	< d.l.	< d.l.
Co	6,0	< d.l.	6,3	< d.l.	< d.l.	< d.l.	2,4	2,2	1,9	1,2	< d.l.
Ni	< d.l.	< d.l.		< d.l.	< d.l.	10,3		9,7	14,8	< d.l.	< d.l.
Zn	48	74	137	96	< d.l.	< d.l.	70	40	61	37	113
Rb	491	460	376	473	358	416	411	454	517	447	525
Sr	< d.l.	3,3	38,8	< d.l.	< d.l.	6,9	2,9	8,4	1,3	6,2	6,2
Y	68	48	61	51	45	52	56	64	69	61	76
Zr	661	649	537	587	418	648	564	629	634	612	804
Nb	104	99	77	101	82	111	102	104	103	118	116
Cs	29	32	24	26	28	29	28	29	29	31	36
Ba	4,5	< d.l.	37,6	< d.l.	< d.l.	2,7	< d.l.	2,5	< d.l.	13,2	< d.l.
La	131	122	110	127	84	124	104	124	132	121	149
Ce	252	238	239	232	180	240	224	229	233	227	293
Pr	23	22	24	25	20	28	22	22	22	23	29
Nd	89	90	70	87	63	103	72	83	78	80	93
Sm	11	9	14	23	12	20	11	19	7	20	14
Eu	0,4	1,4	< d.l.	< d.l.	< d.l.	0,8	1,1	< d.l.	< d.l.	0,9	1,6
Gd	10	12	16	13	9	18	11	11	7	14	32
Tb	2,2	2,6	1,5	1,8	0,8	0,9	2,2	1,0	1,3	1,6	2,1
Dy	15	9	10	15	10	14	9	10	7	7	10
Ho	1,6	1,8	1,1	2,3	2,7	1,1	0,9	1,1	1,4	1,5	2,1
Er	5,1	4,9	7,7	10,8	1,3	5,4	2,4	3,7	3,9	3,8	7,6
Tm	0,9	0,7	0,7	1,2	0,3	0,6	1,0	0,6	0,8	0,4	0,9
Yb	8,7	5,0	9,4	10,0	4,6	10,3	6,6	5,6	6,0	3,1	2,9
Lu	0,9	0,8	1,8	1,1	0,7	< d.l.	0,9	1,3	1,6	0,8	1,4
Hf	14	13	14	10	12	13	10	14	17	10	29
Ta	7,2	6,3	4,7	5,5	2,6	3,0	4,4	5,2	4,2	4,6	5,9
Pb	52	64	59	56	55	60	49	61	58	57	75
Th	43	46	39	41	35	44	42	39	45	43	61
U	13	14	14	15	13	12	12	14	13	14	14
Eu/Eu*	0,1	0,4				0,1	0,3			0,2	0,2
$(La/Yb)_N$	10	16	8	9	12	8	11	15	15	26	35
$(La/Sm)_N$	7,2	8,1	4,9	3,4	4,3	3,9	6,2	4,0	11,6	3,9	6,7
$(Gd/Yb)_N$	1,0	1,9	1,4	1,0	1,6	1,4	1,4	1,6	1,0	3,8	8,9

Chemical analysis of tephras from the ODP Leg 160, Site 963A core

Major (wt.%) and trace (ppm) element composition of the tephra layers. All analysis recalculated water-free to 100. Agpaitic index (A.I.) McDonald 1974. Tephra components: GS=glass shards, SC=scoria, P=pumice. Chemistry: HK= high K, ALK=alkaline, CA=calc-alkaline; RHY= rhyolite, PAN=Pantellerite, TRA-AND=trachy-andesite, TRA-DAC= trachy-dacite, TRA-COM=thrachy-comendite.

Tephra layer	**ODP3/5-1**															
Sample	**ODP3/5-1 a**								**ODP3/5-1 b**							
Material	**GS**															
Classification	**TRA-DAC**			**PAN**	**TRA-DAC**				**PAN**		**TRA-DAC**		**PAN**			
SiO_2	64,9	63,3	65,4	73,4	64,9	65,2	65,1	65,4	73,1	73,0	65,3	65,8	73,1	73,7	73,6	73,4
TiO_2	0,91	0,84	0,88	0,45	0,86	0,88	0,86	0,90	0,47	0,50	0,92	0,91	0,48	0,53	0,49	0,49
Al_2O_3	15,3	16,9	14,9	8,7	16,3	14,6	15,0	14,8	8,2	8,0	14,7	14,6	8,1	8,3	8,4	8,3
FeO	6,98	6,75	6,78	8,07	6,30	7,12	6,54	6,67	8,17	8,58	6,83	6,86	8,82	8,29	8,31	8,05
MnO	0,35	0,40	0,27	0,38	0,34	0,30	0,41	0,31	0,41	0,39	0,35	0,27	0,38	0,30	0,37	0,37
MgO	0,47	0,44	0,44	0,11	0,43	0,44	0,43	0,42	0,10	0,11	0,44	0,43	0,10	0,09	0,13	0,10
CaO	1,36	1,47	1,40	0,39	1,31	1,29	1,38	1,48	0,38	0,32	1,31	1,26	0,36	0,39	0,37	0,35
Na_2O	5,08	5,30	5,34	4,39	4,95	5,50	5,54	5,25	4,88	4,70	5,18	5,06	4,27	4,12	4,03	4,53
K_2O	4,47	4,38	4,52	4,07	4,46	4,52	4,60	4,57	4,28	4,29	4,67	4,60	4,31	4,32	4,26	4,35
P_2O_5	0,17	0,14	0,12	0,03	0,17	0,16	0,14	0,20	0,05	0,06	0,21	0,20	0,08	0,02	0,03	0,04
Tot.	95,8	96,8	98,9	95,4	99,0	95,9	97,6	97,5	93,8	93,4	97,9	98,4	91,8	92,9	93,3	93,1
Alkali	9,5	9,7	9,9	8,5	9,4	10,0	10,1	9,8	9,2	9,0	9,9	9,7	8,6	8,4	8,3	8,9
A.I.	0,9	0,8	0,9	1,3	0,8	1,0	0,9	0,9	1,6	1,5	0,9	0,9	1,4	1,4	1,3	1,5

Tephra layer	**ODP3/5-1**							
Sample	**ODP3/5-1 a**	**ODP3/5-1 b**						
Li	18	63	34	< d.l.	69	68	42	50
Be	< d.l.	< d.l.	< d.l.	< d.l.	< d.l.	< d.l.	29	11
Sc	14,5	< d.l.	< d.l.	17,8	< d.l.	4,5	7,8	5,9
V	< d.l.	< d.l.	< d.l.	< d.l.	< d.l.	< d.l.	1,7	12,0
Cr	< d.l.	< d.l.	< d.l.	< d.l.	< d.l.	10,9	<9.96	41,0
Co	< d.l.	< d.l.	< d.l.	3,7	< d.l.	< d.l.	< d.l.	3,4
Ni	10	< d.l.	7	< d.l.	< d.l.	3	3	19
Zn	139	202	297	352	442	423	434	245
Rb	41	203	210	187	191	178	187	183
Sr	15	2	3	4	2	2	3	18
Y89	26	142	142	148	131	151	144	143
Zr	191	1447	1558	1599	1513	1621	1612	1534
Nb	70	349	341	333	327	356	336	323
Cs	0,5	3,3	2,6	3,7	2,4	2,3	2,2	2,1
Ba	561	37	35	39	32	41	37	70
La	38	183	197	208	183	203	197	199
Ce	75	360	393	391	370	396	382	373
Pr	8,9	33,9	38,6	43,3	42,0	40,6	38,3	41,2
Nd	39	134	122	145	141	151	143	137
Sm	6,3	27,0	27,4	27,0	22,5	29,6	30,2	28,0
Eu	2,6	3,2	4,4	3,8	3,6	4,0	4,6	4,1
Gd	6,8	17,6	24,6	23,7	23,0	31,6	26,8	23,9
Tb	0,7	2,9	3,6	3,0	3,6	4,0	4,2	3,9
Dy	4,0	21,5	27,5	26,7	26,7	27,7	25,6	23,0
Ho	1,2	4,1	4,1	6,3	4,9	4,9	5,6	4,6
Er	3,2	12,5	17,0	16,0	13,2	15,7	15,9	15,2
Tm	0,5	1,8	2,5	1,4	1,5	2,3	2,2	2,2
Yb	3,0	13,4	20,3	14,5	12,3	16,4	15,2	14,4
Lu	0,7	1,8	< d.l.	1,4	2,2	1,8	2,2	1,6
Hf	4,9	31,1	39,0	38,3	36,1	40,1	38,1	31,5
Ta	3,3	20,7	19,0	18,3	20,9	20,6	20,6	20,8
Pb	2,2	22,6	13,5	16,4	14,2	14,8	15,1	20,3
Th	3,5	25,5	30,0	24,8	30,0	30,3	30,1	29,1
U	1,3	9,8	8,9	11,2	9,0	10,5	9,7	13,6
Eu/Eu*	1,2	0,4	0,5	0,5	0,5	0,4	0,5	0,5
$(La/Yb)_N$	8,4	9,2	6,6	9,7	10,0	8,4	8,8	9,3
$(La/Sm)_N$	3,8	4,3	4,5	4,9	5,1	4,3	4,1	4,5
$(Gd/Yb)_N$	1,8	1,1	1,0	1,3	1,5	1,6	1,4	1,3

Tephra layer	ODP6/3-3										
Sample	ODP6/3-3 a										
Material	GS										
Classification	TRA-DAC			PAN	TRA-DAC		PAN	TRA-DAC			
SiO_2	64,9	64,7	65,1	73,9	65,4	65,0	74,0	64,6	64,8	64,8	65,5
TiO_2	0,76	0,73	0,75	0,38	0,82	0,80	0,37	0,77	0,78	0,72	0,73
Al_2O_3	16,1	15,7	15,7	8,6	15,8	15,6	8,5	15,6	15,6	15,6	15,4
FeO	5,68	5,71	5,46	7,25	5,38	5,49	7,27	5,68	5,89	5,67	5,43
MnO	0,24	0,27	0,30	0,30	0,26	0,32	0,38	0,31	0,28	0,33	0,22
MgO	0,40	0,39	0,42	0,07	0,40	0,44	0,06	0,45	0,44	0,39	0,35
CaO	1,37	1,42	1,45	0,30	1,46	1,46	0,34	1,45	1,53	1,49	1,21
Na_2O	5,97	6,06	6,04	4,75	5,77	5,86	4,65	6,14	5,94	6,02	6,06
K_2O	4,46	4,82	4,70	4,42	4,63	4,88	4,34	4,84	4,65	4,79	4,98
P_2O_5	0,13	0,16	0,15	0,04	0,17	0,16	0,00	0,11	0,13	0,19	0,16
Tot.	98,0	98,1	97,8	93,6	94,3	95,3	92,8	96,7	96,9	98,3	97,8
Alkali	10,4	10,9	10,7	9,2	10,4	10,7	9,0	11,0	10,6	10,8	11,0
A.I.	0,9	1,0	1,0	1,5	0,9	1,0	1,4	1,0	0,9	1,0	1,0

Tephra layer	ODP6/3-3								
Sample	ODP6/3-3 a								
Li	< d.l.	< d.l.	9,5	20,9	10,8	15,3	21,0	56,4	7,2
Be	7,7	44,1	20,8	< d.l.	< d.l.	10,0	< d.l.	< d.l.	< d.l.
Sc	9,4	5,7	6,8	8,9	11,1	8,3	11,0	6,4	10,8
V	< d.l.	< d.l.	< d.l.	< d.l.	0,7	< d.l.	3,3	1,4	< d.l.
Cr	20,7	32,7	< d.l.	28,8	< d.l.	< d.l.	< d.l.	17,0	< d.l.
Co	0,6	1,4	< d.l.	2,1	0,6	1,2	1,0	1,4	0,7
Ni	< d.l.	< d.l.	5,1	< d.l.	< d.l.	< d.l.	2,4	< d.l.	< d.l.
Zn	167	208	128	151	185	121	183	392	262
Rb	61	60	56	58	62	61	62	233	59
Sr	52	55	52	50	56	57	54	6	60
Y89	40	44	38	35	43	44	43	202	50
Zr	353	367	324	334	362	357	371	2232	395
Nb	102	100	93	94	100	93	100	439	107
Cs	0,2	0,4	0,4	0,5	0,6	0,6	0,6	2,6	0,7
Ba	863	867	911	901	927	898	939	47	996
La	60	64	57	55	61	57	65	277	68
Ce	117	122	114	109	122	119	124	513	136
Pr	14	12	13	12	14	14	14	53	15
Nd	49	58	52	54	57	57	57	199	66
Sm	11	9	9	12	12	11	12	40	17
Eu	2,5	2,7	2,9	2,4	2,6	2,9	3,1	4,0	3,5
Gd	8,5	8,5	9,5	6,7	9,1	10,5	8,7	36,1	9,8
Tb	1,4	1,1	1,2	1,3	1,4	1,4	1,5	5,9	1,4
Dy	7,9	7,8	8,6	7,9	8,9	8,5	9,5	36,3	10,0
Ho	1,5	1,6	1,2	1,9	1,5	1,6	1,4	6,9	1,4
Er	5,4	3,5	5,1	4,0	4,3	5,0	3,7	19,5	4,2
Tm	0,6	0,4	0,5	0,7	0,6	0,7	0,6	3,2	0,5
Yb	5,0	4,2	3,9	4,7	4,3	4,6	3,2	20,3	4,1
Lu	0,7	0,5	0,6	0,7	0,6	0,8	0,8	2,8	0,7
Hf	8,1	5,9	7,9	8,4	8,9	9,1	8,9	48,8	10,6
Ta	5,3	5,6	5,4	4,5	5,7	5,7	5,5	26,5	6,1
Pb	3,3	4,7	4,2	6,9	3,8	5,5	4,5	17,9	4,8
Th	7,0	6,1	5,8	6,1	6,7	5,8	6,8	42,0	8,8
U	2,6	2,8	2,0	2,1	2,1	2,1	2,3	12,9	2,3
Eu/Eu*	0,8	0,9	0,9	0,8	0,8	0,8	0,9	0,3	0,8
$(La/Yb)_N$	8,2	10,3	9,7	8,0	9,7	8,4	13,8	9,2	11,3
$(La/Sm)_N$	3,3	4,6	3,9	2,9	3,3	3,4	3,3	4,4	2,5
$(Gd/Yb)_N$	1,4	1,6	2,0	1,2	1,7	1,8	2,2	1,4	2,0

Tephra layer	ODP6/3-3														
Sample	ODP6/3-3c														
Material	GS														
Classification	PAN	RHY	TRA-DAC		PAN	TRA-DAC		PAN			TRA-DAC	PAN		PAN	TRA-DAC
SiO_2	75,1	73,0	65,2	65,8	73,5	65,2	64,8	74,7	74,0	74,9	72,0	74,7	73,7	74,7	64,9
TiO_2	0,34	0,37	0,70	0,74	0,42	0,70	0,71	0,35	0,31	0,35	0,41	0,36	0,40	0,38	0,79
Al_2O_3	8,5	11,0	15,6	15,8	8,5	15,3	15,4	8,4	9,3	8,5	11,5	8,8	8,7	8,6	15,4
FeO	7,37	6,95	5,68	5,64	8,46	5,71	5,94	7,46	7,27	7,17	5,20	7,03	7,05	6,91	5,94
MnO	0,35	0,36	0,30	0,23	0,39	0,33	0,24	0,32	0,27	0,38	0,31	0,33	0,34	0,33	0,37
MgO	0,09	0,10	0,43	0,43	0,07	0,41	0,41	0,07	0,10	0,10	0,19	0,07	0,06	0,09	0,41
CaO	0,26	0,34	1,46	1,38	0,29	1,42	1,50	0,27	0,35	0,33	0,32	0,32	0,29	0,27	1,46
Na_2O	3,51	3,50	5,74	4,92	4,00	5,88	6,04	3,93	4,09	3,94	5,51	3,88	5,16	4,36	5,48
K_2O	4,43	4,32	4,73	4,88	4,32	4,81	4,74	4,47	4,25	4,33	4,58	4,46	4,27	4,39	5,07
P_2O_5	0,00	0,00	0,14	0,16	0,03	0,16	0,20	0,02	0,01	0,01	0,02	0,00	0,02	0,00	0,14
Tot.	92,2	92,9	95,4	94,2	89,6	97,3	98,2	92,4	92,6	91,4	98,6	93,4	93,5	92,1	97,1
Alkali	7,9	7,8	10,5	9,8	8,3	10,7	10,8	8,4	8,3	8,3	10,1	8,3	9,4	8,8	10,6
A.I.	1,2	0,9	0,9	0,8	1,3	1,0	1,0	1,3	1,2	1,3	1,2	1,3	1,5	1,4	0,9

Tephra layer	ODP6/3-3				
Sample	ODP6/3-3 c				
Li	55	66	62	42	48
Be	< d.l.	< d.l.	< d.l.	< d.l.	46
Sc	< d.l.	4,2	< d.l.	2,5	< d.l.
V	6,0	< d.l.	< d.l.	2,3	< d.l.
Cr	< d.l.	< d.l.	< d.l.	< d.l.	< d.l.
Co	< d.l.	0,4	< d.l.	< d.l.	< d.l.
Ni	< d.l.	2,6	< d.l.	< d.l.	< d.l.
Zn	297	441	388	265	320
Rb	219	219	229	220	223
Sr	5,3	3,7	3,3	7,6	2,5
Y89	193	207	193	199	195
Zr	2113	2400	2204	2529	2140
Nb	416	449	441	452	422
Cs	2,5	2,6	3,2	2,9	3,4
Ba	34	27	25	33	32
La	235	269	247	296	231
Ce	418	470	463	491	427
Pr	46,3	51,0	47,1	53,8	42,2
Nd	189	191	184	208	177
Sm	37	38	32	36	37
Eu	3,0	4,9	3,7	5,0	4,0
Gd	21	35	42	41	29
Tb	5,2	5,6	5,7	5,1	5,3
Dy	29	39	36	47	33
Ho	8,2	8,2	5,7	8,9	6,8
Er	21	20	16	22	17
Tm	2,5	3,1	2,6	2,7	2,9
Yb	17	21	24	23	16
Lu	2,3	2,8	4,0	3,3	2,8
Hf	40	53	50	61	43
Ta	27	30	26	34	27
Pb	20	16	16	19	15
Th	45	40	38	46	39
U	11	12	12	13	12
Eu/Eu*	0,3	0,4	0,3	0,4	0,4
$(La/Yb)_N$	9,5	8,7	6,9	8,6	9,8
$(La/Sm)_N$	4,0	4,4	4,8	5,2	3,9
$(Gd/Yb)_N$	1,0	1,4	1,4	1,4	1,5

Tephra layer	ODP6/3-3														
Sample	ODP6/3-3c														
Material	GS														
Classification	PAN	RHY	TRA-DAC		PAN	TRA-DAC		PAN			TRA-DAC	PAN		PAN	TRA-DAC
SiO_2	75,1	73,0	65,2	65,8	73,5	65,2	64,8	74,7	74,0	74,9	72,0	74,7	73,7	74,7	64,9
TiO_2	0,34	0,37	0,70	0,74	0,42	0,70	0,71	0,35	0,31	0,35	0,41	0,36	0,40	0,38	0,79
Al_2O_3	8,5	11,0	15,6	15,8	8,5	15,3	15,4	8,4	9,3	8,5	11,5	8,8	8,7	8,6	15,4
FeO	7,37	6,95	5,68	5,64	8,46	5,71	5,94	7,46	7,27	7,17	5,20	7,03	7,05	6,91	5,94
MnO	0,35	0,36	0,30	0,23	0,39	0,33	0,24	0,32	0,27	0,38	0,31	0,33	0,34	0,33	0,37
MgO	0,09	0,10	0,43	0,43	0,07	0,41	0,41	0,07	0,10	0,10	0,19	0,07	0,06	0,09	0,41
CaO	0,26	0,34	1,46	1,38	0,29	1,42	1,50	0,27	0,35	0,33	0,32	0,32	0,29	0,27	1,46
Na_2O	3,51	3,50	5,74	4,92	4,00	5,88	6,04	3,93	4,09	3,94	5,51	3,88	5,16	4,36	5,48
K_2O	4,43	4,32	4,73	4,88	4,32	4,81	4,74	4,47	4,25	4,33	4,58	4,46	4,27	4,39	5,07
P_2O_5	0,00	0,00	0,14	0,16	0,03	0,16	0,20	0,02	0,01	0,01	0,02	0,00	0,02	0,00	0,14
Tot.	92,2	92,9	95,4	94,2	89,6	97,3	98,2	92,4	92,6	91,4	98,6	93,4	93,5	92,1	97,1
Tot. Alkali	7,9	7,8	10,5	9,8	8,3	10,7	10,8	8,4	8,3	8,3	10,1	8,3	9,4	8,8	10,6
A.I.	1,2	0,9	0,9	0,8	1,3	1,0	1,0	1,3	1,2	1,3	1,2	1,3	1,5	1,4	0,9
R1	3129	3028	2038	2191	2923	1998	1949	3013	2997	3064	2586	3036	2786	2968	1976
R2	116	150	332	324	118	322	332	115	134	124	156	125	119	118	328

Tephra layer	ODP6/3-3				
Sample	ODP6/3-3 c				
Li	55,0	65,5	61,9	42,1	48,0
Be	< d.l.	< d.l.	< d.l.	< d.l.	45,9
Sc	< d.l.	4,2	< d.l.	2,5	< d.l.
V	6,0	< d.l.	< d.l.	2,3	< d.l.
Cr	< d.l.	< d.l.	< d.l.	< d.l.	< d.l.
Co	< d.l.	0,4	< d.l.	< d.l.	< d.l.
Ni	< d.l.	2,6	< d.l.	< d.l.	< d.l.
Zn	296,8	441,1	387,9	265,3	320,1
Rb	218,9	219,2	229,4	219,8	223,5
Sr	5,3	3,7	3,3	7,6	2,5
Y89	193,3	206,9	193,1	198,9	194,7
Zr	2112,6	2400,5	2204,1	2529,4	2139,6
Nb	416,2	448,9	441,4	451,8	422,3
Cs	2,5	2,6	3,2	2,9	3,4
Ba	33,9	27,1	25,4	32,6	32,4
La	235,1	268,9	247,0	295,9	231,1
Ce	417,8	470,0	462,5	490,8	427,1
Pr	46,3	51,0	47,1	53,8	42,2
Nd	189,1	190,5	184,0	207,7	177,5
Sm	36,7	38,4	32,2	35,8	37,1
Eu	3,0	4,9	3,7	5,0	4,0
Gd	21,4	35,4	42,3	41,2	29,0
Tb	5,2	5,6	5,7	5,1	5,3
Dy	29,0	38,9	36,3	46,5	33,4
Ho	8,2	8,2	5,7	8,9	6,8
Er	20,9	20,0	15,6	22,2	17,2
Tm	2,5	3,1	2,6	2,7	2,9
Yb	16,7	20,8	24,3	23,1	16,0
Lu	2,3	2,8	4,0	3,3	2,8
Hf	39,8	53,4	50,3	61,5	42,7
Ta	27,5	29,6	25,9	33,5	27,0
Pb	19,8	16,5	15,8	19,3	14,7
Th	44,7	39,6	38,2	46,0	38,9
U	11,4	12,5	11,8	12,9	11,7
Eu/Eu*	0,3	0,4	0,3	0,4	0,4
$(La/Yb)_N$	9,5	8,7	6,9	8,6	9,8
$(La/Sm)_N$	4,0	4,4	4,8	5,2	3,9
$(Gd/Yb)_N$	1,0	1,4	1,4	1,4	1,5

Tephra layer	ODP6/3-4																										
Sample	b										d									e							
Material	GS																										
Classification	TRA-DAC				PAN		TRA-DAC	DAC	TRA-DAC		TRA-COM	TRA-DAC	PAN	TRA-COM	TRA-DAC					TRA-DAC	PAN			TRA-DAC	PAN	TRA-DAC	
SiO_2	65,5	64,9	65,5	66,0	74,6	73,9	66,3	67,1	65,4	66,5	65,9	65,4	74,4	66,0	65,3	65,0	68,2	64,4	64,0	65,5	74,6	74,3	74,4	65,7	74,8	66,1	65,5
TiO_2	0,72	0,70	0,72	0,73	0,39	0,39	0,05	0,75	0,69	0,61	0,64	0,75	0,38	0,70	0,74	0,76	0,83	0,73	0,72	0,71	0,38	0,39	0,36	0,71	0,43	0,74	0,74
Al_2O_3	15,4	15,3	15,7	15,9	8,7	9,1	20,4	15,8	15,9	15,0	15,2	15,6	9,0	14,9	16,0	16,5	16,5	17,1	16,9	15,6	8,7	8,7	8,7	15,5	8,7	15,8	15,8
FeO	5,85	5,80	5,98	5,67	7,00	7,17	0,23	6,65	5,92	5,73	5,67	5,64	7,07	5,78	5,57	5,71	5,99	5,81	5,74	5,77	7,02	6,95	7,07	5,59	7,00	5,45	5,54
MnO	0,27	0,30	0,34	0,34	0,28	0,34	0,05	0,30	0,25	0,17	0,31	0,37	0,31	0,30	0,27	0,32	0,34	0,27	0,30	0,32	0,33	0,41	0,39	0,34	0,43	0,30	0,29
MgO	0,39	0,40	0,36	0,37	0,07	0,06	0,00	0,42	0,45	0,28	0,31	0,02	0,15	0,28	0,40	0,38	0,43	0,42	0,40	0,40	0,05	0,08	0,09	0,32	0,09	0,40	0,40
CaO	1,41	1,49	1,39	1,43	0,30	0,30	1,72	1,48	1,48	1,17	1,04	1,41	0,32	1,09	1,47	1,39	1,44	1,46	1,42	1,39	0,27	0,28	0,30	1,26	0,30	1,39	1,36
Na_2O	5,55	6,00	5,11	4,67	4,20	4,17	7,95	2,35	5,10	5,44	5,98	5,87	4,11	5,99	5,41	5,22	1,55	5,03	5,74	5,43	4,24	4,64	4,32	5,79	3,90	4,92	5,41
K_2O	4,81	4,88	4,80	4,73	4,42	4,55	3,33	4,90	4,70	5,02	4,97	4,78	4,28	4,91	4,71	4,61	4,55	4,65	4,66	4,73	4,39	4,19	4,27	4,71	4,32	4,83	4,77
P_2O_5	0,15	0,15	0,10	0,19	0,05	0,01	0,00	0,21	0,13	0,11	0,03	0,18	0,02	0,08	0,11	0,16	0,17	0,12	0,14	0,15	0,00	0,05	0,03	0,10	0,02	0,13	0,17
Tot.	95,9	96,3	95,1	93,4	93,1	92,7	99,8	95,7	95,2	95,8	99,0	98,5	91,6	98,8	97,5	95,3	94,1	93,7	98,6	94,7	93,2	94,1	92,7	97,9	93,4	95,2	94,4
Alkali	10,4	10,9	9,9	9,4	8,6	8,7	11,3	7,3	9,8	10,5	11,0	10,6	8,4	10,9	10,1	9,8	6,1	9,7	10,4	10,2	8,6	8,8	8,6	10,5	8,2	9,7	10,2
A.I.	0,9	1,0	0,9	0,8	1,3	1,3	0,8	0,6	0,8	1,0	1,0	1,0	1,3	1,0	0,9	0,8	0,5	0,8	0,9	0,9	1,4	1,4	1,3	0,9	1,3	0,8	0,9

Tephra layer	ODP6/3-4																		
Sample	f								g										
Material	GS																		
Classification	TRA-DAC			PAN	TRA-DAC				TRA-DAC				PAN	TRA-DAC					
SiO_2	64,8	65,1	64,9	71,1	64,5	64,7	64,7	64,9	65,1	64,6	64,6	63,9	74,1	65,2	65,2	64,6	67,2	64,4	64,5
TiO_2	0,71	0,70	0,68	0,55	0,75	0,73	0,74	0,74	0,69	0,79	0,77	0,78	0,38	0,76	0,75	0,69	0,68	0,76	0,74
Al_2O_3	15,9	15,8	15,7	11,5	16,3	16,2	16,4	15,8	16,1	16,1	16,0	16,6	8,6	15,8	15,9	16,0	16,5	15,8	15,9
FeO	5,69	5,61	5,87	6,33	5,77	5,79	5,59	5,79	5,48	5,53	5,56	5,88	7,16	5,93	5,69	5,85	6,07	5,73	5,79
MnO	0,25	0,26	0,28	0,35	0,35	0,30	0,28	0,37	0,31	0,21	0,34	0,31	0,45	0,34	0,33	0,25	0,29	0,34	0,24
MgO	0,42	0,40	0,40	0,26	0,45	0,45	0,40	0,42	0,40	0,41	0,42	0,41	0,10	0,40	0,39	0,42	0,42	0,42	0,43
CaO	1,45	1,42	1,52	0,41	1,44	1,54	1,49	1,49	1,34	1,40	1,45	1,45	0,30	1,40	1,37	1,49	1,46	1,57	1,53
Na_2O	5,92	5,94	5,79	4,85	5,57	5,37	5,70	5,63	5,88	6,14	6,05	5,84	4,65	5,45	5,45	6,03	2,58	6,17	6,01
K_2O	4,68	4,60	4,74	4,63	4,77	4,77	4,56	4,76	4,49	4,73	4,61	4,67	4,31	4,61	4,72	4,50	4,65	4,69	4,73
P_2O_5	0,18	0,12	0,18	0,03	0,16	0,15	0,12	0,15	0,16	0,12	0,22	0,14	0,04	0,10	0,18	0,15	0,17	0,13	0,13
Tot.	96,3	97,8	98,6	95,2	97,3	96,1	96,0	98,0	96,3	95,6	97,8	94,7	90,8	96,3	94,7	97,5	95,3	94,3	96,3
Alkali	10,6	10,5	10,5	9,5	10,3	10,1	10,3	10,4	10,4	10,9	10,7	10,5	9,0	10,1	10,2	10,5	7,2	10,9	10,7
A.I.	0,9	0,9	0,9	1,1	0,9	0,9	0,9	0,9	0,9	0,9	0,9	0,9	1,4	0,9	0,9	0,9	0,6	1,0	0,9

Tephra layer / Sample	ODP8/1-5												
Material	GS												
Classification	PAN												
SiO_2	69,5	70,4	70,6	70,2	70,3	70,1	69,5	70,2	71,1	70,8	70,3	70,5	70,1
TiO_2	0,63	0,57	0,62	0,27	0,62	0,54	0,62	0,64	0,19	0,67	0,64	0,48	0,4
Al_2O_3	11,3	11,3	11,7	11,3	11,9	11,3	11,6	11,6	11,7	11,7	12,0	11,7	11,5
FeO	6,73	6,28	5,96	6,61	5,97	6,54	6,77	6,18	6,69	5,83	6,53	6,46	6,33
MnO	0,28	0,24	0,23	0,15	0,59	0,23	0,09	0,42	0,57	0,2	0,06	0,40	0,01
MgO	0,25	0,33	0,09	0,19	0,23	0,29	0,14	0,32	0,26	0,28	0,22	0,18	0,33
CaO	0,36	0,47	0,44	0,44	0,51	0,4	0,5	0,56	0,36	0,54	0,39	0,42	0,6
Na_2O	6,31	5,73	5,89	6,18	5,32	5,99	6,41	5,67	4,63	5,53	5,13	5,31	6,1
K_2O	4,66	4,66	4,49	4,71	4,59	4,57	4,42	4,44	4,47	4,5	4,8	4,56	4,64
P_2O_5	n.d.	n.d.	n.d.	n.d.	n.d.	n.d.	n.d.	n.d.	n.d.	n.d.	n.d.	n.d.	n.d.
Tot.	98,5	99,2	95,2	97,9	97,7	98,2	97,1	96,1	96,5	96,2	99,0	97,4	98,2
Alkali	11,0	10,4	10,4	10,9	9,9	10,6	10,8	10,1	9,1	10,0	9,9	9,9	10,7
A.I.	1,4	1,3	1,2	1,4	1,2	1,3	1,3	1,2	1,1	1,2	1,1	1,2	1,3

Tephra layer / Sample	ODP8/1-5				
Li	28	30	27	33	38
Be	42	69	10	18	< d.l.
Sc	5,4	< d.l.	5,5	6,1	4,7
V	< d.l.	2,2	< d.l.	2,9	< d.l.
Cr	< d.l.	< d.l.	13,8	< d.l.	< d.l.
Co	< d.l.	1,1	0,5	0,6	0,7
Ni	4,1	6,0	11,2	< d.l.	72,7
Zn	201	201	230	352	247
Rb	144	149	140	141	136
Sr	5,7	6,5	10,6	4,6	7,5
Y89	146	107	125	115	131
Zr	1544	1322	1440	1321	1534
Nb	318	282	290	266	285
Cs	0,9	1,6	1,5	1,3	2,6
Ba	102	93	103	93	103
La	175	140	155	142	162
Ce	315	253	275	263	294
Pr	34	27	31	25	29
Nd	138	105	108	105	139
Sm	20	18	20	22	22
Eu	3,3	2,7	2,9	2,8	2,8
Gd	26	17	19	22	11
Tb	3,3	3,6	3,6	2,9	3,3
Dy	22	23	20	19	22
Ho	5,3	3,7	4,1	4,0	3,8
Er	12	11	13	13	11
Tm	2,2	1,7	2,1	1,9	1,6
Yb	16	13	9	13	14
Lu	1,7	1,9	1,3	1,5	2,6
Hf	35	29	31	29	38
Ta	20	16	18	16	18
Pb	18	17	16	17	18
Th	27	23	23	24	30
U	7,9	6,8	7,5	7,4	8,9
Eu/Eu*	0,4	0,5	0,4	0,4	0,5
$(La/Yb)_N$	7,5	7,5	11,2	7,1	7,9
$(La/Sm)_N$	5,6	5,0	4,9	4,0	4,7
$(Gd/Yb)_N$	1,3	1,1	1,6	1,3	0,7

Tephra layer / Sample	ODP8/3-6									
Material	GS									
Classification	TRA-COM									
SiO_2	65,6	66,5	66,0	66,1	65,5	66,0	65,3	65,6	66,1	66,4
TiO_2	0,72	0,56	0,68	0,97	0,86	0,77	0,84	0,85	0,57	0,62
Al_2O_3	14,5	14,2	14,2	14,1	14,7	13,3	14,6	14,5	14,0	14,1
FeO	5,68	6,21	5,94	6,46	5,8	7,05	6,45	6,28	6,22	5,95
MnO	0,55	0,41	0,44	0,16	0,34	0,43	0,37	0,4	0,35	0,4
MgO	0,51	0,33	0,28	0,48	0,42	0,35	0,36	0,35	0,49	0,43
CaO	0,78	0,82	0,69	0,95	1,22	0,91	1,12	0,99	0,92	1,06
Na_2O	6,45	5,96	6,64	5,98	6,11	6,19	6,01	6,18	6,45	6
K_2O	5,24	4,95	5,07	4,82	5,01	4,93	4,97	4,8	4,89	5,04
P_2O_5	n.d.	n.d.	n.d.	n.d.	n.d.	n.d.	n.d.	n.d.	n.d.	n.d.
Tot.	96,8	94,4	98,3	97,1	99,0	95,2	98,5	98,2	97,5	96,2
Alkali	11,7	10,9	11,7	10,8	11,1	11,1	11,0	11,0	11,3	11,0
A.I.	1,1	1,1	1,2	1,1	1,1	1,2	1,1	1,1	1,1	1,1

Tephra layer / Sample	ODP8/3-6							
Li	25	12	11	10	12	10	7	15
Be	< d.l.	6,5	< d.l.	< d.l.	2,3	8,0	7,3	< d.l.
Sc	9,8	11,3	10,1	9,7	10,8	9,2	10,3	9,0
V	8,9	0,4	0,5	< d.l.	1,0	2,3	< d.l.	< d.l.
Cr	< d.l.	< d.l.	< d.l.	5,0	< d.l.	24,0	< d.l.	< d.l.
Co	0,8	0,3	0,4	0,5	0,4	< d.l.	< d.l.	1,3
Ni	7,9	0,6	< d.l.	< d.l.	< d.l.	< d.l.	< d.l.	< d.l.
Zn	135	158	147	171	137	124	148	102
Rb	86	63	61	71	57	68	74	69
Sr	22	10	10	6	23	12	3	8
Y89	59	47	47	52	43	44	55	50
Zr	523	425	427	485	381	417	491	472
Nb	124	105	101	116	90	102	121	117
Cs	1,0	0,5	0,5	0,6	0,5	0,5	0,6	0,4
Ba	133	508	514	297	901	468	198	185
La	78	66	64	71	60	63	73	73
Ce	146	124	123	133	115	120	130	134
Pr	17	14	14	15	13	13	16	14
Nd	63	57	56	58	53	55	63	52
Sm	13	12	12	11	10	7	12	11
Eu	1,7	2,9	2,8	2,5	2,8	2,2	2,8	2,5
Gd	13	11	10	13	9	12	11	12
Tb	2,2	1,7	1,5	1,7	1,4	1,4	1,7	2,0
Dy	12	10	9	10	9	11	9	11
Ho	2,0	1,7	1,7	2,0	1,7	1,7	2,3	2,2
Er	6,3	5,6	4,3	5,0	3,6	3,6	6,5	5,3
Tm	0,9	0,7	0,8	0,7	0,6	0,6	0,6	0,9
Yb	3,9	4,6	4,7	5,2	3,9	3,5	6,9	4,7
Lu	0,8	0,6	0,7	0,8	0,5	0,7	0,7	0,7
Hf	11	10	9	10	9	9	13	13
Ta	8,8	6,2	5,9	7,2	5,4	7,1	8,5	7,4
Pb	13	3	4	5	3	4	5	6
Th	11	8	8	9	7	8	9	8
U	2,5	2,5	2,2	2,4	2,0	2,3	2,6	2,2
Eu/Eu*	0,4	0,8	0,8	0,6	0,9	0,7	0,8	0,7
$(La/Yb)_N$	14	10	9	9	10	12	7	10
$(La/Sm)_N$	3,8	3,6	3,5	4,0	3,6	5,4	3,8	4,1
$(Gd/Yb)_N$	2,7	1,9	1,7	2,0	1,7	2,9	1,3	2,1

APPENDIX D

Primitive mantle and chondrite values used for normalization trace elements

Element	Primitive mantle (Sun & McDonough, 1989)	CI chondrite (Boynton 1984)
Rb	0,635	
Ba	6,989	
Th	0,085	
Nb	0,713	
La	0,687	0,3100
Ce	1,833	0,8080
Sr	21,1	
Nd	1,354	0,6000
Sm	0,444	0,1950
Zr	11,2	
Eu	0,168	0,0735
Ti*	1300	
Gd	0,596	0,2590
Dy	0,737	0,3220
Y	4,55	
Er	0,48	0,2100
Yb	3,05	0,2090
Lu	0,074	0,0322
Pr		0,1220
Tb		0,0474
Ho		0,0718
Tm		0,0324

APPENDIX E

Whole-cores photos of KC01B

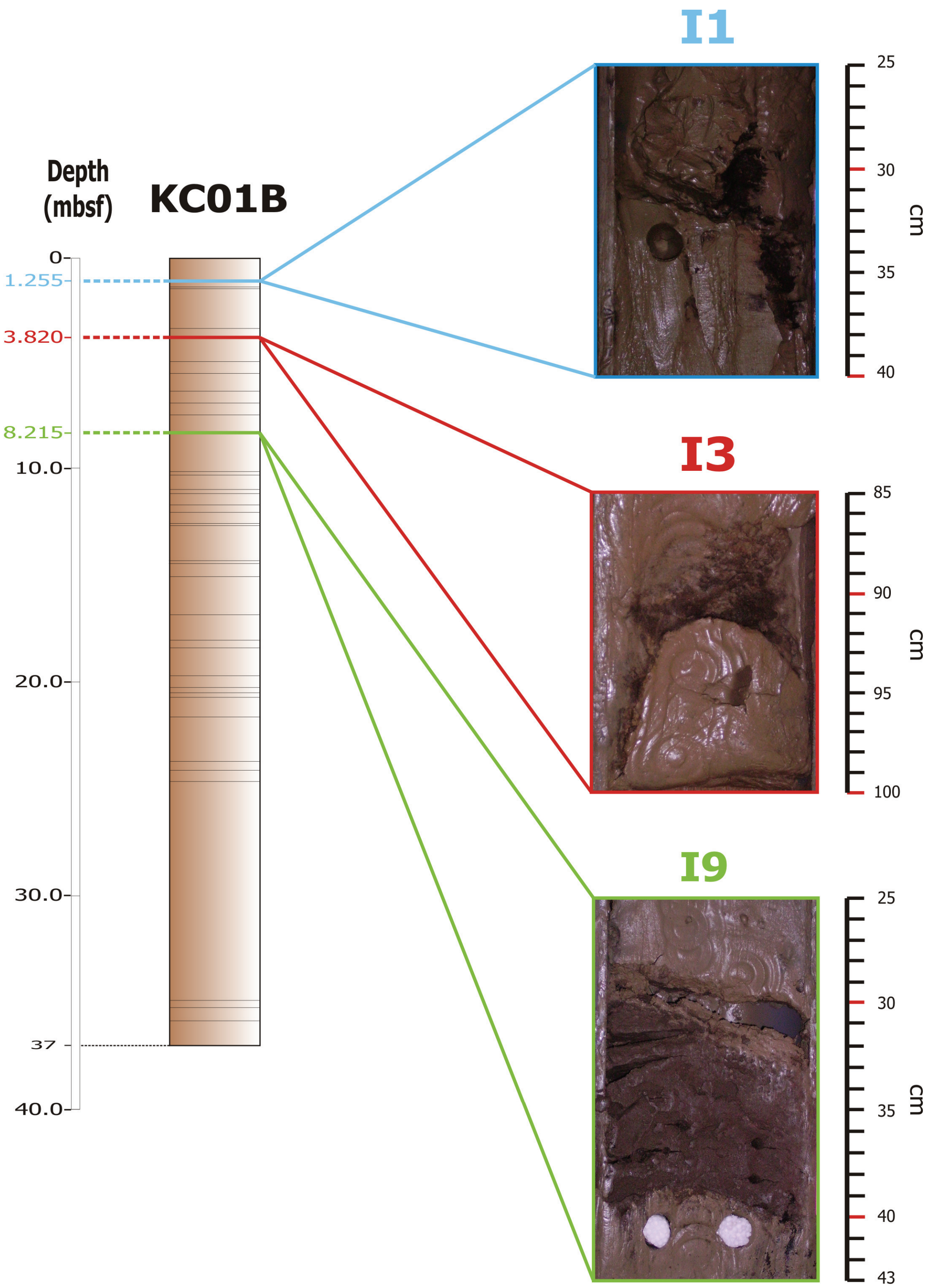

Whole-cores photos of MD01_2474G

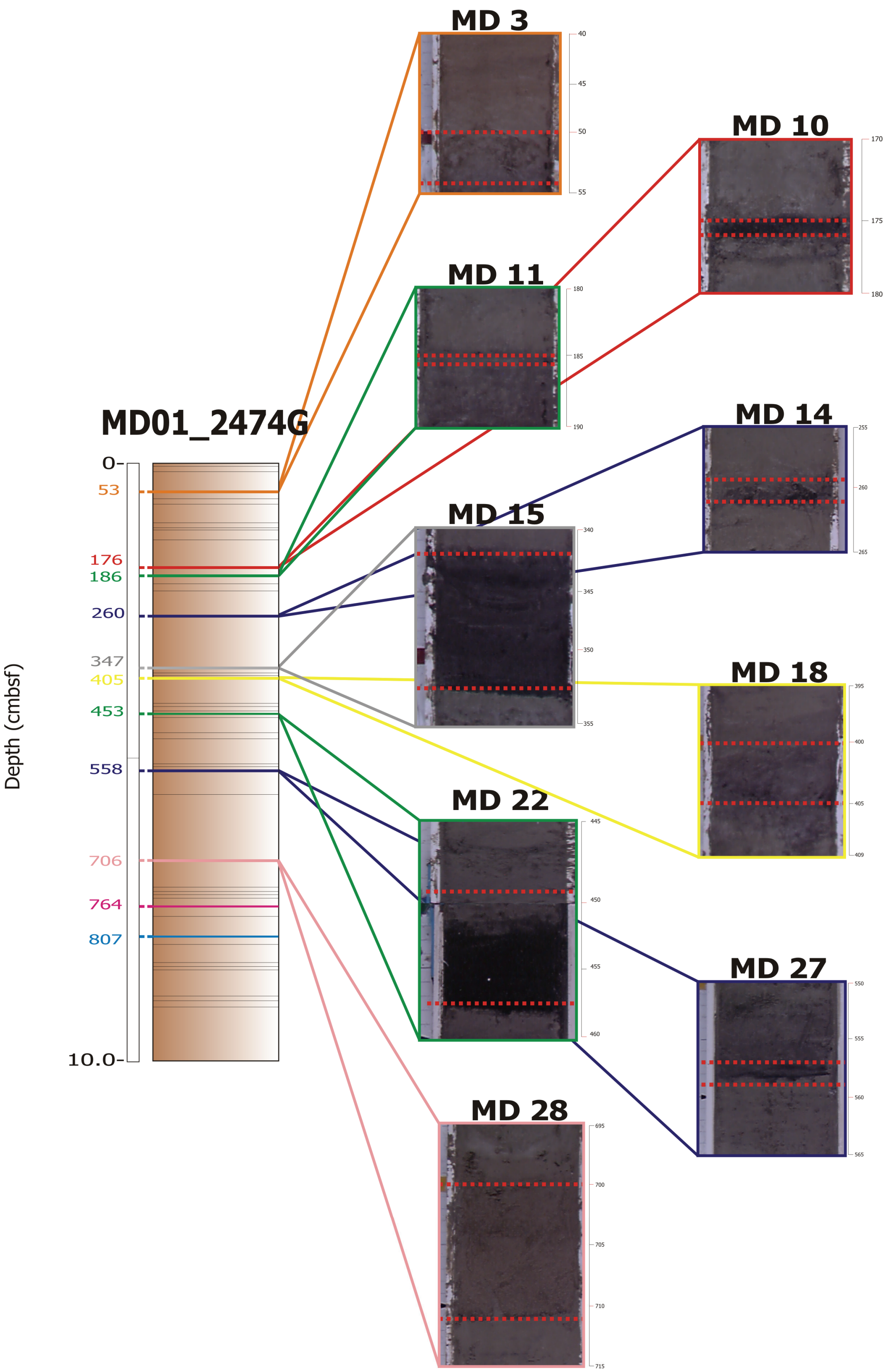

PhD thesis

Whole-cores photos of ODP Leg 160, Site 963A